AGARD-AG-148-71

AGARD

ADVISORY GROUP FOR AEROSPACE RESEARCH & DEVELOPMENT

7 RUE ANCELLE 92 NEUILLY SUR SEINE FRANCE

AGARDograph No. 148

on

Heat Transfer in Rocket Engines

by

H. Ziebland and R. C. Parkinson

NORTH ATLANTIC TREATY ORGANIZATION

DISTRIBUTION AND AVAILABILITY
ON BACK COVER

NORTH ATLANTIC TREATY ORGANIZATION

ADVISORY GROUP FOR AEROSPACE RESEARCH AND DEVELOPMENT

(ORGANISATION DU TRAITE DE L'ATLANTIQUE NORD)

HEAT TRANSFER IN ROCKET ENGINES

H.Ziebland
Explosives Research and Development Establishment
Waltham Abbey, Essex, England

and

R.C.Parkinson
Rocket Propulsion Establishment
Westcott, Bucks., England

This AGARDograph has been sponsored by the Propulsion and
Energetics Panel of AGARD-NATO

THE MISSION OF AGARD

The mission of AGARD is to bring together the leading personalities of the NATO nations in the fields of science and technology relating to aerospace for the following purposes:

- Recommending effective ways for the member nations to use their research and development capabilities for the common benefit of the NATO community;
- Providing scientific and technical advice and assistance to the North Atlantic Military Committee in the field of aerospace research and development;
- Continuously stimulating advances in the aerospace sciences relevant to strengthening the common defence posture;
- Improving the co-operation among member nations in aerospace research and development;
- Exchanging of scientific and technical information;
- Providing assistance to member nations for the purpose of increasing their scientific and technical potential;
- Rendering scientific and technical assistance, as requested, to other NATO bodies and to member nations in connection with research and development problems in the aerospace field.

The highest authority within AGARD is the National Delegates Board consisting of officially appointed senior representatives from each Member Nation. The mission of AGARD is carried out through the Panels which are composed of experts appointed by the National Delegates, the Consultant and Exchange Program and the Aerospace Applications Studies Program. The results of AGARD work are reported to the Member Nations and the NATO Authorities through the AGARD series of publications of which this is one.

Participation in AGARD activities is by invitation only and is normally limited to citizens of the NATO nations.

Published September 1971

536.2:629.76

Printed by Technical Editing and Reproduction Ltd
Harford House, 7-9 Charlotte St, London, W1P 1HD

PREFACE

In its continual effort to make available in book form pertinent work in the areas of propulsion, combustion and power systems, the Propulsion and Energetics Panel of AGARD is pleased to sponsor this AGARDograph by Ziebland and Parkinson.

Coverage of the complex heat transfer problems which arise in rocket motors is inadequate in most books dealing with rocket propulsion. Indeed, it is difficult to find all aspects of the rocket heat transfer problem in texts devoted exclusively to heat transfer. In this concise effort, Ziebland and Parkinson manage to cover practically all facets of heat transfer that enter into the performance of rocket motors. The approaches are both fundamental and practical. Thus, this AGARDograph should be of great value to the practising propulsion engineer, as well as those beginning their studies in this field. Its contents should find application, as well, to problem areas arising in other propulsive devices and various aerospace technologies.

Irvin Glassman
Chairman
Propulsion and Energetics Panel

September, 1971

SUMMARY

In the first part of this book the various basic heat transfer processes are considered,– simple convective heat transfer from hot gases to the engine walls under various conditions, radiation heat transfer, and coolant heat transfer processes. This part is followed by one describing the various methods of cooling used in liquid propellant rocket engines, such as regenerative, film, ablation and radiation cooling. The final part concerns the properties of materials that will have to be known by the engine designer, from the transport properties of the hot combustion gases to those of the materials from which the engine will be constructed.

Emphasis was placed on presenting simple methods for calculating the magnitude of heat transfer rather than providing the most modern and rigorous theories, particularly in the field of developing boundary layers.

ACKNOWLEDGEMENT

First and foremost the authors' thanks are due to the many workers who through their research in the field of rocket propulsion have contributed so much to the wealth of knowledge on which the authors have freely drawn. Dr I.Smith formerly of Rolls Royce Ltd, kindly advised in the preparation of the chapter dealing with heat transfer to rocket injectors.

It is a most pleasant duty to record the moral support of Dr R.Hagerty of AGARD whose patience was a continuing source of encouragement to the senior author to complete a difficult task.

Last, but by no means least, we must mention the many colleagues and friends who at various times lent a hand in the preparation of the manuscript, the illustrations, etc. To all these colleagues, too numerous to mention individually, our heartfelt thanks.

CONTENTS

HEAT TRANSFER IN ROCKET ENGINES

by

H.Ziebland and R.C.Parkinson

CHAPTER 1

FOREWORD

The flame temperatures attained in liquid propellant rockets considerably exceed the safe operating temperatures of all conventional materials of construction and the need to protect in some way the surfaces directly exposed to the hot gas stream has been recognised by the earliest workers (Tsiolkowski, Oberth, Goddard).

Rocketry in the first half of this century was pursued by a handful of enthusiasts who received little, if any, public support and had to work with very limited funds. As there were so many new problems to solve, it was inevitable that their efforts were concentrated in the more spectacular field of rocket flight and problems associated with the cooling of the rocket engine received scant attention and were considered of secondary importance.

This situation did not materially change when the military potential of rocket propulsion was realised during the years immediately before and during World War II. Emphasis was almost exclusively placed upon objectives dictated by military demands and hardly any effort was devoted to back up the work of the development engineers by parallel, fundamental studies. One of the major problems of that time was to provide adequate protection for the walls of combustion chamber and nozzle and the "cooling problem" proved to be a continuing headache to the designers and test engineers alike. Only by adopting trial and error methods, and often down-grading the propellant, as e.g. in the case of the well-known V-2 rocket, was it possible to attain the development objectives.

The importance of the heat transfer processes in rocket engines had been realised for a long time but the details of many of the processes involved were not so obvious. A general qualitative picture of heat transfer in rocket thrust chambers can be derived from the energy flux distribution in the hot combustion gases themselves, reaching a maximum at the nozzle throat where the flow area is a minimum and velocity a maximum. It was also understood that the heat transfer will increase if higher energy propellant combinations are used, and if the chamber pressure is increased. However, if we wish to extend this broad picture of heat transfer for the purpose of making quantitative estimates, problems arise. A full understanding of the heat transfer will involve an understanding of nearly every other sort of process occurring in a rocket engine. The distribution and mixing of the propellant streams by various types of injectors and hence the development of the combustion process has a pronounced effect on the heat transfer in the combustion chamber while the aerodynamic processes in the expansion nozzle will affect the heat transfer further downstream. Further, the use of certain cooling techniques, e.g. film cooling, will cause an interaction of the coolant with the hot gas boundary layers and thus affect engine and system performance.

The lack of knowledge in many important areas was a considerable handicap and resulted in much wasted effort. The senior author's own experience, who for several years was head of rocket engine design and development under the German pioneer worker Dr Sänger, is perhaps worth recalling in this connection. At one critical stage in the development of a high pressure oxygen-kerosine rocket engine it proved impossible to adequately cool certain areas of the nozzle. While the engineering branch needed as much as five days to produce a new rocket engine, their work was often reduced in a few seconds to unrecognisable lumps of molten metal by test stand personnel. As the two branches came under different heads there existed for some considerable time an almost permanent state of tension between the two groups. As it was the author's responsibility to provide the necessary hardware it was an act of sheer self-preservation that during the period 1943-45 a programme of research was initiated that was probably the first systematic study of various factors influencing the heat transfer in regeneratively cooled rocket engines. The results of this work had considerable influence on subsequent design studies.

Since these early days considerable progress has been made in the field of heat transfer, and cooling and protection of rocket engines as evidenced by the successful launchings of space vehicles in the USA and the USSR. The high degree of reliability could not have been achieved by mere trial and error processes but was due to the thorough and detailed work of numerous scientists and engineers in many countries. There is no doubt that the

most important contributions to this field of knowledge were made by workers at the Jet Propulsion Laboratory, Pasadena, who under the direction of D.R.Bartz investigated systematically numerous aspects of heat transfer in liquid propellant rocket engines and thus considerably advanced our knowledge of both gas-side and coolant-side heat transfer phenomena. The published account of work from this and other laboratories is widely dispersed and may be found in the internal reports of various research organisations, in various journals, proceedings of symposia and other sources and it is very difficult and time-consuming for the non-specialist to acquaint himself adequately with the nature and the technical solutions of such an important aspect of rocket engine design.

Although no doubt better and more elegant solutions to problems relating to the thermal protection of rocket engines will be found it must be agreed that the period of rapid advancement in this field has come to an end. It seemed therefore an appropriate point in time to make an attempt to reflect and sum up the present state of the art.

In writing this book the authors intended to provide the designer of rocket engines with a basic understanding of the various heat transfer processes within a rocket engine and the cooling methods that are available. Emphasis was placed on methods and procedures for calculating the magnitude of heat transfer so that the usefulness of various designs can readily be assessed rather than on providing the most modern and rigorous theories – particularly in the field of developing boundary layers. While one safely may assume the presence of electronic computers at everybody's elbow, there remains also a continuing demand for simple, if only approximate pictures of the way the various factors interact.

In the first part of this book the various basic heat transfer processes are considered – simple convective heat transfer from hot gases to the engine walls under various conditions, radiation heat transfer, and coolant heat transfer processes. This part is followed by one describing the various methods of cooling used in liquid propellant rocket engines, such as regenerative, film, ablation and radiation cooling. The final part concerns the properties of materials that will have to be known by the engine designer, from the transport properties of the hot combustion gases, through the properties of some coolants to those of the materials from which the engine will be constructed.

The methods of cooling and of predicting heat transfer are not complete. In particular the factors influencing the heat transfer to the propellant injector are insufficiently understood and it is agreed that the only sure method of showing accurate heat transfer predictions and a satisfactory design in the end is to actually fire the engine. However, it is hoped that through the methods presented it will be possible to design rocket engines in which the number of development firings to solve heat transfer problems is kept to a minimum, ideally one.

For the most part this book is concerned with liquid propellant rocket engines. Many of the problems, but not all of the solutions, are equally applicable to solid propellant motors. These have, however, not been given special attention and the reader may therefore assume that wherever the context is not explicit the authors had liquid propellant rocket engines in mind.

CHAPTER 2

TURBULENT BOUNDARY LAYER FLOWS

2.1 GENERAL

The principal process by which heat is transferred to the walls of a rocket engine from the hot combustion gases is by convection. Heat is conducted out of the layer of hot gases immediately adjacent to the wall, and a little further from the wall turbulent processes will transport hot gas from the main stream in to mix with the outer part of this region cooled by conduction to the wall. Heat transfer rates will then be controlled by the fluid-dynamic phenomena occurring within this boundary layer.

Successive attempts at the prediction of heat transfer in rocket engines have resulted in a series of theories of increasing mathematical complexity. Factors of especial importance in rocket engines are the varying free stream velocity, the large temperature differences between the free stream and the wall, and the effects of varying free stream and wall temperatures. Account must be taken of the developing combustion within the initial part of the engine, the high accelerations given to the gas in the nozzle, compressibility effects and the effects of chemical non-equilibrium in the flow.

This chapter will present the basic theory of a turbulent boundary layer in a compressible flow. Following chapters will then identify and describe the main phenomena associated with particular areas of the engine, developing this basic theory to a point where the heat transfer rate to each part of a rocket engine can be reliably calculated.

2.2 NON-DIMENSIONAL CORRELATIONS

A most convenient way of representing the heat transfer in a rocket engine is by the Stanton number (St) – the ratio of the heat transfer rate ($\ddot{q}$) perpendicular to the wall to the available heat flux ($\rho U \Delta H$) carried along in the gas stream parallel to the wall. The enthalpy difference (ΔH) is that between the gas at the free stream condition and the gas at the temperature of the wall. The basic heat transfer equation is thus:

$$\ddot{q} = St\, \rho U \Delta H \,. \tag{2.1}$$

Typically, in rocket engines, the Stanton number is about 0.002.

Various simple heat transfer correlations have been proposed relating the Stanton number to other non-dimensional characteristics of the flow – in particular the Reynolds number (Re) and the Prandtl number (Pr). The Reynolds number is a measure of the viscous effects close to the wall, and the Prandtl number the ratio of the thermal and momentum diffusivities. For fully developed turbulent flow in a circular pipe, for instance, the correlation is

$$St = 0.023\, Re_D^{-1/5} Pr^{-2/3} \,, \tag{2.2}$$

the Reynolds number in this case being based on the pipe diameter.

Early workers attempted to correlate rocket engine heat transfer data by using variants of this equation. Unfortunately, full "pipe flow" generally does not develop until approximately twenty pipe diameters from the entrance – greater than the total length of a rocket engine. In practice, such an approach gives little improvement on the assumption of an arbitrary, constant Stanton number.

However, Equation (2.2) basically states, for fully developed pipe flow, a relationship characterised by Re_D between the heat transfer and viscous forces acting on the flow. The general statement of this relationship between heat and momentum transfer is known as *Reynolds analogy*.

$$\frac{\ddot{q}}{\rho c_p dT/dy} = \frac{\tau}{\rho du/dy} \,.$$

In this form the relationship is only strictly true for a Prandtl number of unity. Colburn[1] has provided a more general relationship for incompressible flow as

$$St = \tfrac{1}{2} C_f Pr^{-2/3} \tag{2.3}$$

where C_f is the skin-friction coefficient.

This analogy suggests the possibility of using other skin-friction formulae to correlate heat transfer data. In particular, since it is apparent that the boundary layer in a rocket engine is developing, a better correlation might be obtained by using a Reynolds number Re_x based on the increasing axial distance down the bounding wall.

$$\boxed{St = B\, Re_x^{-b}\, Pr^{-2/3}} \tag{2.4}$$

The choice of the index b in this equation is not, however, arbitrary. Any particular choice implies a particular form of the development of the momentum boundary layer, and a particular velocity distribution close to the wall.

2.3 FLAT PLATE BOUNDARY LAYERS

A simple formula for the skin-friction on a flat plate can be obtained by assuming that the velocity in the boundary layer varies according to some power law with the distance away from the wall. The skin-friction can then be calculated from the momentum integral equation

$$\frac{d\delta_2}{dx} + \frac{1}{u_s}\frac{du_s}{dx}\,\delta_2(H_{12} + 2) = \frac{\tau_w}{\rho u_s^2}. \tag{2.5}$$

This equation is of fundamental importance in the dynamics of boundary layers. The two characteristic quantities of the boundary layer are the displacement thickness

$$\delta_1 = \int_0^\infty \left(1 - \frac{u}{u_s}\right) dy$$

and the momentum thickness

$$\delta_2 = \int_0^\infty \frac{u}{u_s}\left(1 - \frac{u}{u_s}\right) dy .$$

The shape factor is defined as

$$H_{12} = \delta_1/\delta_2 ,$$

and τ_w is the shear stress at the wall, u_s the velocity of the free stream.

The "universal" velocity profile of a boundary layer in a constant velocity stream has been found to be defined by two non-dimensional quantities, one a velocity (u^+), the other a distance from the wall (y^+):

$$u^+ = \frac{u}{u_\tau}$$

and

$$y^+ = \frac{y u_\tau}{\nu},$$

where

$$u_\tau = \left(\frac{\tau_w}{\rho}\right)^{1/2}$$

and is known as the "friction velocity". The actual shape of this "universal" boundary layer profile (see Figure 2.1) is complex – showing as distinct regions a laminar sub-layer $(y^+ < 8)$, where transport is effected by molecular processes only, and a turbulent wake region $(y^+ > 30)$ in which turbulent mixing controls the various transport processes. In between these two regions there is a "buffer" regime where molecular diffusion processes are gradually replaced by turbulent mixing.

A simple assumption, quite adequate for many purposes, is that this universal profile can be approximated by a power-law of the form

$$u^+ = C_1 (y^+)^{1/n} , \tag{2.6}$$

from which it follows that

$$\frac{u_s}{u_\tau} = C_1 \left(\frac{u_\tau \delta}{\nu} \right)^{1/n} = C_1 \left(\frac{u_s \delta}{\nu} \right)^{1/(n+1)} ,$$

where δ is the distance of the assumed "edge" of the boundary layer from the bounding surface in Equation (2.6).

With zero pressure gradient, the momentum integral Equation (2.5) becomes simply

$$\frac{d\delta_2}{dx} = \frac{\tau_w}{\rho u_s^2} = \frac{u_\tau^2}{u_s^2} \tag{2.7}$$

and with the present assumptions it also follows that

$$\frac{\delta_2}{\delta} = \frac{n}{(1+n)(2+n)} .$$

Substituting for δ_2 and u_s/u_τ in Equation (2.7) an equation in δ is obtained

$$\frac{n}{(1+n)(2+n)} \frac{d\delta}{dx} = C_1^{-2n/(n+1)} \left[\frac{u_s \delta}{\nu} \right]^{-2/(n+1)} . \tag{2.8}$$

With the boundary conditions $\delta = 0$ for $x = 0$, this can be integrated to give

$$\frac{\delta}{x} = C_2 \, Re_x^{-2/(n+3)}$$

where

$$C_2 = \left[\frac{(2+n)(n+3)}{n} C_1^{-2n/(n+1)} \right]^{(n+1)/(n+3)}$$

It follows that the local skin-friction coefficient is

$$\boxed{C_f = \frac{2\tau_w}{\rho u_s^2} = C_3 \, Re_x^{-2/(n+3)}} , \tag{2.9}$$

where

$$C_3 = C_2 \frac{2n}{(2+n)(n+3)} .$$

Experimental measurements have established that, in the range $5 \times 10^5 < Re_x < 10^7$, good agreement is obtained by the equation

$$C_f = 0.0592 \, Re_x^{-1/5} ,$$

indicating a value for n of 7.

In these equations, the index n is a measure of the "shape" of the boundary layer. The constants derived from C_1, less obviously, provide a measure of the growth rate of the boundary layer, and thus depend on the way in which gas is entrained into the boundary layer from the free stream. This is illustrated by Equation (2.8), in which the growth rate of the boundary layer depends directly on C_1, together with a weak function of the

Reynolds number of the boundary layer thickness.

Equation (2.6) may be rewritten in terms of the skin-friction coefficient and the distance from the wall. At the outer edge of the boundary layer,

$$Re_\delta^{-1} = C_1^{-n}\left(\frac{C_f}{2}\right)^{(n+1)/2} . \qquad (2.10)$$

The constant C_1 then also defines a relationship between the surface skin-friction and the boundary layer thickness. The assumption of "similarity" in the boundary layer will contain equally that the values of C_1 and n remain constant. This will be important later when cases will be considered in which the value of this constant differs from its value for the equilibrium flat plate boundary layer, and where a redistribution of shear stress in the boundary layer must take place.

By assuming other mathematical laws for the shape of the boundary layer it is possible to obtain further, potentially more exact relations for the skin-friction coefficient on a flat plate. A number of such formulae have used the von Kármán logarithmic law[2] for the velocity profile. The Schultz-Grunow equation, for example, is

$$C_f = \frac{0.370}{(\log_{10} Re_x)^{2.584}} . \qquad (2.11)$$

For the Reynolds number range with which we shall normally be concerned in rocket engines, the difference between these alternative forms is small (see Figure 2.2), and can safely be ignored.

However, before such simple theories can be applied to rocket engines, it is necessary to extend this "flat plate" solution to take account of the compressibility of the flow, and the large temperature variations across the boundary layer. This is the subject of the next section.

2.4 COMPRESSIBLE BOUNDARY LAYERS

The flat plate boundary layer may be seen as a limiting condition of compressible boundary layer theories. A wide variety of approaches to this more general problem exist, but in seeking a solution suitable for application to rocket engines one not only seeks a correlation of existing data to a satisfactory degree of accuracy, but also a theory of sufficient simplicity to give insights into the boundary layer phenomena, and capable of use as *part* of an overall design problem.

A useful approximation is to assume that the boundary layer at each point along the wall develops as if it were part of an equivalent boundary layer on a flat plate, and then to find the overall solution accounting for changing mass-flux, temperature, etc, by a process of integration. The general theory of solutions of this kind was developed by Ambrok[3]. Different assumptions about the effects of changing gas properties and conditions will provide different solutions of greater or less relevance to a particular problem. For rocket engines, the theory of Mayer[4] will be adopted.

The thermal boundary layer thickness, δ_θ, on a surface is given by

$$\delta_\theta = \frac{\int_0^\infty \rho u \Delta H \, dy}{\rho_s u_s \Delta H_s} , \qquad (2.12)$$

where ρ, u and ΔH are the density, velocity and enthalpy difference respectively. The heat flux, $\ddot{q}$, at a distance x from the leading edge is therefore

$$\ddot{q} = \frac{d}{dx}(\rho_s u_s \delta_\theta)\, \Delta H_s \qquad (2.13)$$

for a flat-plate, or for axi-symmetric flow with r as the temperature recovery factor

$$r\ddot{q} = \frac{d}{dx}(\rho_s u_s r \delta_\theta)\, \Delta H_s . \qquad (2.14)$$

Because, from the definition of the Stanton number (St),

$$r\dot{q} = St\, \rho_s u_s \Delta H_s\, r ,$$

it follows that

$$\frac{d\delta_\theta}{dx} + \frac{\delta_\theta}{\rho_s u_s \Delta H_s r} \frac{d}{dx} (\rho_s u_s \Delta H_s r) = St . \tag{2.15}$$

If a Reynolds number based on the thermal boundary layer thickness is now defined as

$$Re_\theta = \frac{\rho_s u_s \delta_\theta}{\mu_s}$$

and it is noted that for an isothermal flat-plate with zero pressure gradient, ρ, u and ΔH are independent of x, it follows from Equation (2.15) and Equation (2.4) that

$$St = \frac{d\delta_\theta}{dx} = B\, Re_x^{-b}\, Pr^{-m} . \tag{2.16}$$

Thus

$$\delta_\theta = \int_0^x B\, Re_x^{-b}\, Pr^{-m}\, dx$$

and hence

$$Re_\theta = \frac{B\, Pr^{-m}}{1-b}\, Re_x^{1-b} .$$

Substituting for Re_x in Equation (2.16) one obtains

$$St = B^{1/(1-b)} \left(\frac{1-b}{Pr^{-m}} Re_\theta \right)^{-b/(1-b)} Pr^{-m} . \tag{2.17}$$

This equation describes the dependence of the heat transfer rate on Re_θ for a flat plate in the absence of a pressure gradient. It will now be assumed that this relation is also valid for axi-symmetric flow with variation of the pressure gradient and the wall temperature. This is the fundamental assumption made by Ambrok[3].

Substituting Equation (2.17) into Equation (2.15) yields

$$\frac{d\delta_\theta}{dx} + \frac{\delta_\theta}{\rho_s u_s r} \frac{d}{dx} (\rho_s u_s r) = B^{1/(1-b)} \left(\frac{1-b}{Pr^{-m}} Re_\theta \right)^{-b/(1-b)} Pr^{-m} . \tag{2.18}$$

The integral of this equation is*

$$\rho_s u_s r = \frac{B}{1-b} \left[\int_0^x (\rho_s u_s) r^{1/(1-b)}\, \mu^{b/(1-b)}\, Pr^{-m/(1-b)}\, dx \right]^{1-b}$$

---

*To integrate Equation (2.18), we may write it in simple form as

$$\frac{d\delta_\theta}{dx} + \frac{\delta_\theta}{R} \frac{dR}{dx} = \delta_\theta^{-b/(1-b)} F ,$$

where R, F and δ_θ are functions of x. Re-arranging, this becomes

$$(R\delta_\theta)^{b/(1-b)} \frac{d}{dx} (R\delta_\theta) = R^{1/(1-b)} F ,$$

whence

$$(1-b)\, (R\delta_\theta)^{1/(1-b)} = \int_0^x R^{1/(1-b)} F\, dx .$$

Equation (2.15) now gives the Stanton number

$$St = \frac{B\, r^{b/(1-b)}\, \mu^{1/(1-b)}\, Pr^{-m/(1-b)}}{\left[\int_0^x \left(\frac{\rho_s u_s}{\mu}\right) r^{1/1-b)}\, \mu^{1/(1-b)}\, Pr^{1/(1-b)} dx\right]^b} . \tag{2.19}$$

This leaves only the property variation through the boundary layer to be taken into account. For compressible flows, Eckert[5] has provided a "reference" temperature for the boundary layer at which the various gas transport properties should be evaluated. This point will be discussed in more detail in Section 3.6. For the moment it is sufficient to know that it is a mixture of the "adiabatic recovery" stagnation temperature (T_{ad}), the free-stream static temperature (T_s), and the temperature of the wall (T_w).

$$\boxed{T_{ref} = 0.50\, T_w + 0.28\, T_s + 0.22\, T_{ad} .} \tag{2.20}$$

In most practical cases it may be assumed that the density of the gas in the boundary layer varies according to the ideal gas law

$$\rho \sim T^{-1} \tag{2.21}$$

and that the viscosity varies according to a simple exponential law

$$\mu \sim T^{\omega} \tag{2.22}$$

where ω is an exponent characteristic of the particular gas mixture, and has a typical value of 0.7. The Prandtl number and the specific heat of the gas have a relatively weak temperature dependence, and for the moment can be taken as constant at the reference temperature.

According to this method, the ratio of the modified Stanton number to that for a flat-plate with uniform free stream conditions can be calculated from

$$\frac{St}{St_0} = \left(\frac{\mu_s}{\mu_{ref}}\right)^{-b} \left(\frac{\rho_{ref}}{\rho_s}\right)^{1-b} = \beta .$$

It follows from Equations (2.21) and (2.22) that the ratio β is a function of the ratio between the static and the reference temperature,

$$\beta = \left(\frac{T_s}{T_{ref}}\right)^{1 - b(1+\omega)} . \tag{2.23}$$

Substituting reference properties into Equation (2.19), and making the appropriate re-arrangements, yields the result given by Mayer[4]

$$\boxed{St = \frac{B\, r^{b/(1-b)}\, Pr_{ref}^{-m}\, \beta^{1/(1-b)}}{\left[\int_0^x (\beta r)^{1/(1-b)} \left(\frac{\rho u}{\mu}\right)_s dx\right]^b} .} \tag{2.24}$$

As has been indicated in Section 2.2, the two constants B and b are functions of the processes occurring within the boundary layer, and may be derived from the basic friction laws of Blasius for a flat plate. Values for the constants in both laminar and turbulent flows are given in Table 2.I.

Because the original flat plate "law" is only approximate, the values of these constants will change slowly with the local Reynolds number, but this variation is not sufficient to concern most calculations in rocket engines.

2.5 CONCLUSION

The development of prediction methods for turbulent boundary layers continues apace. Much of this effort is directed towards obtaining solutions of general applicability to a wide range of conditions, and is not immediately suitable for rocket engine design purposes.

In the somewhat more restricted conditions in rocket engines, Equation (2.24) provides a useful starting point for making heat transfer predictions. Modifications will be required to allow for the acceleration forces existing in the nozzle, and for the chemical reactions taking place within the boundary layer, but with these provisions the theory presented in Section 2.4 has been found to correlate available data to the accuracy expected from the experiments.

The specific effects on the heat transfer to be found in the rocket nozzle and the combustion chamber will be dealt with in the next two chapters.

REFERENCES

1. Colburn, A.P. — *A method of correlating forced convection heat transfer data and a comparison with fluid friction.* Trans. A.I.Ch.E., Vol. 29, 1933, pp.174-210.

2. von Kármán, Th. — *The analogy between fluid friction and heat transfer.* Trans. ASME, Vol. 61, 1939, pp.705-710.

3. Ambrok, G.S. — *Approximate solution of equations for the thermal boundary layer with variations in boundary layer structure.* Sov. Phys: Tech. Phys., Vol. 2, 1957, pp.1979-1986.

4. Mayer, E. — *Analysis of convective heat transfer in rocket nozzles.* ARS Journal, Vol. 31, 1961, pp.911-916.

5. Eckert, E.R.G. — *Survey on heat transfer at high speeds.* WADC Tech. Rept. 54-70, 1954.

TABLE 2.I

Flow in boundary layer	B	b	m
laminar	0.332	0.5	0.67
turbulent	0.0296	0.2	0.67

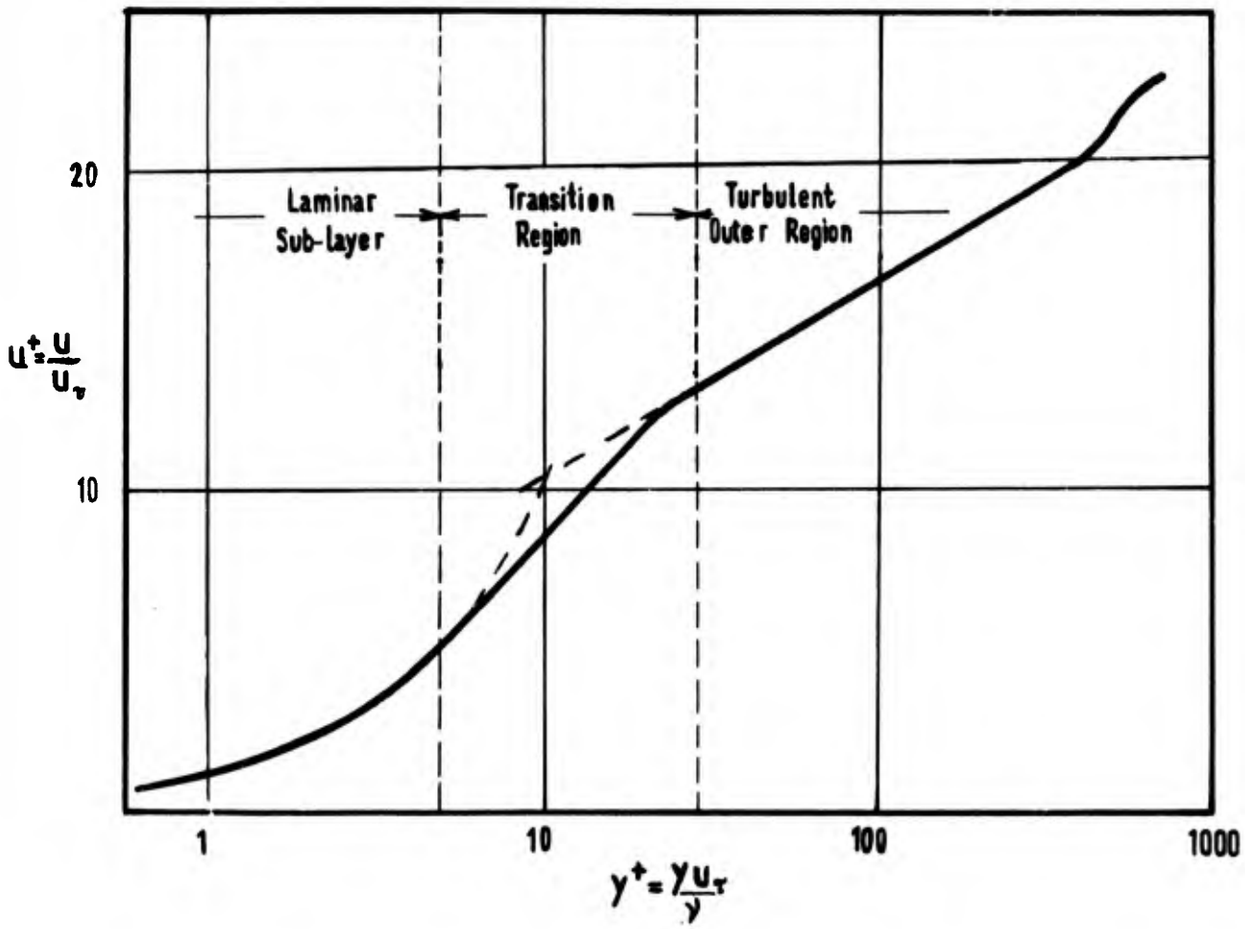

Fig.2.1 "Universal" velocity profile of a turbulent boundary layer

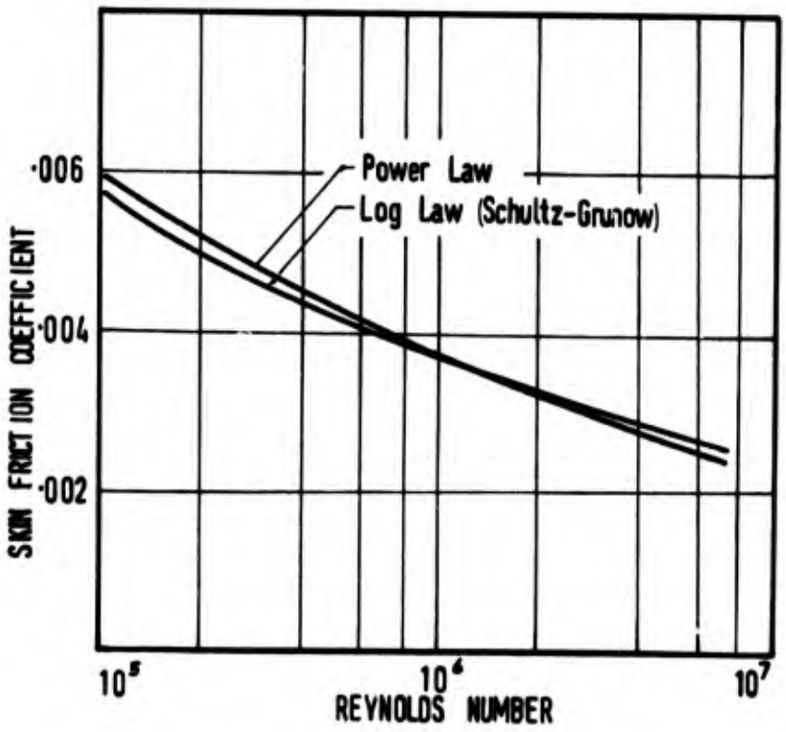

Fig.2.2 Comparison of power-law and log-law skin-friction correlations

CHAPTER 3

HEAT TRANSFER TO THE NOZZLE

3.1 GENERAL

In the convergent-divergent nozzle of a rocket engine thermal energy released by combustion is converted into kinetic energy. At the nozzle throat the flow becomes sonic, and the convective heat transfer rate is a maximum. Downstream, the flow is supersonic, and compressibility assumptions play an increasingly important part in the heat transfer process.

In addition, the accelerations imposed on the gas in the nozzle are extremely high (typically 10^7 m/sec^2 – one million "g"!), and can cause distortions of the boundary layer shape, forcing a reversion towards laminar flow. An adequate theory for the heat transfer in the nozzle will therefore also have to provide a description of such laminarization processes.

This chapter will deal with the phenomenon of boundary layer laminarization, and the effects of supersonic flow in the nozzle.

3.2 LAMINARIZATION

The assumed velocity profile of a turbulent boundary layer is an equilibrium condition, achieved on a flat plate in the absence of disturbing pressure gradients. It is known that if a sufficiently strong accelerating force is applied to the flow, the turbulent boundary layer structure at the wall can be suppressed, and a partial or complete reversion to a laminar boundary layer obtained. As has already been pointed out in Chapter 2, the structure of the boundary layer is important in determining the heat transfer rate. If laminarization occurs, there will be a reduction in the heat transfer rate.

Launder[1] has given a very simple method of calculating the approximate point at which the pressure gradient accelerating the flow begins to affect the boundary layer shape by comparing the pressure gradient forces with the shear forces in the boundary layer. Laminarization effects will become important when these two forces become comparable, i.e. when

$$-\frac{dp}{dx}\,y \sim \tau_w .$$

Now the outer, "logarithmic" region of the boundary layer velocity profile in which turbulence exists only applies for $y^+ > 30$ (Section 2.3). If the acceleration is such that $-(dp/dx)y \sim \tau_w$ for $y^+ = 30$ or less, then departure from the established boundary layer shape can be expected to take place. Translating this condition into the parameters of the flow, it follows that the turbulent boundary layer shape will suffer distortion approximately as

$$\boxed{\frac{\mu}{\rho u^2}\,\frac{du}{dx}\left(\frac{C_f}{2}\right)^{-3/2} \sim 10^{-2} .} \qquad (3.1)$$

For a typical value of the skin friction coefficient (e.g. $C_f = 0.004$), an approximate value for the onset of laminarization, confirmed by experiment, is obtained

$$K \equiv \frac{\mu}{\rho u^2}\,\frac{du}{dx} \simeq 10^{-6} . \qquad (3.2)$$

This parameter K, which is non-dimensional, and behaves in some respects as an inverse Reynolds number, shall be referred to as the *acceleration number*. As might be expected, no sudden reversal to laminar flow conditions occurs at $K = 10^{-6}$. Instead, there is a progressive change in the boundary layer shape from turbulent to laminar as the acceleration number increases to about 4×10^{-6}.

A fundamental understanding of the laminarization process must be based upon knowledge of the detailed turbulence structure of the boundary layer. It is known that turbulence is generated deep within the boundary layer, apparently in those layers just above the laminar sub-layer. Kline[2] has described experiments which indicate that turbulence originates from the break-up of longitudinal, sinuous, momentum-deficient "streaks" existing within the laminar sub-layer and diffusing outward from the wall. Because turbulence is generated *within* the boundary layer, its rate of development is little affected by disturbances in the free stream.

Under accelerating conditions, Kline found that the "burst frequency" of break-up of these momentum deficient streaks in the laminar sub-layer decreased with increasing values of the acceleration number, vanishing altogether at $K > 4.5 \times 10^{-6}$. This is in agreement with the experiments on the change-over from turbulent to laminar boundary layer flow.

3.3 HEAT TRANSFER WITH LAMINARIZATION

Comparing the values of the acceleration number and the ratio of the experimental heat transfer to that expected with a turbulent boundary layer (Fig.3.1), it will be observed that the heat transfer falls progressively below that for simple turbulent flow as long as the acceleration number is above a certain value (here marked as 2.4×10^{-6}). No sudden change in the Stanton number occurs, but the rate of development becomes more appropriate to a value of b (Equation (2.24)) of 0.5, rather than the turbulent value of 0.2.

With a range of experiments providing different values of K , it is possible to find a corresponding series of values for b accounting for the experimental variation in the heat transfer (Fig.3.2). Below $K \simeq 10^{-6}$, the boundary layer remains essentially turbulent. Above $K = 3.4 \times 10^{-6}$ the boundary layer has become laminar. And in between there is a progressive change in the boundary layer shape.

Because there is no discontinuity in the Stanton number curve at any point in the laminarization process, while it is possible to substitute values for b into Equation (2.24) corresponding to the local value of K , the value of the constant B must be recalculated with each change. It is generally more convenient to assume a series of step changes in the shape index b during laminarization, and then to use

$$B_2 = B_1 \left[\frac{\beta_1^{1/(1-b_1)} I_2^{b_2}}{\beta_2^{1/(1-b_2)} I_1^{b_1}} \right] r^{(b_1-b_2)/\{(1-b_1)(1-b_2)\}} , \qquad (3.3)$$

where

$$I = \int_0^x (\beta y)^{1/(1-b)} \, d(Re_x)$$

and

$$\beta = \left(\frac{T_s}{T_{ref}} \right)^{1-(1+b)\omega}$$

Similarly, when the acceleration parameter falls again, there is a continuous transition back to a turbulent boundary layer, and the constant B will assume a value somewhat below the familiar value of 0.0296 characteristic of a turbulent boundary layer. Values for a "stepped" boundary layer shape change are recommended in Table 3.I.

Because, after a period of laminarization, the constant B does not return to its original value, a situation obtains in which the boundary layer thickness is greater than would be expected from the surface skin friction (see Equation (2.10)). The equilibrium shape appears to have been regained, but the boundary layer is not yet in complete equilibrium. As a consequence, it might be expected that the renewed turbulence will tend to reduce the boundary layer thickness, shifting the value of the constant B back towards its equilibrium value.

This is observed. While there is insufficient experimental information to allow an accurate description of the processes involved, for the small nozzle illustrated in Figure 3.1 an approximate variation with position was found as

$$B = B_0(1 + 0.105\, x) , \qquad (3.4)$$

where x is the distance downstream of the re-transition point in centimetres. This continues until the constant has recovered its equilibrium value.

Simple calculations indicate that the boundary layer does not stop growing until the skin friction coefficient has, as it were, "caught up". Instead, the rate of entrainment of free stream gas is slightly reduced until the shear forces in the boundary layer have achieved full equilibrium.

There is a similar slow drift towards fully laminar heat transfer at extreme accelerations ($K > 5.0 \times 10^{-6}$). The rate of drift in this case is much smaller, as might be expected due to the laminar nature of the flow.

$$B = B_0(1 - 0.02\,x)\,, \tag{3.5}$$

x once more being measured in centimetres. In this case the effect is to *increase* the thickness of the boundary layer, and so reduce the value of the constant b .

3.4 SUPERSONIC HEAT TRANSFER

In addition to the process of laminarization reducing the heat transfer in the nozzle, a sharp drop in the heat transfer has been found when the flow becomes supersonic. Evidence from nozzles with different throat curvatures has shown that this fall in the heat transfer occurs just upstream of the geometric throat, at a point at which the Mach number close to the wall will just be unity (see Figure 3.3).

The reduction in heat transfer may be described by a reduction in the constant B (Equation (2.24)) to 0.0203. Thus, if the boundary layer is recovering from a period of laminarization – so that the constant is still below its "preferred" value of 0.0296 – the reduction taking place will still be to B = 0.0203 , and not simply by 30%. Indeed, if severe laminarization has taken place, the constant B may continue to *increase*, but now towards the lower value of B .

The phenomena underlying this effect are not understood. The reduction in heat transfer appears specific to turbulent boundary layers, and is generally evident in rocket engine heat transfer experiments.

It is possible that the effect is caused by changes in the mechanism whereby turbulent energy is dissipated in the upper levels of the boundary layer. In supersonic flow, the turbulent disturbances can only affect fluid downstream, and so the possibilities for energy dissipation are reduced. The redistribution of shear stress within the boundary layer will then cause an increase in the thickness of the laminar sub-layer. Lobb, Winkler and Persh[4], measuring the profiles of supersonic boundary layers, have found that under these circumstances the outer edge of the laminar sub-layer appears to be at a value of $y^+ \simeq 14$, rather than the more usual value of 10.5.

Because this reduction in heat transfer occurs when the free stream flow becomes supersonic, the maximum rate of heat transfer will occur just upstream of the geometric throat in most nozzles.

3.5 SUPERSONIC SEPARATION

In measurements of the wall static pressure in a nozzle of high throat curvature ($r_c/r_* = 0.63$), Back, Massier and Cuffel[5] found a pressure *rise* immediately downstream of the throat section. The radial accelerations imposed on the gas in this section are high, and the change in direction of the momentum of the gas flowing from the circular arc throat section into the divergent cone can lead to the formation of a weak shock in the flow just downstream of the throat. The effect of this shock will generally be very local, but it was found that, at the lowest stagnation pressures investigated, separation of the boundary layer occurred.

Flow separation was observed in those cases in which laminarization had continued past the throat of the nozzle. The laminar boundary layer is less resistant to the effects of the adverse pressure gradient. Figure 3.4 illustrates the behaviour of the heat transfer. In the separated region the heat transfer falls to about one half of its normal value. If the overall pressure ratio is sufficient to ensure re-attachment, the heat transfer will then recover to its normal turbulent layer value.

Flow separation in the nozzle will also occur near the nozzle exit if the static pressure of the flow falls below about one-third of the ambient pressure. In this region the heat transfer might be expected to behave as above. However, expansion nozzles are generally designed to avoid such separation.

3.6 HEAT TRANSFER AT HIGH MACH NUMBERS

The concept of a "reference" temperature, to take account of transport property variation in the boundary layer at high Mach numbers, has been introduced earlier (Equation (2.20)). This concept was first developed by Rubesin and Johnson[6] for laminar boundary layers, and only later was the idea extended to turbulent boundary layers.

As the flow within the nozzle accelerates, more and more thermal energy is converted into kinetic energy. In the boundary layer, the main flow is decelerated, and kinetic energy transformed back into heat, before the gases are cooled once more by heat transfer to the wall. The temperature profile under these circumstances will look something like Figure 3.5. It is now important to know just how much of the kinetic energy in the flow will be recovered in the boundary layer, and an adiabatic recovery temperature T_{ad} is used in the formulation of a reference temperature,

$$T_{ad} = \left(1 - \frac{\gamma - 1}{2} r Ma^2\right) T_s \,, \tag{3.6}$$

where r is the temperature recovery factor. T_{ad} is the temperature that the wall will assume in the absence of heat transfer. Van Driest[7] has suggested that for turbulent boundary layers

$$r \simeq Pr^{1/3} \,.$$

Few heat transfer measurements have been made in rocket nozzles at Mach numbers greater than about 2.5. At such high Mach numbers the actual rate of heat transfer is quite small, and measurement errors may be large. Nevertheless, such measurements as exist suggest that extraordinarily low recovery factors (~0.5) can exist in rocket nozzles. Typical results are shown in Figure 3.6. On the other hand, the Eckert reference temperature formulation (Equation (2.20)) has been applied successfully to a wide range of flat-plate and two-dimensional nozzle data without the appearance of such low recovery factors.

At high expansion ratios – particularly in the case of contoured nozzles – the flow may be considerably non-uniform across a given cross-section, and detailed knowledge of the flow pattern in the nozzle will be required before adequate heat transfer predictions can be made. The heat transfer rates involved will be small, but can be important in, for example, the design of radiation-cooled nozzles.

3.7 CONCLUSION

In rocket nozzles, laminarization is a phenomenon confined for the most part to smaller and lower pressure engines. It is important to take note of this fact because a number of experimental engines designed to measure heat transfer have exhibited this phenomenon, while most practical engines have not, and so a direct extrapolation of experimental results will not be valid.

Investigation of heat transfer measurements available from experiments on model nozzles using air as a working fluid (and so avoiding problems of combustion, gas radiation and the like), have shown that the theory of laminarization and supersonic heat transfer presented here is capable of correlating the results to a root mean square deviation of 14.5% up to exit Mach numbers of 2.5. This is about the scatter to be expected from experimental inaccuracies.

Further work is obviously required before the phenomena associated with the heat transfer in the supersonic flow regime are fully understood. However, there is no reason to suppose that the phenomena themselves are not general to all rocket engines.

REFERENCES

1. Launder, B.E. — *Laminarization of the Turbulent Boundary Layer by Acceleration.* M.I.T. Gas Turbine Laboratory, Report No.77, 1964.

2. Kline, S.J. — *Some Remarks on Turbulent Shear Flows.* Thermodynamics and Fluid Mechanics Convention, Liverpool, 13th – 15th April, 1966.

3. Back, L.H. et al. — *Convective Heat Transfer in a Convergent-Divergent Nozzle.* JPL Technical Report 32-415, 1963.

4. Lobb, R.K. et al. — *Experimental Investigation of Turbulent Boundary Layers in Hypersonic Flow.* J. Aero. Sci., Vol.22, 1955, p.1.

5. Back, L.H. et al. — *Flow Phenomena and Convective Heat Transfer in a Conical Supersonic Nozzle.* J. Spacecraft, Vol.4, 1967, p.1040.

6. Rubesin, M.W. Johnson, H.A. — *A Critical Review of Skin-Friction and Heat-Transfer Solutions of the Laminar Boundary Layer of a Flat Plate.* ASME Trans., Vol.71, 1949, p.383.

7. Van Driest, E.R. — *Turbulent Boundary Layer in Compressible Fluids.* J. Aero. Sci., Vol.18, 1951, p.145.

TABLE 3.1

Index b	*Value for* K *at transition*
0.3	1.0×10^{-6}
0.4	2.2×10^{-6}
0.45	2.8×10^{-6}
0.5	3.4×10^{-6}

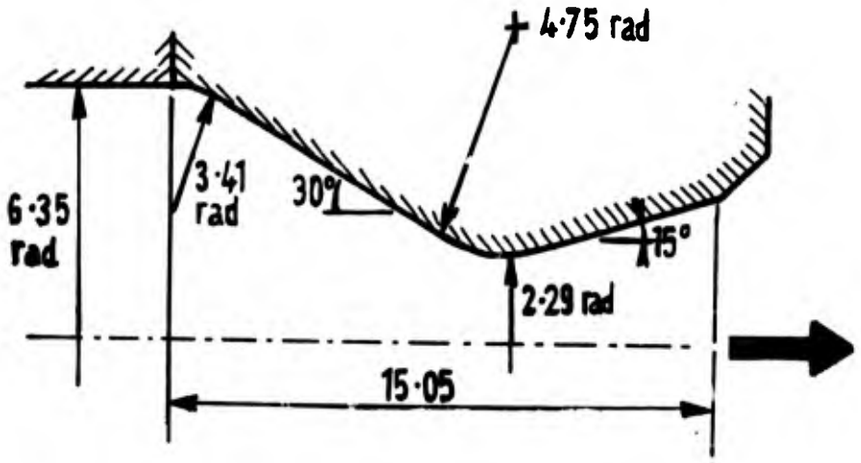

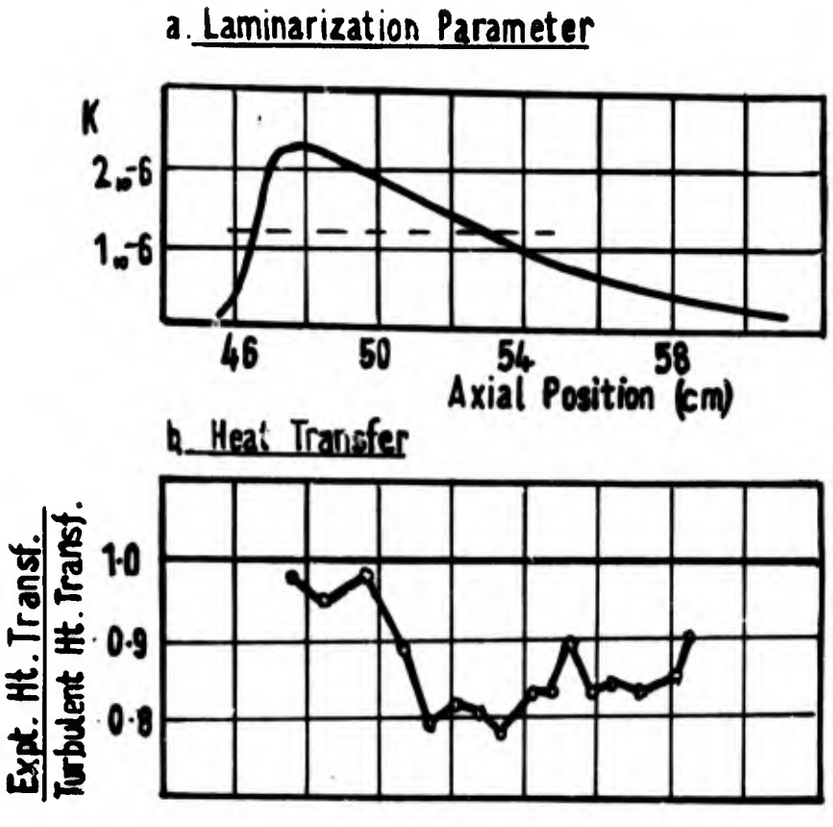

Fig.3.1 Variation of acceleration number and heat transfer in a typical nozzle.

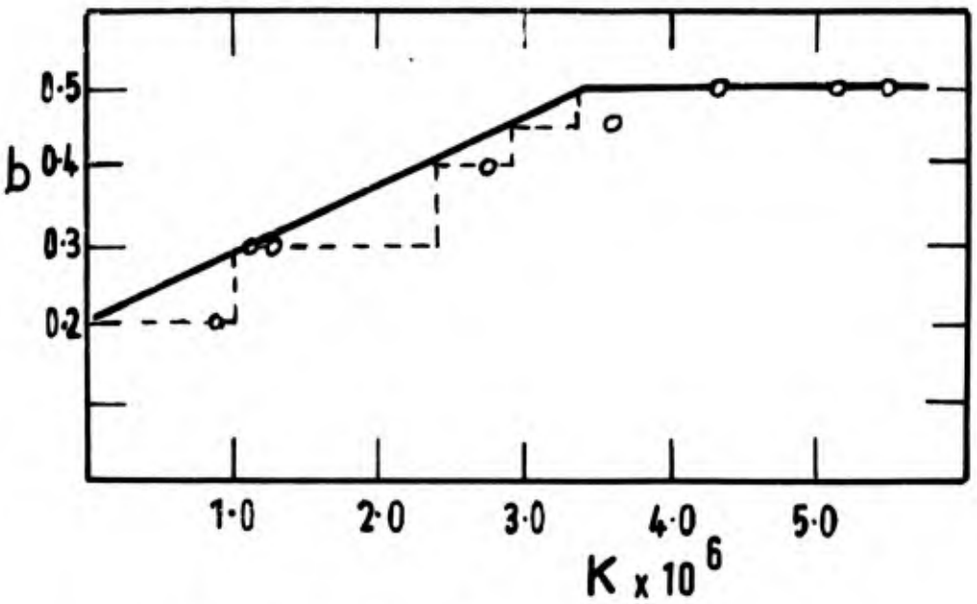

Fig.3.2 Change in boundary layer shape index in acceleration

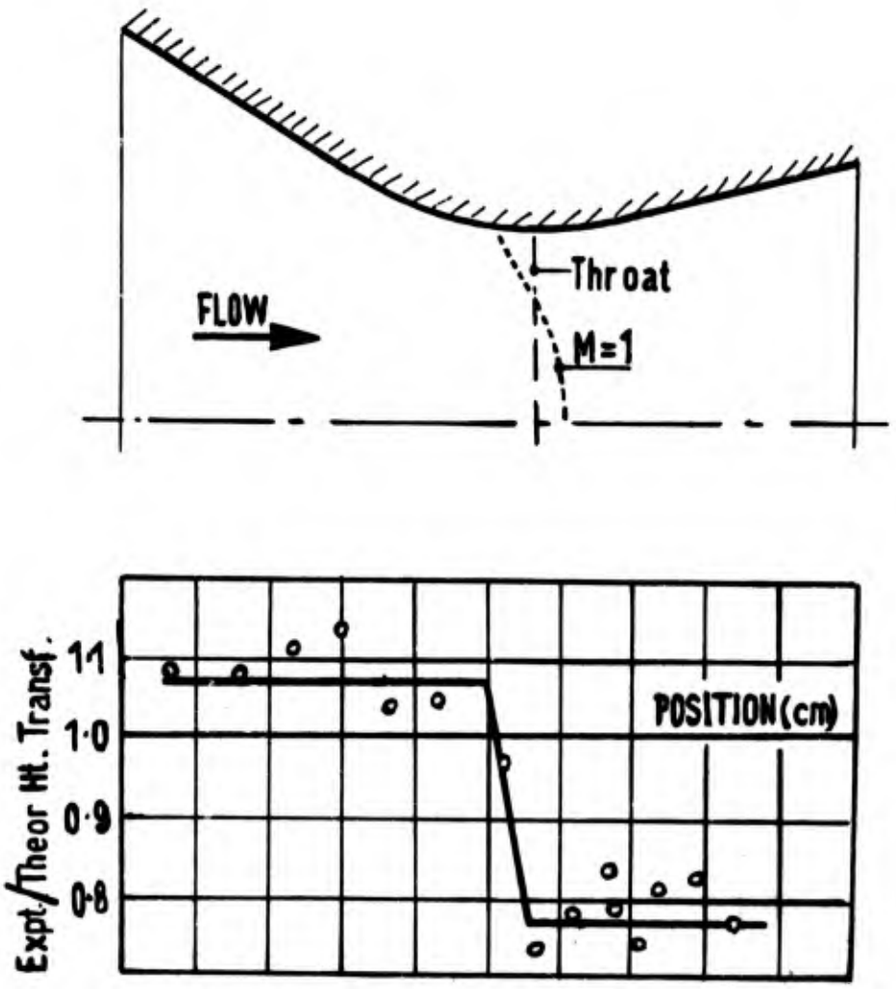

Fig.3.3 Heat transfer at a nozzle throat

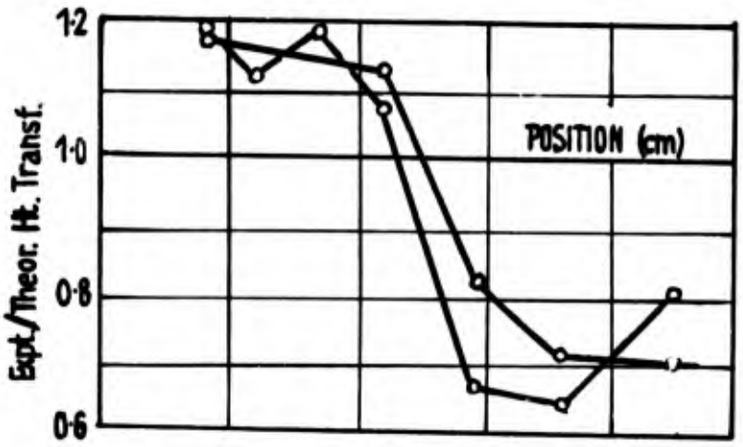

Fig.3.4 Heat transfer in a separated region

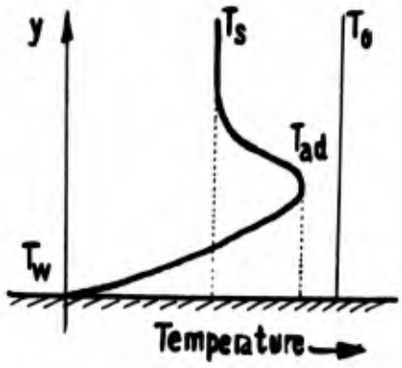

Fig.3.5 Typical temperature profile of a boundary layer at high Mach numbers

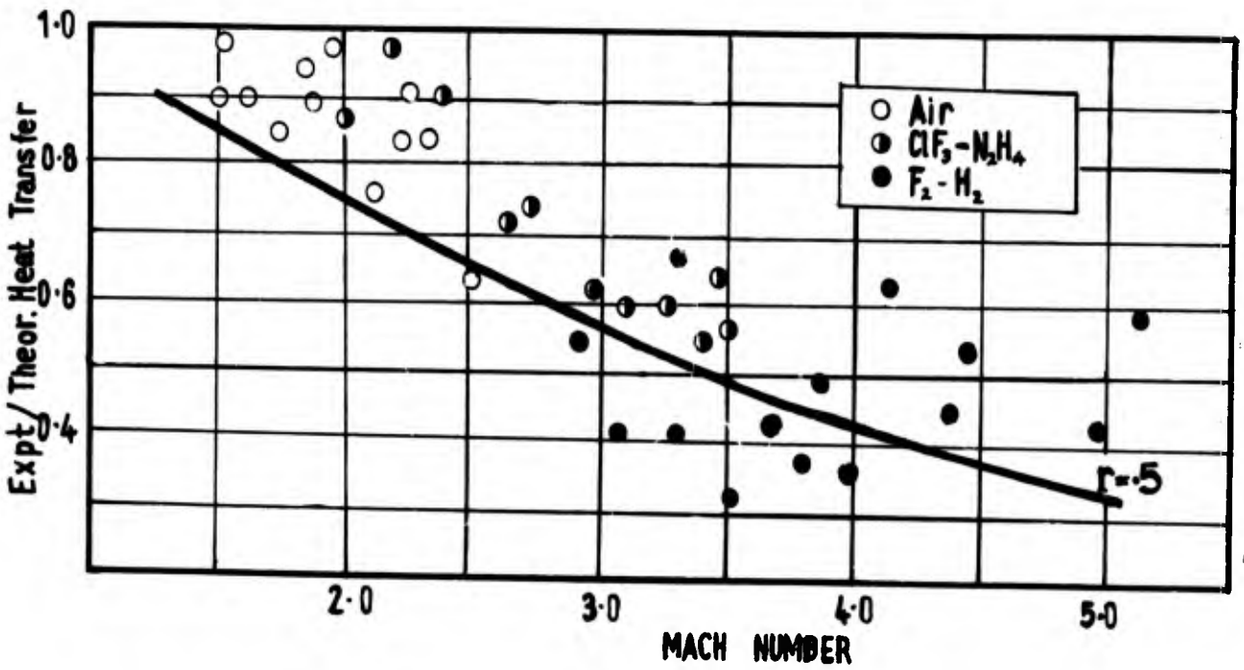

Fig.3.6 Heat transfer at high Mach numbers, showing effect of low recovery factor

CHAPTER 4

HEAT TRANSFER IN THE COMBUSTION CHAMBER

4.1 GENERAL

The heat transfer process within the combustion chamber is complicated by the fact that the main stream of gas is a reacting mixture. Combustion of the fuel and oxidant will progressively release heat as the gases travel downstream, and at the same time non-uniform mixing in the gas mixture will cause circumferential variations in the heat transfer.

Figure 4.1 shows in a schematic way the progression of the combustion processes in a rocket engine. Close to the injector there will be a region controlled by injection processes, with liquid stream break-up, fuel and oxidant impingement, and ignition processes taking place. Hypergolic propellants will ignite on contact, tending to drive apart the opposed propellant streams. Non-hypergolic propellants will ignite by hot gas recirculation and other processes. But whatever the process, shortly downstream of this region the flow will become predominantly axial, and combustion will progress first by droplet evaporation[1], and then by gas-phase mixing.

From the point of view of the heat transfer, it is gas-phase mixing processes that are of greatest importance. Maximum rates of heat transfer will occur in the later stages of the combustion process, and will be controlled by the outer layers of the flow, where gas-phase mixing is likely to predominate. For this reason a simple mixing theory will be presented first and then the distribution of heat transfer in actual rocket engine combustion chambers will be considered.

4.2 MIXING THEORY

The combustion efficiency of a rocket engine chamber is normally measured in terms of the characteristic velocity

$$c^* = \frac{p_0 A_*}{\dot{m}}$$

related to the maximum value of c^* that could be obtained at the nominal oxidant-to-fuel ratio and operating pressure of the engine. For an ideal, isentropic expansion process this is directly related to the stagnation speed of sound in the nozzle (a_0)

$$c^* = a_0 \frac{1}{\gamma}\left(\frac{\gamma+1}{2}\right)^{(\gamma+1)/2(\gamma-1)} \tag{4.1}$$

Many engines are run close to the stoichiometric oxidant-to-fuel ratio, where it is immediately apparent that variations in the mixture-ratio will cause a reduction in the overall c^*, and hence a "c^*-efficiency" (η) of less than one. This is a general result, although it may be possible to find special cases in which poor mixing leads to an increase in c^*.

For calculation purposes it may be assumed that each point in a given cross-section has an individual c^* dependent only on the local mixture ratio, so that the overall c^* achieved (ηc^*) is given by the integral of the mass-flow across the cross-section.

$$\frac{1}{\eta c^*} = \frac{1}{A}\int_A \frac{dA}{f(O/F)} \tag{4.2}$$

Here, $f(O/F)$ is the c^*-value at the local oxidant-to-fuel ratio. In general, exact integration of this equation will not be possible, but modern digital computing techniques make numerical integration across a given cross-section simple.

The range of mixture-ratio values existing across a given section of the engine will be very wide, and it is convenient to know approximate variations of c^* with O/F-ratio covering the entire range of possible mixtures. The following simple, empirical forms have been found to fit a number of propellant combinations with an acceptable accuracy.

$$\left.\begin{aligned} c^* &= D(O/F)^n + E && O/F \leqslant \text{stoichiometric} \\ c^* &= \frac{A}{(O/F) + E} + F && O/F \geqslant \text{stoichiometric} \end{aligned}\right\} \tag{4.3}$$

Values for the various constants are given in Table 4.I.

To calculate the mixture ratio at any point the injector pattern will be simulated by a series of point sources of fuel and oxidant, and mixing by "random-walk" processes. Towle and Sherwood[2] provide a convenient approximation for the turbulent diffusion of material from a continuous point source,

$$\boxed{C = \frac{W}{u}\frac{1}{4\pi\psi}e^{-r^2/4\psi}\,,} \tag{4.4}$$

where C is the concentration of the gas at a radial distance r from the axis of a source of strength W in a gas stream of velocity u. Neglecting molecular diffusion as being small compared with the turbulent diffusion, the spreading factor ψ is given to a moderate accuracy by the equation of Dryden[3],

$$\boxed{\psi = S\bar{v}t + S^2(e^{-\bar{v}t/s} - 1)\,,} \tag{4.5}$$

where t is the time after injection, S the Lagrangian scale of the turbulence, and $\bar{v}$ is the lateral root-mean-square velocity of the turbulence.

The mixture ratio at any point due to an array of oxidant holes (ox), and fuel holes (f) at various radial distances r is therefore

$$O/F = \frac{W_{ox}}{W_f}\frac{\sum_{ox} e^{-r^2/4\psi}}{\sum_{f} e^{-r^2/4\psi}} \tag{4.6}$$

(assuming that the sources of each propellant are all of the same strength).

Experimental measurements, and comparison of the mixing theory with measured values of c^*, indicate that the lateral root-mean-square velocity $\bar{v}$ remains constant as the axial velocity u increases due to continuing combustion. Thus, once a value for $\bar{v}$ has been obtained, the mixing achieved can be calculated at all points downstream. The effect is of an initially high value of turbulence, dying away asymptotically towards some low value as combustion progresses.

The value for $\bar{v}$ may be calculated from the asymptotic value for the turbulence $(Tu)_{inf}$ as the velocity in the combustion chamber approaches that of complete combustion,

$$\bar{v} = (Tu)_{inf}\, u_{inf}\,. \tag{4.7}$$

Now, if ρ_0 is the density of the fully burned gases at pressure p_0, then

$$u_{inf} = \frac{p_0 A_*}{\rho_0 A}c^*\,,$$

and since, for ideal gases,

$$a_0 = \left(\frac{\gamma p_0}{\rho_0}\right)^{1/2}\,,$$

we obtain from Equation (4.1)

$$u_{inf} = \gamma\left(\frac{2}{\gamma+1}\right)^{(\gamma+1)/(\gamma-1)} c^*\frac{A_*}{A}\,. \tag{4.8}$$

Thus,

$$\boxed{\bar{v} = \gamma\left(\frac{2}{\gamma+1}\right)^{(\gamma+1)/(\gamma-1)} (Tu)_{inf}\, c^*\frac{A_*}{A}\,.} \tag{4.9}$$

Experimental evidence from c^*-measurements, from heat transfer results, and from more direct measurements by Hersch[4] indicate that in nearly all cases $(Tu)_{inf}$ has a value of ~0.015. Equation (4.9) thus concludes that the initial turbulence velocities generated close to the injector derive their energy from the available combustion energy characterised by c^*, and $(Tu)_{inf}$ is really no more than a constant of proportionality.

With the assumption of a constant $(Tu)_{inf}$, the mixing theory can be rewritten without involving the flow velocity of gas in the combustion chamber, or the contraction area ratio of the nozzle. To do this one substitutes for the "lateral drift" term $\bar{v}t$, a term containing the local turbulence level (Tu) and a fictitious distance x',

$$x'(Tu) = \bar{v}t \tag{4.10}$$

so that

$$x' = ut = u\int_x \frac{dx}{u} .$$

From Equation (4.8), the local velocity in the combustion chamber is proportional to the achieved overall c^*-efficiency – i.e.

$$\frac{u}{u_{inf}} = \frac{(Tu)_{inf}}{(Tu)} = \eta ,$$

so that

$$x' = \eta\int\frac{dx}{\eta}$$

and

$$\boxed{\bar{v}t = (Tu)_{inf}\int_x \frac{dx}{\eta} .} \tag{4.11}$$

This value may now be substituted in Equation (4.5), and a new distribution of mixture ratio calculated across the cross-section. The Lagrangian scale of turbulence, S, has only a minor effect on the spreading factor, as can be seen by expanding Equation (4.5) as a series.

$$\psi = \frac{(\bar{v}t)^2}{2!} - \frac{(\bar{v}t)^3}{3!S} + \frac{(\bar{v}t)^4}{4!S^2} \ldots .$$

This is fortunate, because the Lagrangian scale measures the degree of auto-correlation of the turbulent velocity in a point of the fluid as it travels downstream, and hence is very difficult to measure experimentally. A recommended value, taken from the measurements of Uberoi and Corrsin[5], is 9 mm.

The assumption made in this theory that the injection points act as "point" sources, while being reasonable enough for simple, showerhead injectors, needs a little more justification for other injectors. With hypergolic propellants, injectors of the impinging jet type are in widespread use. However, with such injectors reactions between the propellant streams will tend to force the streams apart once more, so that after a brief initial reaction zone the source approximation may very well be a reasonable description. The fact that it has been found possible to predict the gross behaviour of a number of complex injector patterns by this comparatively simple simulation suggests that the essential feature of importance may well be the relative spacing of the injector element array.

4.3 AXIAL HEAT TRANSFER

In practice one finds that both c^* and heat transfer approach the "completed combustion" values following a simple asymptotic, exponential rise with distance down the chamber. Since c^* is proportional to the square root of the available energy released by combustion, the similarity of the behaviour of the two quantities is to be expected.

Good correlations of a number of experimental measurements of the heat transfer in rocket engine combustion chambers can, therefore, be achieved by assuming that the enthalpy of the gas stream at any point is

$$H = H_0(1 - e^{-(x+x_0)/L}) , \tag{4.12}$$

where H_0 is the enthalpy of the gases after combustion has been completed. The constants x_0 and L are functions of the particular injector and propellant combination. In general terms, x_0/L represents the amount of

combustion that takes place in the immediate vicinity of the injector, and $1/L$ the rate at which combustion subsequently progresses towards completion down the chamber.

It has been found that for very many cases the simple mixing theory presented in Section 4.2 will predict L, but not x_0.

The constant x_0 will be a complex function of the injection processes – involving such phenomena as liquid-phase mixing, reaction rates, droplet break-up and hot gas recirculation. Except in very simple circumstances, x_0 values must for the moment be determined empirically.

It should be noted, however, that x_0 will be *positive* in the case of hypergolic propellants and impinging jet injectors where a degree of initial mixing can take place. In the case of the "showerhead" and "coaxial jet" injectors used with oxygen-hydrogen and similar propellant combinations where there is a region close to the injector where no reaction takes place, x_0 will be *negative*.

This second case provides one example where moderately good predictions of x_0 can be made. Combs and Schuman[6] have made a study of coaxial oxygen-hydrogen injectors, showing that this initial zone without combustion is associated with the break-up of the central liquid oxygen jet. In this simple case, and also with the very similar showerhead type of injector, x_0 values correlate well with liquid oxygen hole diameter, indicating an initial combustion zone between twenty and thirty hole diameters downstream of the injector.

Table 4.II summarizes a number of experiments from which values of x_0 and L have been determined. Estimates for the rms deviation of the theory from the experimental results have been made, and the overall correlation is about 0.15 for a total of 524 experimental measurements. This is agreeably close to the experimental accuracy which might be expected from the results.

4.4 CIRCUMFERENTIAL VARIATIONS

For the moment it has been assumed that the heat transfer is uniform around the circumference of the combustion chamber at any station downstream. However, the mere fact that combustion is incomplete indicates that there must be wide variations in the mixture ratio across a given cross-section. As a consequence one must expect that there will also be variations in the heat transfer rate.

Figure 4.4 shows a not untypical distribution of heat transfer over a quadrant of a combustion chamber. This information was built up from a number of experimental firings[15]. Even though attempts have been made to reduce the fuel-rich and oxidant-rich areas to a minimum, the heat transfer about a typical cross-section still can vary by a factor of five. In addition, it is apparent that fuel or oxidant-rich streams are persisting in the vicinity of the wall throughout the chamber, even though the obtained c^*-efficiencies of the overall engine may be quite good.

In an axial direction, the heat transfer will still rise towards the theoretical "completed combustion" value as the gases progress down the chamber, as described in the previous section. In most cases, the designer will be interested in the *maximum* rate of heat transfer at any station, and this has been found to follow the sort of exponential rise given by Equation (4.12). This is useful, and will tend to make the maximum heat transfer around any circumference easier to predict than the overall distribution.

In addition, the circumferential variation in heat transfer will tend to diminish as combustion progresses. However, the accuracy with which one may hope to predict circumferential variations in the heat transfer by a simple mixing theory of the sort presented in Section 4.2 will depend far more on the accuracy with which it is possible to simulate the injector by a source pattern than with values for the degree of *overall* combustion achieved. The simpler the injector pattern, and the farther downstream the predictions are made, the more likely it is that mixing calculations will predict the local available gas enthalpies correctly.

4.5 CONCLUSION

The heat transfer distribution in the rocket engine combustion chamber is probably the most difficult single aspect of heat transfer in rocket engines to deal with. It is affected by injector patterns, propellant behaviour, droplet evaporation and mixing processes, and all the other processes that are lumped together under the single heading "combustion".

It is encouraging, therefore, that a simple mixing theory of the sort presented in Section 4.2 should be so successful in giving overall rates at which combustion progresses down the chamber. For many systems, the only important unknown remaining is the amount of initial mixing and combustion that occurs immediately after injection – characterized by the constant x_0 in Equation (4.12).

The mixing theory reduces to a series of numerical integrations quite suited to modern computing techniques. The important equations are (4.2), (4.4), (4.5) and (4.11), which form an "iterative loop". For the axial progress of combustion, the important parameter in simulating a given injector appears to be the spacing of the injector elements. Increasing interest in the circumferential variation of the heat transfer pattern will demand more accuracy in the source pattern chosen.

One more important factor in the basic convective heat transfer processes occurring in rocket engines remains to be discussed – the effects of chemical non-equilibrium in the boundary layer. This is the subject of the next chapter.

REFERENCES

1. Priem, R.J. Heidman, M.F. — *Propellant Vaporization as a Design Criterion for Rocket-Engine Combustion Chambers.* NASA TR R-67, 1960.
2. Towle, W.L. Sherwood, T.K. — *Mass Transfer in the Central Portion of a Turbulent Air Stream.* Ind. Eng. Chem., Vol.31, 1939, p.457.
3. Dryden, H.L. — *A Review of the Statistical Theory of Turbulence.* Quart. Appl. Math., Vol.1, 1943, p.7.
4. Hersch, M. — *Experimental Method of Measuring Intensity of Turbulence in a Rocket Chamber.* ARS J., Vol.31, 1961, p.39.
5. Uberoi, M.S. Corrsin, S. — *Diffusion of Heat from a Line Source in Isotropic Turbulence.* NACA Rept.1142, 1953.
6. Combs, L.P. Schuman, M.D. — *Steady-State Rocket Combustion of Gaseous Hydrogen and Liquid Oxygen: Part 2, Analysis for Coaxial Jet Injection.* Rocketdyne Res. Rept.64-29, 1965.
7. Witte, A.B. Harper, E.Y. — *Experimental Investigation and Empirical Correlation of Local Heat-Transfer Rates in Rocket Engine Thrust Chambers.* JPL Tech. Rept.32-244, 1962.
8. Powell, W.B. et al. — *Chlorine Trifluoride – Hydrazine Liquid Propellant Evaluation and Rocket Motor Development.* JPL Tech. Rept.32-305, 1963.
9. Bartz, D.R. — *Experimental Rocket-Motor Performance and Heat Transfer of the RFNA-Ammonia Propellant System at Chamber Pressures to 2000 psia.* JPL Prog. Rept.20-268, 1955.
10. Canright, R.B. — *Some Studies on the Heat Flux into Rocket Motors Utilizing the Red Fuming Nitric-Acid Aniline Propellant.* JPL Rept.1-33, 1947.
11. Curren, A.N. et al. — *Experimental Heat-Transfer Study of a Regeneratively Cooled Hydrogen-Fluorine Rocket Engine at Low Chamber Pressure.* NASA TN D-4178, 1967.
12. Pavli, A.J. et al. — *Design and Cooling Performance of a Dump-Cooled Rocket Engine.* NASA TN D-3532, 1966.
13. Jeffs, A.T. et al. — *Combustion and Heat Transfer in a Small Rocket Chamber Burning Liquid Oxygen and Gaseous Hydrogen.* Spaceflight, Vol.8, 1966, p.172.
14. Liebert, C.H. Ehlers, R.C. — *Determination of Local Experimental Coefficients on Combustion Side of an Ammonia-Oxygen Rocket.* NASA TN D-1048, 1961.
15. Rupe, J.H. Jaivin, G.I. — *The Effects of Injection Mass-Flux Distribution and Resonant Combustion on Local Heat Transfer in a Liquid Propellant Rocket Engine.* JPL Tech. Rept.32-648, 1964.

TABLE 4.I

Approximate Variation of c^*

$O/F <$ maximum c^*

$$c^* = D(O/F)^n + E$$

Propellants	D m/sec	n	E m/sec	O/F max	*Mean Error*	*RMS Error*
N_2O_4 – N_2H_4	348	0.3	1550	1.0	0.05	0.02
ClF_3 – N_2H_4	1246	0.2	396	2.3	–	–
RFNA – NH_3	920	0.5	216	2.2	–0.04	0.05
HTP – C_7H_{16}	560	0.5	865	8.0	0.02	0.03
O_2 – H_2	777	0.2	1619	2.6	0.08	0.09
F_2 – H_2	689	0.3	1619	4.0	0.05	0.06

$O/F >$ maximum c^*

$$c^* = \frac{A}{(O/F) + E} + F$$

Propellants	D m/sec	E	F m/sec	*Mean Error*	*RMS Error*
N_2O_4 – N_2H_4	8784	5.35	503	–0.01	0.01
ClF_3 – N_2H_4	24230	31.3	1094	–	–
RFNA – NH_3	7516	5.04	504	0.13	0.10
HTP – C_7H_{16}	12660	10.15	890	0.00	0.01
O_2 – H_2	42400	18.3	536	0.00	0.02
F_2 – H_2	137000	53.1	244	0.00	0.05

TABLE 4.II

PROPELLANTS *Oxidant*	*Fuel*	*Injector*	O/F *Ratio*	*Chamber Dia.* mm	$\frac{x_0}{L}$	L mm	*Source Ref.*
N_2O_4	N_2H_4	8-pair Splash-plate	1.0	127	0.61	222	7
ClF_3	N_2H_4	Multiple cup-and-plug	1.9 – 2.4	127	0.21	164	8
WFNA	NH_3	8-pair Splash-plate	1.3 – 3.7	63.5	0.79	59	9
		8-pair Impinging-jet	1.8 – 3.1	63.5	0.74	160	9
RFNA	Aniline	4-pair Impinging-jet	2.6 – 3.3	63.5	0.11	301	10
		Conical sprays	2.6 – 3.3	63.5	0.20	127	10
F_2	H_2	121-element Coaxial	4.5 – 7.3	137	–0.42	66	11
O_2	H_2	19-element Coaxial	2.3 – 5.5	95.5	–1.47	34	12
		Showerhead (fine)	2.3 – 8.0	101	–0.44	58	13
		Showerhead (coarse)	7.3	102	–0.22	134	–
O_2	NH_3	Showerhead	1.5	76	–0.35	93	14

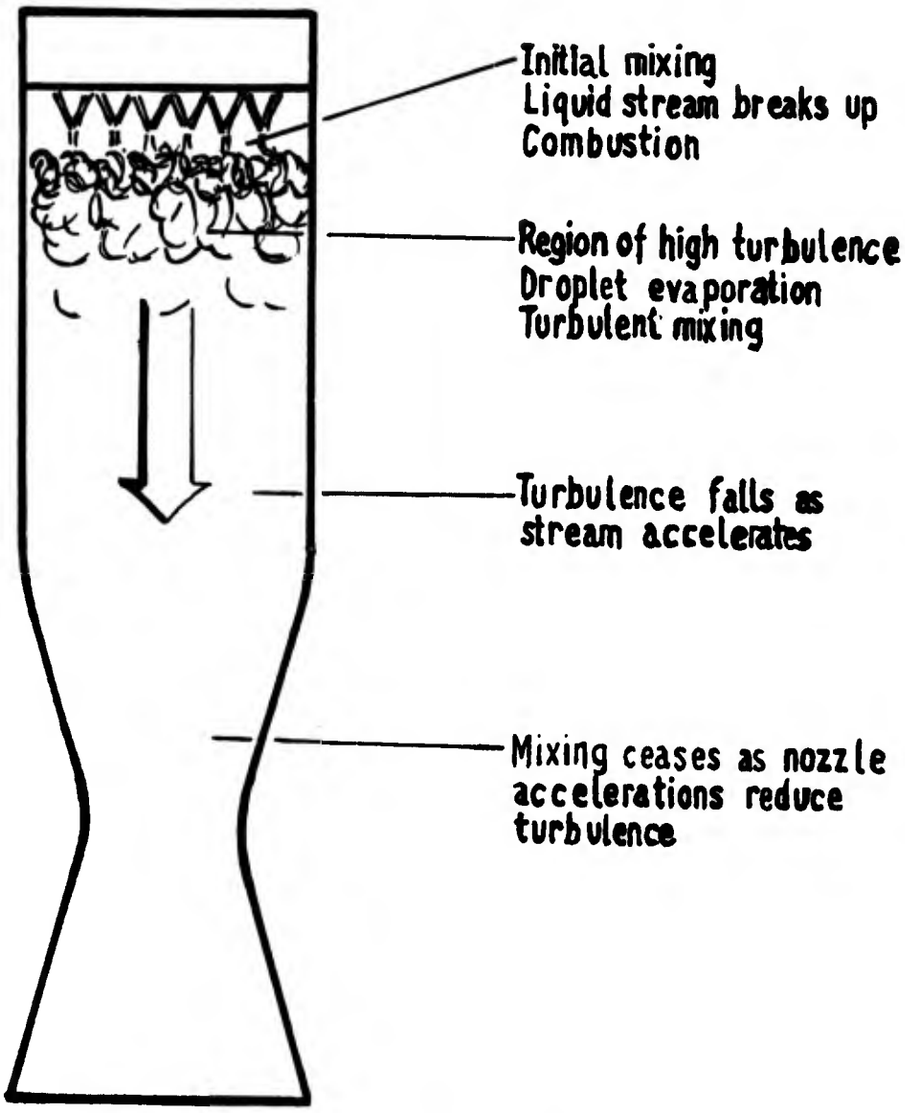

Fig.4.1 Main combustion processes occurring within a rocket engine

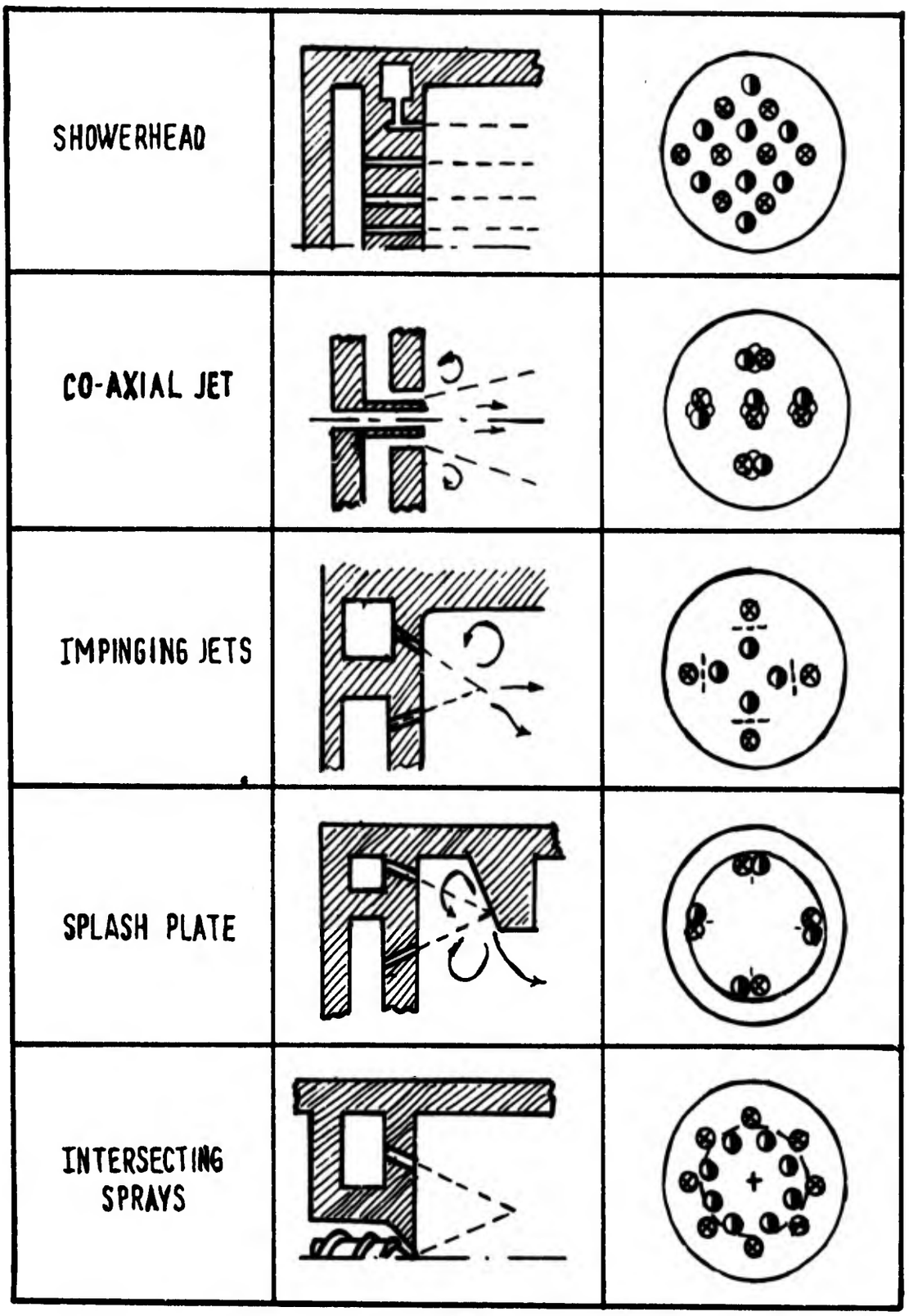

Fig.4.2 Some typical forms of injector, with their source patterns for mixing simulations

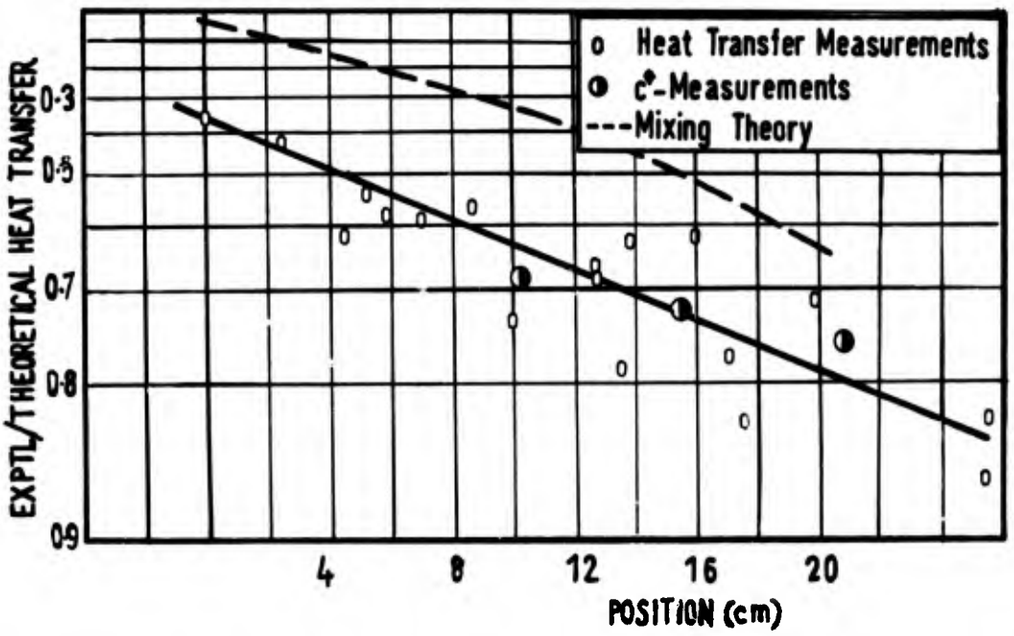

Fig.4.3 Typical variation of heat transfer with position in a combustion chamber, showing the progress of combustion

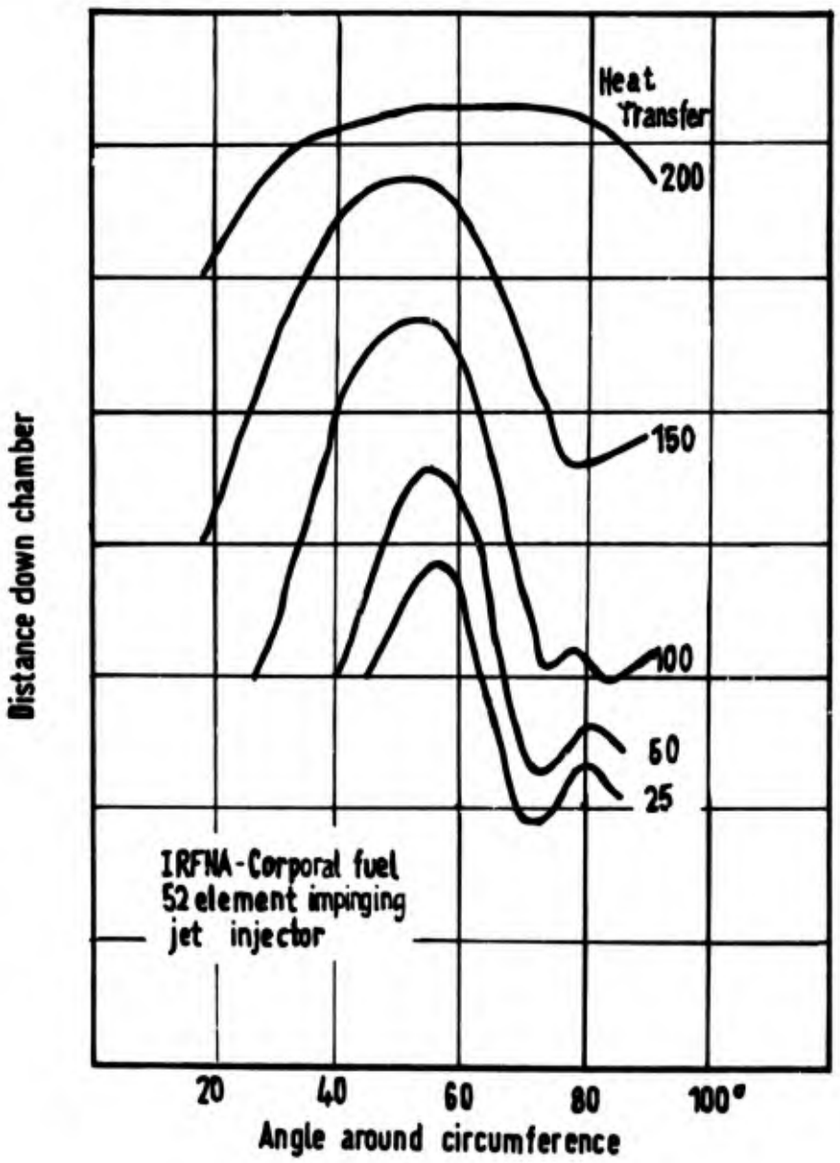

Fig.4.4 A typical distribution of heat transfer over a quadrant of a combustion chamber

CHAPTER 5

CHEMICAL REACTIONS IN THE BOUNDARY LAYER

5.1 GENERAL

The combustion processes liberating energy within a rocket engine will tend to form simple molecules – water vapour, carbon dioxide, and with some propellants, nitrogen. However, because of the high gas temperatures some of the available energy will remain bound up by chemical dissociation. If the gas temperature is subsequently lowered, recombination reactions will take place, releasing energy as the chemical composition of the gas mixture changes.

In particular, the combustion gases will cool in the boundary layer adjacent to the wall. The heat transfer, therefore, will be subject to the effects of chemical reaction and changing gas composition in the boundary layer.

Three main effects exist. First, the available driving enthalpy across the boundary layer will be increased by chemical recombination. Secondly, the effective thermal conductivity of the gas will be enhanced by the diffusion of dissociated species across the temperature gradient of the boundary layer. And lastly, heat transfer may also be increased by the catalytic recombination of dissociated species at the gas-side wall.

The first essential is to determine the probability of a given chemical reaction taking place in the boundary layer.

5.2 CHEMICAL KINETICS IN THE BOUNDARY LAYER

The equilibrium gas composition of the combustion gases will vary with temperature. As the gases enter the cooler boundary layer, reactions will begin among the various molecular species to change the gas composition towards its new, lower temperature equilibrium. The degree of equilibrium actually obtained will depend on the speed of the various chemical reactions, and the residence time for the reacting species within the cooler boundary layer.

The region in which nearly all of the chemical reaction will take place is the laminar sub-layer. Here, with the absence of turbulent mixing, residence times will be longest. In addition the temperature drop across the boundary layer will nearly all take place within this layer (see Figure 5.1).

One may therefore characterize the residence time of a particular species within the boundary layer by the ratio of its mean-free-path (λ) to the thickness of the laminar sub-layer (δ_L). The latter may be obtained, as in Section 2.3, from the non-dimensional profile of the boundary layer.

$$\delta_L = \frac{y_L^+ \nu}{u_\tau}$$

where, for subsonic boundary layers, $y_L^+ = 10.5$. Following the method of Czarnecki and Monta[1], the mean-free-path is given by the relationship

$$\lambda = 1.255 \frac{\nu}{a} \sqrt{\gamma},$$

where a is the speed of sound. A little re-arrangement of this provides the simple formula

$$\boxed{\frac{\lambda_w}{\delta_L} = \frac{1.255\,Ma}{y_L^+} \sqrt{\frac{\gamma C_f}{2}}}, \qquad (5.1)$$

where Ma is the Mach number, and C_f the local skin-friction coefficient.

In the boundary layer of a typical combustion chamber, λ_w/δ_L is of the order of 10^{-3}. A typical molecule may thus be expected to make between ten and one hundred thousand collisions before leaving the laminar sub-layer region. The degree of equilibrium obtained in the laminar sub-layer will depend on the probability of one of these collisions resulting in a chemical reaction.

Considering a typical chemical reaction between species i and species j, the rate of change of concentration of i (measured in mole-fractions) is given by

$$\frac{dx_i}{dt} = -k_r x_i x_j ,$$

where k_r is the reaction rate constant. Practical rate constants in gas-mixture reactions have been found to follow laws of the form

$$k_r = AT^b e^{-E/RT} , \tag{5.2}$$

where A and b are experimental rate constants and E is the activation energy. The exponential term in which E occurs allows for the fact that molecules will have a range of energies, only some of which will be capable of bringing about a reaction.

Theoretical kinetic considerations give the rate constant as

$$k_r = PZe^{-E/RT} \tag{5.3}$$

where Z is the rate at which molecular collisions of the correct kind occur, and P is a "steric factor" bringing theoretical reaction rates into line with those found in practice. This "steric factor" allows mainly for those collisions of sufficient energy that will none-the-less occur without reaction because of misalignment of the molecules.

The probability of a given collision in the gas-mixture bringing about a reaction between species i and species j is

$$f_{ij} = \frac{1}{Z}\frac{dx_i}{dt} = x_i x_j P e^{-E/RT}$$

$$\boxed{= x_i x_j \frac{AT}{Z} e^{-E/RT} .} \tag{5.4}$$

A list of reaction rate data for typical reactions occurring in rocket engines is given in Table 5.I. The rate of bimolecular collisions is given by

$$Z = N\sigma_{ij}\left[\frac{8\pi RT(M_i + M_j)}{M_i M_j}\right]^{1/2} . \tag{5.5}$$

N is Avogadro's number, σ_{ij} the mutual collision diameter, and M_i and M_j are the molecular weights of the two species.

The degree of completion of any given reaction achieved in the boundary layer will be given by a comparison of f_{ij} with λ_w/δ_L. It has been found that the reaction is just complete when

$$\boxed{g_{ij} \equiv f_{ij}\frac{\delta_L}{\lambda_w} \simeq \frac{1}{50} .} \tag{5.6}$$

The small value of this quantity is a consequence of the random walk path followed by a typical molecule during its stay in the laminar sub-layer. At any instant only a relatively small fraction of the molecules in the sub-layer will actually progress directly towards the wall, or away from it.

Now, each reaction will have an enthalpy change, or heat of reaction, associated with it. So that knowing the probability of a given reaction occurring, it is possible to add to the available enthalpy that energy released by the reaction. As an example, the reactions occurring in a typical oxygen-hydrogen engine have been listed in Table 5.II, with the probability of their occurrence, and the energy released. Such calculations indicate that in general two reactions will be dominant, namely

$$\begin{aligned} H + OH + M &\rightarrow H_2O + M \\ H + H + M &\rightarrow H_2 + M . \end{aligned} \tag{5.7}$$

There are three possible situations that will affect the state of chemical equilibrium within a boundary layer.

(i) The chemical reactions may be slow compared to the residence times in the boundary layer so that the composition of the boundary layer is essentially "frozen" at that of the free-stream.

(ii) One, or more of the possible chemical reactions will be essentially complete, and the chemical composition of the boundary layer will be more appropriate to the equilibrium composition of the gas at the temperature

of the wall. In both of these cases minor changes in the conditions of the free-stream (affecting, for instance, Equation (5.1)) will have no effect on the available enthalpy for heat transfer.

(iii) One of the chemical reactions will have reaction times comparable with the residence time of molecules in the laminar sub-layer, and significant changes in the available enthalpy will take place with changes in Mach number, mixture ratio, or development of the boundary layer.

Figure 5.2 illustrates these three cases. In the first case (WFNA-ammonia) the composition in the boundary layer is "frozen". In the second case (oxygen-hydrogen), only the H + OH reaction is complete, and the experimental results lie between the completely "frozen" and the completely "equilibrium" values for heat transfer. In the third case (fluorine-hydrogen), the H + H reaction lies in the balance, and the experimental results shift from completely "frozen" to completely "equilibrium" conditions with changing mixture ratio. In this range, quite small changes in local conditions will affect the achieved equilibrium, and hence the heat transfer.

5.3 CHEMICAL REACTIONS AND HEAT TRANSFER

As already mentioned, chemical reactions will affect the heat transfer by increasing the available enthalpy of the gases close to the wall, by enhancing the effective thermal conductivity of the boundary layer, and by catalytic recombinations occurring at the wall. The first of these has been dealt with in the previous section.

The effective thermal conductivity of the boundary layer will be enhanced by the diffusion of dissociated species across the temperature gradient, and their subsequent recombination closer to the wall. For boundary layers in thermochemical equilibrium Rosner[6] has shown that the conventional convective heat transfer coefficient must be enhanced by a factor

$$\left[1 + (\mathrm{Le} - 1)\frac{\Delta H_{chem}}{\Delta H_e}\right]^{2/3}. \tag{5.8}$$

Here Le is the Lewis-Semenov number $\rho c_p D/k$, measuring the rate at which diffusion of dissociated species occurs in the boundary layer, and ΔH_{chem} is the enthalpy available from a completed chemical reaction. In fact there will be different enhancements for each of the various chemical reactions taking place, but the enhancement of thermal conductivity will take place at a somewhat slower rate than that calculated for the achieved chemical reaction in the boundary layer, and once again only one or two reactions will be important.

For the conditions given in Table 5.II, the maximum degree of enhancement given by (5.8) is 1.194 based on the enthalpy of the *equilibrium* composition as driving force. The major contribution is due to H-atoms diffusing through the boundary layer.

Surface catalysis of reactions will enhance the frozen driving enthalpy. The energy released is by the completion of reactions involving species that diffuse through the boundary layer unreacted as far as the wall. Once again, diffusion controls the maximum enhancement, and Rosner[6] gives as the enhancement factor

$$\left[1 + (\mathrm{Le}^{0.6} - 1)\left(\frac{C}{1+C}\right)\frac{\Delta H_{chem}}{\Delta H_f}\right], \tag{5.9}$$

where C is a "catalytic parameter" defined as the ratio of the interfacial reaction rate to the characteristic rate for convective diffusion,

$$C = \frac{k_{r_w}\rho_w}{\rho u St_D}, \tag{5.10}$$

k_{r_w} being the reaction rate constant at the surface, and St_D the Stanton number for mass-transfer (equal to that for heat transfer for a Prandtl number of unity).

The reaction rate constant of the surface is directly proportional to the catalytic efficiency of the surface (r_A) – that is, the ratio of atoms recombining at the surface to the total number of atoms reaching the surface,

$$k_{r_w} = \left(\frac{2\pi M}{RT}\right)^{-1/2}. \tag{5.11}$$

The main difficulty here is to find a value for the catalytic efficiency of the surface. The catalytic efficiency will vary widely with the nature of the surface and the reaction. Fortunately, the factor given by (5.9) is not too sensitive to values of r_A. A typical value cited by Goulard[7] for the recombination of nitrogen is

$$r_A \sim 4 \times 10^{-7} T_w .$$

Using this, the Rosner catalytic parameter C for a wall at 1000°K is 0.75. For H-atoms diffusing through the boundary layer of an oxygen-hydrogen engine and using the data in Table 5.II, the Lewis-Semenov number is 3.0, resulting in an enhancement on the frozen composition driving enthalpy of 1.082.

Obviously this latter recombination reaction assumes that the boundary layer is essentially frozen, and thus the factors given by (5.8) and (5.9) are mutually exclusive. Both effects will be important mainly where there is a component of low molecular weight (such as H-atoms) in the reacting combustion gases, helping diffusion processes, and where the combustion temperature is sufficiently high for a significant amount of energy to be bound up in chemical dissociation.

5.4 MAIN STREAM FLOW CONDITIONS

When the exhaust gases pass through a rocket nozzle, chemical equilibrium effects will also cause the main stream gas composition to change. As the gases expand in the nozzle, chemical equilibrium will be maintained up to a point, and then fairly rapid "freezing" of the composition will occur as flow processes become comparable in speed to the reaction rates[8]. This freezing point will generally occur somewhere downstream of the throat section, but if significant changes in the gas composition have taken place, the heat transfer will reflect these changes.

Figure 5.3 shows a comparison made of the heat transfer calculated according to changing and frozen composition assumptions in a nitrogen tetroxide-hydrazine engine. The difference amounts to about 2.7% at the throat, and 8.5% far downstream. Such errors will generally be of only minor importance, particularly as the chemical equilibrium condition will not be maintained indefinitely, but for cases of particular accuracy it will be worth recalculating the gas composition and its properties at least at the throat section, and using these values for the supersonic part of the nozzle.

5.5 CONCLUSION

Possibly the most important conclusion to be drawn from this study of chemical reactions in the boundary layer is that the equilibrium achieved will proceed in a series of plateaus – certain reactions being essentially complete, and others almost completely "frozen". This allows us to calculate the effect of boundary layer reactions as a single factor for a given engine. Only in the case where one particular reaction lies somewhere in between the "frozen" and "complete" condition – as, for example, in the fluorine-hydrogen engine illustrated in Figure 5.2(c) – will it be necessary to recalculate the chemical equilibrium at each point along the engine wall.

The main effects of chemical reaction in the boundary layer will be to enhance the available enthalpy for heat transfer. The enhancement of the thermal conductivity of the boundary layer, and the effect of surface catalysis will generally only be of secondary importance.

With this study of the chemical reactions occurring within the boundary layer of a rocket engine, our study of the basic convective heat transfer processes is complete. Radiation remains the only important means by which heat is transmitted from the hot gases to the engine walls, a subject to be dealt with in the next chapter.

REFERENCES

1. Czarnecki, K.R. Monta, W.J. — *Effects of Compressibility and Heat Transfer on the Laminar Sub-Layer of the Turbulent Boundary Layer.* NASA TN D-1998, 1964.

2. Glasstone, S. — *Textbook of Physical Chemistry.* Macmillan, London, 1955, p.1095.

3. Bartz, D.R. — *Experimental Rocket-Motor Performance and Heat Transfer of the RFNA-Ammonia Propellant System at Chamber Pressures to 2000 psia.* JPL Prog. Report 20-268, 1955.

4. Jeffs, A.T. et al. — *Combustion and Heat Transfer in a Small Rocket Chamber Burning Liquid Oxygen and Gaseous Hydrogen.* Spaceflight, Vol.8, 1966, p.172.

5. Waldman, B.J. Shuster, E.B. — *Fluorine-Hydrogen Evaluation: Phase 1. Part II: Nozzle Performance Analysis and Demonstration.* Rocketdyne Report R-6636-2, 1967 (NASA CR-72038).

6. Rosner, D.E. — *Convective Heat Transfer with Chemical Reaction, Part 1.* Aerochemical Research Laboratories Inc., Report ARL 99, 1961.

7. Goulard, R.J. — *On Catalytic Recombination Rates in Hypersonic Stagnation Heat Transfer.* Jet Propulsion, Vol.28, 1958, p.737.

8. Bray, K.N.C. — *A Simplified Sudden Freezing Analysis for Non-Equilibrium Nozzle Flows.* University of Southampton, AASU Report 161, 1960.

TABLE 5.I

Reaction Rate Data

Reaction	*Experimental Rate Constants* a	b	E k cal/mole	ΔH k cal/mole	ΔS/R k cal/mole °K
$H_2 + OH \rightarrow H_2O + H$	$6.3_{10}10$	0	5.9	14.01	1.290
$H + O_2 \rightarrow OH + O$	$7.2_{10}11$	0	16.9	−14.84	−2.336
$H_2 + O \rightarrow OH + H$	$2.6_{10}9$	0	7.7	−1.968	−0.847
$H_2 + M \rightarrow H + H + M$	$7.7_{10}18$	−1.5	104.2	−104.2	−2.309
$H_2O + M \rightarrow OH + H + M$	$2.0_{10}19$	−1.5	114.7	−114.7	−3.599
$O + O + M \rightarrow O_2 + M$	$1.9_{10}11$	0.5	0	122.7	3.798
$N_2 + O \rightarrow NO + N$	$7.0_{10}10$	0	75.5	−75.47	−1.549
$O_2 + N \rightarrow NO + O$	$1.0_{10}10$	0.5	6.2	32.52	−1.468
$NO + M \rightarrow N + O + M$	$1.4_{10}18$	−1.5	150.0	−151.6	−2.348
$O_2 + N_2 \rightarrow 2NO$	$2.7_{10}10$	0	107.0	−42.95	−2.999
$H + F + M \rightarrow HF + M$	$3.4_{10}8$	0	138.8	−141.81	−2.660
$H_2 + F \rightarrow HF + M$	$2.5_{10}7$	1.0	8.0	31.97	0.697
$F_2 + H \rightarrow HF + F$	$5.3_{10}9$	0.5	4.0	97.78	1.056
$F + F + M \rightarrow F_2 + M$	$5.2_{10}6$	0.5	16.2	−16.22	−3.191

$$k_{f+} = AT^b e^{-E/RT}$$

$$k_{f-} = \frac{AT^b}{e^{\Delta S/R}} e^{-(E+\Delta H)/RT} .$$

$R = 1.98726$ k cal/mole^{-1} deg K^{-1}

$N = 6.023 \times 10^{26}$ molecules/mole

Units for reaction rate data are dm^3, gram-mole, sec and deg K.

TABLE 5.II

Reactions Occurring in an Oxygen-Hydrogen Engine

Stagnation pressure = 3 MN/m^2

Mixture = 15% hydrogen

Wall temperature = 1000°K

Composition

	H	OH	H_2	H_2O	O	O_2
T = 3410°K	0.045	0.044	0.282	0.621	0.004	0.004
T = 1000°K	–	–	0.286	0.714	–	–

Reaction	*Probability* ij	ΔH k cal/mole
$H_2 + OH \rightarrow H_2O + H$	$6.82_{10}-11$	14.01
$H_2O + H \rightarrow H_2 + OH$	$3.10_{10}-14$	−14.01
$H + O_2 \rightarrow OH + O$	$2.46_{10}-13$	−14.84
$OH + O \rightarrow H + O_2$	$1.56_{10}-8$	14.84
$H_2 + O \rightarrow OH + H$	$2.06_{10}-13$	−1.968
$OH + H \rightarrow H_2 + O$	$1.65_{10}-12$	1.968
$H_2 + M \rightarrow H + H + M$	$8.67_{10}-28$	−104.2
$H + H + M \rightarrow H_2 + M$	$3.87_{10}-6$	104.2
$H_2O + M \rightarrow H + OH + M$	$1.54_{10}-28$	−114.7
$H + OH + M \rightarrow H_2O + M$	$1.13_{10}-4$	114.7

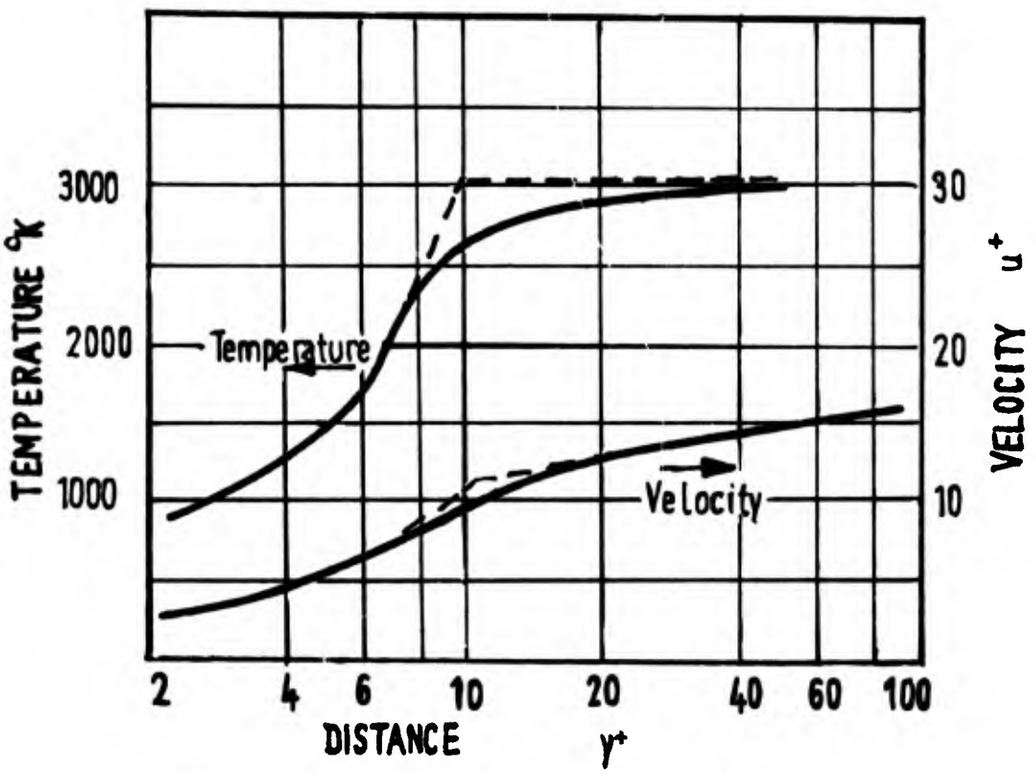

Fig.5.1 Temperature and velocity distributions in a boundary layer

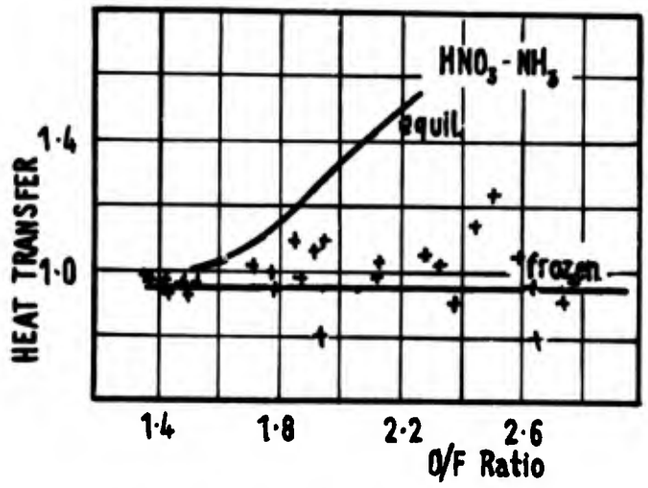

(a)

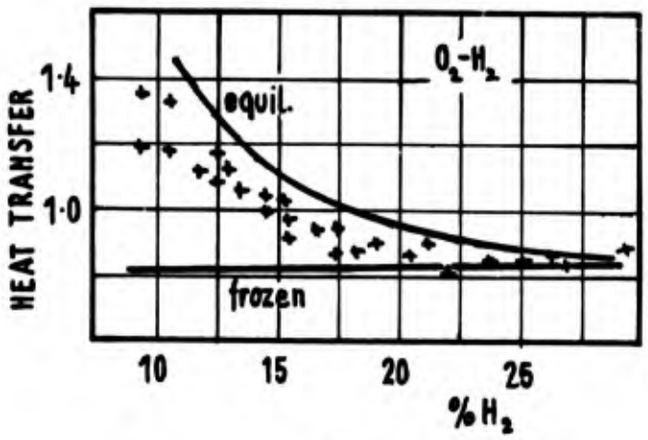

(b)

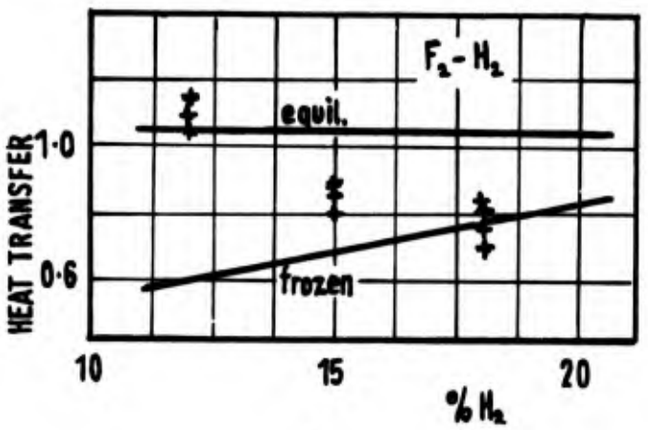

(c)

Fig.5.2 Degree of equilibrium obtained in a boundary layer from heat transfer measurements

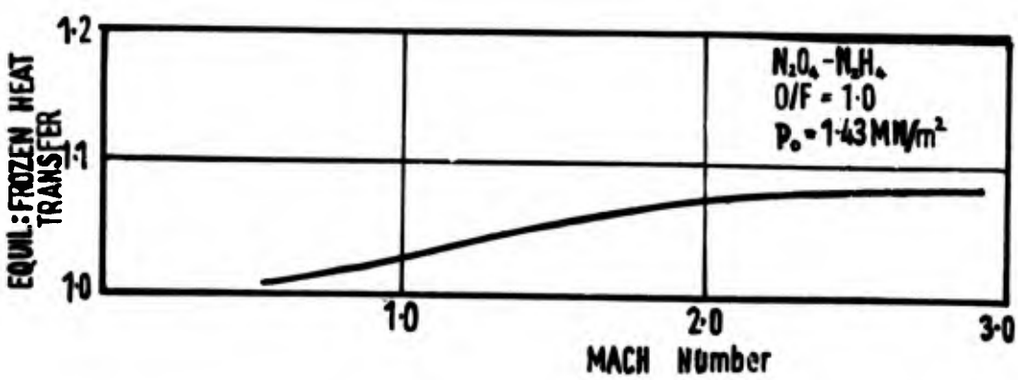

Fig.5.3 Effect of chemical equilibrium in main flow on the heat transfer

CHAPTER 6

RADIATION

6.1 GENERAL

Convective heat transfer from dissociated combustion gases has received considerable attention from theoretical and experimental workers, but few systematic attempts have been made to enlarge our understanding of thermal radiation at conditions of state characteristic of those occurring in high-energy rocket thrust chambers, i.e. temperatures up to 4000°K at pressures ranging from 10 to 200 bar.

In view of the lack of pertinent numerical data the radiative heat transfer is usually calculated from the equilibrium concentrations of the polar gas constituents and their respective emissivities. As the experimentally verified emissivities for the two major radiating gases, water vapour and carbon dioxide, extend only to about 1600°K, the respective emissivity values at rocket thrust chamber conditions have to be obtained by extrapolation, and contributions from other radiating equilibrium constituents, e.g. carbon monoxide, or the hydroxyl radical, are usually neglected, mainly on account of lack of sufficiently accurate data.

Radiative heat fluxes calculated in this manner showed that, relative to the total heat flux (convective plus radiative heat flux) the radiative heat flux constituted but a small fraction. From the development engineer's point of view it must have seemed unjustifiable to devote a great deal of effort to undertake the difficult task of a thorough experimental study in this field. This, coupled with the fact that studies of thermal radiation phenomena are traditionally the domain of the physicists, were probably the primary reasons for the lack of experimental effort and understanding of an extremely complex problem.

It cannot be the task of this brief chapter to provide a thorough account of the phenomenon of thermal radiation but it is thought essential for an appreciation of the physical phenomena involved to provide some qualitative information on thermal emission from gaseous media and on the influence of parameters such as absolute pressure and absolute temperature on this quantity. This will lead not only to a better understanding of the physical problems encountered in high temperature gases but will also serve to appreciate the limitations of the engineering approximations currently used.

6.2 GAS RADIATION

A gas emits radiation as a result of quantized rotational, vibrational and electronic transitions from excited energy levels to the ground state. In the spectrum of an excited gas or a gas mixture we may find individual lines, groups of very closely spaced lines, so as to give the impression of a continuous, but narrow band, or even a complete continuum extending over a wide spectral range.

Line spectra are only emitted by atoms or atomic ions, while band spectra are characteristic for emission from molecules. Continuous spectra cannot be ascribed to the nature of the substance, but are an indication of the nature of a non-quantized deactivation process.

6.2.1 Line Spectra

According to Bohr's theory each atom possesses a number of stable electron orbits along which an electron can move without a change in the energy state of the atom. The orbit of the smallest radius represents the stable ground state of the atom. To force an electron into an orbit of larger diameter a certain quantum of energy is required, the so-called excitation energy. By imparting more energy to the atom the electron jumps successively into orbits of increasing diameter. The quanta of energy required for each electron jump diminish with increasing distance from the nucleus on account of the diminishing attractive forces between nucleus and electron. Continuing this process a state will eventually be reached at which the electron separates completely from the nucleus; the atom breaks down into an atomic ion and a free electron. Suppose the energy imparted to the atom was in excess of that required for ionisation, the liberated electron will carry the excess energy in form of kinetic energy $m_e v^2/2$, where m_e is the mass of the electron and v its velocity. As the free electron can absorb any arbitrary amount of energy, the energy states of an atom above its ionisation level are therefore continuous as opposed to the quantized states of the stable atom. An ionised atom will therefore display a continuum in a characteristic spectral range. The excitation energy required for ionisation of monatomic or diatomic gases is fairly high and this process is unlikely to be of any importance in rockets utilising the chemical energy of propellants.

A semi-schematic graphical presentation of the energy levels of an atom will be found in Figure 6.1.

6.2.2 Spectra of Molecules

At equilibrium conditions energy imparted upon a molecule is distributed equally amongst all degrees of freedom, viz. translation, rotation and vibration. Whereas translational changes of energy are continuous, the excitation of a molecule to higher frequencies of rotation and/or vibration takes place in discrete steps, that is to say, it is quantized.

In the far infrared a spectrum of such a molecule shows equidistant lines or line sequences, whereas in the near infrared clearly separated lines and line groups will be found. These are known as the rotational and rotational-vibrational spectra, respectively.

From the near-infrared through the visible regime into the ultraviolet region, closely spaced, complex line systems, and often continua will be observed. The complexity of the band spectrum arises from the fact that excitation may be due to several processes, such as (a) electron excitation, similar to that observed for an atom, (b) vibrational excitation of the atomic nuclei, and (c) rotational excitation.

A change in any of these states may lead to the emission of energy by radiation. Spectra in the near-infrared and in the visible regime are considered to be of greatest importance in high temperature gas systems, and are predominantly due to changes of the vibrational-rotational levels of excitation.

To provide an approximate scale for the quantitative importance of various possible changes in the energy level of a molecule it ought to be borne in mind that an energy change consequent upon an electron jump is an order of magnitude larger than that caused by a vibrational quantum jump, and the latter an order of magnitude larger than a rotational quantum jump.

Deactivation of excited states in the rotation-vibration spectrum by direct emission can only take place if the electric moment of the system is changed during the transition. Because of the symmetry of the charge distribution in homonuclear molecules the electric moment remains unchanged for internal vibrations. Hence, molecules such as O_2, H_2 and N_2 normally do not possess a vibration-rotation band spectrum. There is, however, an important exception to this general rule. At very high pressures, energetic, close-range, two-body collisions between such molecules can lead to a distortion of the electronic charge distribution. The resulting electric moments can be of considerable magnitude permitting the activation of the ground frequencies of the rotational band structure. This phenomenon is known as collision induced emission and has been studied for pure hydrogen and gas mixtures containing hydrogen at pressures up to 1500 atm by Chrisholm and Welsh[1].

The nature of the vibrational-rotational spectrum is of importance in assessing thermal radiation from high temperature gases and gas mixtures in technical applications. As a typical example the spectrum of water vapour based on measurements by E.Schmidt[2] is shown in Figure 6.2.

The spectrum possesses a series of active bands within which radiation can be emitted and absorbed which are separated by fairly wide wave length regions within which the gas is completely transparent. An examination of the fine structure of these bands with a spectroscope possessing ultra-high resolving power would show it to consist of thousands of closely spaced individual lines, each line representing a distinct quantum change. With all the possible combinations of simultaneous rotational and vibrational energy changes, a nearly infinite number of energy levels seems possible. The spectrum of a single radiating molecule would only produce lines on different parts of the spectrum. The band spectrum emitted by a very large number of radiating molecules is simply a measure of the relative probabilities of various possible combinations of energy levels within that molecule.

6.2.3 Continuous Spectra

Continuous spectra in gases are associated with transitions in which at least one of the states involved is unquantized. Such continua correspond to certain characteristic changes of the atom or molecule, such as ionisation, dissociation and association. From the examination of the line spectra and band spectra the type of the emitting species can be determined while continua provide information on the nature of the molecular processes taking place.

6.2.4 Ionisation Continuum

Absorption spectra of atoms consist of a series of converging lines beyond which a region of unquantized continuous radiation and absorption is observed. As has already been stated these lines correspond to various characteristic levels of quantized electronic states; the continuum, however, is the consequence of the liberation of an electron from the positive atomic ion. Supposing the excitation leading to partial ionisation was sufficiently powerful, the liberated electron would move with a velocity v and thus possess the kinetic energy $m_e v^2/2$. As the velocity of the free electron may vary continuously the same must apply to its kinetic energy. Changes in the states of the atom above its ionisation limit are therefore unquantized and ionized gases will in the appropriate part

of the spectrum emit a continuum. Ionisation brought about by the thermal motion of atoms is known as thermal ionisation and is generally only of importance at temperatures of, say, more than 5000°K. This temperature lies outside the limit attainable with chemical fuels but may eventually be reached in nuclear powered rockets. The concentration of ionised atoms and molecules increases exponentially with the absolute gas temperature according to the Eggert-Saha equation.

It must be remembered that, however small the concentration of ionised atoms or molecules may be, their presence in a gaseous system will lead to the emission of a continuum.

6.2.5 Association Continuum

A frequent cause of the existence of a continuum in high temperature gases is molecular association of atoms or molecules into more stable molecular complexes. The process is easiest explained for the case of two atoms forming upon collision a molecule.

Bimolecular association of homonuclear atoms such as $H + H \rightarrow H_2$ can only take place by three-body collisions

$$A + A + B \longrightarrow 2A + B_{fast} \ ,$$

where the third body B which may be a molecule on the surface of a bounding wall absorbs the energy liberated in the process.

The situation is different, however, when two ion atoms collide, as the potential curve of the excited state is different from that of the ground state of the ion molecule. The recombination in this case may take place by a two-body collision according to

$$A + B \longrightarrow A^+ B^- + hc\bar{\nu}_k \ ,$$

in which the energy released is emitted as a continuum between the wavelength region lying between the transition steps F'F'' and G'G'' as indicated in Figure 6.3.

Similar considerations apply also to the recombination of polyatomic molecules (radicals) to either transient intermediates or stable complexes. In this case, however, the complexity is increased as the potential curves are to be replaced by potential surfaces.

6.3 METHODS OF PREDICTING GAS RADIATION

Before proceeding with a discussion of the two main methods, a few general principles governing the emission and absorption from gaseous media will be introduced.

Radiation incident upon a layer of a substance, be it in the solid, liquid or gas phase, is progressively attenuated as the radiating beam passes through the substance. In contrast to solids, and also many liquids, for which a very thin layer may prove adequate for complete absorption, a radiating beam may penetrate a gas layer to a considerable depth before appreciable absorption takes place. According to the law of Lambert and Beer the energy flux dI_ω absorbed in a layer of elementary thickness dX is proportional to the flux I_ω entering the layer and a proportionality constant k_ω. This factor is a physical constant for the substance and the wave number ω in question and is termed the monochromatic absorption coefficient. Hence

$$dI_\omega = I_\omega k_\omega dX \ . \tag{6.1}$$

Integrating the above equation with the boundary conditions $I_\omega = I^0_\omega$ for $X = 0$, yields for the beam leaving the layer of effective thickness X

$$I_\omega = I^0_\omega \exp(-k_\omega X) \tag{6.2}$$

and the energy absorbed within the gas layer of thickness X is therefore

$$I^0_\omega - I_\omega = I^0_\omega[1 - \exp(-k_\omega X)] \ . \tag{6.3}$$

Gases possess a high degree of transmittance and in consequence k_ω is a relatively small quantity. Absorption of radiation involves an interaction with the molecules of the absorbing gas and must therefore be a function of the number of molecules lying within the path length L of the radiating beam. For an ideal gas the number of molecules of a radiating gas in gas mixture is proportional to the partial pressure P_g. It thus follows that emission and absorption of radiation must increase with increasing partial pressure of the absorbing gas constituent. For the spectral emissivity of a system of uniformly distributed radiators the following relation obtains

$$\epsilon_\omega = 1 - \exp(-k_\omega P_g L) \ , \tag{6.4}$$

where k_ω is the spectral absorption coefficient at wave number ω, and L the thickness of the emitting gas layer.

The effective path length for absorption, represented by the product $(P_g L)$, is usually referred to as the optical density of the gas. The Lambert-Beer Law (Eqn (6.4)) which predicts identical values for ϵ_ω for different combinations of P_g and L, is not universally valid and deviations for strongly polar molecules, such as water vapour, have to be considered.

As is seen from an inspection of Equation (6.3) the emissivity of the substance diminishes with increasing values of X. This quantity corresponds to the optical density $(P_g L)$ for gases. However, the optical density required for complete absorption of a monochromatic beam does not require infinitely large values of either P_g or L. In general, the critical optical density for black-body emission varies with the nature of the gas and is smaller the higher the absorption coefficient.

With the aid of these general relations, and bearing in mind the multi-band structure of a hetero-polar molecular spectrum, it is possible to make a numerical estimate of that quantity which is of utmost interest in engineering heat transfer calculations, viz. the radiative heat flux.

6.3.1 The Spectral Absorption Method

Provided the absorption spectrum for the gas in question is known the total radiative flux emanating from a volume of gas can be obtained by integrating Planck's distribution law over the spectral range of each individual band.

The energy emitted by a spectral band is

$$I_{band} = \int_{\omega_1}^{\omega_2} k_\omega I^0_\omega \, d\omega \ , \tag{6.5}$$

where k_ω is the spectral emissivity,

ω_1 and ω_2 are the wave numbers at the extreme limits of the band,

$I^0_\omega d\omega$ is the spectral radiancy for a black-body emitter in the wave number region $\omega + d\omega$, given by Planck's distribution function as

$$I^0_\omega d\omega = C_1 \omega^3 d\omega / [\exp(C_2 \omega / T) - 1] \ . \tag{6.6}$$

The spectral emissivity is given by Equation (6.4) in which the mean effective beam length L depends on shape and size of the radiating gas volume.

At sufficiently high gas densities the individual spectral lines in the vibrational-rotational spectrum become pressure broadened in which case the emissivity may be calculated by integrating the measured intensities below each band and replacing the resulting area by a rectangular box having an effective band width $\Delta\omega$ and a mean spectral absorption coefficient $\bar{k}_\omega$. The integrated intensity of an absorption band is given by

$$\phi = \Delta\omega \bar{k}_\omega = \int_{Band} k_\omega \, d\omega \tag{6.7}$$

and, after introducing $\phi/\Delta\omega$ for the mean absorption coefficient in (6.4), yields the band emissivity

$$\epsilon_{Band} = 1 - \exp(-\phi P_g L / \Delta\omega) \ . \tag{6.8}$$

Thus the radiancy of a single band centred around wave length ω is given by

$$I_{Band} = [1 - \exp(-\phi P_g L / \Delta\omega)] \, C_1 \omega^3 \Delta\omega / [\exp(C_2 \omega / T) - 1] \ . \tag{6.9}$$

The total radiancy of a gas is then found as the algebraic sum of the individual band radiancies.

Values of integrated band emissivities for water vapour have been determined by Goldstein[6] at temperatures up to 1000°K and up to 2200°K by Ferriso et al.[7] from spectral measurements on water vapour at pressures up to 15 atm. Table 6.I contains the values from Reference 6.

Values at higher temperature may be calculated from Table 6.I with the help of two semi-empirical relations. The integrated band intensity varies inversely with the absolute temperature

$$\phi = \phi_{300}(300/T) \tag{6.10}$$

and the effective band width may be considered proportional to the square root of the absolute temperature

$$\Delta\omega = \Delta\omega_{300}(T/300)^{1/2} \quad . \tag{6.11}$$

Similar information on carbon dioxide will be found in Reference 8.

Spectral emissivities of hot CO_2-H_2O mixtures in the 2.7 μm region have been reported by Ferriso et al.[9]. This region is of particular interest as the H_2O fundamental level and the CO_2 combination levels overlap. The analysis of the experimental data showed that the emissivity of such mixtures can be calculated from Beer's law, which yields the explicit formula

$$\epsilon(H_2O + CO_2) = \epsilon(CO_2) + \epsilon(H_2O) - \epsilon(H_2O)\epsilon(CO_2) \quad . \tag{6.12}$$

The numerical values of the mixture emissivities are valid over reasonably broad regions of the spectrum.

6.3.2 The Total Emissivity Method

The alternative approach to obtaining information on the radiative properties of gases and gas mixtures is by direct measurement of the total energy emitted by an isothermal volume of gas. Such measurements have been performed by several workers on the two most important combustion products, viz. CO_2 and H_2O (Refs.2, 4, 5). Their results are still widely used for engineering calculations of the radiative heat flux from non-luminous gases.

In these experiments the emission from an isothermal volume of gas is directly compared with that of a black-body emitter at the same reference temperature. The gas emissivity is then defined as the ratio of the energy emitted by the gas divided by that of the black-body. The gas is thus treated as if it were a continuous, grey emitter and the complexities of the true physical nature of gas radiation are taken care of by the choice of suitable variables and the introduction of semi-empirical correction terms.

The practical advantage of this approach lies in the fact that the radiative heat flux can readily be evaluated from the Stefan-Boltzmann equation,

$$\ddot{q}_R = \sigma_B \epsilon_g T_g^4 \quad , \tag{6.13}$$

where σ_B is the Stefan-Boltzmann constant,

ϵ_g the appropriate gas emissivity, which is a function of the absolute temperature and the optical density P_gL ,

T_g the absolute temperature of the gas.

Nearly all experimental data on gas emissivities refer to a total pressure of 1 bar and temperatures below 1500°K. The essential variation of the effective optical density was achieved by either varying the partial pressure of the radiating gas through addition of a non-polar gas, such as nitrogen or argon, or by altering the path length of the beam.

Figures 6.4 and 6.5 represent the emissivity isotherms for CO_2 and H_2O as a function of the optical density. Full lines indicate experimentally verified, broken lines extrapolated isotherms. Owing to the deviation of water vapour from Beer's law, values taken from Figure 6.5 have to be multiplied with a correction factor f , values of which are found in the appropriate textbooks. For gas conditions encountered in rocket thrust chambers, i.e. large optical densities and high partial pressure ratios P/P_{tot} , the correction term f tends towards unity.

In liquid propellant rockets gas temperatures of up to 4000°K are not uncommon and it may at first glance appear questionable to consider extrapolating the existing emissivity data over more than twice the experimentally confirmed temperature range. The coincidence of two favourable circumstances, however, tends to increase the precision of the extrapolated data. As is seen from Figures 6.4 and 6.5 the emissivity isotherms rapidly converge with increasing optical densities and for values of this latter quantity of 1000 and more, the emissivity must be close to an asymptotic value which for CO_2 and H_2O has been estimated to be 0.23 and 0.9, respectively. For a typical case, a hydrogen-oxygen rocket thrust chamber of 30 cm diameter, operating at 60 atm combustion pressure and with a propellant equivalence ratio of 0.8, the optical density would amount to about 1200. Owing to the relative temperature insensitivity of ϵ_g at large values of P_gL even widely extrapolated data may prove to be reasonably reliable for engineering predictions. It is for this reason that the total emissivity method is recommended until reliable new spectroscopic data obtained at the working conditions in rockets, have become available.

6.4 METHOD OF PREDICTING GAS RADIATION IN COMBUSTION CHAMBERS

Heat transfer by radiation in the thrust chamber of a rocket engine is normally calculated by assuming that the sources of thermal emission are the strongly polar equilibrium combustion products. For the hydrogen/oxygen propellant combination this is water vapour, and for propellants based on hydrocarbon fuels, water vapour and carbon dioxide. The partial pressures of these constituents and their adiabatic flame temperatures can readily and accurately be obtained from thermal equilibrium calculations and such data have been compiled for the more widely used propellant combinations[10,11].

Of the various methods of predicting the radiative heat flux from such gas mixtures the "Spectral Absorption Coefficient Method" would probably be the most accurate one, but also more demanding in its application. Bearing in mind that under normal conditions the contribution by thermal radiation to the total heat flux in a thrust chamber is generally a relatively small one, it seems justifiable under these circumstances to recommend the less accurate, but simpler "Total Emissivity Method".

According to this method the radiative heat flux from an isobaric, non-isothermal gas can be written as

$$\ddot{q}_r = (1/\pi) \int_\omega \int_X \sigma_B T^4 (\partial\epsilon/\partial X) \cos\theta \, d\omega dX \quad . \tag{6.14}$$

The quantity $\sigma_B T^4$ is derived from Planck's black-body function $B_\lambda(T)$.

Introducing into Equation (6.14) the angle factor F defined as

$$F = (1/\pi) \int_\omega \cos\theta \, d\omega \quad , \tag{6.15}$$

where θ is the angle between the line of sight of the radiating pencil and the normal to the surface receiving radiation and by combining Equations (6.14) and (6.15) and introducing $X = P_g L$, we obtain

$$\ddot{q}_r = F\sigma_B \int_{P_g L} T^4 [\partial\epsilon/\partial(P_g L)] \, d(P_g L) \quad . \tag{6.16}$$

For easy numerical evaluation by computer programme the total emissivity as a function of the effective optical beam length for various values of the temperature T may be obtained by curve-fitting with polynomials the data presented e.g. by Eckert[12].

For calculations involving the radiative heat transfer in the combustion chamber of a rocket, isothermal conditions for gas and wall may be assumed and the radiative heat exchange between the gas and a bounding black wall is given by

$$\ddot{q}_r = F\sigma_B(\epsilon_g T_g^4 - \epsilon_w T_{wg}^4) \quad , \tag{6.17}$$

where T_g and T_{wg} are the absolute temperatures of the gas and the gas-side wall respectively,

ϵ_g the emissivity of the gas at temperature T_g, and

ϵ_w the absorptivity of the gas for radiation emitted by the wall at temperature T_{wg}.

The surfaces of a combustion chamber radiate, however, as so-called grey surfaces ($\epsilon < 1$) and the calculation of the radiative heat exchange between the gas and the wall is further complicated by the fact, that the energy emitted by the gas is only partially absorbed by the wall, and the rest is reflected back into the gas body. During this process a fraction of the reflected energy is absorbed again by the gas before the remainder reaches another part of the bounding surface. The net effect of these repeated interactions is that only a certain part of the total energy emitted by the gas is actually absorbed by the wall. According to Eckert[12] this effect can be taken care of by introducing a so-called radiation interchange coefficient $\bar{\epsilon}$. Of the energy emitted by the gas, the fraction absorbed by the wall is given by $\bar{\epsilon}_g \sigma_B T_g^4$ and, in the same way the part of the energy emitted by the grey wall and absorbed by the gas amounts to $\bar{\epsilon}_w \sigma_B T_w^4$. The total energy flux exchanged between wall and the enclosed gas body is thus the difference between the two fluxes,

$$\ddot{q}_r = F\sigma_B[\bar{\epsilon}_g T_g^4 - \bar{\epsilon}_w T_{wg}^4] \quad . \tag{6.18}$$

For the radiation interchange factors $\bar{\epsilon}_g$ and $\bar{\epsilon}_w$, in Equation (6.18), Eckert[12] proposed the following approximate relation

$$(1/\bar{\epsilon}) = (1/\epsilon) + (1-\alpha)/(\alpha - \epsilon_\infty) \quad , \tag{6.19}$$

which may be used for evaluating either $\bar{\epsilon}_g$ or $\bar{\epsilon}_w$ at the reference temperatures T_g and T_{wg}. In Equation (6.19), ϵ is the emissivity of the gas for a given optical density and ϵ_∞ is the emissivity of the same gas for an infinitely thick layer. The absorptivity α of the grey wall may be assumed to be independent of wave length.

Elgeti[13] derived an exact equation for ϵ_g in the form of an infinite series

$$\epsilon_g = \alpha^2[\epsilon_{g(1)} + (1-\alpha)\epsilon_{g(2)} + (1-\alpha)^2\epsilon_{g(3)} + ... + (1-\alpha)^{n-1}\epsilon_{g(n)}] \qquad (6.20)$$

which, in comparison with Equation (6.19), showed that for large values of α the above equation by Eckert is a good approximation, but is less accurate for small values of this quantity.

With this relation $\bar{\epsilon}_g$ can readily be computed, provided ϵ_g is known as function of the optical density P_gL. The quantities $\epsilon_{g(1)}$, $\epsilon_{g(2)}$ and $\epsilon_{g(n)}$ represent the emissivity of an isothermal, homogenous gas volume of optical density P_gL, $2P_gL$ and nP_gL, respectively.

An expression analogous to Equation (6.20) can be derived for $\bar{\epsilon}_w$ which differs from Equation (6.20) insofar as the ϵ_g-values are to be replaced by the gas emissivity values ϵ_w evaluated at the corresponding wall temperature.

Values of the emissivity of carbon dioxide and water vapour from an analysis of existing experimental data have been compiled by various authors. The emissivity isotherms shown in Figures 6.4 and 6.5 are due to Eckert[12] and may be further extrapolated to the temperatures and pressures encountered in rocket combustion chambers.

To calculate the radiation interchange coefficient $\bar{\epsilon}$, values of the emissivity of the radiating gas are required for the appropriate reference temperature as functions of the equivalent effective optical beam lengths P_gL, $2P_gL$ to nP_gL. Figure 6.6 shows schematically the procedure involved.

Intuitively it could be expected that $\bar{\epsilon}_g$ and $\bar{\epsilon}_w$ will not only depend on the respective initial values $\epsilon_{g(1)}$ or $\epsilon_{w(1)}$, but also on the absorption coefficient of the wall and, for water vapour, in view of the deviation of this substance from Beer's law, also to a somewhat lesser extent on the partial pressure P_g.

The surprising fact emerging from the analysis presented in Reference 13 is that, for a given value P_gL, a unique value of $\bar{\epsilon}$, independent of temperature is obtained. For both carbon dioxide and water vapour such a correlation may be obtained if instead of ϵ and $\bar{\epsilon}$ the new reduced variables ϵ/ϵ_∞ and $\bar{\epsilon}/\epsilon_\infty$ are introduced, where ϵ_∞ is the emissivity of an infinitely thick gas layer of equal temperature.

The values recommended in Reference 13 for this latter quantity are:

$$H_2O \quad : \quad \epsilon_\infty = 0.90$$

$$CO_2 \quad : \quad \epsilon_\infty = 0.23 \ .$$

These data were shown to be in good accord with values obtained by numerical integration over all relevant absorption bands, and seem to concur with analytically extrapolated values of the total emissivity to large values of P_gL.

The application of this prediction method can also be extended to the practically important mixtures of carbon dioxide and water vapour by introducing a correction term $\Delta\epsilon_\infty$ which allows for the partially overlapping absorption bands of the two gases. The emittance of such a gas mixture is thus given by

$$\epsilon_\infty(H_2O + CO_2) = \epsilon_\infty(H_2O) + \epsilon_\infty(CO_2) - \Delta\epsilon_\infty \ . \qquad (6.21)$$

The corrective term $\Delta\epsilon_\infty$ is not constant and should decrease with increasing temperature. A value of 0.15 was chosen as the best average value for the temperature range considered.

For the numerical value of the emissivity of a carbon dioxide-water vapour gas mixture of infinite layer thickness, one thus obtains

$$\epsilon_\infty(H_2O + CO_2) = 0.90 + 0.23 - 0.15 = 0.98 \ .$$

Figure 6.7, taken from Reference 13, represents a universal diagram for the rapid estimation of the radiation interchange coefficient $\bar{\epsilon}$ for carbon dioxide, water vapour and mixtures of these two gases with grey surfaces of different absorptivities.

The practical use of the diagram is as follows: First, determine the emissivity ϵ at the given temperature and known partial pressure P_g, and effective optical density from Figure 6.4 or Figure 6.5 respectively. With this quantity and the appropriate value of ϵ_∞ the ratio ϵ/ϵ_∞ is obtained. The ratio $\bar{\epsilon}/\epsilon_\infty$ is then readily read from

Figure 6.7 at the point of intersection of ϵ/ϵ_∞ with the line representing the assumed, or known value of the absorptivity α of the wall. Multiplying with ϵ_∞ yields eventually the desired quantity $\bar{\epsilon}$.

For first order approximations it is recommended in Reference 13 to use a simple relation according to which the radiation interchange coefficient is given by

$$\bar{\epsilon} = \alpha\epsilon_{L^*} \tag{6.22}$$

where ϵ_{L^*} is the emissivity at a notional layer thickness $L^* = \alpha^{-0.85} L$. This empirical interpolation equation represents the data in Figure 6.7 with an uncertainty of less than 5 per cent, which in view of the uncertainty of the published emissivity data as such does not seem excessive.

6.5 RADIATION FROM LUMINOUS, PARTICULATE FLAMES

In a rocket combustion chamber burning a hydrocarbon fuel, solid carbon may be formed either as an equilibrium constituent, or in the reaction zone as a transient species. To accurately predict the radiation of such a flame the temperature and the population density of the carbon particles has to be known.

It is probable that in the combustion chamber and in the expansion nozzle the particles will be in thermal equilibrium with the gaseous combustion products. As far as the concentration of solid carbon is concerned thermochemical calculations can only predict the conditions at equilibrium. A large uncertainty in making any prediction arises from the distinct possibility that the propellant mixture ratio may be non-uniform in certain regions of the thrust chamber, thus giving rise to local variation of free carbon formation. A comparatively small increment in the oxidiser/fuel ratio may result in a large increment of carbon concentration..

To treat radiation from carbon particles adequately the mechanism of their formation and their optical properties must be known, and the emittance of a gas stream containing carbon particles must be calculable.

According to Paushkin[14] the formation of carbon depends on several factors, such as degree of atomisation and the temperatures of the fuel and oxidiser, the operating conditions in the combustion chamber (pressure, O/F-ratio) and the chemical nature of the hydrocarbon fuel. It is generally believed that the greater part of the carbon formed originates from the decomposition of the aromatic fractions of the fuel which is comparatively high in certain types of kerosine.

Quantitative predictions are difficult to make and recourse to empirical relations has to be made. For a wide variety of hydrocarbon fuels the amount of carbon formed can be predicted by the following empirical relation proposed by Penner et al.[15],

$$C = (1/K_3) \log_e (K_1 R - K_2) + (T_b/K_4) - K_5 \quad , \tag{6.23}$$

where C is the rate of carbon formation

R the carbon/hydrogen ratio,

T_b the boiling temperature of the fuel,

K_1 to K_5 are empirically determined constants numerical values of which are given in Reference 16.

A knowledge of the particle size in flames is an important factor in determining the thermal emission from such flames. Observations on flames from many different fuels showed that carbon particle diameters ranged from 100 Å to 2000 Å. A carbon particle size analysis performed on the exhaust of an RP1/LOX rocket engine gave an average particle size of 350 Å, the size distribution being Gaussian[16]. This observation agrees well with measurements on particles from the exhaust of an $F-1$ engine where particle sizes varied from 200 Å to 600 Å (Ref.17). Comparatively little information seems to have been published on particle concentration. Tesner[18] found from a study of the thermal degradation of various hydrocarbons that carbon particle concentration ranged, depending on the nature of the substance, from 2×10^{10} to 2×10^{12} particles per cm^3. From these and other supporting observations not referred to here, a particle diameter of 400 Å can be considered a representative value for most luminous hydrocarbon flames.

6.5.1 Radiation from a Particle Cloud

Several methods of predicting the emittance of carbon particles and particle clouds have been proposed and the one presented here, the so-called "inverse wave length method" was chosen on account of the relative simplicity with which numerical predictions of the radiative heat flux can be made. This method has widely been used for predicting the monochromatic mass absorption coefficient $k_{m,\lambda}$ and the monochromatic emittance ϵ_λ of particulate clouds. According to this empirical relation the above quantities are related by

$$k_{m,\lambda} = C\lambda^{-A} \tag{6.24}$$

and

$$\epsilon_\lambda = 1 - \exp(-k_{m,\lambda} VL) = 1 - \exp(-C\lambda^{-A} VL) , \tag{6.25}$$

where C is a constant, independent of wave length,

V the volume fraction of carbon particles*

L the thickness of the luminous flame.

The term A is not constant over a wide spectral range but its variation is small. From an analysis of the results of various experimental studies Siddall and McGrath[19] concluded that for the visible range of the spectrum the exponent A may, as a first approximation, be assumed independent of wavelength, but for the infra-red regime a relation of the following form

$$A = a - b \log_e \lambda , \tag{6.26}$$

(where a and b are numerical constants) is preferred for correlating the available experimental data. The total emittance is then obtained by integrating over all wave lengths,

$$\epsilon_P = \int_0^\infty [1 - \exp(-C\lambda^{-A} VL)] B_\lambda \, d\lambda \Big/ \int_0^\infty B_\lambda \, d\lambda , \tag{6.27}$$

where B_λ is Planck's black-body intensity function.

According to Schack[20] the mass absorption coefficient for the near-infrared and visible region is satisfactorily expressed by

$$k_{m,\lambda} = 0.57/\lambda . \tag{6.28}$$

With the assumption of isothermal conditions within the particle cloud, Sato and Matsomoto[21] evaluated the integral (Eqn (6.27)) and gave the following solution for the total emittance of a cloud of particles

$$\epsilon_P = 1 - (15/\pi^4)\psi'''(X + 1) , \tag{6.29}$$

where $X = CVLT/C_2$,

C_2 is the second Planck constant

T the temperature of the particles.

$$\psi'''(X + 1) = (d^4/dX^4) \log_e \Gamma(X + 1) , \tag{6.30}$$

where $\Gamma(X + 1)$ is the Gamma function.

The above relation can readily be evaluated with the aid of the Gamma function tables. As was shown in Reference 21 the results of this analysis closely approximate those of Schack[20]. Figure 6.8 which was taken from Reference 20 analytically extrapolated to 3400°K, shows the dependence of the emittance of the luminous flame as a function of the variable (CVL) with the temperature as a parameter. It will be noticed that the emittance of the flame increases with rising temperature, a consequence of the fact that the intensity maximum of black-body emission moves towards shorter wave lengths and the emittance of carbon particles is larger for short wave length radiation.

6.5.2 Radiation from a Luminous Flame Containing Solid Particles

The radiation from a luminous flame consists of two contributions, viz. that of the cloud of particles which has already been discussed at length in the preceding section, and that of the non-luminous gaseous atmosphere in which the particles are carried in suspension. This atmosphere contains gas constituents which themselves emit thermal radiation, e.g. water vapour and carbon dioxide. Assuming that the radiating gas constituents are uniformly distributed in the flame and that the temperature of the suspended particles is equal to that of the surrounding gases, the monochromatic emittance of the luminous flame can be written as the algebraic sum of the two contributions

---

* The volume fraction V is related to the particle density, N_p , by:

$$N_p \bar{m}_c / c = V$$

where N_p is the number of particles per cm^3 of gas

$\bar{m}_c$ the average mass of one carbon particle, and

c the density of carbon

$$\epsilon_{\lambda,f} = 1 - \exp\left[-(k_{m,\lambda}V + k_{mg})L\right] . \tag{6.31}$$

This simplified approach is restricted to optically thin flames ($CVL < 0.4$). For flames with a high particle cloud emittance the contribution due to gas radiation must be progressively reduced as the sum of both contributions cannot exceed black-body emission in any part of the spectrum. For large values of CVL the contribution to $\epsilon_{\lambda,f}$ due to gas radiation can therefore be completely neglected.

With these reservations the total emittance of the luminous flame can be evaluated in a way analogous to that for the particle cloud. The result given in Reference 21 reads

$$\epsilon_f = 1 - (15/\pi^4)(1 - \epsilon_g)\psi'''(X + 1) . \tag{6.32}$$

Luminous flames and the receiving bounding surfaces of a thrust chamber may be considered diffusely emitting and reflecting surfaces and it is further permissible to consider them optically grey surfaces.

The evaluation of radiative heat exchange between such bodies depends on the knowledge of their geometric configuration. The quantity which provides information on the fraction of diffusely distributed energy emitted by one surface and received by the other is commonly known as the view factor, or the angle factor; the latter term will be used in this presentation.

The analytical methods employed in determining angle factors are described in detail in various textbooks. Before carrying out the tedious computations involving the determination of angle factors it is advisable to consult available compilations of angle factors. An excellent survey of such information with numerous useful references, will be found in the textbook by Sparrow et al.[22]. Configurations which are commonly met in calculation of radiative heat transfer in rockets are:

(a) A cylinder filled with a grey-body emitter (luminous gas).

(b) A circular surface emitting to a cylindrical surface element.

(c) Two circular surfaces a certain distance apart radiating to each other.

The analytical expressions for these factors as a function of various non-dimensional lengths are given in Reference 22, but for most practical calculations the accuracy attainable by reading values from the graphical presentations of the angle factors in the above reference will be found adequate.

The net radiative heat flux received at any part of the internal surface of the thrust chamber further depends on the emissivity of the solid surface and the wall temperature T_{wg}. Whilst reliable values of the emissivity of a clean metallic surface may be found in literature, in practice the surfaces of rocket thrust chambers very quickly change either through oxidation of the metallic wall, or by the deposition of solid combustion products, e.g. a layer of carbon. In particular, the latter has frequently been observed in kerosine fuelled rockets and was considered to be the cause of a pronounced reduction of the total heat flux. Owing to the relatively poor conductivity of a thin, porous carbon layer in comparison with that of a metallic material, the surface temperature of a wall covered with a carbon layer attains a much higher value than that of a clean surface. Hence the driving temperature difference between the gas stream and the wall is diminished, and both convective and radiative heat fluxes are markedly reduced. However, these beneficial effects of a carbon deposit are difficult to predict numerically, and for evaluation of the radiative heat flux, unless specific conditions apply, it is best to consider the surface as mildly oxidised. Appropriate values for the emissivity of clean and oxidised surfaces pertaining to metals used in rocket chamber construction are found in Chapter 17.

With this information to hand the radiative heat flux between a luminous flame and the walls of the rocket chamber can be evaluated from

$$\dot{q}_r = \sigma_B F \epsilon_f \epsilon_w [T_f^4 - T_{wg}^4] , \tag{6.33}$$

where F is the angle factor between the two surfaces

ϵ_f, ϵ_w the emissivity of the flame and the receiving wall respectively,

T_f, T_{wg} the respective temperatures of flame and gas-side wall.

6.6 RADIATION MEASUREMENTS IN ROCKET THRUST CHAMBERS

In the previous section on the recommended procedure for the numerical evaluation of radiation from combustion gases it was tacitly assumed that the complex dissociated gas mixture in the combustion chamber is in thermal and chemical equilibrium. Only for this condition can the gas temperature and the partial pressures of the various

gas constituents be predicted from thermochemical calculations. In a combustion chamber chemical equilibrium is attained at a certain distance from the injector face which depends largely on the efficiency of the propellant evaporating and mixing process. Immediately upstream of this zone is the reaction or flame zone which is characterized by the absence of thermochemical equilibrium and in which short-lived, transient molecules and atoms may be formed at concentrations exceeding by far those in the equilibrium zone. Apart from qualitative observations on flames there is no known method by which numerical estimates of either the concentrations, or indeed the nature and the state of excitation of some of these transient species can be made.

One might be inclined to query the significance of this non-equilibrium zone with respect to the calculation of radiative heat transfer processes in rocket engines and to provide an explanation, reference must be made to certain steps in the practice of rocket development.

In a new rocket propulsion system the diameter of the combustion chamber is usually determined by injector requirements, and a length chosen to provide nearly complete combustion of the propellants. In its later stages, this combustion process follows a more-or-less exponential law (see Chapter 4) achieving complete combustion only at an infinite distance. Usually the chamber length is chosen at some point where nearly all of the combustion will have taken place, and specific impulse values of perhaps 92-98% of the theoretical equilibrium values are obtained.

From this it is apparent that, as far as the combustion chamber is concerned, equilibrium conditions are never really attained in highly efficient propulsion systems, but the gas composition in the nozzle itself and just beyond the exit cone, are very close to chemical equilibrium. Estimates of the radiative heat flux in these zones can therefore be made in the manner outlined above.

It is obvious that predictions of radiative heat transfer in the combustion chamber based on equilibrium gas conditions must remain suspect and the question arises as to how the problem can be approached. Fortunately, there have been a few isolated experimental studies conducted exclusively on small scale chambers which have thrown some light on the subject of flame radiation in liquid propellant rockets.

Power and Omori[23] studied the total radiation at the downstream end of a 2.5 in. diameter RFNA/Hydrazine combustion chamber at pressures between 300-600 lb/in^2 and found that the radiative heat flux, according to temperature and pressure, varied from 0.17 to 0.47 Btu/in^2 sec, a result which expressed in terms of black-body emission, amounts to overall emissivities between 0.13 and 0.27. Using a similar but somewhat improved experimental set-up, Robinson and Van Grouw[24] measured the total and the spectral emissivity of radiation emitted from the high pressure combustion products (nominally at 700 lb/in^2) of three propellants. Water vapour was for these propellants the dominant radiating gas constituent.

Figure 6.9 shows the variation of the experimental emissivity with combustion gas temperature. Attention is drawn to the fact that the results obtained by the "spectral absorption method" consistently fell below those obtained by the "total emissivity method". It was suggested by the authors of Reference 24 that radiation emitted at wave lengths below the cut-off limit of the spectrometer used (1.14 μm) remained undetected in their tests and may have been the cause of this discrepancy. Such wave bands do in fact exist for H_2O as is evident from Figure 6.2 and it seems not unlikely that at higher temperatures and elevated pressures their contribution may become significant.

Using a novel flow variation technique, Ziebland[25] reported values of the radiative heat flux in a small, kerosine-oxygen combustion chamber for various pressures and equivalence ratios. The experimental results were always markedly higher than those calculated by the equilibrium emissivity method, an observation which was repeated in subsequent studies on the hydrogen-oxygen system by the same author[26].

It will be seen from Figure 6.10 which represents the experimental results of Reference 26 for two injector configurations, that all experimental points lie within 10% of a curve representing 22% black-body emission at the appropriate temperatures for each equivalence ratio.

The concurring evidence on the magnitude of the radiative flux from this and the two earlier observations tend to support the postulate that the excessive radiative heat flux must be due to a flame continuum, i.e. emission from transient, excited species in the non-equilibrium, or reaction zone of the system, which in the case of water vapour, cannot be associated with radiation from solid particles, as has always been assumed the cause with hydrocarbon flames.

It is known that the low pressure (atmospheric) H_2–O_2 flame is almost completely transparent, but visual observation on this flame at high pressures inside the combustion chamber indicated strong emission of bright, bluish-white light, i.e. a continuum extending into the visible region of the spectrum. This unexpected light emission from a high pressure H_2–O_2 flame was already observed as early as 1890 by Liveing and Dewar[27] and later by others[28,29] who found from direct absorption measurements that the OH concentration was more than an order of magnitude larger than the corresponding equilibrium concentration and that recombination reactions involving excited OH molecules were the probable cause of the intense continuum[30]. In contrast, calculated data by Bonner[34] using the spectral emissivity method amounted to only 20-25% of the experimental results, as is seen in Figure 6.10.

Conclusive proof of the reality of flame radiation was provided by the qualitatively and quantitatively concurring observations of two independent workers viz. Burrows[31,32] and Ziebland[33] who investigated the emission from the combustion gases in hydrogen-oxygen combustion chambers normal to the flow path of the gas at various distances from the injector face. Figure 6.11 taken from an unpublished report[33] shows the axial variation of the total radiative heat flux in a combustion chamber of 5 cm diameter at a total pressure of 45 bar. As is seen, the radiative heat flux rises sharply at a certain distance from the injector face and with increasing distance falls equally steeply to a slowly diminishing value of about 1/5 to 1/4 of the peak value.

It is believed that the zone around the peak radiative heat flux represents the non-equilibrium (reaction) zone and the following, flattish part of the heat flux curve, the equilibrium zone. Support for this interpretation is lent by the results of some calculations which showed that the observed radiative heat flux from the equilibrium zone exceeds by only a relatively small amount that predicted by the total emissivity method, whereas, of course, the peak radiative heat flux was about 2.5 to 3 times the calculated value. If we identify the end of the falling branch of the heat flux curve of Figure 6.11 with the attainment of chemical equilibrium, the design engineer would prefer not to extend the cylindrical combustion chamber beyond this point. It is unfortunate, however, that our present state of knowledge is insufficient to suggest a way to numerically predict from basic data the radiative heat flux due to luminous gas radiation such as has been observed e.g. with the hydrogen-oxygen system.

6.7 CONCLUSIONS

Although the spectral absorption method is claimed to be more accurate a recent examination of many papers on spectral measurements on water vapour disclosed a large measure of disagreement in the absorption coefficients reported in literature. Differences by a factor of 2 to 3 among various researchers were fairly common, and were as high as a factor of 10 in some wave band regions[35]. Extensive measurements at high temperatures and for optical densities between 100 and 1000 cm-bar for which there is apparently no data at all available, are badly needed.

Likewise the total emissivity method suffers from a similar lack of directly relevant data, but certain trends in the behaviour of emissivity with increasing temperature and optical density tend to make numerical predictions not quite as uncertain as might be expected.

First, for the currently used large thrust chambers and their operating conditions, optical densities for the major radiating gas, i.e. water vapour, of the order of 1000 and more could be expected. Under these conditions, even the equilibrium gas radiation from water vapour alone will attain values of 60% and more of the appropriate black-body radiation. It seems therefore probable that the quantitative differences between flame radiation and the equilibrium gas radiation will tend to diminish with increasing optical densities and that for large combustion chambers and/or high operating pressures, near-black-body emission will be attained. Hence, the extrapolation of the total emissivity data shown in Figure 6.5 to rocket conditions, is probably the most economic method to date.

Likewise, luminous radiation due to carbon particle emission in hydrocarbon-oxygen propellants will also tend to raise the emissivity to values approaching unity as is seen from Figure 6.8. To what extent the radiation directed towards the injector will be attenuated by the partial absorption and scattering of hydrocarbon fuel droplets has not yet been evaluated.

Tables 6.II and 6.III show that the resultant heat fluxes are by no means negligible as has been often assumed and must be considered in the design studies of the cooling requirements for the least protected part of the combustion chamber, viz. the surface of the injector. It is not improbable that the failures encountered with injectors for high pressure hydrogen-oxygen engines can be attributed to this circumstance.

As neither oxygen, nor hydrogen possess absorption bands in the near-infrared and visible region of the spectrum, protection against excessive radiative heat transfer to the injector by propellant droplets is negligible. It should also be noted that the efficacy of normal film cooling involving fluids transparent to radiation, is markedly reduced. Highly reflecting surface coatings and external cooling may provide the best method of protection under these conditions.

REFERENCES

1. Chisholm, H.L. Welsh, D.A. — *Induced Infrared Absorption in Hydrogen and Hydrogen Foreign Gas Mixtures at Pressures up to 1500 atm.* Canad. J. Phys., Vol.32, 1954, pp.291-311.

2. Schmidt, E. — *Messung der Gesamtstrahlung des Wasserdampfes bei Temperaturen bis 1000°C.* Forschg. Ing. Wes., Vol.3, 1932, pp.57-70.

3. Schack, A. — *Die Strahlung von Feuergasen.* Arch. Eisenhüttenw, Vol.13, 1939, p.241.

4. Eckert, E.R.G. — *Messung der Gesamtstrahlung von Wasserdampf und Kohlensäure bei Temperaturen bis zu 1300°C.* VDI-Forschg.H.387, 1937, pp.1-20.

5. Hottel, H.C. Mangelsdorf, H.G. — *Heat Transmission by Radiation from Non-Luminous Gases.* Trans. Am. Inst. Chem. Eng., Vol.31, 1935, pp.517-549.

6. Goldstein, R. — *Measurements of Infrared Absorption by Water Vapour at Temperatures to 1000°K.* J.Quant. Spectrosc. Radiat. Transfer, Vol.4, 1964, pp.343-352.

7. Ferriso, C.C. Ludwig, C.B. — *Spectral Emissivities and Integrated Intensities of the 2.7 m H_2O Band between 530°K and 2200°K.* J. Quant. Spectrosc. Radiat. Transfer, Vol.4, 1964, pp.215-227.

8. Ferriso, C.C. Ludwig, C.B. — J. Opt. Soc. Am., Vol.54, 1964, p.651.

9. Ferriso, C.C. Ludwig, C.B. — *High Temperature Spectral Emissivities of CO_2-H_2O Mixtures in the 2.7 μm Region.* Appl. Opt., Vol.3, 1964, pp.1435-1443.

10. Svehla, R.A. — *Thermodynamic and Transport Properties for the Hydrogen-Oxygen System.* NASA SP-3011, 1964.

11. Ziebland, H. — *Some Computed Thermodynamic Data for the Products of Combustion of the Oxygen-n-Heptane Propellant.* ERDE Rep.18/R/60, 1961.

12. Eckert, E.R.G. — *Heat and Mass Transfer.* McGraw Hill Book Co., New York, 1959.

13. Elgeti, K. — *Ein neues Verfahren zur Berechnung des Strahlungsaustausches zwischen einem Gas und einer grauen Wand.* BWK, Vol.14, 1962, pp.1-6.

14. Paushkin, Ya. M. — *The Chemical Composition and Properties of Fuels for Jet Propulsion.* Pergamon Press, New York, 1962.

15. Penner, S.S. Datner, P.R. — *Combustion Problems in Liquid Fuel Rocket Engines.* International 5th Symposium on Combustion, Reinhold Publishing Co., New York, 1955.

16. Boynton, F.P. — *Studies of Carbon Particles Formed by Small, Hydrocarbon-Fuelled, Rocket Engines.* General Dynamics/Convair, ERR-AN-007, 1960.

17. – — *Radiation and Structural Characteristics of Rocket Exhaust Gases.* Rocketdyne R-6742, 1966.

18. Tesner, P.A. — *Formation of Dispersed Carbon by Thermal Decomposition of Hydrocarbons.* Seventh Symposium (International) on Combustion, Butterworths, London, 1959.

19. Siddall, R.G. McGrath, I.A. — *The Emissivity of Luminous Flames.* 9th Symposium on Combustion, Academic Press, 1963.

20. Schack, A. — *Strahlung von leuchtenden Flammen.* Z.F. tech, Phys., Vol.6, 1925, p.530.

21. Sato, T. Matsomoto, R. — *Radiant Heat Transfer from Luminous Flames.* International Developments in Heat Transfer, ASME, New York, 1963.

22. Sparrow, E.M. Cess, R.D. — *Radiation Heat Transfer.* Brooks/Cole Publishing Co., Belmont, California, 1966.

23. Powell, W.B. Omori, T.H. — *Radiation of Rocket Motor Combustion Gases.* J.P.L. Progr. Rep. No.20-166, 1953.

24. Robinson, D.E. Van Grouw, S.I. — *Observed Emissivities of Rocket Combustion Gases.* Final Rep. AFOSR 1904, 1961.

25. Ziebland, H. — *Radiation and Convection in High Energy Liquid Propellant Rocket Engines.* 1961 International Heat Transfer Conference, Boulder, Colorado, USA.

26. Ziebland, H. — *An Introduction to Heat Transfer in Hydrogen-Oxygen Rocket Combustion Chambers.* Unpublished Ministry of Technology Report.

27. Liveing, G.D. Dewar, J. — *On the Influence of Pressure on the Spectra of Flames.* Proc. Roy. Soc. XLIX, 1891, p.217.

28. Avramenko, L. Kondratjew, V. — Acta physicochimica USSR, Vol.7, 1937, p.567.

29. Kondratjew, V. Zirkin, M. — Acta physicochimica USSR, Vol.6, 1936, p.307.

30. Wolfhard, H.G. Diederichsen, J. — *Spectrographic Examination of Gaseous Flames at High Pressures.* Proc. Roy. Soc., Vol.A.236, 1956, p.89.

31. Burrows, M.C. Povinelli, L.H. — *Emission Spectra from High Pressure Hydrogen-Oxygen Combustion.* NASA TN D-1305, 1962.

32. Burrows, M.C. — *Radiation Processes Related to Oxygen-Hydrogen Combustion at High Pressures.* NASA TN D-2541, 1964.

33. Ziebland, H. — Unpublished Ministry of Technology Report.

34. Bonner, B.H. — *Calculation of the Thermal Radiation Emitted by Water Vapour at High Pressures and Temperatures.* RPE Tech. Memo 347, 1965.

35. Ferriso, C.C. et al. — *Empirically Determined Infrared Absorption Coefficients of H_2O from 300°K to 3000°K.* J. Quant. Spectrosc. Radiat. Transfer, Vol.6, 1966, p.241.

TABLE 6.I

Integrated Band Intensities Normalised to 300°K for Water Vapour

Band Centred at Wave Length μm	*Integrated Intensity at 300°K* $cm^2 atm^{-1}$
1.38	16.1
1.87	21.6
2.7	194
6.3	225

TABLE 6.II

Variation of Black-Body Radiative Heat Flux with Absolute Temperature

T	*Radiative Heat Flux*	
°K	cal/cm^2 *sec*	W/cm^2
1400	5	21
1600	9.5	38
1800	14.5	61
2000	22	92
2200	32	134
2400	45.5	190.5
2600	63	264
2800	84	352
3000	110.5	462
3200	144.5	605
3400	184	770
3600	233	974
3800	284	1188

TABLE 6.III

Adiabatic Flame Temperatures for Stoichiometric Mixtures of the Kerosine-Oxygen and Hydrogen-Oxygen Propellant at Various Pressures

P *Bar*	*Kerosine-Oxygen* °K	*Hydrogen-Oxygen* °K
10	3410	3400
30	3580	3560
60	3690	3660
100	3760	3750

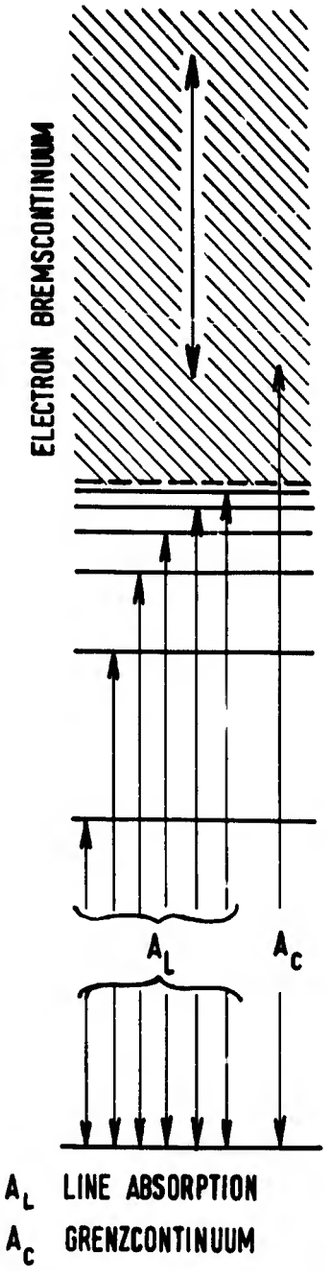

Fig.6.1 Energy levels within an atom

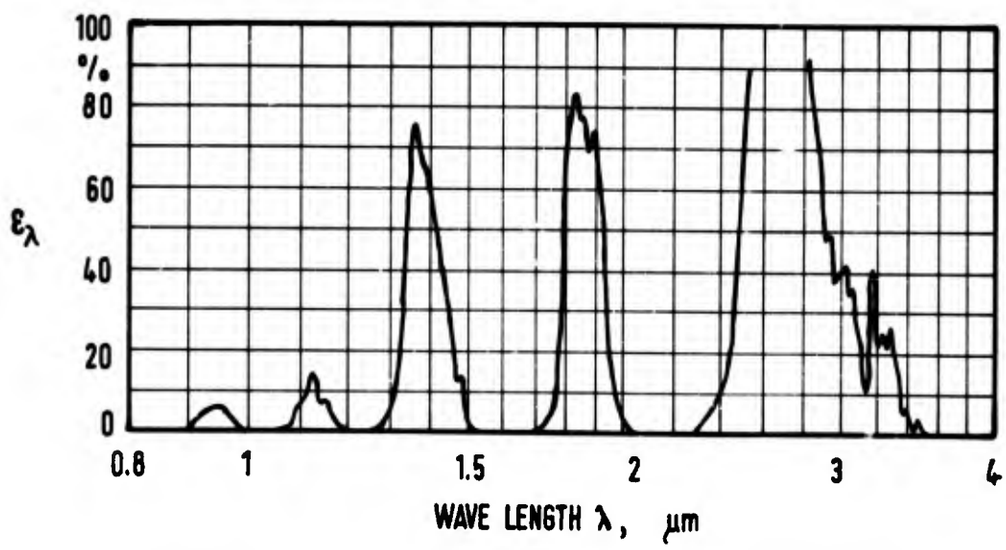

Fig.6.2 Spectrum of water vapour (according to Schmidt[2])

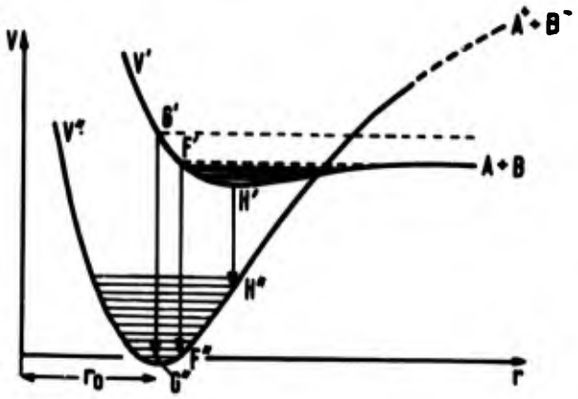

Fig.6.3 Potential curves showing the formation of an ion molecule with simultaneous emission of a recombination continuum

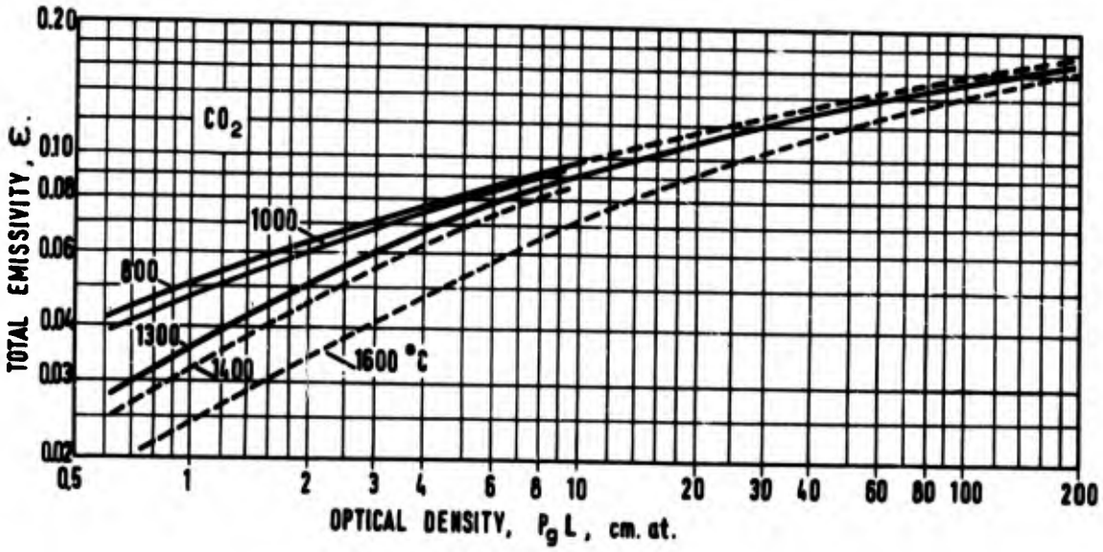

Fig.6.4 Emissivity isotherms for CO_2 (according to Eckert[4])

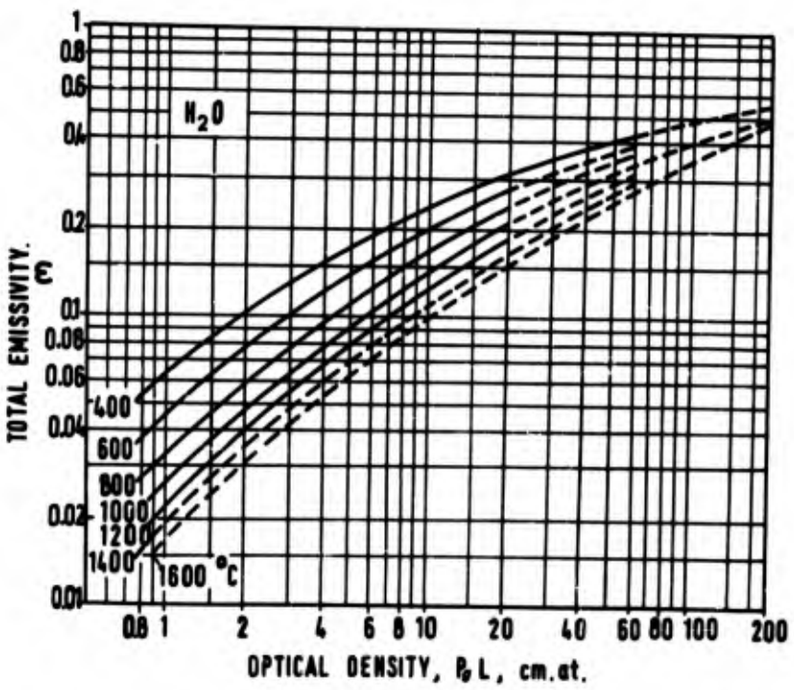

Fig.6.5 Emissivity isotherms for H_2O (according to Eckert[4])

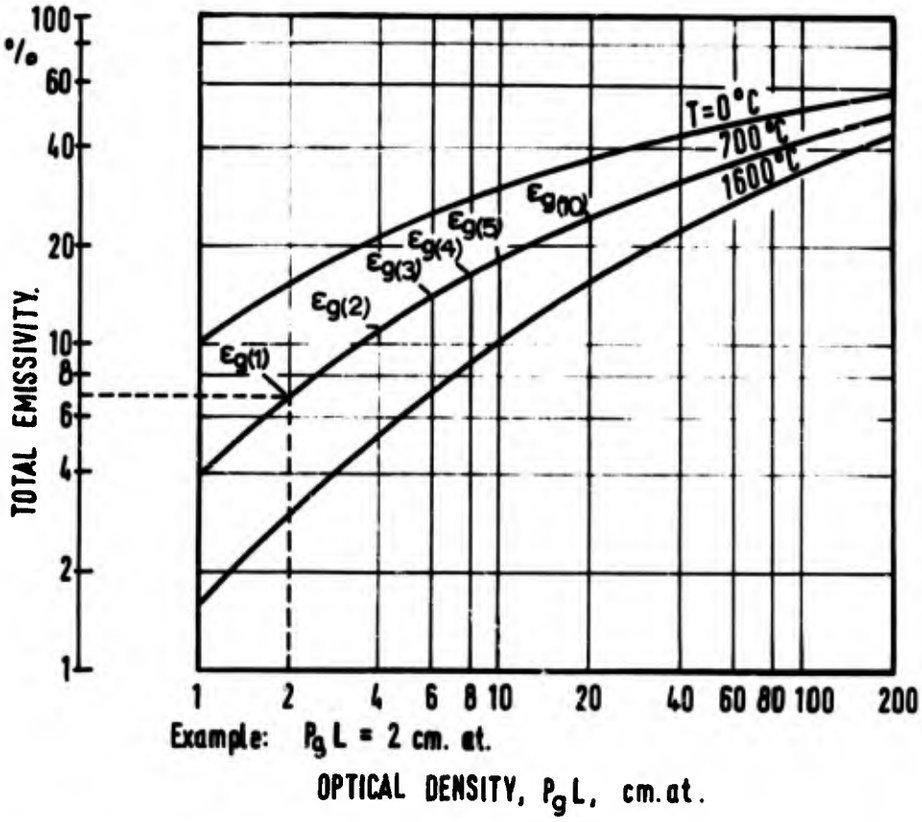

Fig.6.6 Graphical method of evaluating the radiation interchange coefficient $\bar{\epsilon}_g$ according to Equation (6.20). Data refer to a layer of water vapour at 700°C

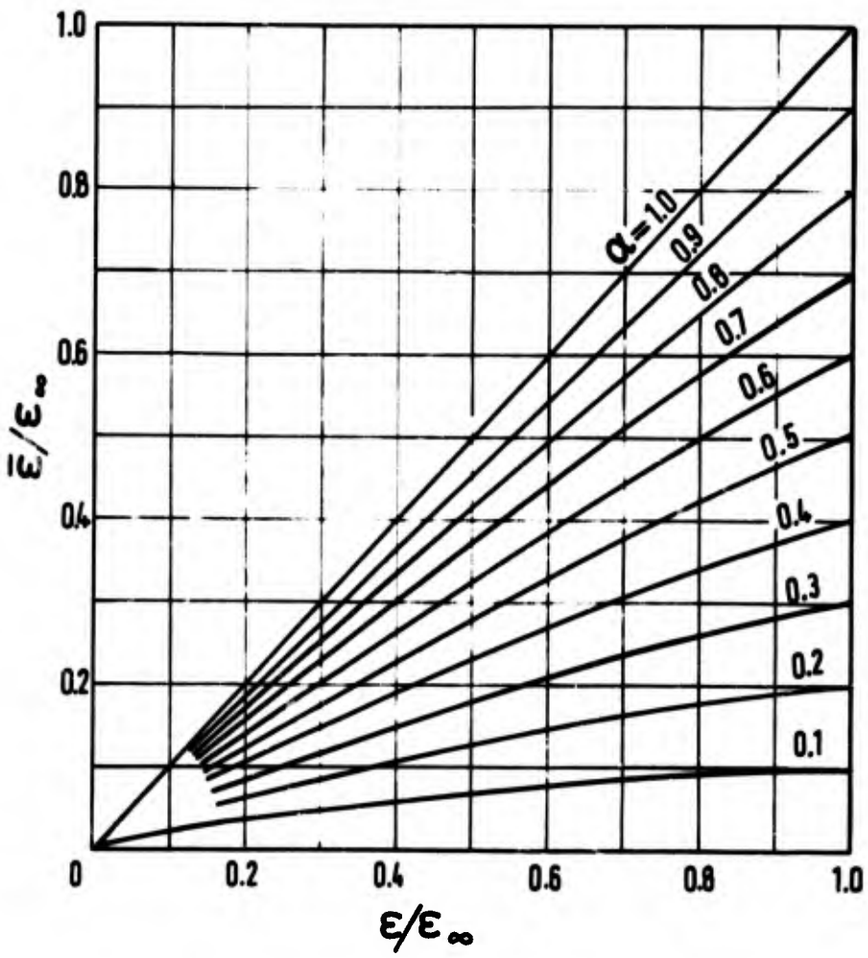

Fig.6.7 Universal diagram for estimating the radiation interchange coefficient $\bar{\epsilon}$ for CO_2, H_2O and mixtures of these gases (according to Elgeti[13])

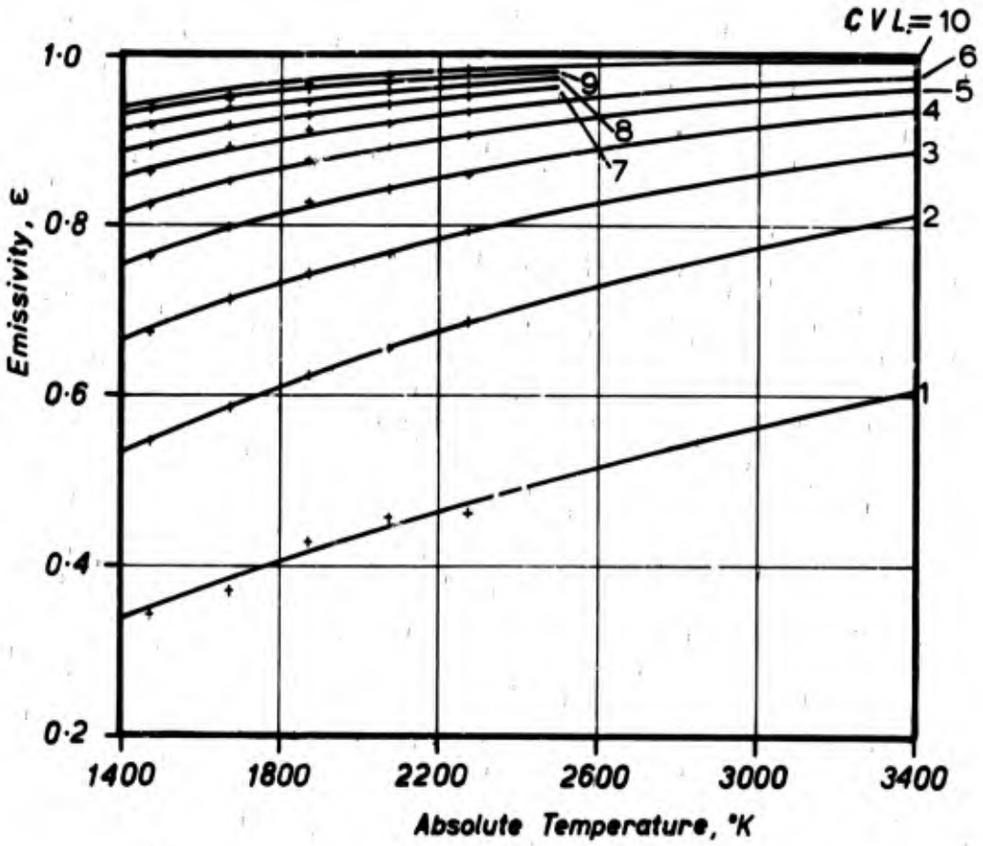

Fig.6.8 The emittance of flames containing luminous carbon particles as a function of optical thickness and temperature (data analytically extrapolated from Reference 20)

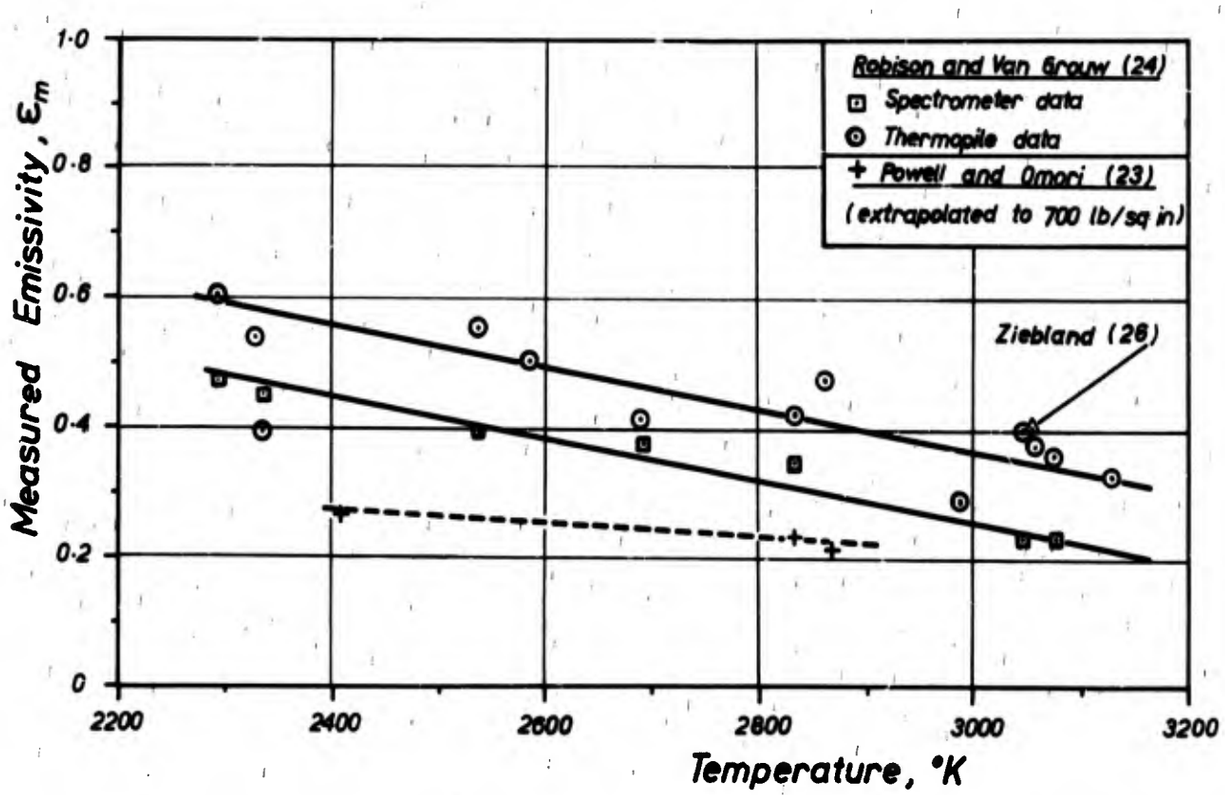

Fig.6.9 Measured emissivities of rocket engine combustion gases at elevated pressures (Ziebland[25])

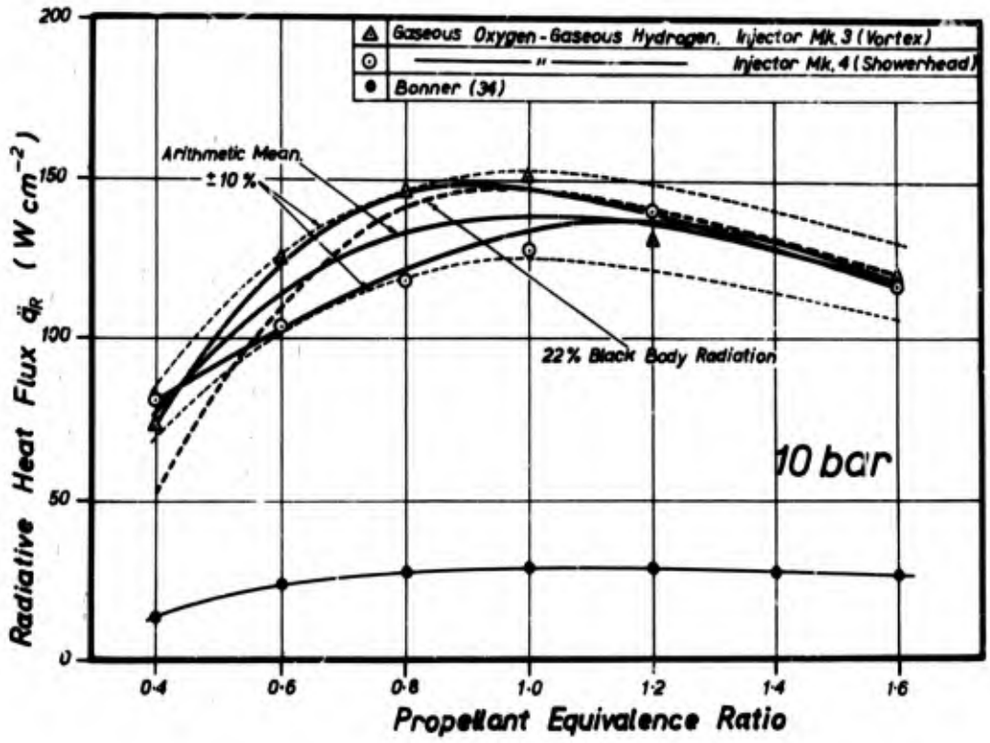

Fig.6.10 Experimental radiative heat flux in a hydrogen-oxygen rocket combustion chamber (Ziebland[26]). Crown Copyright Reserved

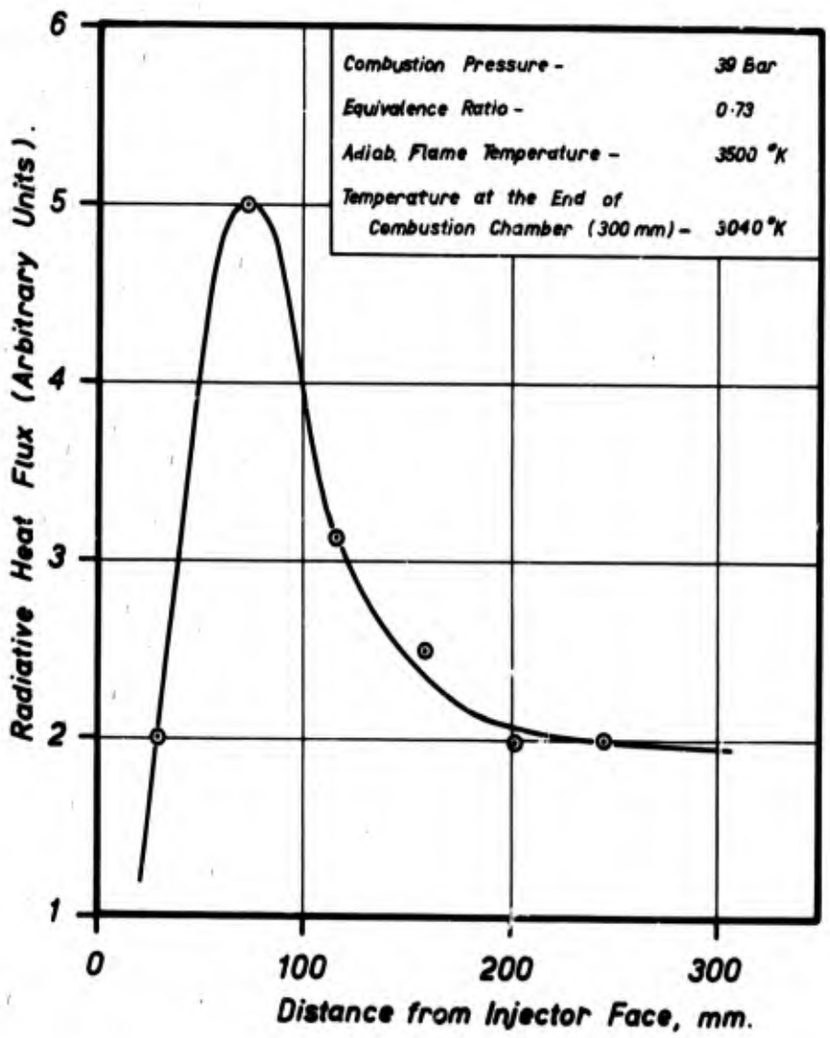

Fig.6.11 Variation of radiative heat flux in a hydrogen-oxygen combustion chamber measured normal to the flow path of the combustion gases (Ziebland[33]). Crown Copyright Reserved

CHAPTER 7

COOLANT HEAT TRANSFER

7.1 GENERAL

In view of the wealth of information available on forced convective heat transfer to fluids it could be assumed that the prediction of the required local coolant flow velocities for the adequate protection of all areas of the thrust chamber would not present any unusual difficulty. The analysis of practical experience on rocket engines, however, has revealed a number of interesting novel phenomena which are the consequence of peculiar operating conditions, such as the high rates of heat flux in liquid propellant rocket engines, the conditions of state of the coolant, etc. It seems indicated therefore, to give at first a brief qualitative survey of forced convection processes at high heat fluxes, followed by recommended procedures for the numerical prediction of the influence of the various phenomena on coolant heat transfer.

As long as the coolant remains in the liquid phase in all areas of the duct -- and that includes the fluid in immediate contact with the heated surface – heat transfer is by single-phase, forced-flow convection. Assuming the property variation of the coolant is not excessive, the heat transfer coefficient at different rates of heat transfer may be considered approximately constant and the heat flux from the wall to the coolant is proportional to the temperature difference between the coolant-side wall and the bulk of the fluid.

$$\ddot{q} = h(T_{w,c} - T_b) .$$

This single phase regime is represented by the line linking points 1 and 2 in Figure 7.1.

With increasing heat flux the temperature difference between wall and liquid progressively rises until the wall temperature on the coolant side has reached the boiling point of the respective coolant. This latter temperature, of course, varies with the local coolant pressure. At this point small vapour bubbles are being formed at preferred sites on the heated surface which, after having detached themselves from the surface, are immediately condensed as the bulk of the coolant has a temperature well below the boiling point.

The frequency of the bubble formation and collapse, and the number of active sites both increase with heat flux. Owing to the disturbance produced in the boundary layer by this phenomenon and the disruption of the laminar sub-layer which represents the largest resistance to heat exchange, the heat transfer rates attainable under these conditions are markedly higher than those for single phase convection. This regime is generally known as forced convection nucleate boiling.

For identical flow conditions and the same temperature difference between wall and bulk coolant as much as seven times the heat flux for the single-phase regime can be transferred in the nucleate boiling regime, and it is understandable that considerable attention was paid by researchers to the study of this phenomenon.

With further rising heat flux the vapour forming nuclei on the heated surface become so numerous that small localized vapour blankets of transient existence are being formed at sites of high nucleation density until at 3 a maximum heat flux is reached. Exceeding that unstable point, an even very small incremental increase in heat flux will cause the numerous bubbles to coalesce into a more or less continuous vapour blanket which separates the bulk of the coolant from the heated wall. This condition is a stable one even if the wall temperature on the fluid side exceeds by several hundred degrees the bulk coolant temperature and has been termed the "burn out" point.

In this case the temperature drop across the boundary layer is no longer controlled by the properties of the coolant in its liquid phase but by those of the stable vapour film, whose thermal conductivity is about an order of magnitude less than that of the corresponding liquid phase. In consequence in order to sustain heat flux just above point 3, the required driving temperature difference jumps to point 4 which may be one to two orders of magnitude larger than that needed for the nucleate boiling regime. The consequent increase of the wall temperature is such that unless special precautions are taken instantaneous overheating and destruction of the wall would result if this condition were allowed to take place.

Suppose a transient situation exists whereby point 4 in Figure 7.1 has been reached. By progressively reducing the heat flux below the level of 3–4, the stable film boiling regime can be sustained up to point 5, below which a sudden transition to the stable nucleate boiling regime, accompanied by an appropriate marked drop in the driving temperature difference, takes place.

It is obvious that the regime of stable nucleate boiling is of primary interest to the rocket engineer as very large heat fluxes can be absorbed with comparatively small temperature differences between coolant-side wall and bulk fluid.

As nucleate boiling is a predominantly vapour phase controlled phenomenon, it follows that the state of the cooling fluid, notably its pressure, must have a marked effect on the phenomenon. Not only will the onset of nucleate boiling be delayed at higher coolant pressures but also the maximum values of nucleate boiling heat flux will change, as shown schematically in Figure 7.1. Nucleate boiling, being a two-phase phenomenon, will cease to exist when the pressure of the coolant sufficiently exceeds its critical value. Heat transfer in the region close to the critical point of the coolant is markedly affected by the rapid changes of all its physical properties with temperature.

Additional complications arise from the geometric shape of the cooling ducts which usually have a rectangular cross-section and are strongly curved in the region of the expansion nozzle. Further, the cooling ducts are heated on one side only and the effect of non-uniform heating on flow and heat transfer must also be examined.

Apart from these problems which are common to many regenerative cooling systems, due attention must also be paid to the thermal behaviour of the selected coolant at elevated temperatures. Although it may be possible to keep the bulk coolant temperature below a critical level, owing to the high fluxes in certain areas, e.g. around the nozzle throat, and local wall temperatures may closely approach, or even exceed the safe operating temperature for the fluid in question. It is in these cases that provisions have to be made for the coolant velocity to be raised in order to effect the necessary drop in the wall temperature or additional cooling, such as film cooling, may have to be provided locally.

The influence of these various factors will be discussed in greater detail in the following sections.

7.2 SINGLE-PHASE, FORCED FLOW CONVECTION

Most workers who studied high-intensity heat transfer in forced flow convection systems found it adequate to correlate their results with the aid of simple variants of the basic Nusselt equation. To allow for certain specific effects e.g. that of the large temperature difference between the wall and the bulk of the fluid on the transport properties of the coolant, specific reference temperatures for the evaluation of certain properties and/or dimensionless functions of those properties which are most temperature sensitive were introduced.

A relation of this type is the well-known Sieder-Tate equation which allows for the effect of property variations through a viscosity ratio function,

$$St = Nu/Re\,Pr = 0.027\,Re^{-0.2}Pr^{-0.67}(\mu_b/\mu_w)^{0.14} \quad . \tag{7.1}$$

In this equation all physical properties are to be evaluated at the average bulk temperature of the fluid, with the exception of μ_w which is the viscosity of the fluid at the coolant-side wall temperature.

From the analysis of the extensive experimental results of high-intensity heat transfer to supercritical hydrogen and supercritical helium McCarthy et al[1,2] and Taylor[3] proposed a general equation for local values of single-phase, forced convection heat transfer which includes the so-called entrance effects, i.e. the effect of developing flow and temperature profiles on convection:

$$Nu = Nu_b(T_{wc}/T_b)^{-(0.57-1.59/X/D_e)} \tag{7.2}$$

in which

$$Nu_b = 0.023\,Re_b^{0.8}Pr_b^{0.4} \quad , \tag{7.2a}$$

where X/D_e is the dimensionless entrance length, i.e. the linear distance from the entrance of the fluid into the duct and the area considered over the equivalent duct diameter D_e,
T_{wc} and T_b are the coolant-side wall and fluid bulk temperatures, respectively.

All physical properties in Equation (7.2) are to be evaluated at the fluid bulk temperature.

The introduction of a function of the temperature ratio takes account of the variation of the physical properties across the boundary layer in a similar way, as in the Sieder-Tate equation. Friction factors for the same fluid regime were also determined by Taylor[4] and can be evaluated from

$$f/2 = 0.0007 + 0.0625\,Re_w^{-0.32}(T_b/T_{wc})^{0.5} \quad , \tag{7.3}$$

where Re_w is the wall Reynolds number, in which the viscosity is to be evaluated at the local wall temperature.

Although the above relations were derived from experimental data on gases they are expected to be adequately accurate for single-phase liquid heat transfer with perhaps some minor modification to the numerical constant in Equation (7.2a).

7.3 NUCLEATE BOILING

Nucleate boiling commences when the surface in contact with the coolant attains a temperature slightly in excess of the local saturation temperature of the coolant. The driving potential for the formation of vapour bubbles is therefore the difference between the coolant-side wall temperature T_{wc} and the saturation temperature T_{sat} of the liquid. This temperature difference remains remarkably constant in the entire regime of the nucleate boiling and rarely exceeds about 30°C between the inception of nucleate boiling and the ultimate heat flux at which transition to film-boiling will occur (points 2 and 3 respectively in Figure 7.1). Coolant-side wall temperature in the nucleate boiling regime can therefore be adequately estimated by adding about 20 to 30°C to the local saturation temperature.

While the beneficial effects of nucleate boiling through the perturbation of the laminar sub-layer are quite marked at low and medium coolant velocities, at high velocities conventional boundary layer effects become again the controlling factor. This is seen clearly in Figure 7.2 which shows the heat flux as a function of wall temperature at constant fluid bulk temperature. It is interesting to note that at a fluid velocity of 0.90 m/sec the nucleate boiling regime extends from about 54 W/cm^2 to 460 W/cm^2 whereas at a velocity of 42 m/sec the corresponding limiting values are 1340 W/cm^2 and 2000 W/cm^2.

Clearly of primary interest to the designer of a cooling system is the ultimate heat flux, $\bar{q}_{ult}$ that can be attained at the given conditions before the discontinuous transition from nucleate to the film boiling takes place (points 3 to 4 in Figure 7.1. Owing to the complex relationship between the various property and flow variables no generally valid method of predicting $\bar{q}_{ult}$ is yet available and recourse to experimental determinations is usually taken to establish the heat transfer characteristics of coolants.

However, despite the lack of a reliable analytical procedure, the examination of many experimental data on different fluids revealed a phenomenologically consistent behaviour. This can best be demonstrated by referring to a study of forced convection nucleate boiling by Noel[5] on ammonia.

Figure 7.3 shows the heat flux at the upper limit of nucleate boiling ($\bar{q}_{uit}$) as a function of pressure for three main stream velocities. Apart from the initially strong increase of the ultimate heat flux with pressure it will be noticed that after having passed through a maximum, $\bar{q}_{ult}$ diminishes with further increasing pressure. For the two higher velocities this maximum occurs at a reduced pressure of about 0.55, whereas at zero velocity the peak value of $\bar{q}_{ult}$ occurs at a reduced pressure of approximately 0.3. This observation tends to be in agreement with results obtained on other liquids.

The effect of main stream velocity on the ultimate heat flux is shown in Figure 7.4 where it will be noted that $\bar{q}_{ult}$ is a linear function of velocity. The gradients of the lines diminish with increasing bulk temperature. At zero velocity, i.e. for the case of nucleate pool boiling, the three lines converge towards a common value which can be predicted with the aid of a semi-empirical relation by Kutadeladze[6].

The effect of liquid bulk temperature is shown in Figure 7.5 for various velocities and at constant pressure. Values of $\bar{q}_{ult}$ are seen to decrease with increasing bulk temperature and converge at the saturation temperature to a common value which incidentally is similar to that for zero flow velocity in Figure 7.4. Bulk temperature effects on $\bar{q}_{ult}$ are more pronounced at high velocities.

A point worth noting concerns the options open to the designer who wishes to use the nucleate boiling phenomenon for cooling an area of known thermal load. Assume a heat flux of 250 W/cm^2, reference to Figure 7.2 shows that operation within the nucleate boiling region is feasible and that a very modest flow velocity of 0.9 m/sec resulting in a low pressure drop, is adequate to achieve the desired protection. Should, however, the resultant wall temperature be too high, operating conditions can be transferred into the single-phase convective regime by raising the flow velocity to 9.2 m/sec. The latter choice may be dictated by secondary effects, e.g. the thermal stability of the coolant in contact with the wall as has been mentioned in the introductory section.

The difficulties in developing a satisfactory analytical model for predicting heat transfer in forced-flow nucleate boiling not only stem from the complex interaction of fluid flow and thermal phenomena but also from our lack of knowledge of many essential properties of the cooling fluids. It has been therefore a widely accepted technique to determine by experiment the essential data, such as the ultimate heat flux, with various rocket propellants at conditions likely to be met in a real engine, and to empirically correlate such data with readily measured quantities.

Forced convection heat transfer to the widely used jet engine fuels JP–3 and JP–4 have been studied by Hatcher[7] and Beighley[8] respectively. Hatcher correlated his data for $\bar{q}_{ult}$ by means of the empirical equation

$$(\bar{q}_{ult}/\bar{q}_{conv})^{3.5} = 2 \times 10^4/P\bar{m} \quad , \tag{7.4}$$

where $\bar{q}_{conv}$ is the predicted heat flux for forced flow convection at the same coolant-side wall and bulk temperatures that pertain to $\bar{q}_{ult}$

P the absolute pressure in lb/in^2

$\bar{m}$ the mass flux of the coolant in lb/in^2 sec.

Confirmation of this method of correlation was provided by Beighley who found for his data for $\ddot{q}_{ult}$ on JP–4 the following equation

$$(\ddot{q}_{ult}/\ddot{q}_{conv})^{2.54} = 1.11 \times 10^4/Pfn \quad . \tag{7.5}$$

7.4 HEAT TRANSFER TO NEAR-CRITICAL FLUIDS

In the two previous sections it was tacitly assumed that the bulk of the fluid stream remained in the liquid phase, although vapour formation may occur in the immediate vicinity of the heated surface. A different situation must exist when the bulk coolant temperature is raised to its saturation point and the coolant is partly, or completely evaporated during its passage through the cooling duct. The practical difficulties attendant upon a two-phase mode of operation are quite considerable and to the authors' knowledge no such system has ever operated successfully in practice. However, if the pressure of the fluid over the entire length of the duct is above the critical pressure these considerations do not apply, as by definition the existence of a second co-existent phase is excluded.

The interest in the heat transfer behaviour of super-critical fluids was stimulated by the use of hydrogen as a rocket propellant and regenerative coolant. Hydrogen is an unusual coolant in that it is possible for the fluid while at supercritical pressures to be heated from subcritical bulk temperatures around the normal boiling point of 20°K, through its critical temperature of 33°K, to final temperatures above 100°K on passing through the cooling ducts. At some location in the coolant duct the bulk fluid temperature will pass through the critical temperature region in which the physical properties of all fluids are very strongly temperature dependent.

It is therefore essential to examine how the flow and heat transfer processes differ from those predicted by the modified constant property relations of Sections 2 and 3, and to provide improved relations for reliably estimating heat transfer in cooling ducts of rocket engines operating under such conditions.

As an immediate consequence of operating in the near-critical region of temperature and pressure, large changes in the fluid density and thus flow velocity, will occur along some section of the cooling channels. These ought to be estimated reliably to ensure that momentum pressure drops remain within design limits.

It must be emphasised that these unusual property variations and their effect on heat transfer phenomena are confined to a rather narrow range of pressure just above the critical value. Examination of the physical and transport property data of various fluids has shown that at reduced pressures $P/P_c > 3$ the characteristic anomalies of the near-critical regime have almost disappeared and the fluid can be considered to have monotonically varying properties. Comprehensive surveys of forced convection heat transfer to near-critical fluids have been published by Hendricks et al.[9] and by Beech[10], the latter concentrating on the use of hydrogen as a coolant.

Summing up the current forced convection work on near-critical fluids Hendricks et al. stated that, despite the fact that analysts have been able to substantiate their work with data, subsequent investigators found it necessary to modify the methods to suit their own results. No analysis is currently widely accepted, nor has any analysis been thoroughly tested against the available data. Against this unsatisfactory background a few general observations can be made, however, which might provide at least a guide as to how to approach the task of making numerical estimates.

One of the earliest attempts to correlate heat transfer data near the critical point was that of Miropolskii and Shitsman[11] who, using experimental data on water and steam, derived a remarkably simple modification to the conventional Nusselt equation

$$Nu_b = 0.023\ Re^{0.8} Pr_{min} \quad , \tag{7.6}$$

where Pr_{min} is the minimum Prandtl number defined as

$$Pr_{min} = Pr_b \text{ , for } Pr_b < Pr_w \quad \text{and} \quad Pr_{min} = Pr_w \text{ , for } Pr_w < Pr_b \text{ ,}$$

where Pr_b and Pr_w are the Prandtl numbers evaluated at bulk and wall temperature, respectively.

Although satisfactory in a number of cases there are specific situations where this relation has failed to predict the experimental observations.

Another entirely empirical approach consists in introducing a series of correction terms to the standard Nusselt equation which assumes the following form

$$Nu = Nu_b(\mu_w/\mu_b)^a(\lambda_w/\lambda_b)^b(\rho_w/\rho_b)^c[\bar{C}_p/C_{p_b}]^d \quad , \tag{7.7}$$

where $\underline{Nu}_b$ is the Nusselt number evaluated at the bulk fluid temperature
$\bar{C}_p = (H_w - H_b)/(T_w - T_b)$, is the integrated specific heat
H_b and H_w the enthalpies of the fluid at bulk and at wall temperature.

The novelty in the above relation is the introduction of a property value integrated over the driving temperature difference $(T_w - T_b)$. The concept of using integrated properties was further extended by Brokaw[12] who proposed that all temperature dependent variables should be presented as integrated average values

$$\bar{\phi}(T) = 1/(T_w - T_b) = \int_{T_b}^{T_w} \phi(T)\, dT \quad , \tag{7.8}$$

where $\phi(T)$ is any fluid property.

Since some authors have compared a near critical fluid with a dissociating polymer and had some success in predicting certain thermodynamic and transport properties with this concept, the above approach might have some merit.

Reporting on their heat transfer experiments to kerosine at sub-critical and supercritical pressures, Beech and Ziebland[13] observed at slightly supercritical pressures and temperatures boiling-like modes of heat transfer. The heat transfer surface was surrounded by a cloudy envelope which appeared to have the same optical effect as a large number of minute bubbles. At the onset of this condition the heat transfer was found to be enhanced above the value for single-phase convection, although much less marked than in nucleate boiling. Photographic evidence seemed to support the notion that the enhancement of heat transfer was due to a strong natural convection contribution to forced flow convection induced by the steep density gradients in this regime.

In the absence of a more refined and generally valid treatment the use of Equation (7.7) but with all property data temperature averaged appears to be at present the best approach for quantitative predictions of forced convection heat transfer in the near-critical regime.

7.5 SQUARE DUCTS, NON-UNIFORMLY HEATED

The previous equations for forced convection heat transfer were derived from experiments on circular tubes, uniformly heated over their entire periphery. Thrust chambers of rockets, however, usually consist of bundles of thin-walled, square tubes, the aspect ratio of which varies in accordance with coolant flow velocities required at each section. Further, only one side of the rectangular passage is heated by the hot combustion gases. The question arises as to what extent the previous relation will have to be modified to adequately take into account the effects of duct geometry and of non-uniform heating.

Previous theoretical analyses by Barrow[14] of asymmetric heat flow between unbounded parallel walls predicted that the heat transfer coefficient will be lower when heat is transferred on one side only. The cause of this difference between symmetric and asymmetric heat transfer conditions was thought to be the higher turbulent core resistance for the asymmetric case. The predictions of these analyses, however, cannot readily be transferred to asymmetric heat transfer in flow passages of arbitrary cross-section.

Forced convection heat transfer to RP–1 kerosine was investigated by Hines[15] in a rectangular, asymmetrically heated duct at conditions similar to those encountered in a single coolant passage of a liquid propellant rocket engine. All experimental data were satisfactorily correlated by Equation (1) provided the equivalent hydraulic diameter,

$$D_e = 4\, A/U_f \quad ,$$

where A is the cross-sectional area of the duct, and U_f the wetted perimeter of the duct, is introduced as the characteristic length into Nusselt and Reynolds numbers of Equation (7.1).

With this single modification forced convection heat transfer to RP–1 kerosine flowing in asymmetrically heated rectangular ducts has been predicted satisfactorily for bulk Reynolds numbers between 10×10^3 to 200×10^3.

A summary of the experimental conditions for which the validity of the modified Sieder-Tate equation has been proved is given below.

Inlet liquid temperature	30° to 40°C
Exit liquid temperature	31° to 45°C
Average coolant-side wall temperature	81° to 260°C
Heat flux	45 to 400 W/cm²
Liquid pressure	50 to 52 bar
Liquid velocity	600 to 3600 cm/sec .

As the critical pressure of RP–1 kerosine is below 30 bar, all experimental results were obtained in the single-phase convective regime.

Careful measurements of forced convection heat transfer from one side of a duct of rectangular cross section to an internally flowing fluid for a wide range of height-to-width ratios were conducted by James et al[16]. Data were obtained at temperature differences between the wall and the bulk fluid from 40°C to 150°C and refer to single phase heat transfer only.

In contrast to the opinion expressed in Reference 15 it was not found possible to correlate all data by using an equation of the Sieder-Tate type and a complex empirical relation, linking the Nusselt number with the other influential variables was developed which successfully correlated the experimental results within 10 per cent. This equation is:

$$Nu = 0.104^{(0.0016\,Pr+0.75)}\,Pr^{0.4}\,\mu_r(213\,Re - 0.9)/(2.05 + 1.62\,e^{-H_r})\,e^{0.0134\,Pr}, \qquad (7.9)$$

where in Re and Nu the characteristic length is the equivalent hydraulic diameter of the duct as defined above,

μ_r is the ratio of the viscosity at the fluid bulk temperature to the viscosity at the wall temperature

H_r the duct aspect ratio i.e. the width of the heated duct over its height.

All physical properties of the fluid are to be evaluated at the bulk fluid temperature except where indicated.

The range of validity of this equation extends over the following ranges of variables:

With reasonable certainty:	With moderate confidence:
Re: 3×10^3 to 1×10^5	3×10^3 to 2×10^5
Pr: 6.5 to 100	0.7 to 100
H_r: 0.5 to 4	any practically reasonable value
μ_r: 1.5 to 9	1 to 10

The above correlation fits the already published data of other observers for heat transfer in asymmetrically heated rectangular ducts and agrees also with theoretical predictions of heat transfer between a heated and an unheated parallel flat plate.

7.6 CURVILINEAR DUCT FLOW

Cooling channels in a shell type rocket engine are arranged in form of a continuous helix and in the more common, multi-tube thrust chamber design, individual ducts are bent to match the required axial profile of engine and nozzle. In either case the resultant curvature is bound to have an effect on the flow conditions of the coolant and thus on the convective heat transfer.

A detailed study of the secondary flow in curved pipes has been conducted by Ito[17]. The basic effect of duct curvature is that the fluid particles flowing along the more central flow lines are forced sideways and a resultant secondary flow in the form of a double vortex is created, as illustrated in Figure 7.6(a). As far as heat transfer is concerned the secondary flow causes a reduction of the thickness of the boundary layer on the concave surface and an appropriate increase on the convex surface. Qualitatively at high Reynolds numbers the local convective heat transfer at the concave surface will be enhanced. The magnitude of this effect will depend on geometric factors such as the ratio of duct curvature to tube radius (for square duct the appropriate hydraulic radius must be used) and on the distance from the commencement of the curved section, and to some considerable extent on the thermodynamic state of the fluid (see Figure 7.7).

Further, entrance conditions, profile similarity and the previous fluid conditions may have a considerable effect on the local heat transfer coefficients. It should also be noted that the effects of curvature as evidenced by pressure drop and velocity profile measurements[17] tend to persist downstream of the bend.

According to Reference 17 for high Reynolds numbers the average friction factor for a curved tube was increased over that for a straight tube by the following relation:

$$f_c/f_{st} = Re(r/R)^2 = I^{0.05}, \qquad (7.10)$$

where f_c and f_{st} are the friction factors for the curved and straight tube, respectively

r the radius of the duct

R the radius of the bend

I the so-called Ito parameter .

Taylor[18] found that by introducting the Ito parameter heat transfer data could also be adequately correlated.

For the concave surface: $Nu = Nu_c I^{0.05}$

For the convex surface: $Nu = Nu_c I^{-0.05}$,

where Nu_c corresponds to Equation (7.9) of the previous section.

7.7 CONCLUSIONS

Provided the coolant remains in the liquid phase at all points in the flow, predictions of forced convection heat transfer in the cooling ducts of rocket engines can be made with sufficient accuracy. Exponential relations between the pertinent, non-dimensional quantities, Nu, Re and Pr, have been found adequate. Relatively simple modifications to the basic Nusselt equation have been proposed to take into account the effect of duct geometry (rectangular cross section and curved flow path) and of non-uniform heating. Likewise, the influence of the high rates of heat transfer leading to high temperature differences across the laminar sub-layer and hence, variable fluid properties, may be taken care of by introducing temperature-averaged property values. The most likely difficulty to be met in practice might be a lack of accurate property data for the chosen coolant-propellant. However, even this gap is being steadily narrowed. A fairly comprehensive account of the properties of rocket propellants with an extensive bibliography will be found in Reference 18.

No completely satisfactory relation has yet been proposed to enable accurate predictions to be made for the nucleate boiling regime, and the only information available is derived from experimental studies with specific rocket propellants. A reference to a comprehensive review of these tests, almost exclusively conducted at NASA, will be found in Chapter 10. Apart from some general statements concerning the ultimate heat flux apparently applicable to a variety of fluids, the prediction of the limiting heat fluxes in terms of the physical and transport properties of the coolant is yet an uncompleted task.

Even less well understood is the heat transfer by forced convection in the near-critical region. The proximity of the critical temperature either at the wall or for the bulk of the fluid has produced in some experiments sharp temperature rises. The mechanism leading to this phenomenon is yet to be satisfactorily explained. Even at slightly supercritical pressures there is evidence of a distinct discontinuity in the convective heat flux bearing resemblance to, but being smaller than the steep rises observed for nucleate boiling.

In cases where the coolant remains at supercritical pressures and is heated from a subcritical to a supercritical temperature (e.g. hydrogen) the fluid will rapidly expand in the critical regime and be subject to large acceleration forces. Experiments have suggested[19] that the influence of the acceleration (laminarisation) will have to be taken into consideration when the characteristic quantity $Gr/Re^2 > 5 \times 10^3$.

REFERENCES

1. McCarthy, J.R. Wolf, H. — *The Heat Transfer Characteristics of Gaseous Hydrogen and Helium.* Report RR60-12 (NP-10572), Rocketdyne Div. North American Aviation Inc., 1960.

2. McCarthy, J.R. Wolf, H. — *Forced Convection Heat Transfer to Gaseous Hydrogen at High Heat Fluxes and High Pressures in a Smooth, Round, Electrically Heated Tube.* ARS J., Vol.30, 1960. pp.423-425.

3. Taylor, M.F. — *Correlation of Local Heat Transfer Coefficients for Single-Phase Turbulent Flow of Hydrogen in Tubes with Temperature Ratios up to 23.* NASA TN D-4332, 1968.

4. Taylor, M.F. — *A Method of Correlating Local and Average Friction Coefficients for Both Laminar and Turbulent Flow of Gases through a Smooth Tube with Surface to Fluid Bulk Temperature Ratios from 0.35 to 7.35.* Int. J. Heat Mass Transfer, Vol.10, 1967, pp.1123-1128.

5. Noel, M.B. — *Experimental Investigation of the Forced-Convection and Nucleate Boiling Heat Transfer Characteristics of Liquid Ammonia.* NASA TR 32-125, 1961.

6. Kutadeladze, S.S. — *Fundamentals of Heat Transfer.* E. Arnold, London, 1963.

7. Hatcher, J.B. — *High Flux Heat Transfer and Coke Deposition of JP-3 Fuel Mixture.* JPL Progr. Rep.20-157, 1951.

8. Beighley, C.M. Dean, L.E. — *Study of Heat Transfer to JP-4 Jet Fuel.* Jet Propulsion, Vol.24, 1954, pp.180-186.

9. Hendricks, R.C. et al. — *Survey of Heat Transfer to Near Critical Fluids.* NASA TM X-52612, 1969.

10. Beech, J. — *Forced Convection Heat Transfer to Supercritical Cryogenic Hydrogen. Part I. Literature Survey.* Unpublished Ministry of Technology Survey, 1969.

11. Miropolskii, L. Shitsman, M.E. — *Heat Transfer to Water and Steam at Variable Specific Heat in the Near-Critical Region.* Soviet Phys – Tech Phys, Vol.2, 1957, pp.2196-2208.

12. Brokaw, R.S. — *Correlation of Turbulent Heat Transfer in a Tube for the Dissociating System* $N_2O_4 \rightarrow 2NO_2$. NACA RM E57K19a, 1958.

13. Beech, J. Ziebland, H. — *Heat Transfer to Kerosene, D Eng R D 2495, at Supercritical and Subcritical Pressures.* ERDE 5/R/63, 1963.

14. Barrow, H. — *Convection Heat Transfer Coefficients for Turbulent Flow between Parallel Plates with Unequal Heat Fluxes.* Int. J. Heat Mass Transfer, Vol.1, 1961, p.306.

15. Hines, W.S. — *Heat Transfer to RP-1 Kerosene in Turbulent Flow under Asymmetric Heating Conditions.* Chem. Eng. Progr. Symposium, Houston, 1962.

16. James, D.D. et al. — *Forced Convection Heat Transfer in Unsymmetrically Heated Rectangular Ducts.* Spaceflight, Vol.9, 1967, p.129 and International Heat Transfer Conference, Chicago, 1966.

17. Ito, H. — *Friction Factors for Turbulent Flow in Curved Pipes.* J. Basic Eng, Vol.81, 1959, pp.123-134.

18. Dadieu, A. et al. — *Raketentriebstoffe.* Verl.Springer, Wien-New York, 1968.

19. Shiralkar, B.S. Griffith, P. — *Deterioration in Heat Transfer to Fluids at Supercritical Pressures at High Heat Fluxes.* Paper 68-HT-39, ASME, August 1968.

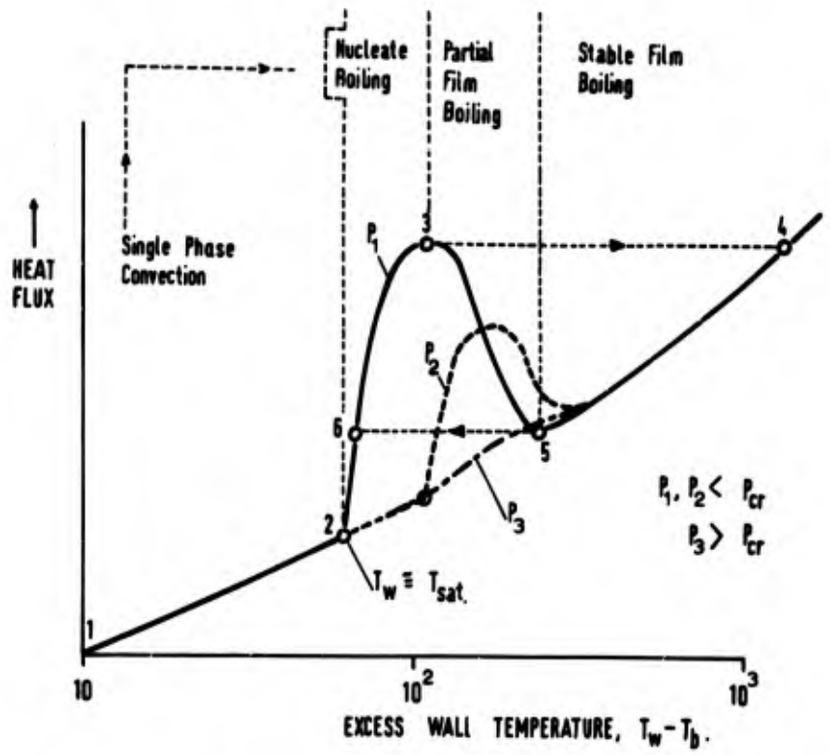

Fig. 7.1 Convective heat flux regimes

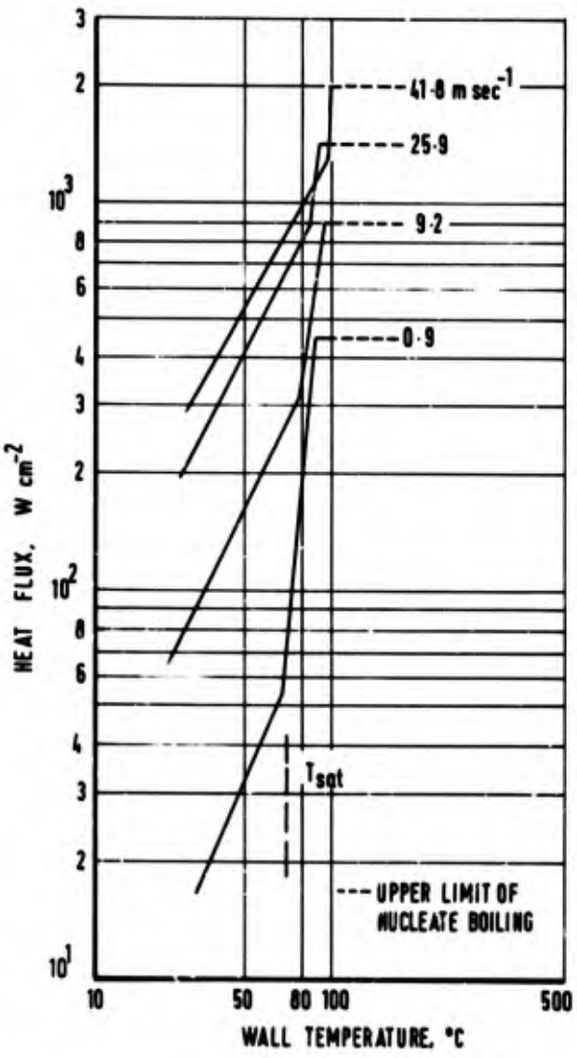

Fig. 7.2 Nucleate boiling heat flux for ammonia as a function of wall temperature for various velocities (according to Noel[5])

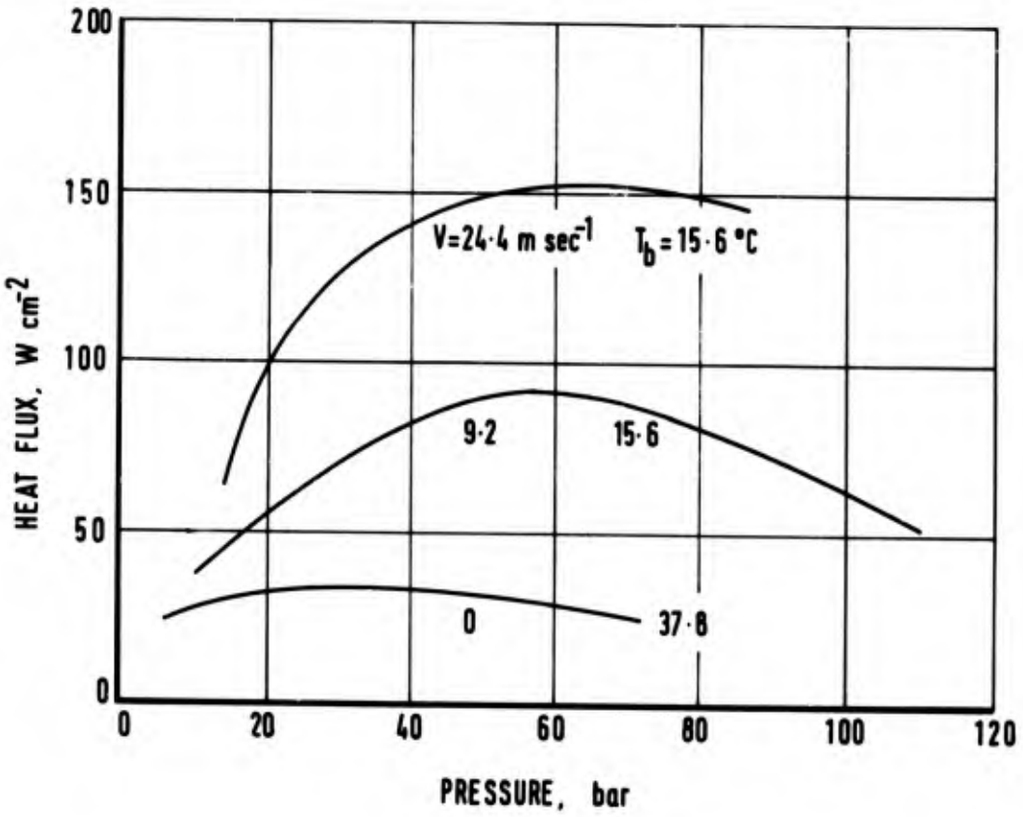

Fig. 7.3 Upper limit of nucleate boiling for ammonia as a function of pressure at various flow velocities (according to Noel[5])

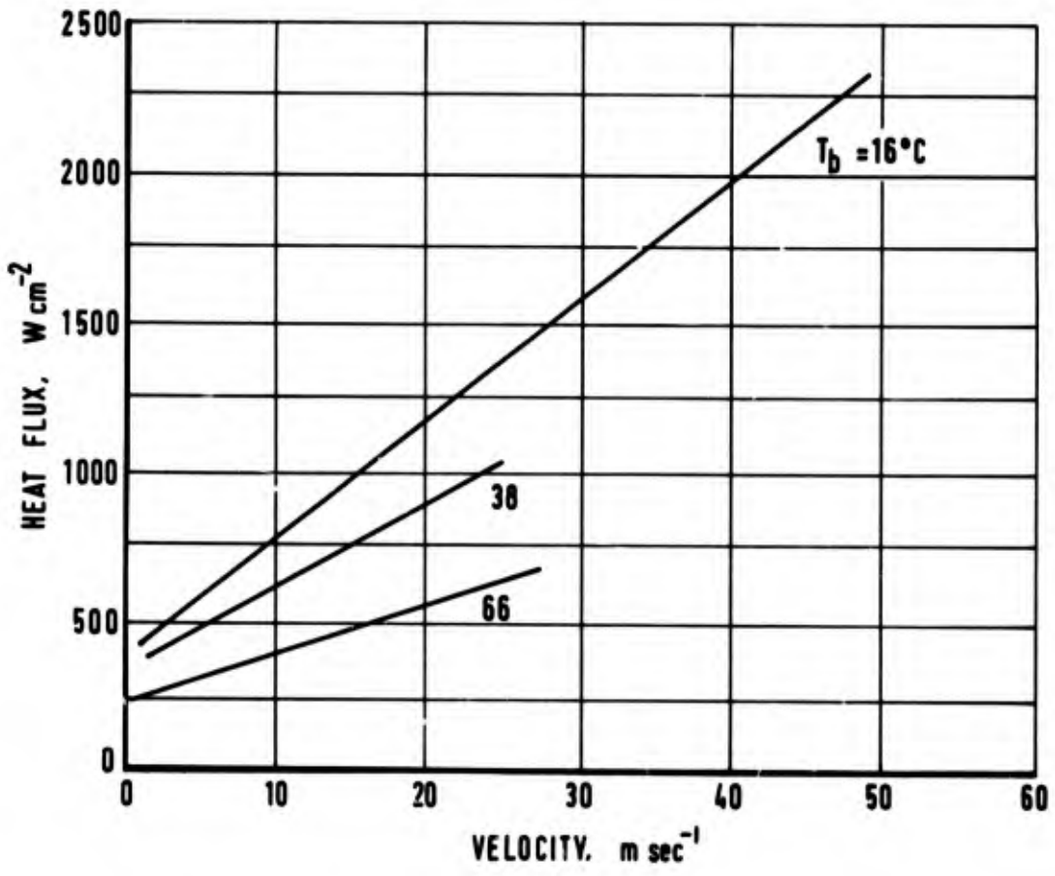

Fig. 7.4 The influence of main stream velocity on the ultimate nucleate boiling heat flux (according to Noel[5])

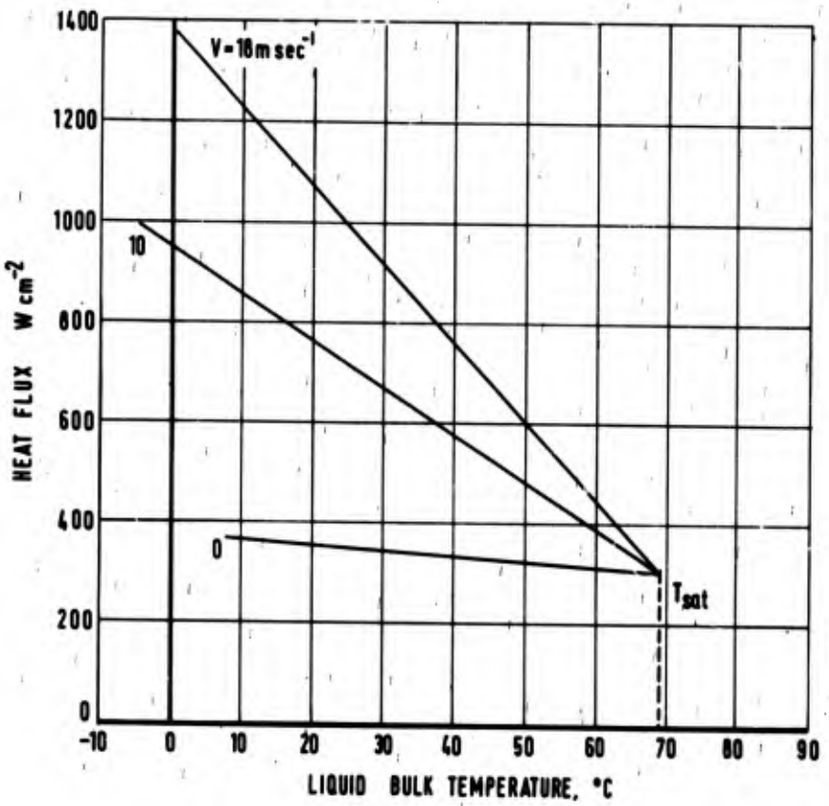

Fig. 7.5 The effect of liquid bulk temperature on the ultimate heat flux (according to Noel[5])

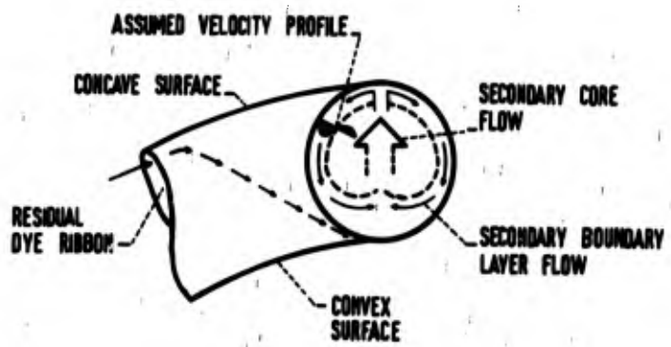

(a) Single-Phase Flow.

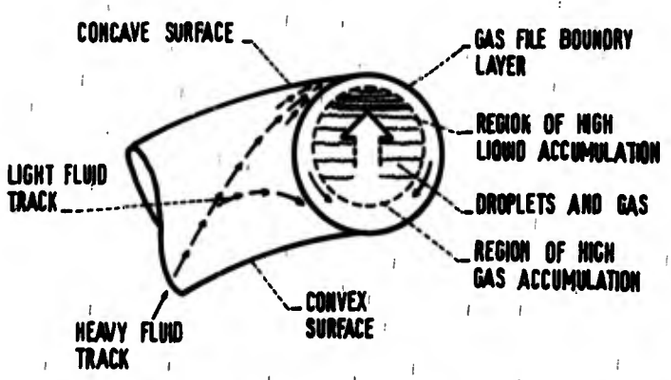

(b) Two-Phase or Near Critical Flow.

Fig. 7.6 Typical flow patterns in a curved duct for single and two-phase flow (according to Hendricks et al.[9])

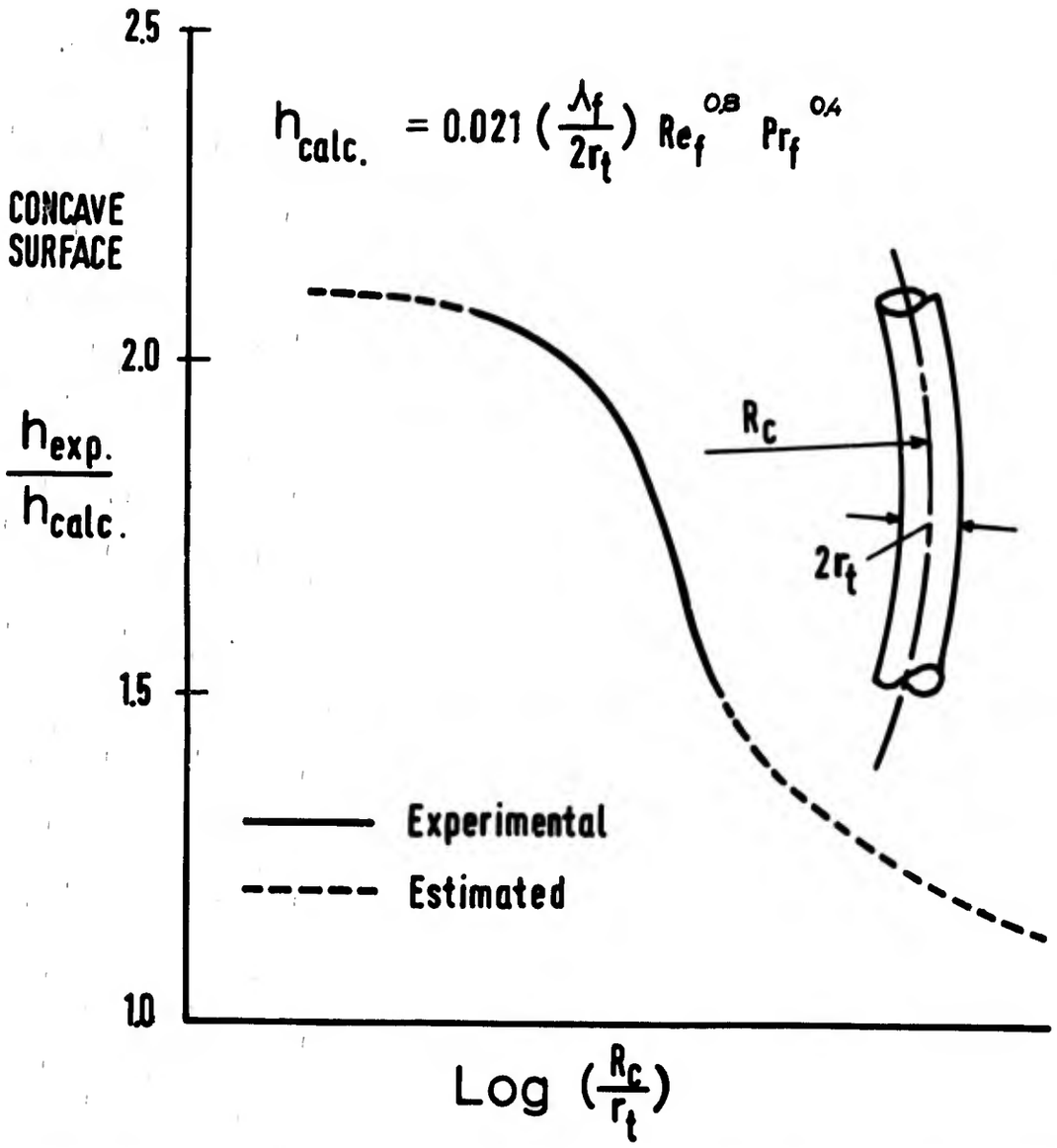

Fig. 7.7 Relative enhancement of the convective heat transfer coefficient in a curved duct (according to Hendricks et al.[9])

CHAPTER 8

LAMINAR HEAT TRANSFER

8.1 GENERAL

In nearly all rocket engines the flow will be turbulent, and most of this book has been written with this assumption. However, there exists a limited class of applications in which the flow will be laminar; small rocket engines used for attitude control, and the thermal-electric resistojet and plasmajet engines.

It is well known that in simple pipe flow the flow will remain laminar until the Reynolds number based on diameter exceeds ~2000. On flat plates the critical Reynolds number (this time based on distance from the leading edge) is ~ 5×10^5. General stability criteria can be complex[1], but with these typical figures we find that the tendency for laminar flow will increase with decreasing engine size, low chamber pressure and high stagnation temperature.

In laminar flow the possibility arises of providing exact solutions to the fluid flow and heat transfer equations. However, such solutions are not always easy to apply to practical problems. Once again the aim of this chapter will be to recommend approximate calculation methods which are moderately easy to apply to practical problems without sacrificing too much accuracy.

8.2 HEAT TRANSFER IN A CIRCULAR TUBE

One of the simplest cases of laminar heat transfer occurs with steady, fully developed, incompressible flow within a circular tube. The Nusselt number in this region was shown by Graetz[2] to be constant. The Nusselt number is defined in terms of the duct radius r

$$Nu = \frac{\ddot{q}}{T_w - T_b} \frac{2r}{k},$$

where T_w is the temperature of the wall, T_b the bulk temperature of the flow, $\ddot{q}$ the heat flux, and k the thermal conductivity of the fluid.

Two extreme cases are generally considered of interest – that in which the wall temperature is constant, and that of constant heat flux to the wall. In the former case the limiting Nusselt number is 3.65. In the latter case the limit is 4.36.

For most cases of interest in the present instance, however, this limit will not be reached. As a typical example, for RePr = 1000 (the Reynolds number here being based on diameter), and with a constant heat flux, the entrance length for the Nusselt number to approach to within 5 per cent of its fully developed value is 42.5 diameters.

Sellars et al.[3] have given good approximations for the behaviour of the heat transfer close to the tube entrance. For a constant wall temperature

$$\boxed{Nu = 1.3565\, x^{*-1/3}, \qquad x^* < 0.01} \tag{8.1}$$

and for the constant heat flux problem

$$\boxed{Nu = 1.6393\, x^{*-1/3}, \qquad x^* < 0.01} \tag{8.2}$$

where

$$x^* = \frac{x}{r} \frac{1}{RePr}.$$

Referring back to Equations (2.9) and (2.6), it will be seen that this implies a one-third power-law for the velocity distribution in the developing boundary layer.

It is apparent that these two equations cannot be followed indefinitely into the tube, since they imply that the Nusselt number at infinity tends to zero. However, if they are used with the proviso that the Nusselt number shall not be smaller than its limiting value, even at the worst case the difference between this value and the more exact solutions is only about 10%. Equations (8.1) and (8.2) will tend to predict low values for the Nusselt number.

More exact solutions tend to involve series solutions. Siegel et al.[4], for instance, give for the constant heat flux case

$$Nu = \frac{2}{\frac{11}{24} + \sum_{n=1}^{\infty} C_n e^{-(\beta_n^2/RePr)(x/r)} R_n(1)} \tag{8.3}$$

instead of Equation (8.2). The first seven values of the various constants involved are given in Table 8.1 from Siegel et al.'s paper[4]. A comparison of the two solutions is given in Figure 8.1.

In comparison with experimental data, Kays and Nicholl[5] have found that the above solutions are accurately applicable without correction for both heating and cooling for absolute temperature ratios of up to 2.0 if all fluid properties are evaluated at local "mixed mean" temperature.

8.3 COMPRESSIBLE LAMINAR HEAT TRANSFER

For heat transfer in compressible flow conditions (e.g. in a nozzle), one of the simplest of applications is the similarity solution of Cohen and Reshotko[6]. As previously with turbulent boundary layers, the similarity assumption requires that the velocity and temperature profiles may always be expressed in terms of a single parameter. For *exact* laminar flow solutions this places restrictions on the velocity distribution in the free-stream, and the method is only approximate for other cases.

The equations of the steady two-dimensional compressible laminar boundary layer are

Continuity:
$$\frac{\partial}{\partial x}(\rho u) + \frac{\partial}{\partial y}(\rho v) = 0 \tag{8.4}$$

Momentum:
$$\rho u \frac{\partial u}{\partial x} + \rho v \frac{\partial u}{\partial y} = -\frac{\partial p}{\partial x} + \frac{\partial}{\partial y}\left(\mu \frac{\partial u}{\partial y}\right), \qquad \frac{\partial p}{\partial y} = 0 \tag{8.5}$$

Energy:
$$\rho u \frac{\partial H}{\partial x} + \rho v \frac{\partial H}{\partial y} = u \frac{\partial p}{\partial x} + \frac{\partial}{\partial y}\left(\frac{\mu}{Pr} \frac{\partial H}{\partial y}\right) + \mu \left(\frac{\partial u}{\partial y}\right)^2 . \tag{8.6}$$

As with turbulent boundary layers, it is also necessary to assume a viscosity-temperature law for the boundary layer. Cohen and Reshotko use a simple linear variation

$$\frac{\mu}{\mu_0} = \zeta \frac{T}{T_0} . \tag{8.7}$$

The velocities in the equations of motion can be replaced through the definition of a stream function:

$$\left.\begin{aligned} \psi_y &= \frac{\rho u}{\rho_0} \\ \psi_x &= -\frac{\rho v}{\rho_0} . \end{aligned}\right\} \tag{8.8a}$$

Cohen and Reshotko[6] then proceed by using a slightly modified form of Stewartson's transformation, in which

$$\left.\begin{aligned} X &= \int_0^x \zeta \frac{p_s}{p_0} \frac{a_s}{a_0} dx \\ Y &= \frac{a_s}{a_0} \int_0^x \frac{\rho}{\rho_0} dy \end{aligned}\right\} \tag{8.8b}$$

and the subsequently transformed velocities are

$$U \equiv \Psi Y$$

$$V \equiv -\Psi X$$

so that the relationship between the transformed and the physical longitudinal velocities is

$$U = \frac{a_0}{a_s} u \ .$$

The transformed equations of motion can now be written as

$$\left.\begin{aligned} U_X + V_Y &= 0 \\ UU_X + VV_Y &= U_s U_{sX}(1 + S) + \nu_0 U_{YY} \\ US_X + VS_Y &= \nu_0 \left[\frac{S_{YY}}{Pr} - \frac{1 - Pr}{Pr} \left(\frac{\frac{\gamma - 1}{2} Ma^2}{1 + \frac{\gamma - 1}{2} Ma^2} \right) \left(\left\{ \frac{U}{U_s} \right\}^2 \right)_{YY} \right] , \end{aligned}\right\} \tag{8.9}$$

where U_X represents $\partial U/\partial X$ etc., U_s is the value of U at the edge of the boundary layer, and S is an enthalpy function

$$S = \frac{H}{H_0} - 1 \ ,$$

H being the local stagnation enthalpy.

The question at this point is, what conditions are necessary to reduce Equations (8.9) to a system of ordinary differential equations for a non-adiabatic flow with a pressure gradient with the assumption that the boundary-layer profiles are functions of a single variable η ? One of the two possible cases requires that

$$U_s = CX^m \tag{8.10}$$

and by then using the two equations

$$\left.\begin{aligned} \Psi &= f(\eta) \sqrt{\frac{2\nu_0 U_s X}{m + 1}} \\ \eta &= Y \sqrt{\frac{m + 1}{2} \frac{U_s}{\nu_0 X}} \end{aligned}\right\} \tag{8.11}$$

Cohen and Reshotko are able to reduce Equations (8.9) to the simultaneous ordinary differential equations

$$\left.\begin{aligned} f''' + ff'' &= (f'^2 - 1 - S) \\ S'' + PrfS' &= (1 - Pr) \left[\frac{(\gamma - 1)Ma^2}{1 + \frac{\gamma - 1}{2} Ma^2} \right] (f'f''' + f''^2) \ . \end{aligned}\right\} \tag{8.12}$$

One must now inquire how realistic these assumptions are when applied to a rocket nozzle with laminar flow. The viscosity-temperature function, for instance, will not be precisely linear, but this approximation will have only a slight effect on the calculated heat transfer. The results obtained by Cohen and Reshotko will not always be met with in practice. However, once again this assumption can often be made without sacrificing too much accuracy.

The most important assumption is that of the free-stream velocity distribution (Eqn (8.10)).

The velocity distribution in a nozzle having a hyperbolic profile is shown in Figure 8.2. It can be seen that the power-law distribution provides a good description of the flow in the subsonic and supersonic portions of the flow, but that deviation from this form occurs in the vicinity of the throat. While it is reasonable to suppose that

the heat transfer at the throat will lie in between the values extrapolated from the subsonic and supersonic parts of the flow, this still leaves the region of maximum uncertainty at just that point at which heat transfer is likely to be greatest. For most cases this can be tolerated. At other times it will be necessary to use more complex, less restricted methods of calculation.

The solution to Equations (8.12) given by Cohen and Reshotko involves numerical integration. However, this simply involves the evaluation of the appropriate function of f in terms of the pressure gradient parameter $\beta = 2m/(m+1)$, and the enthalpy function at the wall, S_w. The shear stress, for instance, can be found from the identity

$$\tau \equiv \mu \frac{\partial u}{\partial y},$$

and the skin-friction coefficient at the wall is given by the relation

$$C_f = \frac{\tau_w}{\frac{1}{2}\rho_w u_s^2} = f''_w \left[2\xi(1+S_w) \sqrt{\frac{m+1}{2} \frac{\nu_0}{U_s X}} \right]. \tag{8.13}$$

Values of the function f''_w for a favourable pressure gradient are given in Figure 8.3.

For the heat transfer coefficient, it is convenient to use a simple modified Reynolds analogy parameter to give the Stanton number,

$$\frac{C_f}{St} = \frac{2(h_0 - h_w)}{\rho u} \frac{\partial u/\partial y}{\partial h/\partial y} = \frac{2f''_w}{-S'_w/S_w}. \tag{8.14}$$

Once again, this function is determined by β and S_w alone, and the values for a favourable pressure gradient are given in Figure 8.4.

Closer examination of the heat transfer distribution in a laminar flow nozzle shows that superficially it resembles that for turbulent flow nozzles (see Figure 8.5). The heat transfer still reaches its maximum in the vicinity of the throat – but now visibly upstream of the throat due to the developing boundary layer. There is no longer a sudden drop in the heat flux as the flow enters the supersonic region, and the effects of laminarization are absent. Heat fluxes will be higher than for turbulent flow nozzles under the same conditions of mass-flux and stagnation temperature, but in general laminar flow nozzles will be operated at lower stagnation pressures, tending to ease this problem.

As we have already mentioned, free stream velocity distributions of the form required by similarity considerations are not generally encountered in practice. Where velocity distributions of the correct form cannot be approximated, more complex integral methods may be required, taking into account the whole history of development of the boundary layer. Such a solution, still based on similarity solutions, has been given by Beckwith and Cohen[7], but the details of this method will not be quoted here. Carden[8] has found good agreement for both of these methods with experimental data taken from a nozzle using nitrogen at stagnation temperatures to 3600°K, and stagnation pressures to 1.5 atmospheres.

8.4 CONCLUSION

In some ways there are fewer difficulties in predicting the heat transfer to laminar flows than for turbulent flows. Exact solution of the appropriate equations, at least by numerical methods, is often possible, and even with approximate solutions there are less imponderables to be accounted for. The major unresolved difficulty will probably come with gas dissociation effects as the stagnation temperatures increase in – for example– electrothermal thrusters. However, even here the methods given in Chapter 5 should still be valid, and the number of different chemical species in the system will generally be smaller than for chemical propulsion systems.

REFERENCES

1. Schlichting, H. — *Boundary Layer Theory.* McGraw-Hill, New York, 1960, p.375 et seq.

2. Graetz, L. — Ann. Phys. (Lpz) N.F., Vol.25, 1885, p.337.

3. Sellars, J.R. et al. — Trans. ASME, Vol.78, 1956, p.441.

4. Siegel, R. et al. — *Steady Laminar Heat Transfer in a Circular Tube with Prescribed Wall Heat Flux.* Appl. Sci. Res. A, Vol.7, 1956, p.387.

5. Kays, W.M. Nicholl, W.B. — *Laminar Flow Heat Transfer to a Gas with Large Temperature Differences.* J. Ht. Transf., Vol.85c, 1963, p.329.

6. Cohen, C.B. Reshotko, E. — *Similar Solutions for the Compressible Laminar Boundary Layer with Heat Transfer and Pressure Gradient.* NACA Rept.1293, 1956.

7. Beckwith, I.E. Cohen, N.B. — *Application of Similar Solutions to Calculation of Laminar Heat Transfer on Bodies with Yaw and Large Pressure Gradient in High-Speed Flow.* NASA TN D-625, Jan.1961.

8. Carden, W.H. — *Local Heat Transfer Coefficients in a Nozzle with High-Speed Laminar Flow.* AIAA J., 1965 (3), p.2183.

TABLE 8.I

n	β_n^2	$R_n(1)$	C_n
1	25.68	−0.4925	0.4035
2	83.86	0.3955	−0.1751
3	174.2	−0.3459	0.1056
4	296 5	0.3140	−0.0733
5	450.9	−0.2913	0.0550
6	637.4	0.2738	−0.0435
7	855.9	−0.2599	0.0356

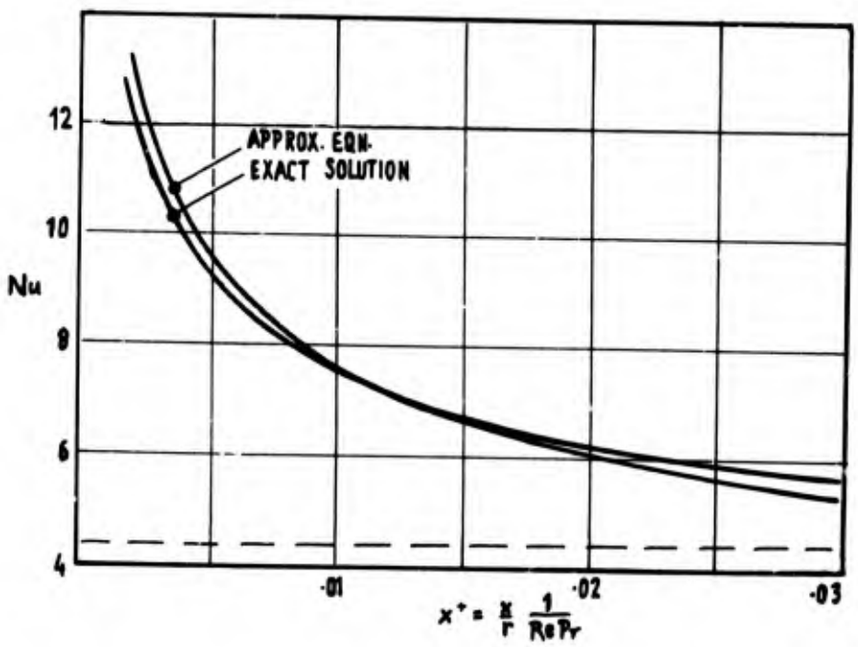

Fig.8.1 Comparison of approximate and exact solutions for the entry length heat transfer in a circular pipe

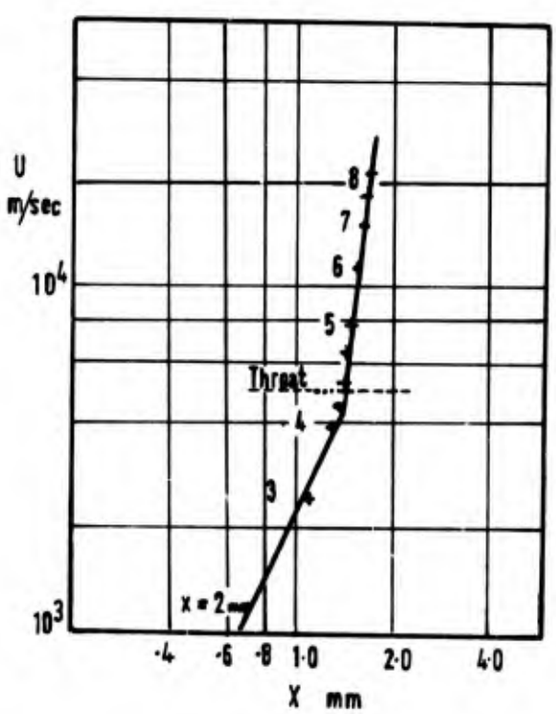

Fig.8.2 Velocity distribution in a hyperbolic nozzle

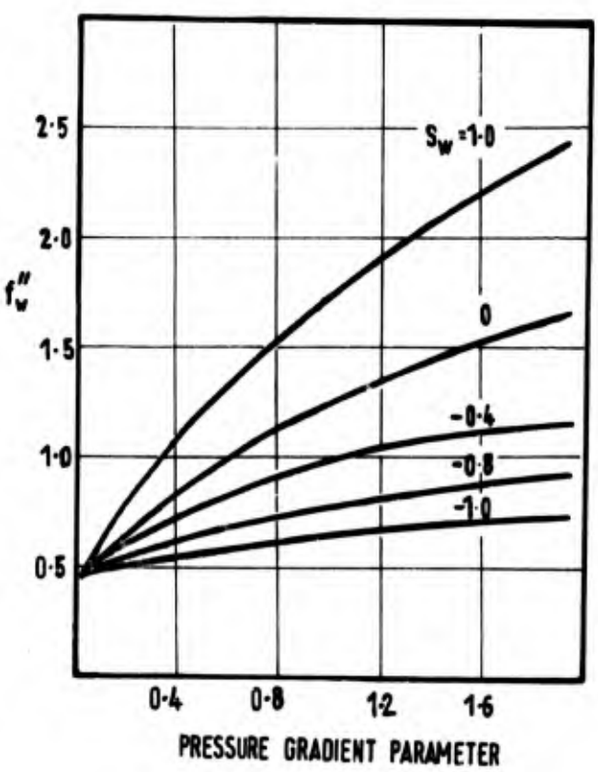

Fig.8.3 Effect of pressure gradient on wall shear function

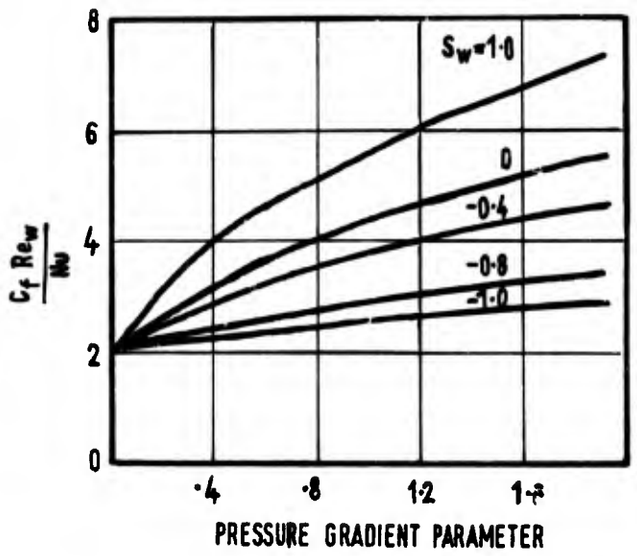

Fig.8.4 Effect of pressure gradient on Reynolds analogy parameter

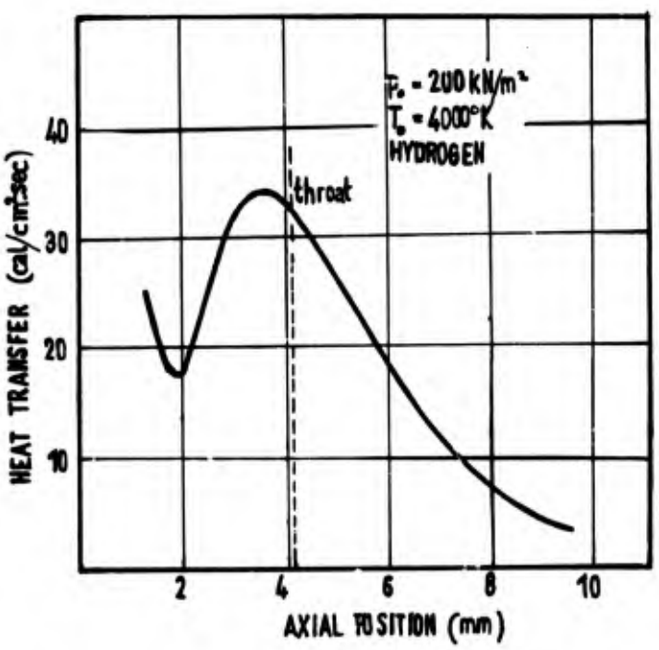

Fig.8.5 Heat transfer in a typical laminar flow nozzle

CHAPTER 9

HEAT TRANSFER TO THE PROPELLANT INJECTOR

9.1 GENERAL

Whilst considerable effort has been expended on studying the heat transfer within the combustion chamber and the nozzle, no detailed attention seems to have been given to the heat transfer processes which determine the temperature of the injector face. Before discussing the heat transfer processes occurring around the propellant injector it is important to consider briefly the main functions of the injector since it is these which generally determine the design rather than heat transfer considerations. This partly arises on account of ignorance regarding the relative importance of various mechanisms of energy transfer, for it is true to say that very few rocket injectors have been deliberately designed with a particular operating temperature in mind.

The four main injector functions are: Propellant atomisation, propellant dispersion and mixing following atomisation, flame front stabilisation and lastly, transmission of thrust and pressure loads. In the early stages of rocket development injector design was more of an art than a logical engineering process. With the vastly increased experience now accumulated certain preferred arrangements have evolved which not only incorporate the requirements to fulfil the above functions but also permit rational construction. The design shown in Figure 9.1 may be considered typical for a modern bi-propellant injector. In order to provide as simple a feed system as possible the injector is formed of a series of concentric rings with alternate rings feeding the fuel and the oxidiser, respectively. Internal passages and ports are formed by conventional machining. Consequently, as may be seen from Figure 9.1, the injector is a fairly complex structure which is subject to both mechanical stresses and considerable thermal stresses induced by the temperature gradients that are established during operation.

The majority of injector failures fall within two categories:

(a) Face burning and/or erosion due to the combination of a high local surface temperature and a high oxidiser concentration close to the injector face.

(b) Face cracking as a result of excessive thermal stresses due to large temperature differences, most likely severest during the transient conditions preceding, or following the stable operating period.

Both modes of failure can be avoided if the heat flux to the injector could be reduced by applying a suitable protection technique, or by certain design modifications to make better use of the cooling potential of the propellant jets.

9.2 HEAT TRANSFER PROCESSES

Heat transfer to the injector face may be postulated as taking place by one, or a combination of several of the following mechanisms:

(a) Radiation from the combustion products.

(b) Radiation from the surrounding walls of the combustion chamber and the nozzle.

(c) Turbulent diffusion.

(d) Convection from recirculatory flows.

The relative importance of these individual processes for a given configuration and propellant combination will depend on various parameters, such as the propellant mixture ratio and combustion pressure and the total propellant flux which in turn affects through the convective heat flux the gas-side wall temperatures of the combustion chamber and nozzle. The heat flowing to the injector face is removed by conduction through the bounding metal wall into the propellant filled annuli and by convection from the hot injector wall into the propellant jets prior to their leaving the orifices.

Efforts of predicting reasonably accurately the contribution of the individual heat transfer processes to the total heat flux are met with considerable difficulties. Let us consider the radiative contribution as an example.

Heat radiated towards the injector face emanates from two sources, from the polar gas constituents of the combustion products, and from the intensely radiating, luminous reaction zone. It is this latter, quantitatively more important source, about which we possess comparatively little well-founded information. To complicate matters further, the finely atomised propellant sprays located between the flame front and the injector face provide an absorbing curtain whose effectiveness depends not only on the optical properties of the propellants, but also on parameters such as droplet size, density of droplet population etc. Most of these quantities can only be obtained through extensive experimental studies and generally speaking, defy analytical prediction.

As far as the prediction of convection from the hot combustion gases is concerned, the condition seems even worse. Not only is the flow pattern around the injector considerably affected by the geometry of the injector, but also by even small deviations of the operating conditions from the design point. In the absence of an analytical study the observations based on two experimental studies will be reported here for reference and discussion.

The first published record of an attempt to throw some light on what at first glance might appear an intractable problem is due to Bragg and Smith[1] who conducted a largely qualitative examination of the heat transfer to an injector similar to that shown in Figure 9.1, for a liquid oxygen/kerosine rocket engine of about 60 tons thrust. By carefully analysing the "picture" presented by the face of the injector which, before the experiment, had been treated with several layers of temperature sensitive paints, it was found that the temperature of the injector face was remarkably uniform and ranged from 370°C to 460°C. Further a closer examination of the area around individual orifices revealed a hot region at the side of the orifice adjacent to its impinging neighbour (see Figure 9.2) a situation which was particularly marked in the case of the oxygen injectors. The conclusion drawn by the authors of Reference 1 from this and other supporting evidence was, that the preponderant fraction of the heat transferred to the injector face was transferred by convection from recirculatory gas flows which were supported, or sustained by the entrainment of combustion products in the developing boundary layer around each propellant jet. Neither wall, nor indeed gas or flame radiation, was thought to have contributed significantly to the total heat flux. Using the values of the injector face temperature referred to above it was estimated that the heat flux must have amounted to the equivalent of about 0.18 kW/cm^2 over the entire surface of the injector. It was thought improbable by the authors that this heat flux could be accounted for by radiation from either chamber or nozzle walls, or by the emission from the polar gas constituents. As we shall see in the following section, it is not inconceivable, however, that a fraction of this heat flux may have its origin in the radiative emission from the flame front which for these propellants owes its luminosity to the presence of minute carbon particles.

Accepting the postulate that convection of combustion gases around the injector face is brought about by the entrainment of gas by the high velocity liquid jets as shown schematically in Figure 9.2 the amount of gas recirculated will clearly depend on many factors such as jet velocity, exposed surface area and particularly the roughness of the jet. It is also obvious that only entrainment from the initial region of the jet will induce a recirculation that affects the conditions at the injector face.

Under these conditions the convective heat flow to the injector face may be expected to be proportional to a function of the flow rate of the entrained gas and to the enthalpy difference between the hot gas and the gas at surface temperature. This situation further impeded an analytical approach as the mixture ratio and thus the enthalpy of the recirculated gas will have a composition considerably different from the overall mixture ratio in the combustion chamber and thus will be unknown. There is evidence in support of the suggestion that the mixture ratio of the recirculated gases depends on the relative momenta of the propellant jets[2].

The second known source of information on heat transfer around the injector surface was from unpublished test results obtained by Ziebland[3] on a 4 cm diameter model combustion chamber using gaseous oxygen and kerosine as propellants. The total heat flux was measured over a water cooled area surrounding a single injector element consisting of a centrifugal spray nozzle for kerosine and a coaxial narrow annular passage for oxygen (Fig.9.3). A summary of the experimental data will be found in Table 9.I of this chapter. Experiments were conducted at three combustion pressures and as the nozzle diameter remained unchanged for all tests, the data obtained refer to different total propellant flow rates, and thus should display the effect of jet momenta on entrainment-induced convective heat flux.

A later paper by the same author[4] contains experimental data of the radiative heat flux in a model combustion chamber close to the injector region, using the same propellant combination and mixture ratio as in Reference 3. As a first order approximation the convective heat flux to the injector may be obtained by simply subtracting the radiative heat flux of Row 2 in Table 9.I from the measured total heat flux. The result of this simple analysis shows clearly that the radiative and the convective part of the total heat flux are for the system in question of a similar magnitude and it would clearly be wrong to dismiss the radiative flux for either of the two most widely used propellant combinations, i.e. oxygen/kerosine and oxygen/hydrogen as insignificant. As has been pointed out in the preceding section on radiation, the emissivity of the luminous flame inside the thrust chamber at high chamber pressures, or large optical path lengths tends towards unity and it seems probably that under these conditions the radiative heat flux will become the dominant mode of energy transfer to the injector face.

Bearing in mind the experimentally verified existence of an intense radiation continuum in the flame or reaction zone of the thrust chamber, it is possible with the aid of some simplifying assumptions to obtain an estimate of the radiative heat flux to the injector.

It is probably true to say that in the case of a hydrocarbon fuel the intensity of radiation from the flame front to the injector face might be considerably attenuated by the finely atomised propellant sprays and it does not seem impossible that under these conditions the convective heat flux will preponderate. However, in all cases where the propellants do not possess appreciable absorption bands the energy radiated towards the injector will pass unattenuated to the injector face where, depending on the optical properties of the surface, a fraction of this energy will be directly absorbed. This situation applies to one of the most important propellant combinations, viz, hydrogen-oxygen, as neither of these two substances possesses absorption bands in the wave length region of interest.

In the following an attempt has been made to provide a quantitative estimate of the radiative heat flux and it will be seen that the radiative heat flux is significant and cannot be ignored when assessing the operating conditions, in particular the critical surface temperature of the injector face. The following simplifying assumptions have been made:

(a) The radiating gas body emits a continuum and the location of this continuum is the reaction zone which is assumed to commence at a distance δ from the injector. It is further assumed that the temperature of this zone is uniform through its entire depth. In most cases the radiating gas body will fill the entire cross section of the combustion chamber, but the analysis can easily be extended to cases where the diameter of the flame front is less than that of the combustion chamber.

(b) The surface of the heat receiving injector behaves like a grey body.

Consider thus the circular surface of the flame front as an isothermal, grey body in radiative heat exchange with the injector surface through a non-absorbing medium. The net radiative heat flux at the injector surface is given by

$$\ddot{q}_r = \epsilon_f \epsilon_w F_{f-w} \sigma_B (T_f^4 - T_w^4) \ , \qquad (9.1)$$

where ϵ_f and ϵ_w are the emissivities of the luminous gas body and the wall respectively,

F_{f-w} the so-called angle factor for radiative heat exchange for the configuration shown in Figure 9.4,

σ_B the Stefan-Boltzmann constant,

T_f and T_w the absolute temperature of the gas body and the injector surface, respectively.

The angle factor F_{f-w} for two circular surfaces was first evaluated by Christiansen[5] and Figure 9.4 taken from Reference 6 represents the dependence of this quantity on the dimensionless distance D/δ between the two radiating surfaces. Concerning the estimates for the remaining quantities it is reasonable to assume that D/δ will not be less than 10 for medium and large thrust chambers. Further, using a value of 0.5 for the emissivity of the surface (oxidised) and 0.8 for that of the luminous flame zone, and restricting the average surface temperature of the injector to 700°K, the heat fluxes received at the injector surface as a function of the flame temperature have been calculated and will be found in Table 9.II.

9.3 THERMAL PROTECTION OF THE INJECTOR FACE

The problem of thermal protection of the injector can be attacked from two angles. First, in the light of the preceding considerations on the effects of recirculatory flows on heat transfer, steps should be taken to minimize this contribution by adopting suitable design and operating characteristics. Low gas entrainment demands low velocity liquid injection and small jet diameters. Both of these requirements are, however, in conflict with those for efficient atomisation and stable combustion.

This dilemma could be resolved if the seat of the entrainment were further removed from the injector face by, e.g. extending the injector orifices in form of small tubes downstream of the injector face. Practical experience[1] has shown that designs in which the oxidiser jets impinged farther away from the injector face than the fuel jets proved satisfactory. Thus to prevent preferential recirculation of oxygen rich gases which may react at the injector surface with entrained fuel droplets or, in severe cases with the wall material itself, the oxidiser pressure drop and thus the injection velocity according to Reference 1 should be high with respect to that of the fuel. A pressure drop ratio of 2:1 seems desirable to prevent face erosion. An alternative solution would be to arrange for the oxidiser atomisation to occur downstream of the plane of fuel impingement. The efficacy of these suggestions is difficult to assess and will certainly have to be proved by experiment, particularly if major changes in the operating characteristics, such as changes in combustion pressure, mixture etc., are contemplated during an operating cycle.

To minimize radiative heat transfer, the surface of the injector should have a high reflectivity. Most clean metallic surfaces would meet this requirement but owing to the chemical nature of the combustion products the formation of an oxide film, or the deposition of unburnt fuel residues would rapidly change the favourable initial state. Plating the surface with a highly reflecting noble metal, e.g. silver, might be an advantage in hydrogen/oxygen rocket thrust chambers.

Whilst these arrangements will tend to reduce the heat transfer to the injector face, the heat ultimately reaching it must be absorbed by the propellant jets, unless a separate cooling system is provided. An order of magnitude calculation demonstrates that the heat transfer rate within the injection orifices will exceed that by convection to the propellants in their respective annuli. The problem is therefore to find an expression for forced convection in narrow cylindrical ducts with low aspect ratio (l/d). This latter quantity will have values between 1 to 3 from which it follows that flow conditions in jet orifices will be undeveloped and the conventional equation for convective heat transfer for fully developed turbulent flow will have to be suitably modified for this effect.

A review of the literature concerning the characteristics of liquids flowing through ducts of low aspect ratio reveals disagreement between various workers on recommended heat transfer relations. The situation is further confused by the differing performance of various duct entrance configurations, e.g. sharp-edged orifices, in which flow separation may occur in the entrance region, and smooth, rounded-entry orifices.

A comprehensive investigation on heat transfer in the entrance region of circular ducts employing a variety of different entrance configurations was conducted by Grass[7]. The measurements ranged from aspect ratios of 0.5 to 17 and Reynolds numbers from about 20×10^3 to 50×10^3. This range straddles that of typical propellant jet Reynolds numbers which lie around 30×10^3. In view of the complexity of the results obtained no attempt was made to correlate the results by analytical expressions and a graphical presentation was preferred. The results for two entrance configurations which resembled those of injector orifices, viz. the rounded entrance and the sharp edged entrance were taken from Reference 7 and are shown in Figures 9.5 and 9.6.

It will be noticed that for the rounded entrance the local heat transfer coefficient at an aspect ratio of unity differs by a relatively small amount from that for the fully developed conditions which in this case seem to have become established at $l/d = 7$. In contrast to that the local heat transfer coefficient for the sharp edged orifice for unity aspect ratio is about twice as high as that for fully developed turbulent flow. This latter configuration is therefore to be preferred although the pressure drop will be higher than for a rounded entrance.

The experimental heat transfer coefficients of Figures 9.5 and 9.6 apply only to single-phase convective heat transfer. Should nucleate boiling, or film boiling occur in the orifices, the appropriate relations from Section 7.3 must be applied.

In many injection systems, particularly those described in Russian textbooks[8,9], swirl is introduced deliberately within the orifices in order to assist in atomising and mixing the propellants. Under these circumstances the heat transfer coefficient may be further enhanced and cooling thus be more effective.

In a practical case the design details of an injector, i.e. the distribution, size, etc. of the various injector orifices will primarily be influenced by considerations related to its main functions, viz. atomisation and effective mixing of the propellants. Heat transfer considerations are only of interest in so far as the maximum injector face temperature may have to be restricted in order to prevent damage or undesirable flow conditions (boiling) in the narrow injector orifices.

Provided the total heat flux $\dot{q}_{tot}$ to the injector surface can be estimated or calculated, the average excess temperature of the surface of the propellant orifices can be calculated from a balance between the heat received at the injector face and that removed by the propellants. It is assumed that the heat transported to the propellants in their respective annuli is negligibly small compared with that removed by the propellants in passing through the orifices.

Suppose the total surface of the injector cocled by fuel jets is A_f (normally the projected area of all fuel-filled annuli), the total heat received in unit of time is

$$\dot{q} = \dot{q}_{tot}[A_f - (\pi/4)\Sigma d_f^2] \ , \tag{9.2}$$

where $(\pi/4)\Sigma d_f^2$ is the total cross-sectional area of all fuel jet orifices of diameter d_f.

This heat flow has to be removed by the fuel on passing through the respective orifices of diameter d_f and length l. Hence

$$\dot{q} = \bar{h}_f \pi \Sigma d_f l [\bar{T}_{w,f} - \bar{T}_f] \ , \tag{9.3}$$

where $\bar{h}_f$ is the mean heat transfer coefficient for fuel flowing through a short duct (entrance regime)

$\bar{T}_{w,f}$ and $\bar{T}_f$ are the mean wall temperature of the fuel orifices and the bulk temperature of the fuel, respectively.

Combining Equations (9.2) and (9.3), and solving for $\bar{T}_{w,f}$, leads to

$$\bar{T}_{w,f} = \bar{T}_f + \{\dot{q}_{tot}[A_f - (\pi/4)\Sigma d_f^2]\}/\bar{h}_f \pi \Sigma d_f l \} \ . \tag{9.4}$$

The mean heat transfer coefficient $\bar{h}_f$ for a given value of l/d_f can be obtained from the experimental data presented in Figures 9.5 and 9.6 through the following relations. The average Nusselt number, given by

$$\overline{Nu} = [1/(l/d_f)_a] \int_0^{(l/d_f)=a} Nu \, d(l/d_f) \quad , \tag{9.5}$$

which can be obtained by graphical integration of the relations in Figures 9.5 or 9.6 between $(l/d)=0$ and $(l/d)=a$ from which by definition the average heat transfer coefficient is,

$$\bar{h}_f = \overline{Nu}(\lambda_f/d_f) \quad , \tag{9.6}$$

where λ_f is the thermal conductivity of the fuel at some suitable reference temperature, e.g. $(T_{w,f} + T_f)/2$.

Introducing (9.6) into (9.4) leads to

$$\bar{T}_{w,f} = \bar{T}_f + \{\dot{q}_{tot}[A_f - (\pi/4)\Sigma d_f^2] / \overline{Nu}\, \pi\lambda_f \Sigma d_f l/d_f\} \quad . \tag{9.7}$$

The term in curly brackets represents the average temperature difference between the orifice surfaces and the fuel and will be referred to as

$$\Delta T_{w-f} \quad .$$

For an injector with uniform orifice diameter d_f the denominator in the expression for T_{w-f} assumes the simple value of

$$\overline{Nu}\, \pi\lambda_f \Sigma l \quad .$$

Large values of the above term, other things being equal, will thus result in small values of $T_{w,f}$.

Equation (9.7) is, of course, with the appropriate values for the oxidiser jets, equally valid for that fluid.

Providing the basic assumption, according to which heat is predominantly removed by heat transfer within the jet orifices, holds true, Equation (9.7) can be used for a rapid estimation of the influence of certain design variables and operating parameters on the mean injector orifice temperature. The latter is not identical, but closely related to the maximum wall temperature between two jets as shown by the schematic presentation of the injector face temperature distribution in Figure 9.2.

Typical examples for the use of Equation (9.7) are:

(a) The assessment of surface temperature changes brought about by such changes in the physical conditions of the propellants (pressure and temperature) at the point of entry into the orifice, which are likely to have a marked effect on the thermal conductivity λ .

(b) The prediction of surface temperatures for a given injector intended to be used with a different propellant.

9.4 CONCLUSIONS

Our knowledge of the heat transfer conditions to the injector surface is scant and, as far as experimental evidence is concerned, essentially restricted to two independent experimental studies. Whilst the interpretation by the authors of their results is not in full agreement, the absolute heat fluxes as measured or deduced from the observations are quantitatively similar.

Owing to the large number of injector types proposed, made and tested, it was always felt impossible to make even approximate predictions of the heat flow to the injector face. The suitability of a new design and the efficiency of the thermal protection technique employed, had to be proved by experiments. However, during the last decade or so, some standard injector designs have emerged, of which the multi-orifice showerhead injector, or multi-orifice impinging jet injector have been dominant. In both cases propellants flow through a large number of fairly closely spaced orifices and it should eventually be possible by well designed experiments and their analysis to arrive at a better understanding of the flow and heat transfer phenomena on a multi-orifice, heated plate.

In view of the evidence provided, there seems to be little doubt that radiation to the injector is by no means a quantitatively insignificant process; in some cases it may even exceed the convective contribution caused by recirculatory flows.

The simple equation for estimating the surface temperature of the injector orifice walls can only give first order approximations of the likely injector surface temperatures in the immediate vicinity of the orifice.

At present the basis for making reasonable estimates of the radiative heat transfer exists, but the convective contribution to the total heat flux cannot be even approximately estimated.

REFERENCES

1. Bragg, S.L.; Smith, I.E. — *Heat Transfer to Rocket Injectors.* International Developments in Heat Transfer, ASME, 1961/62.
2. Braisby, A.T. — Rocket Department Development Report No.88, Rolls-Royce Ltd.
3. Ziebland, H. — *Experimental Studies on Heat Transfer in Rocket Thrust Chambers, Part IV: Heat Flux Distribution in Oxygen-Kerosine Thrust Chambers and Nozzles at Various Combustion Pressures,* Unpublished report.
4. Ziebland, H. — *Radiation and Convection in High Energy Liquid Propellant Rocket Engines.* International Developments in Heat Transfer, ASME 1961/62.
5. Christiansen, C. — Wiedemanns Ann., Vol.19, 1883, p.267.
6. Plank, R. (Editor) — Hdb.d.Kältetechnik, Vol.III, Springer Verlag, Berlin, 1959.
7. Grass, G. — *Wärmeübergang an turbulent strömende Gase im Rohreinlauf.* Allgem. Wärmetechn., Vol.7, 1956, p.58.
8. Dobrovolsky, M.V. — *Liquid Rocket Engines.* Moscow, 1968.
9. Kudryashev, M.V. (Editor) — *Elements of the Theory and Design of Liquid Rocket Engines.* Moscow, 1967.

TABLE 9.I

Heat Flux to the Cooled Injector Surface of a Single Element Injector in a 4 cm Diameter Thrust Chamber. Data Taken from Reference 3 Pertain to a Stoichiometric Mixture of Oxygen and Kerosine. Operating Pressures 10, 20 and 40 bar, Respective Adiabatic Flame Temperatures 3410°K, 3515°K and 3620°K.

Heat Flux, W/cm²				
		Pressure, bar		
		10	20	40
1	Total Heat Flux (experimental, Reference 3)	210	290	380
2	Radiative Heat Flux (taken from Reference 4)	109	155	220
3	Convective Heat Flux (row 1 – row 2)	101	135	160

TABLE 9.II

Radiative Heat Flux as a Function of the Temperature of a Luminous Flame to an Injector Having a Surface Temperature of 700°K.

Flame Temperature °K	*Heat Flux*
	W/cm²
1000	1.4
1500	8.8
2000	28.6
2500	70.5
3000	147
3500	272

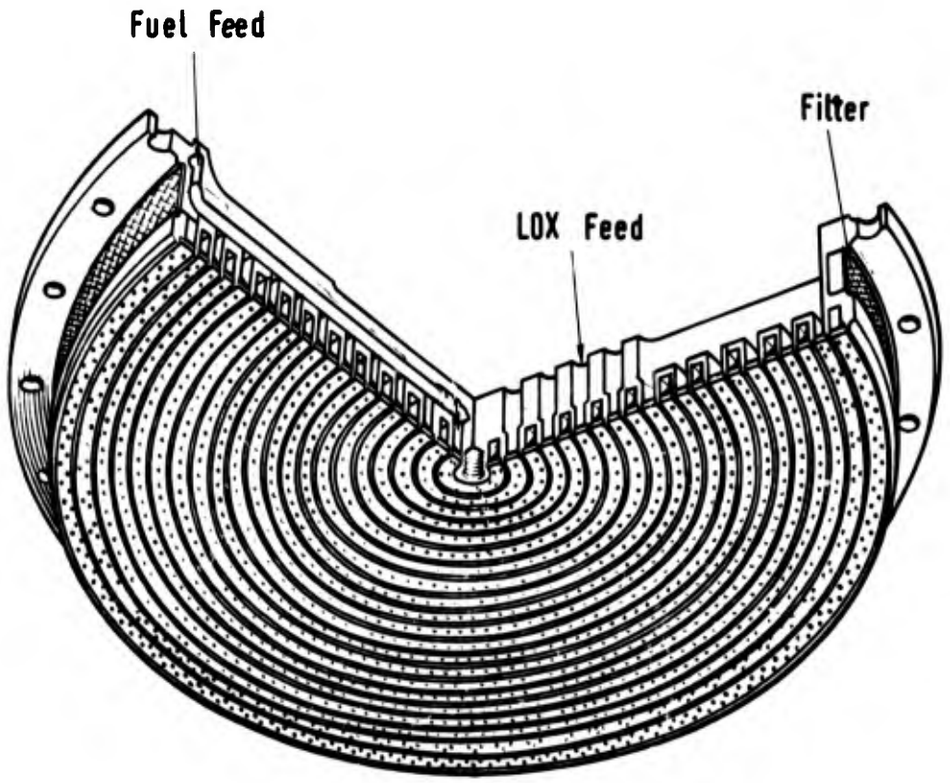

Fig.9.1 Typical liquid propellant injector. (Courtesy Rolls-Royce Ltd)

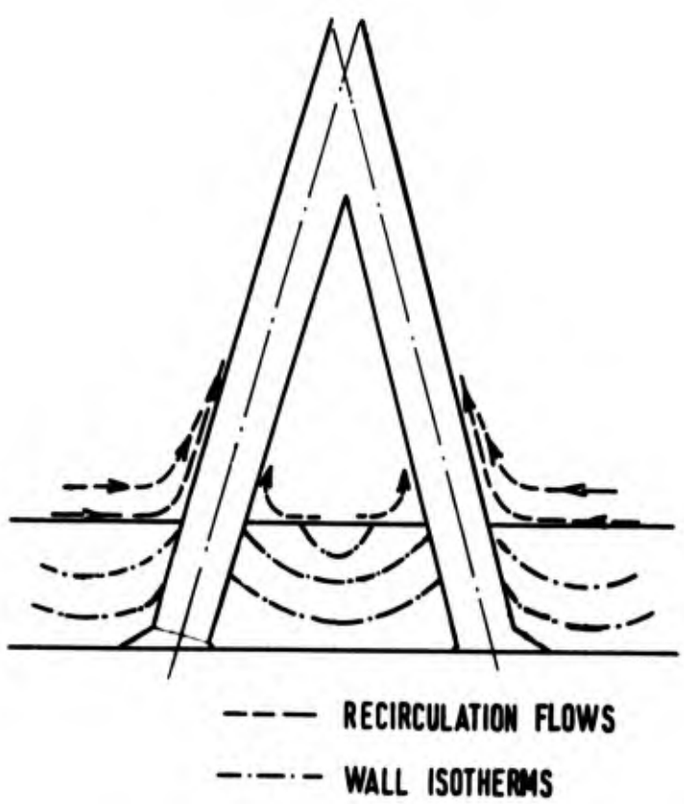

Fig.9.2 Schematic flow and temperature distribution on the wall of a flat plate cooled by emerging jets

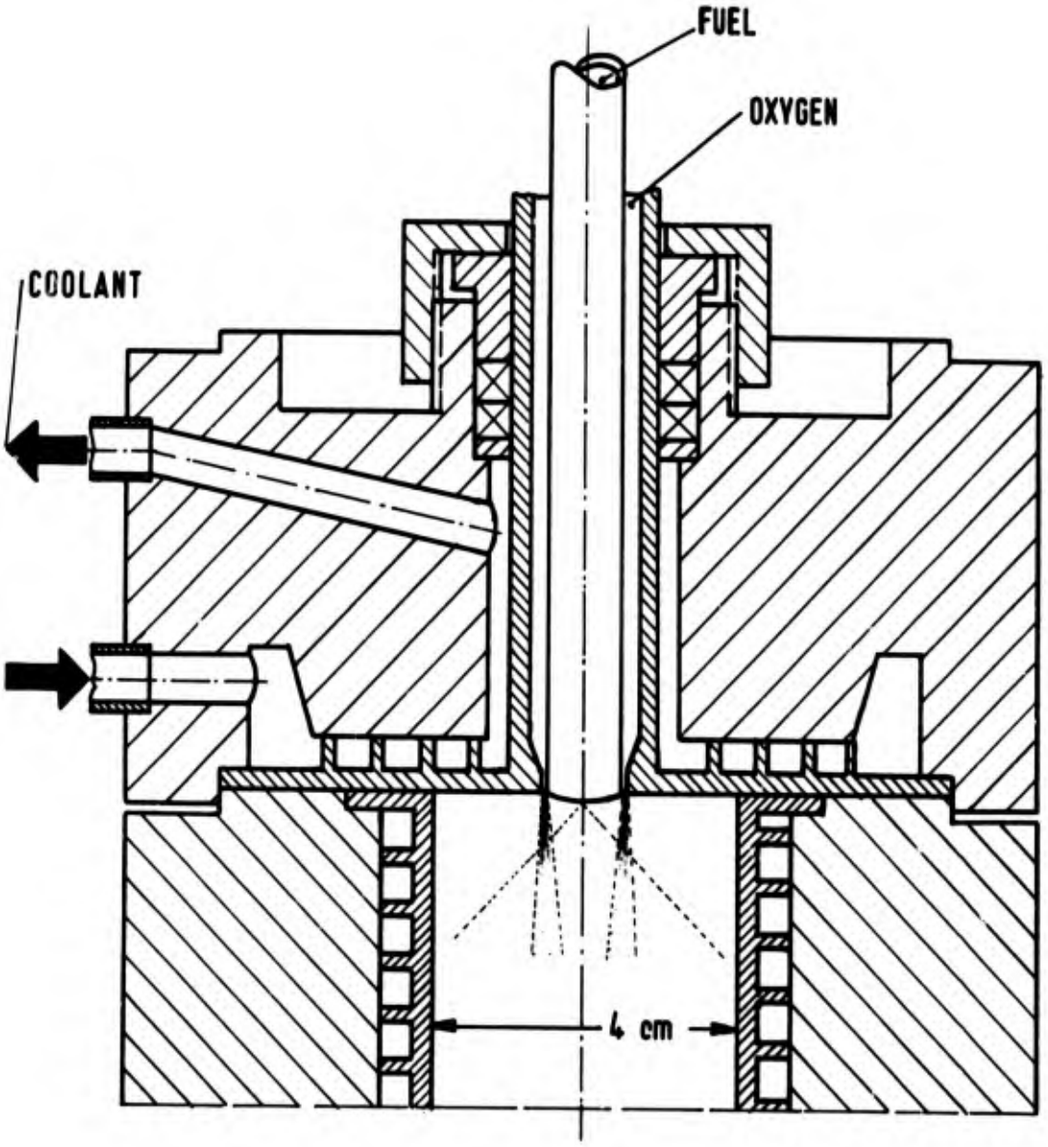

Fig.9.3 Water-cooled, single element bi-propellant injector for gaseous oxygen and kerosine (Ziebland[3])

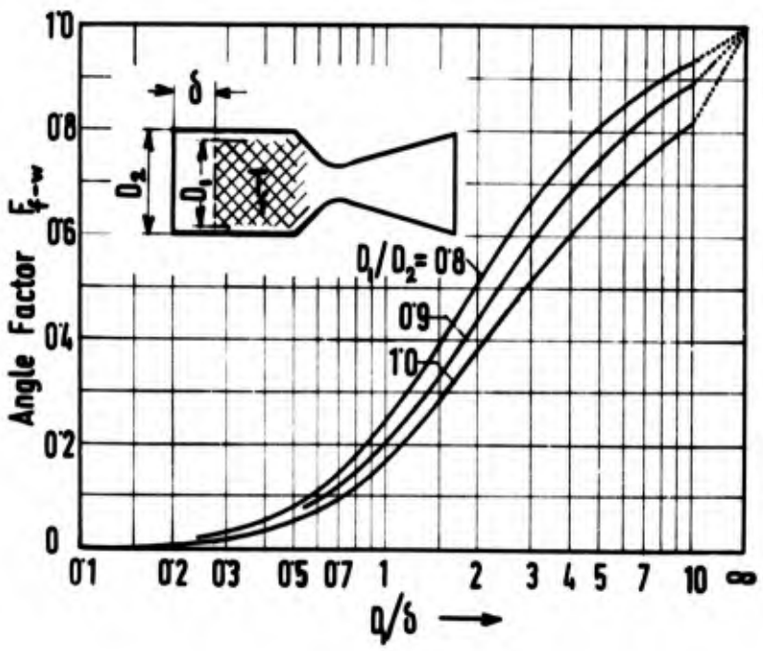

Fig.9.4 Angle factor for radiative heat exchange between the luminous flame front and the injector surface (Christiansen[5])

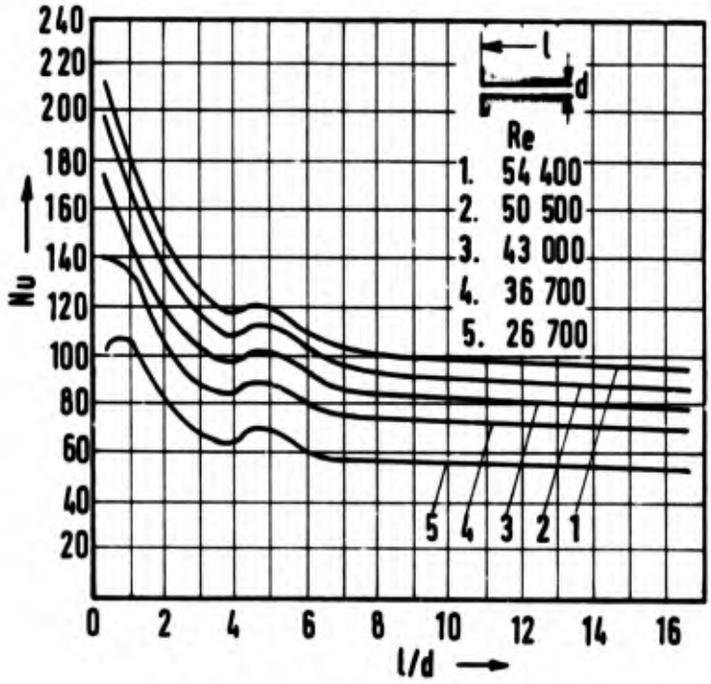

Fig.9.5 Local Nusselt number in the entrance regime of a sharp-edged cylindrical duct. (According to Grass[7])

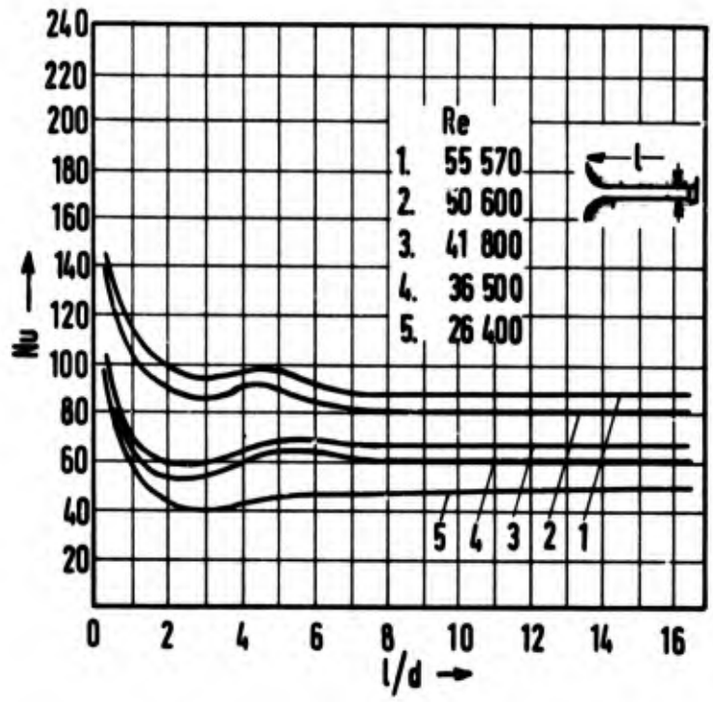

Fig.9.6 Local Nusselt number in the entrance regime of a rounded entry cylindrical duct. (According to Grass[7])

CHAPTER 10

REGENERATIVELY COOLED ENGINES

10.1 GENERAL

Regenerative cooling has a long history in the design of rocket engines, providing a most attractive method of cooling the walls of the combustion chamber. One of the propellants is circulated in a jacket, or through tubular ducts arranged around the outside of the engine before being injected into the combustion chamber (Figure 10.1), and the heat transferred to the thrust chamber walls is recovered as a slight increase in input enthalpy of the propellants. No fraction of the propellant or any other fluid is required solely for cooling purposes, and thus no performance loss of the engine is incurred. Regenerative cooling is therefore of particular interest where extended firing times of the engines are envisaged, e.g. in the propulsion of large space boosters.

Four important design criteria have to be met for regeneratively cooled engines. First, the total heat transferred to the liquid coolant must not raise the bulk temperature to the local boiling point, or to such a temperature at which decomposition reactions in the propellant may commence. Secondly, the local heat transfer rate must not exceed the maximum nucleate boiling heat transfer rate at any point. Thirdly, the pressure drop in the cooling ducts must not be excessive. And finally, the wall temperature must be kept sufficiently low to avoid structural failure, either due to melting erosion or mechanical failure because of the thermal stresses set up in the wall.

This chapter will deal only with simple regeneratively cooled engines. In practice, a combined system of cooling will often be used – in particular film cooling is often employed to reduce maximum local heat transfer rates. For this reason, the performance limits of regeneratively cooled engines are poorly defined, and only trends can be indicated.

10.2 OVERALL HEAT TRANSFER

The first limitation on regeneratively cooled rocket engines is that the total heat transferred to the coolant should not be sufficient to cause vapour formation in the bulk coolant flow. This applies only to coolants below their critical pressure. At supercritical pressures no abrupt change in density will occur with subsequent blockage of the flow, and upper limits to the maximum permissible coolant temperature will be set by other criteria. However, as Table 10.I shows, the only propellants for which supercritical operation is likely to occur at normal combustion pressures are hydrogen and kerosine.

The choice of coolant may be influenced by a variety of factors, such as the physical and chemical properties of the fluid, the engine operating conditions, etc. A brief review of methods of utilizing liquid propellants as coolants and establishing criteria for acceptable cooling has been given by Bartz[1]. Table I of his report contains a comprehensive index to measurements of heat transfer to propellants with and without surface boiling under forced velocity, subcooled conditions.

To indicate the limits imposed on regeneratively cooled engines by propellant boiling, calculations have been made of the overall heat transfer rate expected in a typical engine for various propellant combinations, assuming a constant wall temperature. From this, the expected temperature rise of the coolant, and its eventual vapour pressure can then be calculated (see Table 10.II). Such calculations will serve as the beginning of any regeneratively cooled engine design. From it one can see how easy or difficult regenerative cooling will be for a given situation.

In view of the marked degree of thermal dissociation of the combustion gases of high energy propellants and the consequent influence of mass diffusion and recombination on convective heat transfer, it has been found convenient to introduce in such situations the difference between the combustion gas enthalpies at the gas-side wall temperature and at the temperature of the main flow as the driving potential. With this an "overall energy transfer" coefficient will be defined as the overall heat transferred to the rocket engine walls divided by the driving enthalpy difference ΔH and the total surface area of the engine. Once combustion has been established in the initial part of the chamber, the overall energy transfer coefficient remains very nearly constant – rising to a slight peak just downstream of the nozzle throat and then slowly decreasing (see Figure 10.2). More importantly, the value of this coefficient is largely independent of size. Over a 4:1 range in size (based on throat diameter D_*), the overall energy transfer coefficient typically varies by a mere 20%.

The surface area of the engine will be approximately proportional to the length and the throat diameter $D_\star$ of the engine. Engine length can be divided between the combustion chamber (L_c) – remaining more or less constant -- and the nozzle, which for constant nozzle angle will scale with the throat diameter. Thus

$$\text{surface area} = K_1 D_\star L_c + K_2 D_\star^2 ,$$

and the total heat transferred (Q), assuming a constant overall energy transfer coefficient (h), will be

$$Q = h \Delta H (K_1 D_\star L_c + K_2 D_\star^2) .$$

The mass-flow of coolant, for a given chamber pressure, will be proportional to the throat area, so that the temperature rise (ΔT) in the coolant can be calculated from an expression of the form

$$\boxed{\Delta T = K_3 \frac{h \Delta H}{c_p} \left(\frac{L_c}{D_\star} + K_4 \right) .} \qquad (10.1)$$

Larger engines, therefore, are easier to cool than smaller ones. Because of this constraint, and because of local heat flux considerations (see Section 10.3), there will tend to be a lower size limit to the use of regenerative cooling for a given propellant and operating conditions.

For a given engine size the overall energy transfer coefficient is very nearly proportional to the chamber pressure p_c raised to the 0.8 power. Because the mass-flow of coolant will be directly proportional to the chamber pressure, the temperature rise in the coolant will decrease as the chamber pressure increases. A specific example has been given in Table 10.II. But in addition to the decreasing temperature rise of the coolant with increasing pressure, allowable vapour pressures in the coolant will also increase, and so the cooling problem will diminish.

10.3 LOCAL HEAT TRANSFER

The local rate of heat transfer at any area in the engine may limit the design either by causing excessive nucleate, and even film boiling at the coolant-wall interface, or by causing chemical decomposition of the coolant.

Local nucleate boiling is initially a beneficial process – allowing the coolant to absorb rather more heat for a given temperature difference than is possible by simple, single-phase convection processes. But eventually, with increasing heat flux the vapour bubbles will begin to coalesce on the hot surface, forming an insulating film of gas. The maximum nucleate-boiling heat-flux rate will be dependent in a very complex fashion on the properties of the fluid and the flow conditions (see Chapter 7). For particular fluids it is often possible to develop correlations in terms of the velocity of the flow (U) and the degree of "sub-cooling" of the liquid (ΔT_{sub}) , which is the difference between the liquid bulk temperature and the local boiling point. A proposed correlation has the form

$$\ddot{q}_{ult} = A + BU \Delta T_{sub} , \qquad (10.2)$$

where A and B are individual constants, to be determined by experiment.

In a simple analysis one may assume that the worst condition occurs immediately upstream of the nozzle throat. Once again, the energy transfer coefficient will be proportional to the chamber pressure raised to the 0.8 power, and the equation for the maximum heat transfer rate will be of the form

$$\ddot{q} = K_1 p_c^{0.8} \Delta H . \qquad (10.3)$$

Combining this with Equation (10.2), the minimum velocity of flow in the coolant channels will be

$$U = \frac{K_1 p_c^{0.8} \Delta H - A}{B \Delta T_{sub}} . \tag{10.4}$$

The mass-flow of coolant will be some fixed fraction of the total mass-flow through the engine, and hence proportional to both the chamber pressure and throat area. Knowing the velocity of flow, the coolant flow area at the throat (A_c) may be calculated from

$$A_c = \frac{K_2 p_c B \Delta T_{sub} \pi D_\star^2}{\rho_c (K_1 p_c^{0.8} \Delta H - A)} ,$$

where ρ_c is the coolant density. The ratio of the coolant channel height (d) to the throat diameter ($D_\star$) is thus given by

$$\frac{d}{D_\star} = \frac{K_2 B \Delta T_{sub} p_c}{\rho_c (K_1 p_c^{0.8} \Delta H - A)} \tag{10.5}$$

It follows that the ratio of the channel height to the throat diameter will remain constant for a given chamber pressure. The lower limit to size will be set by problems of fabricating small bore tubes, or, by unacceptably high pressure drops in the coolant ducts.

For the effect of chamber pressure on Equation (10.5), a few simple calculations show that the most important factor is likely to be the consequent variation of ΔT_{sub} . As the chamber pressure is increased, so also is the pressure in the coolant channels, and hence the boiling point of the coolant. The effect of this is that at higher chamber pressures, $d/D_\star$ will increase. Eventually, the critical pressure of the coolant fluid will be attained, and the constraint of the limiting ultimate heat flux will disappear.

At sufficiently low chamber pressures the situation changes. It is probable that there will be a point at lower chamber pressures at which the pressure in the coolant jacket will become relatively independent of the chamber pressure. Below this point only those terms in p_c in Equation (10.5) will affect the ratio of the coolant channel height to the throat diameter, and it is possible for this ratio to increase once more. Eventually the heat flux from the hot gases will no longer cause nucleate boiling in the fluid, and the limitation will again disappear. Figure 10.4 illustrates this effect.

A different limit on the local heat transfer will be set if the coolant undergoes chemical decomposition. In this case the limit on local heat transfer will be set by the local, coolant-side wall temperature. While the rates of the decomposition reaction will increase with temperature, and the limiting temperature of the wall will to some extent depend on the flow rate of the liquid over it, these effects have not been investigated in the detail of – for instance – nucleate boiling effects. It is important, however, to avoid stagnant pockets of the coolant in the design, where even slow reaction rates will have an opportunity to take place.

The main propellants in which propellant decomposition may be important are hydrogen peroxide, the various hydrazine fuels, and hydrocarbon fuels such as kerosine. The two former classes of propellants undergo exothermic decomposition, kerosine presents problems of polymerisation and "cracking" of the fuel leading to the formation of solid deposits within the tube. Suggested temperature limits for surfaces over which there is a continuous flow are 480°K for HTP, 600°K for hydrazine, and 700°K for kerosine. In their experimental study on heat transfer to kerosine, Ziebland and Beech[2] investigated the carbon formation on an electrically heated nickel tube. As the surface temperature exceeded a value of about 300°C an immediate and rapid build-up of carbon was noticed. Thereafter, the rate of deposition increased only slowly with time. By plating the tube with a thin layer of gold the onset of carbon formation could be delayed until a wall temperature around 500°C was reached. From this and other supporting evidence the above authors concluded that the thermal decomposition of kerosine, or that of one of its constituents, e.g. an unsaturated compound, was catalysed by the nickel surface.

10.4 PRESSURE DROP IN COOLANT TUBES

The pressure drop occurring in the coolant ducts can in many cases provide a practical limit to the employment of regenerative cooling. In theory, for instance, it might be possible to construct a chamber from very

narrow bore tubes and so overcome any limit on the local heat transfer given by Equation (10.5). In practice, however, a point will be reached at which the pressure drop in the coolant tubes is unacceptably high. Just what pressure drop is "unacceptably high" will depend very much on the overall system and it is difficult to give any useful generalizations.

The sources of pressure drop in the coolant tubes will be from the change in momentum of the coolant between entrance and exit in the absence of heat transfer, fluid friction in the tubes, and the acceleration of the coolant caused by its increasing density as the coolant is heated on its passage through the duct. If it is assumed that the coolant is incompressible, then Bernoulli's equation for the coolant flow between stations 1 and 2 may be written as

$$\frac{u_1^2}{2} + \frac{p_1}{\rho_1} + Q = \frac{u_2^2}{2} + \frac{p_2}{\rho_2} + \int \frac{2fu^2}{d_{hydr}}\,dx\,, \tag{10.6}$$

where Q is the heat added to unit mass of the coolant through the tube, f the friction factor, and d_{hydr} the hydraulic mean diameter of the coolant channel at any point. From this general relation the pressure drop in the coolant duct can be evaluated from

$$\boxed{\frac{\Delta p}{\rho_1} = \frac{u_1^2}{2}\left[\left(\frac{\rho_1 A_1}{\rho_2 A_2}\right)^2 - 1\right] - Q + p_2\left(\frac{1}{\rho_2} - \frac{1}{\rho_1}\right) + \int \frac{2fu^2}{d_{hydr}}\,dx\,.} \tag{10.7}$$

Equation (10.7) will have to be evaluated for a particular case. For the moment it is not at all apparent how the exit density (ρ_2), for instance, will depend on the total heat transfer. A simple example would be to assume, as for a gas, that

$$\rho \propto T^{-1}$$

and

$$T_2 = T_1 + k\,Q\,.$$

From which

$$\frac{\Delta_p}{\rho_1} = \frac{u_1^2}{2}\left[\left(\frac{A_1}{A_2}\right)^2 - 1\right] + Q\left[\frac{u_1^2}{2}\left(\frac{A_1}{A_2}\right)^2\left\{\frac{2k}{T_1} + \frac{k^2 Q}{T_1}\right\} + \frac{kp_2}{T_1\rho_1} - 1\right] +$$

$$+ \int \frac{2fu^2}{d_{hydr}}\,dx\,. \tag{10.8}$$

In this relation the three sources of pressure drop are separated. It may be observed that the friction loss will be inversely proportional to the fifth power of the hydraulic diameter of the coolant channel, and will thus rise rapidly at small duct sizes. Also, that the terms containing the overall heat transferred are quadratic in Q. The pressure drop will therefore depend both on the local heat transfer rates – principally affecting the friction losses – and the overall heat transfer rates.

A further problem may arise from the effect of excessive circumferential non-uniformities of the heat flux in the chamber on the pressure drop. Excessive local nucleate boiling in particular may increase the pressure drop along a particular duct, lowering the flow rate in that tube and so exacerbating the whole process and leading to tube failure. Most regeneratively cooled engines should be free from any such problem, but where nucleate boiling in the coolant ducts is likely to take place it may be necessary by judicious use of film cooling to moderate indeterminate circumferential non-uniformities in the local heat transfer.

10.5 THERMAL STRESSES

This far only the behaviour of the coolant in a regeneratively cooled engine has been considered. However, as the purpose of cooling the chamber is to keep the temperature of the wall within reasonable bounds it is essential to examine the conditions leading to failure of the cooling duct walls with increasing temperature.

Heat conduction through the tube walls will cause a temperature gradient in the material. With an externally heated duct the outer layers of the duct wall will tend to expand more than the inner layers, causing axial and

circumferential shearing stresses, and some radial tensile stress.

For an otherwise unstressed, thin-walled tube, the thermal stress (σ) in the outer fibres of the wall is given by

$$\sigma = \frac{E\alpha\Delta T}{2(1-\nu)}, \tag{10.9}$$

where E is the Young's modulus of the material, α the coefficient of thermal expansion, and ν the Poisson ratio. Substituting the yield stress $\sigma_{0.2}$ for the left hand side of Equation (10.9) yields the maximum temperature differential (ΔT) allowable in the material for steady state operation. This quantity in turn can be used to evaluate the maximum rate of heat transfer through a given thickness of material.

$$\ddot{q}_{max} = \frac{k}{\Delta x}\Delta T = \frac{2k\sigma_y(1-\nu)}{\Delta x E\alpha} \tag{10.10}$$

To some extent the maximum of heat flux through the duct walls can be increased by decreasing the wall thickness (Δx), but there are practical limits to this imposed by the other loads which the duct walls must carry – those dictated by the need for structural rigidity and to withstand the pressure differential across the tubes.

In Table 10.III, basic calculations have been made for a number of possible structural materials, using Equation (10.10). It is important to note here that the maximum rates of heat transfer do not occur with materials designed to keep their strength at high temperatures, but with the high conductivity materials such as copper.

The results presented in Table 10.III are simplified, in so far as they do not take into account any softening of the material at higher temperatures, nor the effects of pressure and thrust loadings on the structure. Also, in many cases the assumption that the tubes are thin-walled will not hold. Full stress calculations involve dividing the tube wall into a number of thin shells, adding in the pressure and other stresses, and integrating over the tube wall thickness taking account of the varying properties of the material with temperature.

If the behaviour of a practical engine design is examined in detail, it will be found that the main conclusions from Table 10.III still hold. Figure 10.5 shows the calculated bulk coolant and wall temperature distribution in a 60 kN thrust, oxygen-hydrogen engine, designed for operation at a chamber pressure of 3 MN/m². Inconel X-750 has been chosen as the wall material as being typical of the high temperature alloys used in rocket engines, and it can be seen that the inner wall temperature remains very nearly constant at 400°K. About half of the temperature drop between the hot wall and coolant takes place in the wall, half in the coolant, and the maximum wall temperature (880°K) occurs immediately upstream of the throat.

The thermal stresses in the tubes have been calculated assuming a constant coolant-side temperature and a variable gas-side temperature. The results are shown in Figure 10.6 for both Inconel X-750 and a beryllium-copper alloy. Also shown by dotted lines in these figures are the maximum gas-side wall temperatures achieved with each material. It is apparent that the wall of a chamber constructed from Inconel X-750 would be in the yield region near the throat, whereas for beryllium-copper there would still be a reasonable safety factor in the thermal wall stresses.

Refractory materials such as tantalum or tungsten offer somewhat better resistance to thermal stresses. But once again, the important advantage comes from increased thermal conductivity rather than the upper limits of temperature. Such materials are, however, more difficult to fabricate than more conventional materials.

The design limit imposed by thermal stresses in the walls is a limit on the high pressure operation of the engine, unlike previous criteria. Since the maximum heat transfer rate will increase with increasing exhaust velocity, higher performance engines will suffer lower pressure limits to regenerative cooling than will lower performance engines. Depending on the particular propellant combination used, simple regenerative cooling will become impossible at pressures somewhere above 10 MN/m². However, this pressure limitation can be raised by the careful use of film cooling and other methods.

10.6 REFRACTORY COATINGS

One method by which the thermal-stress limit can be improved is to use a coating of refractory material between the hot gas and the metal walls. This will slightly reduce the heat transfer rate, and also provide a thermal barrier to reduce the temperature drop in the load-carrying metal wall.

Figure 10.7 shows the engine previously used for Figure 10.5 with a refractory coating of aluminium oxide applied to it. The maximum temperature of the metal wall has been reduced by 100°K.

There will be very much the same thermal stress limit on the use of refractory coatings as was given for the tube walls in Equation (10.10), although since the coating will not have to carry loads it can be made much

thinner – at the cost of reduced protection of the underlying material. Refractory coatings are brittle, and will fail when the thermal stresses reach the coating yield point.

The coatings themselves can be applied simply by a flame-spray method. The two common coating materials are aluminium oxide and zirconium oxide, and these have been included in Table 10.III. Such coatings will also provide an oxidation resistant surface to the hot exhaust gases, and are used for this purpose with materials such as tantalum and molybdenum in use as radiation-cooled nozzle extensions.

10.7 DUMP COOLING

A variation on the basic method of regenerative cooling is to expel the coolant after it has served its purpose through a separate propelling nozzle. A simple way of doing this is to flow the coolant from the injector parallel to the main gas flow, and simply to terminate the coolant tubes in a sonic nozzle.

With hydrogen, the low molecular weight of the coolant means that exhaust velocities equal to, and perhaps in excess of, the main stream exhaust velocity can be achieved at temperatures below the limiting temperatures of the wall materials. Additional benefit is derived from the fact that the coolant inlet pressure is no longer the sum of the chamber pressure, the injector pressure drop and the coolant duct pressure drop but may be chosen at will. This may ease the burden on the propellant feed system.

Opposed to this is the fact that coolant must now be carried in addition to the propellants required in the combustion chamber. The low density of liquid hydrogen means that this will in its turn reflect on the overall stage mass by increasing propellant tank volume. Dump cooling will have to offset this disadvantage before it is likely to find application.

10.8 CONCLUSION

The limitations on the effective and safe operation of a regenerative cooling system will impose a limit as to the lower size of engine to which this method may be applied, but no upper limit on geometric size has been found. The effect of chamber pressure is, in general, to ease coolant channel fabrication problems, but eventually a limit will be reached resulting from the combined effect of pressure and thermal stresses in the coolant tube walls. However, with the selective use of film cooling, and/or refractory coatings, there is no reason why chamber pressures of at least 10 MN/m^2 cannot be achieved in high performance engines.

Regeneratively cooled engines have found widespread use in large engine applications, and this in itself speaks as testimony to the value of the basic method. It offers the possibility of long firing times without imposing any penalty on the overall performance. The apparent difficulties and expense of fabrication of such engines disappear when the total cost of developing any operational engine system and its attendant vehicle are taken into consideration.

In short, regeneratively cooled engines will occupy a continuing and important place in the family of rocket engines.

REFERENCES

1. Bartz, D.R. — *Factors which Influence the Suitability of Liquid Propellants as Rocket Motor Coolants.* JPL Memorandum No.20-139, 1956.

2. Ziebland, H.
Beech, J. — *Heat Transfer to Kerosine, D.Eng.R.D.2495 at Supercritical and Subcritical Pressures.* E.R.D.E. 5/R/63. Unpublished Ministry of Aviation report.

TABLE 10.I

Propellant	*Critical Point*	
	Pressure MN/m^2	*Temperature* °K
Ammonia	11.3	406
Hydrazine	14.7	654
Hydrogen	1.29	33
HTP	21.7	731
Kerosine	2.17	622
Nitrogen tetroxide	10.1	431
Oxygen	5.04	154
RFNA	8.86	545

TABLE 10.II

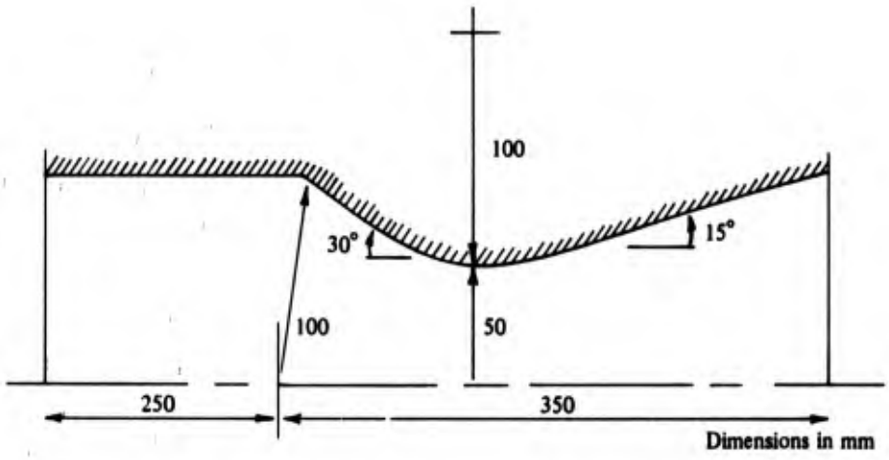

Propellants	*O/F Ratio*	*Coolant*	*Total Heat Transferred* MW	*Temperature Rise* ΔT °K	*Vapour Pressure* MN/m^2
a) Chamber pressure = 2.06 MN/m^2					
N_2O_4 – N_2H_4	1.0	N_2H_4	2.13	148	0.52
RFNA – NH_3	2.2	RFNA	1.04	79.5	0.30
LOX – Heptane	2.3	Heptane	2.22	378	1.72
HTP – Heptane	7.0	HTP	1.28	50.4	0.01
HTP – Heptane	11.0	HTP	1.02	36.5	0.00
b) RFNA-NH_3, Variable chamber pressure					
2.1 MN/m^2	2.2	RFNA	1.06	80.2	0.30
7.0	2.2	RFNA	2.80	63.4	0.20
20.6	2.2	RFNA	6.78	51.0	0.14

TABLE 10.III

	Ref.	σ_{yield} MN/m²	E MN/m²	k watt/m°K	α °K⁻¹	$\dot{q}_{max}$ MW/m²	ΔT °K	*Comments*
Beryllium-Copper		1100	1.31×10^5	133	1.7×10^{-5}	251	755	Limited by upper temperature limit for material
ETP Copper		276	1.17	389	1.75	185	475	
18-8 Stainless Steel		689	2.00	16	1.7	11.5	287	
Rene 41		965	2.06	11	1.2	14.8	538	
Inconel X-750		1070	1.72	19	1.45	29.0	610	
Tantalum		400	1.79	54	0.70	64.6	478	
Tungsten		2200	3.45	121	0.52	53.1	1760	Limited by falling yield
Refractory Coatings								
Aluminium Oxide		216	3.45	6.2	0.85	66	116	
Zirconium Oxide		83	1.24	2.0	0.80	24.5	122	

Metal wall thickness = 0.4 mm

Coating thickness = 0.01 mm

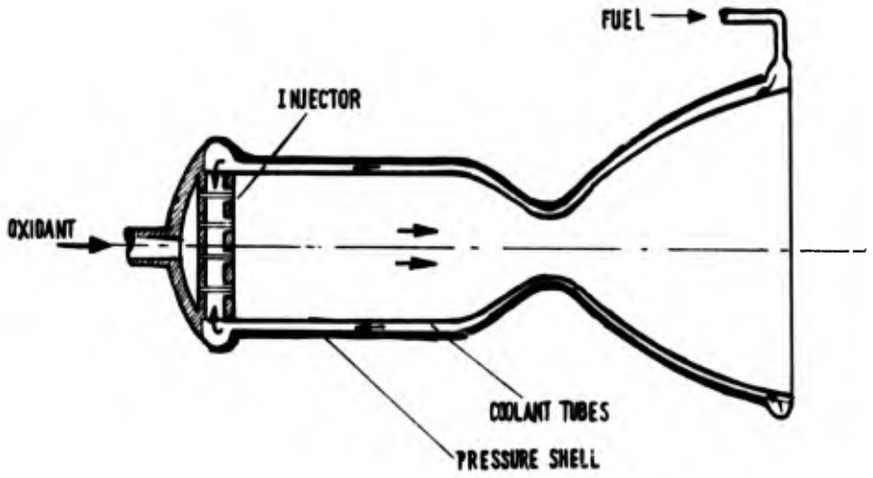

Fig.10.1 Regeneratively cooled engine

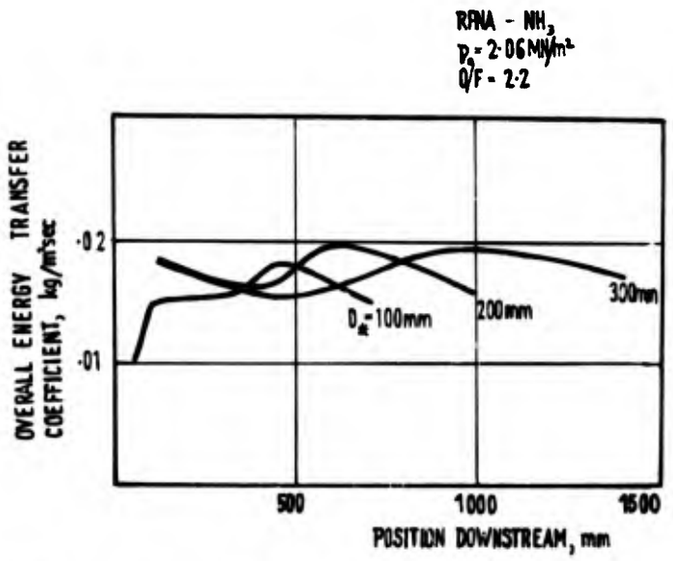

Fig.10.2 Overall heat transfer coefficients for engines of different sizes

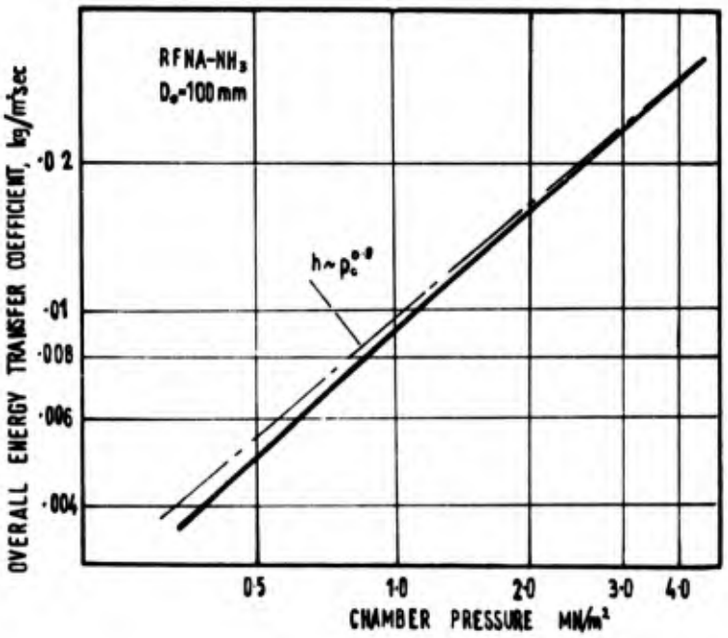

Fig.10.3 Overall heat transfer coefficients at different chamber pressures

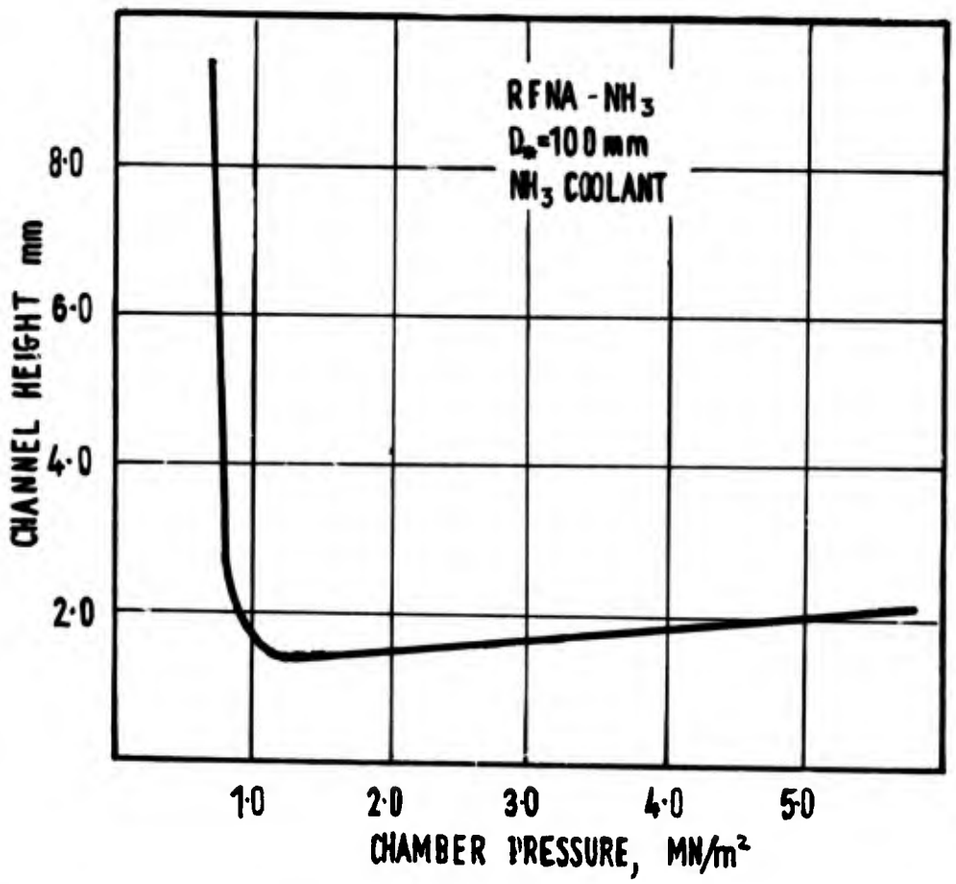

Fig.10.4 Variation of coolant channel height with chamber pressure for a given engine size

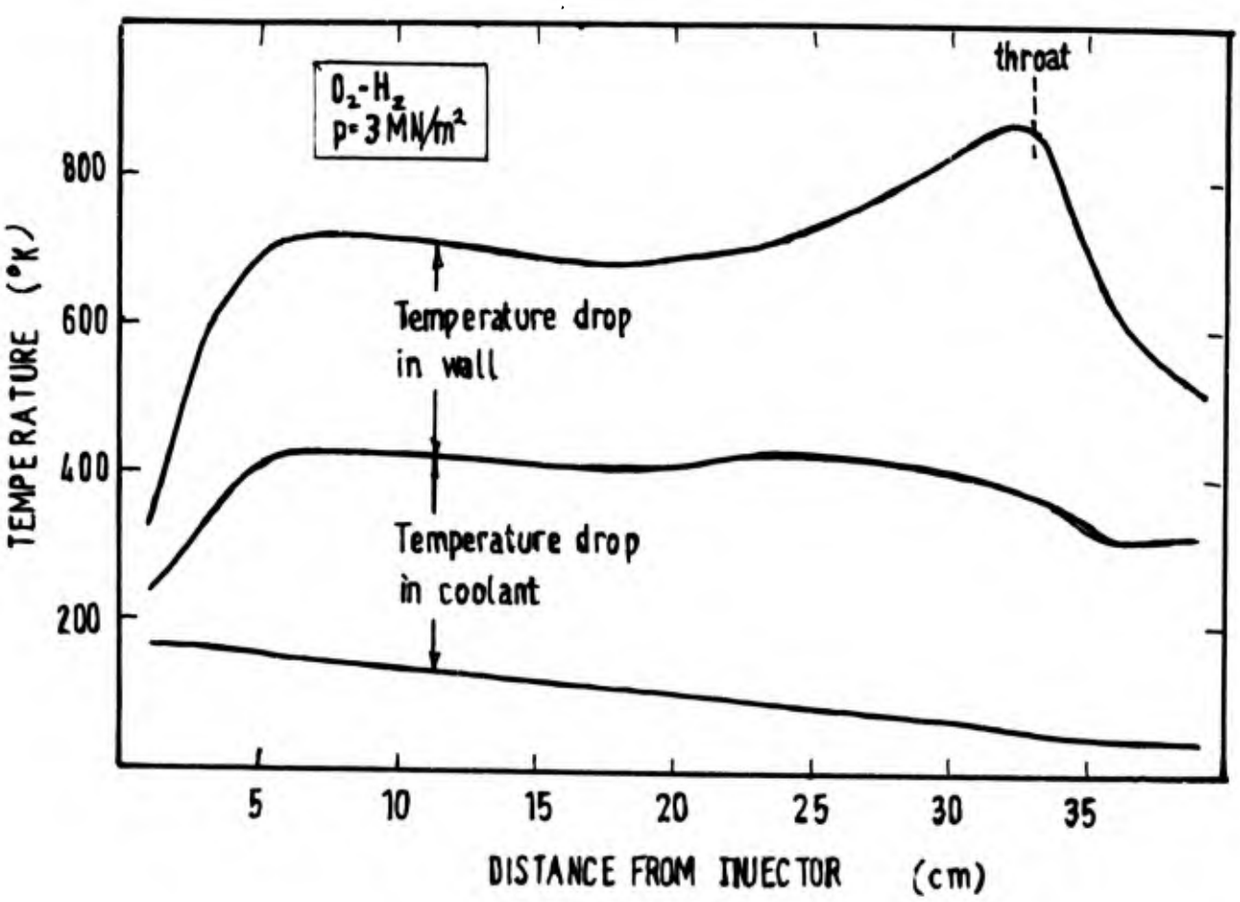

Fig.10.5 Temperature distribution in a regeneratively cooled oxygen-hydrogen engine

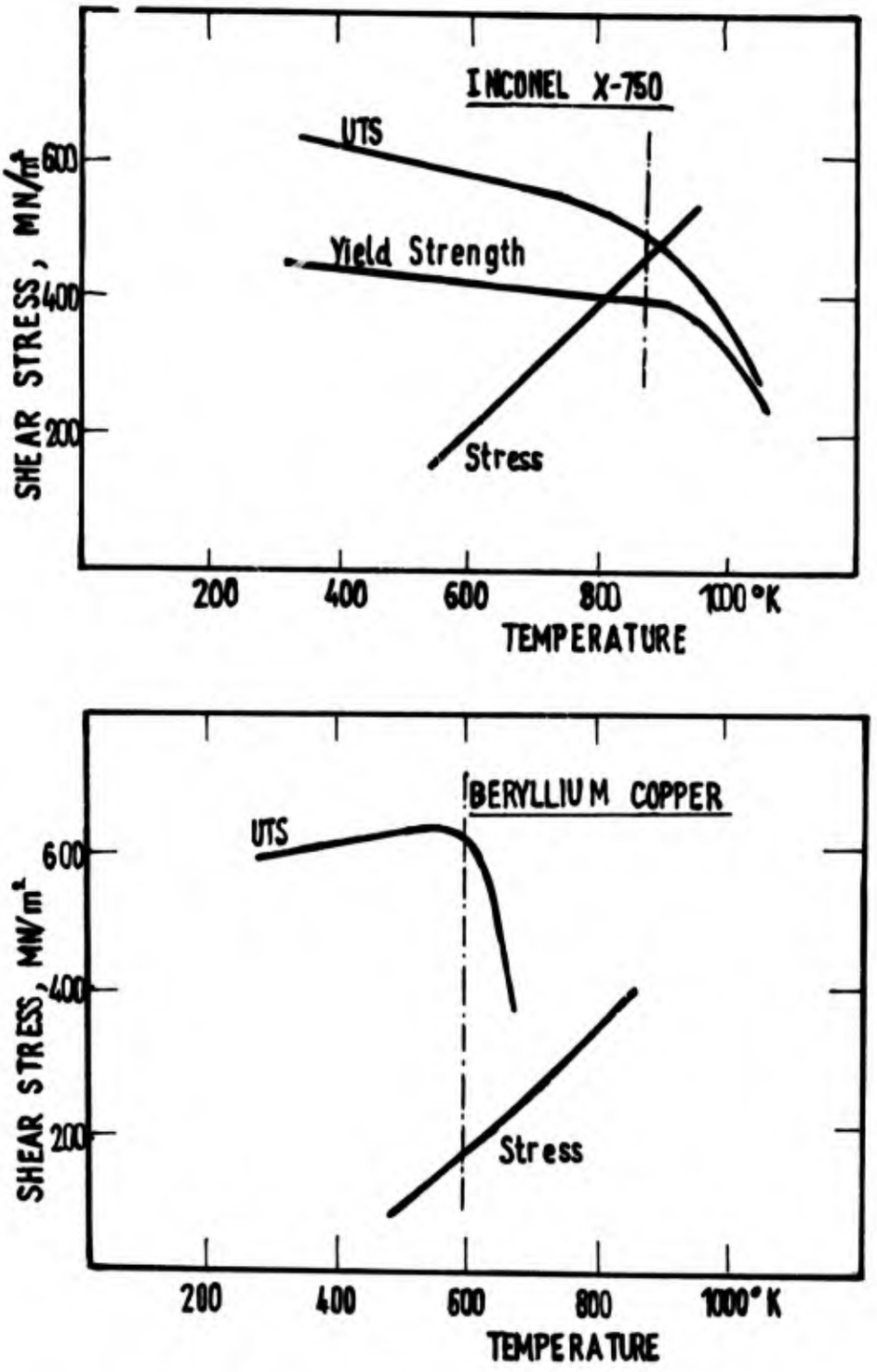

Fig.10.6 Thermal stresses in the wall of a coolant tube

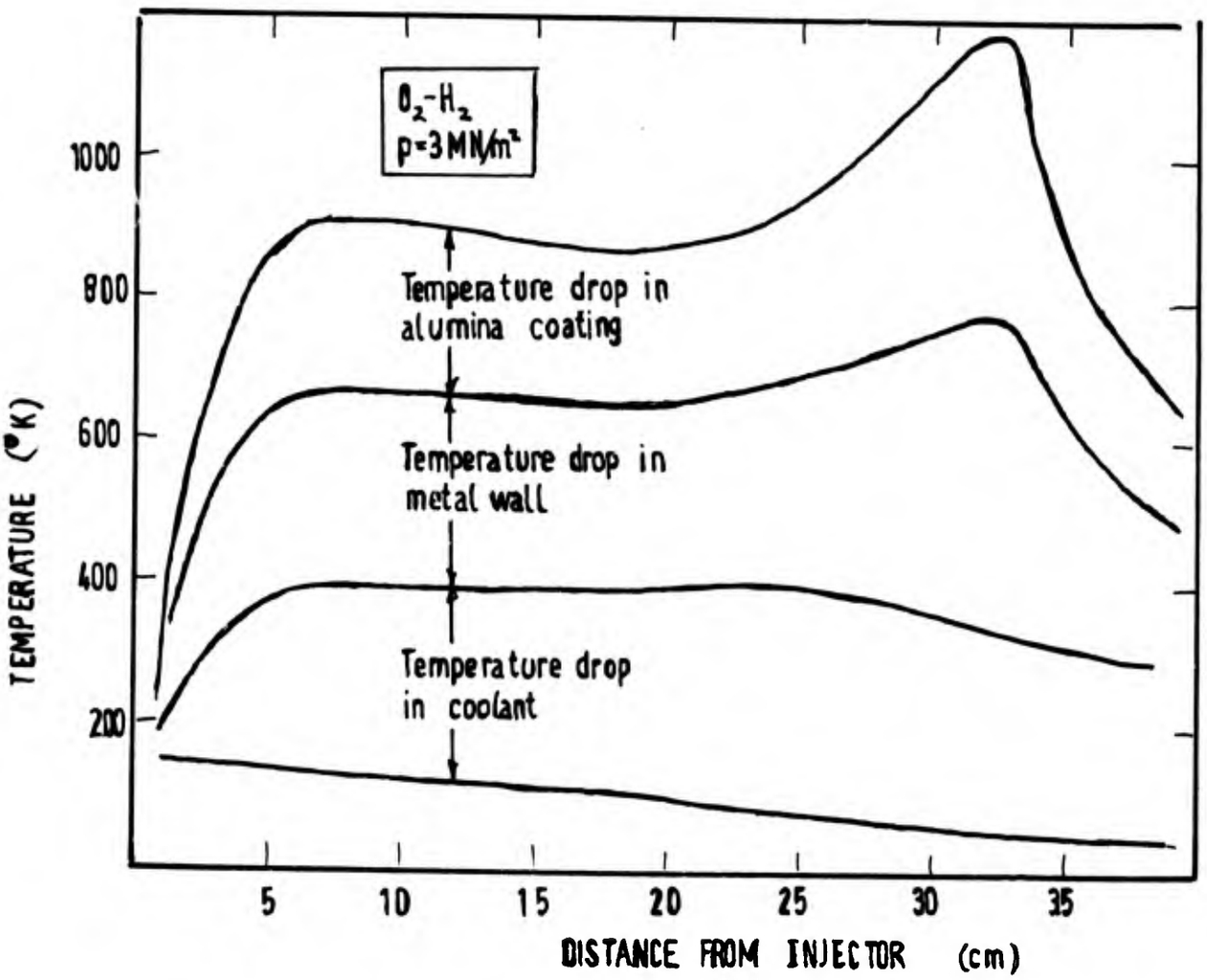

Fig. 10.7 Temperature distribution in a regeneratively cooled oxygen-hydrogen engine with a refractory oxide wall coating

CHAPTER 11

FILM COOLING

11.1 GENERAL

The basic limitation of simple regenerative cooling, particularly at high chamber pressures, comes from the fact that the hot combustion gases are directly in contact with the chamber walls. As the gas-side wall temperature rises, some point will eventually be reached at which the wall materials soften and fail. By injecting one of the propellants in profusion close to the wall it is possible to arrange for a protective cool "film" of gas to separate the wall from the hot combustion gases.

The performance penalty associated with film cooling arises from the fact that the gases close to the wall are cooler than the main stream flow. In consequence the mean exhaust velocity of the engine is reduced, and some part of the propellant is now carried solely for cooling.

A number of variations of film cooling are possible. The coolant may be injected either as gas or liquid. If a liquid it will first evaporate, forming a primary protected zone, and then dissipate as a gaseous film further downstream. If a gas, then the film will lose effectiveness as we progress downstream by heat transfer and turbulent mixing with the hot combustion gases.

Again, the coolant may be introduced as a ring slot about the injector (see Figure 11.1), as a special distribution of propellant holes around the periphery of the injector, or as a separate slot at some point upstream of a location where particular cooling is required (e.g. the nozzle throat). The coolant need not even be injected through a slot. A porous section of wall will serve.

Film cooling is thus a first step towards a condition in which the entire cooled wall is porous (transpiration cooling), and where the coolant material comes from the evaporation or decomposition of special, solid wall material (ablative cooling). These will be the subjects of the next chapters. Here we shall be concerned with simple film cooled layers.

For design purposes we would like to known the rate at which the coolant film is dissipated, and the effects of the various design parameters, including changes from an ideal slot configuration. In the first instance we shall consider film-cooling layers on flat plates without compressible flow.

11.2 FILM COOLING ON FLAT PLATES

A number of theories have been devised to correlate the "film cooling effectiveness" η with the various properties of the flow for gas films on flat plates in uniform, incompressible flows. Usually an "adiabatic wall" (zero heat transfer to the wall) is assumed, and the effectiveness defined as

$$\eta = \frac{T_{aw} - T_0}{T_c - T_0},$$

T_{aw} being the adiabatic wall temperature, T_0 the mainstream temperature, and T_c the temperature of the coolant as it leaves the injection slot. As will be seen later, it is possible to use these correlations to deal with conditions in which there is heat transfer.

The two possible approaches for correlating film cooling data are to assume that the film does not mix with the main stream, and that heat is transferred only to the film, or to assume that mixing takes place and effectiveness is lost by the influx of hot gas.

The former approach is that of Hatch and Papell[1], in which the film is assumed to be of uniform average temperature at any position downstream of the point of injection, and heat is conducted into the film at the same rate as to the wall in the absence of the cooling film. In this case

$$\log_e \eta = -\left[\frac{St\,x}{ms} - 0.04\right]\left(Re_c Pr_c \frac{u_m}{u_c}\right)^{1/8}, \qquad (11.1)$$

where the mass flux ratio is given by

$$m = \rho_c u_c / \rho_m u_m \quad .$$

Here the subscripts c and m refer to conditions at the slot and the main stream respectively, x to conditions at a chosen point downstream. The slot height is s , the Reynolds number Re_x is evaluated at the main stream conditions, and the Stanton number St is that for the solid wall in the absence of the coolant film. The constant (0.04) is introduced to take account of conditions very close to the slot, and is somewhat arbitrary.

The alternative approach is to assume some model for the mixing process between the main stream and coolant film. Stollery and El-Ehwany[2] assume that far enough downstream the film will tend to have similar velocity profiles and mixing characteristics to a simple boundary layer, and in this case

$$\eta = 4.09 \left(\frac{Re_x}{Re_c^{1.25}} \right)^{-0.8} \quad . \tag{11.2}$$

Once again, some variation in the value of the constant term has been derived from different experiments, but it will be shown in Section 11.3 that this equation has its basis in the momentum-integral equation.

As intuitively might be expected, the Hatch-Papell equation tends to give better correlations close to the injection slot, and the model of Stollery and El-Ehwany better correlations further downstream. The main objection to Equation (11.2) is that it does not tend to $\eta = 1$ as $x \to 0$. A simple remedy, asymptotic to the Stollery and El-Ehwany equation at high values of x , is

$$\boxed{\eta = \frac{Re_c}{Re_c + 0.244\, Re_x^{0.8}} \quad .} \tag{11.3}$$

The difference between this expression and Equation (11.2) amounts to no more than a revision of the starting conditions at the coolant film slot, but now the equation provides a good correlation of experimental results at points both close to the slot and farther downstream (Fig.11.2).

Unlike boundary layers, film cooling layers will be sensitive to turbulence generated above the coolant layer. Little account of this has been taken in the simple theory given above. But additional turbulence generated by the bluntness of the slot-lip, or by velocity differentials between film and main stream, will dissipate the coolant film faster than it would be otherwise. And conversely, if the slot Reynolds number is sufficiently low, laminar flow may exist in the initial part of the film, and the effectiveness in cooling will be increased as a consequence.

Figure 11.3 shows a number of results for experiments using hydrogen and helium as coolant gases[3], at slot Reynolds numbers of less than 1000, and close to the slot the effectiveness values are consistently higher than for simple turbulent films. Further downstream, mainstream turbulence encroaches into the laminar coolant flow, and the results return to the values that might be expected from Equation (11.3). By values of $(Re_x/Re_c^{1.25})$ of 100, the laminar layer effects have pretty well disappeared.

Contrariwise, simple velocity differential between the coolant film and the main stream will increase the turbulence, and hence mixing. The simple boundary-layer model of film cooling uses the ratio of the mass-flux in the film to the mass-flux of the main stream (m) as the main variable, and so fails to account for this effect, particularly in those cases where the coolant film and main stream are of differing molecular weights.

To take account of this effect, Hatch and Papell[1] have provided a simple multiplier factor for Re_x .

$$f(u) = 1 + 0.4 \tan^{-1}(u_m/u_c - 1) \qquad \text{for} \quad \frac{u_c}{u_m} < 1.0 \quad . \tag{11.4}$$

This factor is added to Equation (11.3) to give*

$$\eta = \frac{Re_c}{Re_c + 0.107\, f(u)\, Re_x^{0.8}} \quad . \tag{11.5}$$

---

* The change in constant in this equation represents a "best fit" value of 735 experimental results, for which an rms deviation of 16% was found. For cases in which the slot velocity exceeds the free stream velocity ($u_c/u_m > 1$), it was found that the appropriate factor given by Hatch and Papell did not improve the degree of correlation obtained at all, and so this has been omitted.

Film turbulence can also be increased by finite slot-lip thicknesses. For otherwise identical conditions, the effect of increasing slot-lip thickness (t) is to decrease the film cooling effectiveness[4]. A similar effect occurs if the boundary layer on the free stream surface of the slot lip is thick. The geometry in practical rocket engine cases will generally not present geometries of this form, but once again it is possible to achieve a moderately good correlation of flat plate experimental work by using a multiplying factor on the Re_x term in Equation (11.3). The suggested, empirical factor in this case is

$$g(t) = 1.88^{t/s} \tag{11.6}$$

where t/s is the ratio of lip thickness to slot height.

In the preceding analyses it has been assumed that "adiabatic wall" conditions exist. Indeed, a large number of useful experiments have been made using mass-transfer analogues of the heat transfer process, but in practice interest will be confined to cases where heat transfer does occur. Hartnett et al.[5] and other workers have shown that, for most conditions of practical interest, there is little difference in the local heat transfer coefficients with and without film cooling, and that the "adiabatic wall" temperature derived from the effectiveness acts as the driving temperature for heat transfer,

$$\ddot{q} = h_g(T_{aw} - T_w) \ . \tag{11.7}$$

This simple assumption may cease to hold in cases where the slot lip thickness is large, and the flow immediately downstream of the slot ceases to be one-dimensional as a consequence.

11.3 FILM COOLING IN ACCELERATED FLOWS

For cases in which the main-stream velocity is not constant, Nicholl and Whitelaw[6] have provided a convenient method for calculating the film cooling effectiveness based on the boundary layer integral equations.

Re-writing the momentum integral equation [Eqn (2.5)] in terms of the momentum thickness Reynolds number $Re_2 \equiv \delta_2 u_s/\nu$ yields

$$\frac{dRe_2}{dRe_x} + (2 + H_{12} - Ma)K\ Re_2 = \frac{C_f}{2} \ , \tag{11.8}$$

where K is the acceleration number [Eqn (3.2)].

As a second step the conservation equation for enthalpy in the coolant film – assuming, as in Section 2 of this chapter that the wall is perfectly insulating, will be re-written to

$$\frac{d}{dRe_x}\left[\int_0^\infty \rho u(H - H_m)\, dy\right] = 0 \ , \tag{11.9}$$

where H_m is the enthalpy in the main stream. With some re-arrangement this becomes

$$\frac{d}{dRe_x}\left[\frac{u_m}{\nu}\frac{H_{aw} - H_0}{H_c - H_0}\int_0^\infty \frac{u}{u_m}\left(\frac{H - H_0}{H_{aw} - H_0}\right) dy\right] = 0 \ ,$$

or

$$\frac{d}{dRe_x}(\eta\ Re_{\theta,1}) = 0 \ , \tag{11.10}$$

where

$$Re_{\theta,1} \equiv \frac{u_m}{\nu}\int\frac{u}{u_m}\left(\frac{H - H_0}{H_{aw} - H_0}\right) dy \ .$$

The subscripts aw, c and 0 refer to adiabatic wall, coolant and main stream conditions, respectively.

Equation (11.8) can be integrated merely by introducing an expression for the skin-friction coefficient – a convenient version of which, in this case, is Equation (2.9),

$$\frac{C_f}{2} = B\ Re_x^{-b} \ . \tag{11.11}$$

With the aid of an equation relating Re_2 and $Re_{\theta,1}$, the film cooling effectiveness under arbitrary distributions of Mach number and acceleration will immediately follow. At this point the concept of boundary-layer "similarity" will be assumed indicating that the two Reynolds numbers are related by a constant which will be determined for one specific condition. It is simplest to assume that both velocity and enthalpy profiles are straight lines

$$\frac{u}{u_m} = \zeta + (1-\zeta)\frac{y}{y_m}$$

and (11.12)

$$\frac{H - H_0}{H_{aw} - H_0} = 1 - \frac{y}{y_h}$$

While, at first sight, such crude assumptions would appear to be grossly in error, it has been shown by Escudier et al.[7] that these are remarkably satisfactory for predicting integral quantities. By using the velocity profile to predict H_{12} we obtain

$$\boxed{\zeta = \frac{3 - H_{12}}{H_{12}}} \tag{11.13}$$

which by a little algebra yields the desired auxiliary relationship between Re_2 and $Re_{\theta,1}$

$$Re_{\theta,1} = \frac{Re_2}{(1-\zeta)(1+2\zeta)}\left[(\zeta - 1)\left(3 - \frac{1}{\Delta}\right) + 3\Delta\right]. \tag{11.14}$$

The value of the dimensionless thickness $\Delta(\equiv y_h/y_m)$ has been found from examination of available effectiveness measurements, and a value of Δ of 1.25 is suggested[6]. It should be noted, however, that the selection of a constant value for Δ implies that predictions for the effectiveness may be in error where there is a thick boundary layer on the upper lip of the injection slot.

Equations (11.10) and (11.14) may now be combined to give the adiabatic wall effectiveness.

$$(\eta\, Re_{\theta,1}) = \text{constant} = Re_c$$

and

$$\boxed{\eta = \frac{Re_c}{Re_2}\,\frac{(1-\zeta)(1+2\zeta)}{(\zeta-1)(3-1/\Delta)+3\Delta}\,.} \tag{11.15}$$

In order to avoid difficulties associated with defining the flow close to the injection slot, Nicholl and Whitelaw[6] chose to define their initial conditions some 10 slot-widths downstream, and to integrate onwards from this point. However, without sacrificing much accuracy, and gaining considerably in the ease with which conditions in the film may be defined, the same assumption that was made for the flat-plate solution, viz. taking the effectiveness as being unity at the slot, will be used. The lower limit of integration of Equation (11.8) is therefore

$$\boxed{Re_{2,x=0} = Re_c\,\frac{(1-\zeta)(1+2\zeta)}{(\zeta-1)(3-1/\Delta)+3\Delta}\,.} \tag{11.16}$$

Because H_{12} varies only slowly with Re_2, the function of ζ and Δ on the right-hand side of Equation (11.16) may be taken as constant (ξ say). Its value may be found by making a comparison of this integral theory with the empirical flat plate theory of Equation (11.3).

$$K = 0$$

$$Re_2 = \int_0^x B\, Re_x^{-b}\, dRe_x + Re_c$$

and

$$\eta = \frac{Re_c}{Re_c + \dfrac{B}{1-b}\,Re_x^{1-b}}\,. \tag{11.17}$$

"Best fit" values for the various constants can now be obtained from comparison with experimental flat plate film cooling data. The various constants are listed in Table 11.I.

Studies of film cooling in nozzles where the accelerations are sufficient to cause boundary layer laminarization (Section 3.2) have failed to reveal any change in the nature of the film shape (given by b), although the heat transfer is reduced by the reduction in the heat transfer coefficient caused by the laminarization of the underlying boundary layer. This, once again, points to the origin of the laminarization phenomenon in that part of the boundary layer close to the wall. The coolant film mixing, being a function of turbulence in the main stream, is not affected in the same way by accelerations.

11.4 LIQUID FILM COOLING

If the fluid injected as coolant along the walls is a liquid and not a gas there will be an initial region in which the cooling takes place by the evaporation of the liquid film, and only after the liquid has evaporated will the cooling process revert to that with which we have dealt so far in this chapter. Liquid film cooling is very attractive in a number of cases because, for as long as the liquid film exists, the heat transferred to the walls by convection will be effectively zero, and even after the liquid film has disappeared the walls will be protected by the cooler vapour film.

Warner and Emmons[8] have provided a theory for the evaporation of such a liquid film. The heat transfer coefficient (h_f) between the hot gas stream and the liquid film surface is a function of the rate of evaporation per unit surface area of the film (Q), and the properties of the boundary layer,

$$h_f = \frac{k_v \tau_w}{\mu u_m}\left[1 - \frac{13.89\ Q}{\beta \rho_v \sqrt{(\tau_w/\rho)}}\right] , \tag{11.18}$$

where the subscript m refers to conditions in the main stream, and v to the vapour immediately adjacent to the liquid film. The free empirical parameter β was intended to correct for the effects of vapour injection upon the intensity of turbulence within the boundary layer, and also of liquid film surface roughnesses upon the eddy viscosity. The heat required to evaporate unit mass of the coolant is θ_0, and it is assumed that all the heat input to the liquid film is used in evaporating the coolant. Thus

$$h_f = \frac{Q\theta_0}{T_0 - T_v} .$$

Solving these equations for Q, and substituting

$$C_f = \frac{2\tau_w}{\rho u_m^2}$$

yields

$$\boxed{\frac{Q}{\rho u_m} = \left[\frac{\mu\theta_0}{(T_0 - T_v)C_f k_v} + \frac{13.89\ \rho_m}{\beta \rho_c \sqrt{C_f}}\right]^{-1} .} \tag{11.19}$$

The viscosity μ was taken as that of the main gas stream at an average temperature between the gas stream and the liquid surface. The average calculated value of the empirical parameter β was 0.110. Using these results, Warner and Emmons were able to correlate film cooling experiments using a number of different coolants in rocket engine combustion chambers (subsonic flow) to about 15%.

In compressible flow, the effect of acceleration and Mach number is to reduce the effectiveness of the layer of coolant vapour over the liquid film in the same way as for a gas film-cooled wall. However, the problem of calculating this effect is complicated because material is being continuously injected into the boundary layer by evaporation of the liquid film. This is a problem which will be examined in more detail in Chapter 12. Here, however, an approximate theory developed from the flat plate correlation above, will be presented.

For a wall with mass injection at the surface, the momentum integral equation [Eqn (11.8)] becomes

$$\frac{dRe_2}{dRe_x} + (H_{12} + 2 - Ma^2)K\ Re_2 = \frac{C_f}{2} + F , \tag{11.20}$$

where

$$F = \frac{Q}{\rho_m u_m} .$$

The approximate method adopted is to assume that the Nusselt number for heat transfer is proportional to the momentum thickness Reynolds number, and then comparing the incompressible (K = 0) solution of Equation (11.20) with Equation (11.18). This latter equation may for this purpose be re-written as

$$Nu_x = Re_x \frac{C_f}{2} + \frac{13.89\ \rho_m}{\beta \rho_c} \left(\frac{C_f}{2}\right)^{1/2} Re_x\ F \ . \qquad (11.21)$$

In this form, Equation (11.21) does show some remarkable resemblances to the Equation (11.20) for incompressible flow. It should be noted that in Equation (11.20) the skin friction coefficient C_f will be modified by the presence of mass injection at the surface. This is the reason why this equation cannot be integrated directly, whereas in Equation (11.21), derived from Warner and Emmons' theory, C_f is taken to be the skin friction coefficient without mass injection.

The approximate differential equation for the Nusselt number is therefore

$$\frac{d}{dRe_x} Nu_x + (H_{12} + 2 - Ma^2)K\ Nu_x = \frac{C_f}{2} + \frac{13.89\ \rho_m}{\beta \rho_c} \left(\frac{C_f}{2}\right)^{1/2} F \ , \qquad (11.22)$$

where

$$Nu_x = \frac{h_f x}{k_v} = \frac{Q\theta_0}{T_0 - T_v} \frac{x}{k_v} \ .$$

It is no longer possible to obtain an explicit solution for Q , as with the incompressible case. Numerical integration, however, allows to follow the progressive evaporation of the liquid film along the nozzle walls.

Figure 11.4 shows a comparison of this theory with experimental results given by Welsh[9] for film cooling a rocket nozzle using water as coolant. The coolant in this case was injected through a number of discrete holes in the nozzle wall, and it was apparent that in some cases the liquid coolant does not spread over the entire circumference of the nozzle. However, the comparison is remarkably good.

11.5 MULTIPLE SLOT COOLING

For some purposes there may be advantages in injecting the coolant in a number of slots, one downstream of the next. This ensures that the effectiveness of the coolant film is always close to unity, without demanding excessive injection rates at any one point.

With gas injection, the rule for multiple slot injection is simple. If the first slot would give an adiabatic wall temperature T_{aw} at a given distance downstream, then in calculating the effectiveness of the subsequent slot this value should be substituted for the free stream temperature T_0 . Otherwise, the usual calculation procedures apply for each slot.

For liquid film cooling one might expect that, as long as a continuous liquid film was maintained, the effect of two slots would be the same as for one injecting the same mass of coolant. However, Warner and Guinn[10] have provided experimental evidence which indicates that a 10-20% saving in film coolant for a given cooled length may be obtained by dividing the coolant into two injection stations, the second close to the end of the first coolant section.

11.6 CONCLUSION

In rocket engines it is relatively easy to obtain large degrees of reduction in heat transfer to the wall by using film cooling. A few percent hydrogen mass flow in film coolant in an oxygen-hydrogen engine, for instance, can achieve a fifty percent reduction in the heat transfer.

The penalty that must be paid, however, is in exhaust velocity. The cooler gases around the periphery of the chamber will contribute little to the thrust, but must be carried in propellant mass. In the oxygen-hydrogen engine case quoted above, for each three per cent of the total hydrogen mass flow put into film cooling, approximately one per cent loss in specific impulse can be expected. This loss will be reduced, however, as engine size increases.

As high performance engines move out of the range where simple regenerative cooling is possible, film cooling remains the most important method of cooling to allow continued engine operation. It can often be introduced to an existing engine design by no more than a modification to the injector pattern.

And the principles of film cooling eventually merge with those of transpiration and ablation cooling, where the complexities of regenerative engine construction are avoided all together.

TABLE 11.I

"Best-fit" Values for Film Cooling Constants

b	0.2
B	0.029
H_{12}	1.42
ζ	0.3455
Δ	1.25

REFERENCES

1. Hatch, J.E.
   Papell, S.S.
   Use of Theoretical Flow Model to Correlate Data for Film Cooling or Heating an Adiabatic Wall by Tangential Injection of Gases of Different Fluid Properties. NASA TN D-130, 1959.

2. Stollery, J.L.
   El-Ehwany, A.A.M.
   A Note on the Use of a Boundary-Layer Model for Correlating Film-Cooling Data. Int. J. Heat Mass Transf., Vol.8, 1965, p.55.

3. Burns, W.K.
   Stollery, J.L.
   The Influence of Foreign Gas Injection and Slot Geometry on Film Cooling Effectiveness. Int. J. Heat Mass Transf., Vol.12, 1969, p.935.

4. Kacker, S.C.
   Whitelaw, J.H.
   The Effect of Slot Height and Slot Turbulence Intensity on the Effectiveness of the Uniform Density, Two-Dimensional Wall Jet. J. Heat Transf., Vol.90, 1968, p.469.

5. Hartnett, J.P.
   et al.
   Velocity Distributions, Temperature Distributions, Effectiveness and Heat Transfer for Air Injected Through a Tangential Slot into a Turbulent Boundary Layer. J. Heat Transf., Vol.83, 1961, p.293.

6. Nicholl, W.B.
   Whitelaw, J.H.
   The Effectiveness of the Uniform Density, Two-Dimensional Wall Jet. Int. J. Heat Mass Transf., Vol.10, 1967, p.623.

7. Escudier, M.P.
   et al.
   An Explicit Drag Law for Uniform Density Turbulent Boundary Layers. Imperial College, Mech. Engng. Rept TWF/TN/12, June 1966.

8. Warner, C.F.
   Emmons, D.L.
   Effects of Selected Gas Stream Parameters and Coolant Properties on Liquid Film Cooling. J. Heat Transf., Vol.86, 1964, p.271.

9. Welsh, W.E., Jr
   Review of Results of an Early Rocket Engine Film-Cooling Investigation at the Jet Propulsion Laboratory. JPL Tech. Rept.32-58, 1961.

10. Warner, C.F.
    Guinn, G.R.
    An Experimental Study of Liquid Film Cooling Accomplished by Dual Slot Injection. J. Spacecraft Rockets, Vol.3, 1966, p.1547.

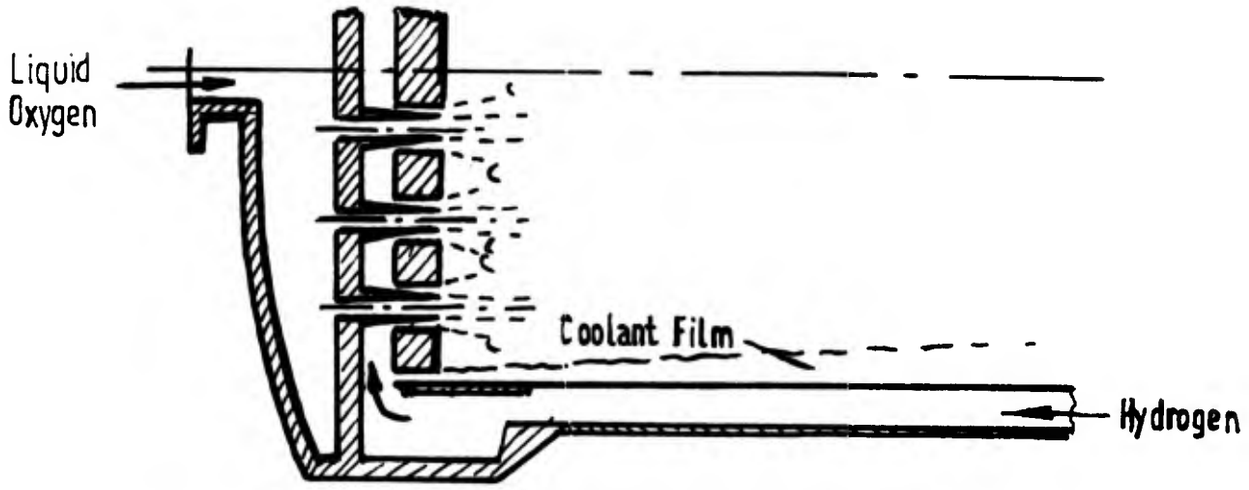

Fig.11.1 Typical film cooling arrangement in an oxygen-hydrogen engine.

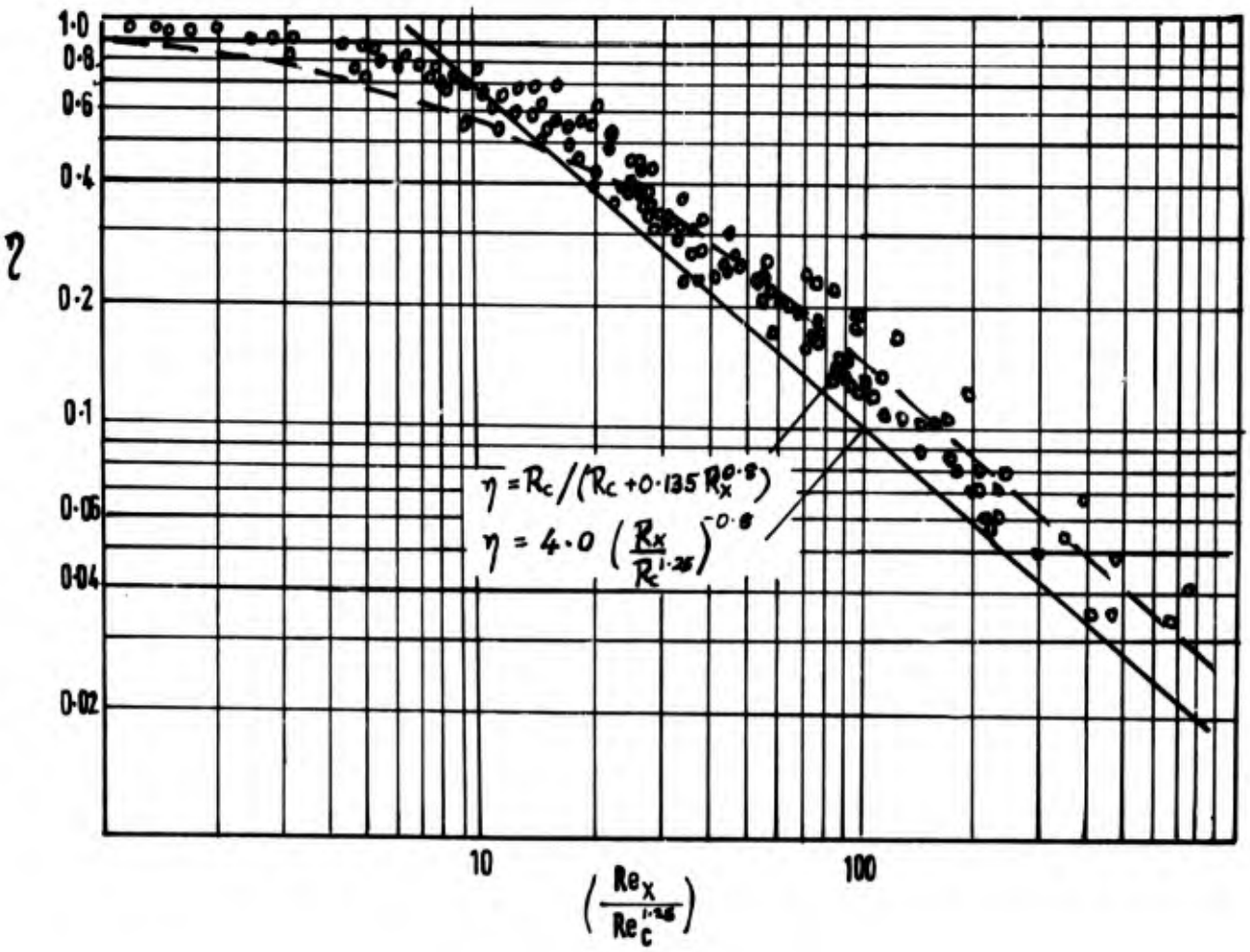

Fig.11.2 Flat-plate film cooling results

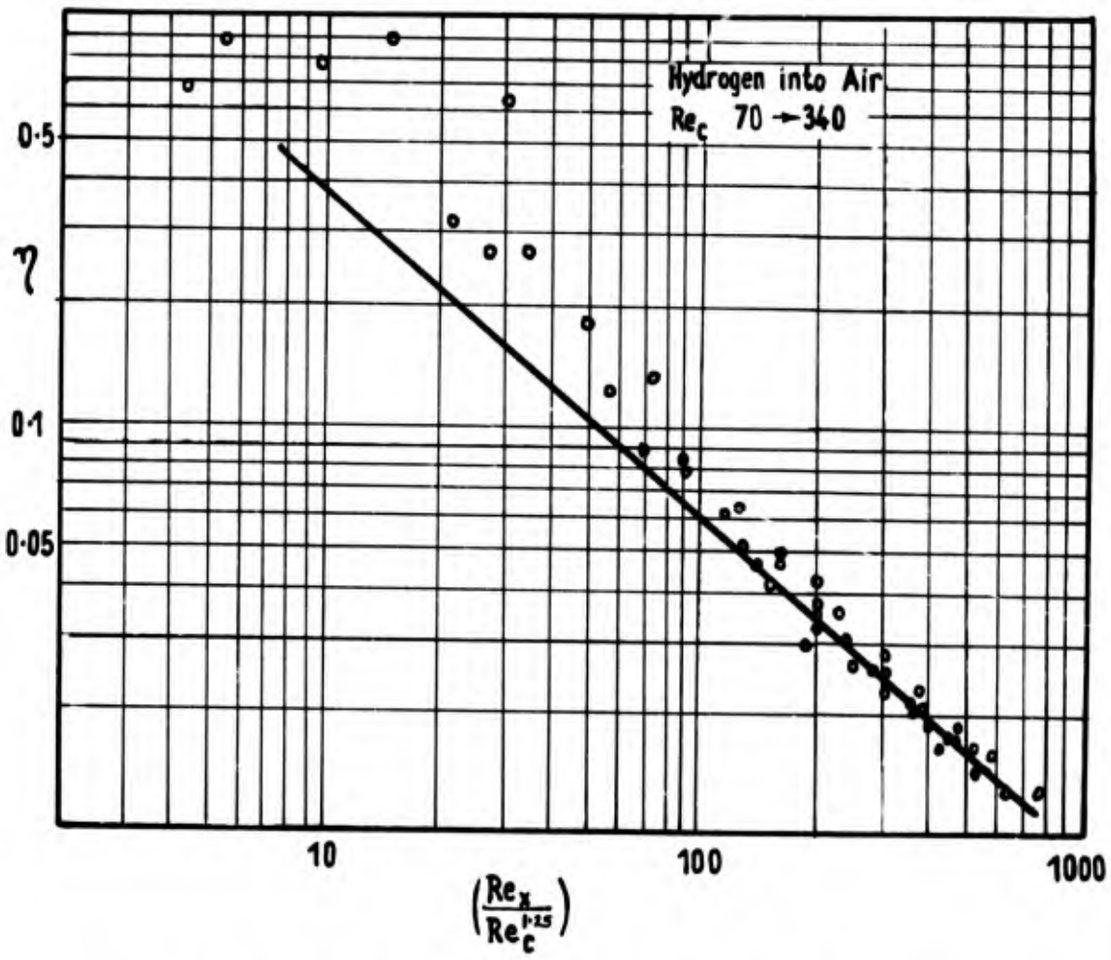

Fig.11.3 Flat-plate film cooling results for low slot Reynolds numbers

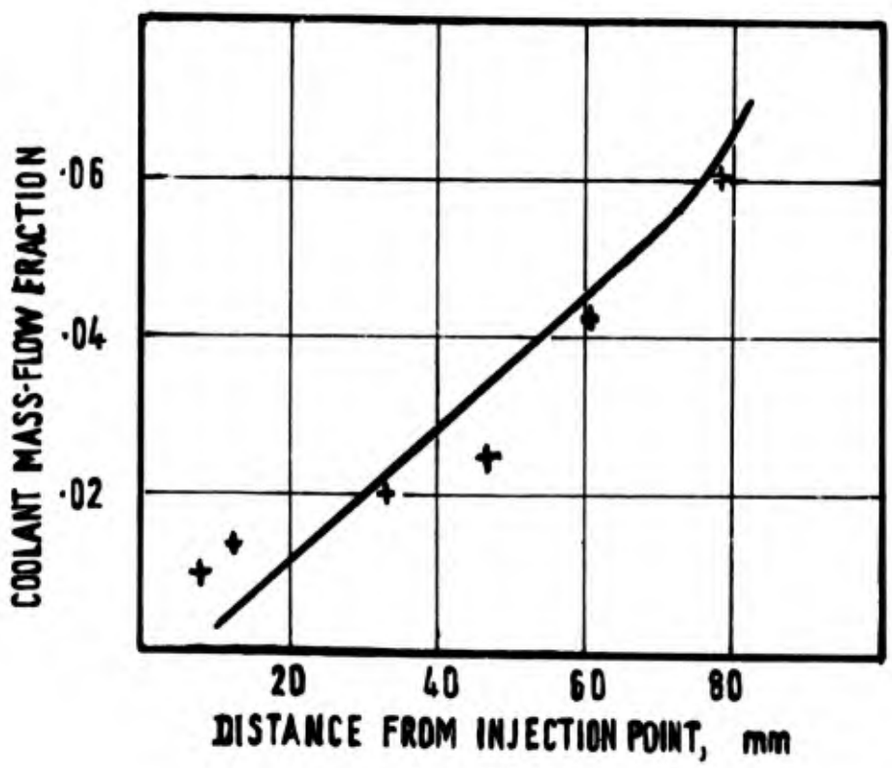

Fig.11.4 Comparison of theory and experiment for liquid film cooling (water) in a rocket nozzle

CHAPTER 12

TRANSPIRATION COOLING

12.1 GENERAL

At first sight, transpiration cooling offers one of the most effective cooling methods available to rocket engines. The coolant passes through a uniformly porous wall, permitting it to absorb the maximum amount of heat from the solid wall. As it is injected into the boundary layer it will provide an additional barrier to convective heat transfer. In theory, the full thermal capacity of the coolant up to the free-stream combustion temperature can be used without achieving excessive wall temperatures. For these reasons, in the early development of high performance rocket engines, transpiration cooling was seen to hold great potential.

The disadvantages with transpiration cooling per se are the difficulties in manufacturing a chamber from materials of uniform porosity, the high pressure drop necessary through the porous walls if flow stability is to be achieved, and the problems of designing for properly distributed coolant supply to the porous walls. As a consequence of these disadvantages, with few exceptions transpiration cooling is now important only as one of the various mechanisms involved with ablation cooling.

In this chapter methods for calculating the heat transfer to a permeable surface with a known blowing rate, will be presented.

12.2 TRANSPIRED BOUNDARY LAYERS ON FLAT PLATES

Gas injection into the boundary layer behaves in the same manner as an adverse pressure gradient, thickening the low velocity part of the boundary layer close to the wall. If sufficient mass is transferred through the wall, the boundary layer will separate.

Perhaps the simplest correlation of transpiration cooling data is to assume that the heat transfer coefficient varies linearly between its value for zero blowing rate and that required for separation. Hacker[1], for instance, found that the skin friction coefficient for a turbulent boundary layer became zero when

$$F\, Re_x^{1/5} \simeq 0.08 ,$$

where F is the blowing rate $(\rho_c u_c/\rho_m u_m)$, $\rho_c u_c$ and $\rho_m u_m$ are the coolant flux and main propellant flux, respectively. Introducing for the zero blowing rate Stanton number

$$St \simeq 0.03\, Re_x^{1/5} ,$$

the following simple correlation is obtained

$$\boxed{St \simeq St_0 \left(1 - 0.375 \frac{F}{St_0}\right),} \qquad (12.1)$$

where St_0 is the Stanton number without transpiration.

A more accurate theory is that of Kutateladze and Leont'ev[2]. These authors assume that injection into the laminar sub-layer at the wall will promote turbulence in this region, and therefore that the conditions in the boundary layer will approach the limiting case as $Re_2 \to \infty$ (where the laminar sub-layer can similarly be disregarded). There is not room here to reproduce the full argument by which these authors arrive at their conclusions, but for a uniform composition, isothermal boundary layer they find

$$\Psi \equiv \frac{C_f}{C_{f,0}} = \left(1 - \frac{b}{b_{cr}}\right), \qquad (12.2)$$

where $b = \dfrac{2F}{C_{f,0}}$, and $C_{f,0}$ is the skin friction coefficient for an impermeable flat plate at the same momentum

thickness Reynolds number (Re_2). Here, b_{cr} is the critical, "blow-off" value of b. In this simple case

$$b_{cr} = 4 .$$

The momentum equation for flows with mass transfer at the surface is

$$\frac{dRe_2}{dRe_x} + (2 + H_{12} - Ma^2)K\, Re_2 = \frac{C_f}{2} + F . \tag{12.3}$$

Thus, in the absence of a pressure gradient

$$\frac{dRe_2}{dRe_x} = (b + \Psi)\frac{C_{f,0}}{2} . \tag{12.4}$$

An auxiliary equation is required for $C_{f,0}$. Kutateladze and Leont'ev prefer to relate this to the momentum thickness. For a power law velocity distribution this is implicit in Equation (2.7),

$$C_{f,0} = E\, Re_2^{-m} , \tag{12.5}$$

where, for a 1/7-power law, $E = 0.0252$ and $m = 0.25$.

The solution to Equation (12.4) turns out to be rather cumbersome. However, a satisfactory approximation, agreeing with the exact solution to within 2%, is

$$\boxed{\left(\frac{C_f}{C_{f,0}}\right)_{Re_x} = (1 - 0.025b)^2(1 + 0.25b)^{-0.5} .} \tag{12.6}$$

For $b \ll b_{cr}$, this in turn may be approximated to

$$\left(\frac{C_f}{C_{f,0}}\right)_{Re_x} = 1 - 0.5\, b ,$$

which is close to Equation (12.1).

For a non-isothermal boundary layer, Kutateladze and Leont'ev modify Equation (12.2) to

$$\Psi = \frac{4\,(1 - b/b_{cr})^2}{(\psi^{1/2} + 1)^2} , \tag{12.7}$$

where

$$\psi = \frac{T_{wg}}{T_m} , \tag{12.8}$$

T_{wg} and T_m being the temperatures of the gas-side wall and main stream respectively. The blow-off parameter (b_{cr}) in the region of interest for rocket engines is given by

$$b_{cr} = \frac{1}{1 - \psi}\left[\log_e\left\{\frac{1 + (1-\psi)^{1/2}}{1 - (1-\psi)^{1/2}}\right\}\right]^2 , \quad \psi < 1 . \tag{12.9}$$

Kutateladze and Leont'ev[2] also deal with the case in which the injected gas is not the same as that of the main stream. Here

$$\begin{aligned} b_{cr} &\simeq 1 + 3\frac{R_m}{R_c} , && R_c > R_m \\ b_{cr} &\simeq 1.47 + 2.53\frac{R_m}{R_c} , && R_c < R_m , \end{aligned} \tag{12.10}$$

where R_m and R_c are the gas constants for the main stream and injected gases. For non-isothermal, non-uniform composition flow, the blow-off parameter is given approximately by

$$b_{cr} \simeq 0.25\, b_{cr,1}\, b_{cr,2}\,, \tag{12.11}$$

where $b_{cr,1}$ and $b_{cr,2}$ are the appropriate values from Equations (12.9) and (12.10).

These equations provide the basic skin friction relationships for transpired boundary layers on a flat plate. However, before these correlations can be converted to heat transfer data, the modifications to Reynolds analogy that have to be made for transpiration cooled surfaces must be examined.

12.3 REYNOLDS ANALOGY FOR TRANSPIRATION COOLING

Writing a conservation equation for energy within the boundary layer, as in Section 11.3, it will be found that, for this case,

$$\frac{d}{dRe_x}\left[\int_0^x \rho u(T - T_m)\, dy\right] = \rho_c u_c (T_c - T_m)\frac{\mu_m}{\rho_m u_m} - \frac{\ddot{q}_w}{c_p}\frac{\mu_m}{\rho_m u_m}\,. \tag{12.12}$$

For most cases it is reasonable to assume that the temperature of the wall and the coolant emerging through it are at the same temperature. It follows, therefore, that

$$\frac{d}{dRe_x}\left[\frac{\rho_m u_m}{\mu_m}\int_0^\infty \frac{u}{u_m}\frac{(T - T_m)}{(T_{wg} - T_m)}\, dy\right] = F + St\,, \tag{12.13}$$

where

$$St = \frac{\ddot{q}_w}{\rho_m u_m c_p (T_m - T_{wg})}\,.$$

It will be noticed here that the Stanton number relates the heat transfer rate ($\ddot{q}_w$) to the full enthalpy difference between the free stream and the wall. Unlike with film cooling, there is no "adiabatic wall" temperature to be considered.

As in Section 11.3 the quantity within the square brackets of Equation (12.13) will be defined as a thickness Reynolds number, so that

$$\frac{dRe_{\theta,1}}{dRe_x} = F + St\,, \tag{12.14}$$

and assuming similarity, so that

$$Re_{\theta,1} = \Delta Re_2\,.$$

Equations (12.14) and (12.3), therefore combine to give

$$F + St = \Delta\left(\frac{C_f}{2} + F\right)\,.$$

Without blowing, this must reduce to the Reynolds analogy of Equation (2.3). If Δ is invariant with blowing rate one obtains

$$\boxed{St = \frac{C_f}{2} Pr^{-2/3} + F\,(Pr^{-2/3} - 1)\,.} \tag{12.15}$$

For Prandtl numbers close to unity the Reynolds analogy in its original form is moderately accurate, but as the Prandtl number moves away from unity an additional term influenced by the blowing rate must be taken into account.

12.4 COMPRESSIBLE FLOW TRANSPIRATION COOLING

At this point transpiration cooling under accelerated and compressible flow conditions will be briefly considered. Here, Equation (12.4) becomes

$$\frac{dRe_2}{dRe_x} + (2 + H_{12} - Ma^2)K\, Re_2 = \frac{C_{f,0}}{2}(b + \Psi)\,. \tag{12.16}$$

Using Equation (12.5) for $C_{f,0}$, the momentum equation becomes a form of Bernoulli's equation, and may be integrated as such. Assuming that $Re_2 = 0$ at $Re_x = 0$,

$$Re_2 = U^{1/(1+m)}$$

$$U = (1+m)\, e^{-\Lambda} \int_{Re_x} E(b + \Psi)\, e^{\Lambda}\, dRe_x \tag{12.17}$$

and

$$\Lambda = (1+m) \int_{Re_x} (2 + H_{12} - Ma^2)K\, dRe_x\,.$$

From these a value for $C_{f/2}$ in terms of Re_x is to be found which may be obtained by substituting the value of Re_2 back into Equation (12.16).

$$\frac{dRe_2}{dRe_x} = \frac{1}{1-m}\, U^{-m/(1+m)}\, \frac{dU}{dRe_x}$$

and

$$\frac{dU}{dRe_x} = (1+m)\left[-\Lambda\,(2 + H_{12} - Ma^2)\, KU + E(b + \Psi)\right],$$

whence

$$\boxed{\frac{C_f}{2} + F = (1 - \Lambda)(2 + H_{12} - Ma^2)\, K\, U^{1/(1+m)} + E(b + \Psi)\, U^{-m/(1+m)}\,.} \tag{12.18}$$

Equation (12.18) will give the skin friction coefficient as a double integral for an arbitrary acceleration and Mach number distribution. The function Ψ is given by Equation (12.7), and the Stanton number can be found from the generalized Reynolds analogy (Equation (12.15)).

12.5 CONCLUSION

Transpiration cooling is a remarkably effective means of cooling a wall. Typically values of the blowing fraction F will be less than 0.001 – so that if the area to be cooled exceeds the cross-sectional area of the flow by a factor of ten, still only one percent of the propellant will be required for cooling. If it were not for the difficulties of reproducibly manufacturing porous wall materials, and in maintaining design coolant flows uniformly over the surface, transpiration cooling might long since have beeome pre-eminent among the various cooling methods for rocket engines.

However, in practice transpiration cooling is most importantly found as one of the processes occurring in ablatively cooled engines, in which the coolant is not one of the propellants but part of the structural material of the thrust chamber being partly converted into gas.

REFERENCES

1. Hacker, D.S. — *Empirical Prediction of Turbulent Boundary Layer Instability along a Flat Plate with Constant Mass Addition at the Wall.* Jet Propulsion, Vol.26, 1956, p.786.

2. Kutateladze, S.S. Leont'ev, A.I. — *Turbulent Boundary Layers in Compressible Gases.* (Translated by D.B. Spalding.) Edward Arnold, London, 1964.

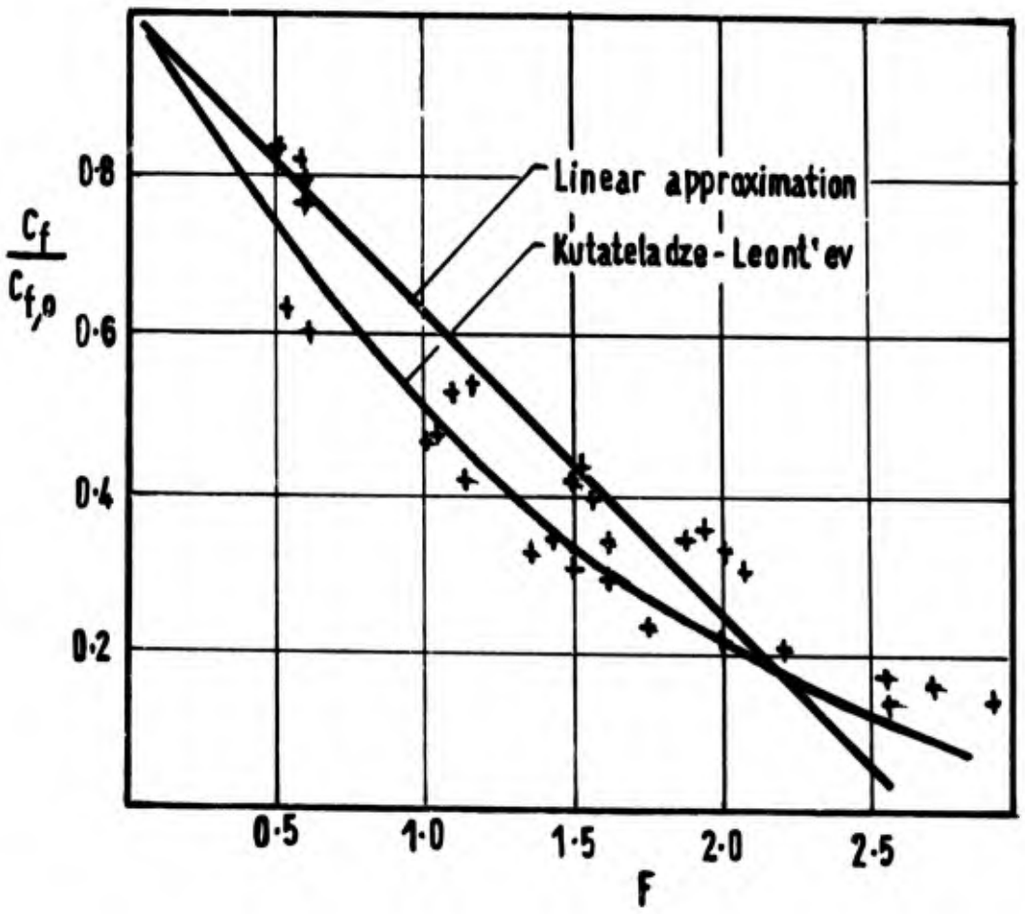

Fig.12.1 Transpiration cooling of a flat plate

CHAPTER 13

ABLATIVE COOLING

13.1 GENERAL

Ablative cooling is a subject that almost requires a book of its own.

With ablative cooling, part of the engine structure is sacrificed to absorb heat and protect the rest. The term covers materials which melt or sublimate only at the surface, those which partially decompose to provide a "char" layer, self-cooled nozzles in which a material having a low vaporization temperature is used to fill a porous, refractory material such as tungsten, and high temperature materials such as graphite which lose surface material only through chemical erosion.

The protection afforded by ablative materials comes both from the heat absorbing capacity of the decomposing or evaporating material, and also from the "blocking" effect of the transpired gases at the surface. Materials that have a low heat absorbing capacity will thus tend to reduce the heat input to the material by transpiration cooling, but at the same time suffer rather more loss of material. Loss of material will generally be the limiting design factor in ablatively cooled engines.

A design of a typical ablatively cooled engine is shown in Figure 13.1. The ablative liner is encased in an outer pressure shell which provides the main structural element of the combustion chamber. Between these two a thermal insulant may be placed to limit the pressure shell temperature. And since changes in the throat diameter are often undesirable, a throat insert of some high temperature material is shown. Finally, for space applications, a radiation cooled nozzle extension may be used.

Historically, ablation cooled engines have tended to be associated with pressure-fed systems, and regeneratively cooled engines with pump-fed systems. However, this division probably reflects both on the size of the engine and on development costs, and not on any inherent advantage in such combined systems. In addition, ablation cooling is useful for solid propellant motors where regenerative cooling is not possible. The principal advantages and disadvantages of ablative cooling when compared with regenerative cooling are summarized in Table 13.I.

Ablation cooling involves transient heat transfer processes, transpiration cooled boundary layer phenomena, reaction kinetics of surfaces, and decomposition processes within the solid. In order to establish full design procedures, therefore, it will generally be necessary to adopt finite-difference methods considering both variations along the wall surface and those within the ablating material. In this chapter it is intended to detail some of the basic mechanisms that would be required to develop a computer program along these lines, and also to provide some simple approximations on which initial designs can be based. Methods of programming finite difference solutions for the heat transfer in the solid material will not, however, be included, but may be found elsewhere!

The reader is warned, however, that the authors' information on ablative cooling is far from complete, and it has not been possible to back the methods presented in this chapter will the same experience as has been possible with other forms of cooling.

13.2 TRANSIENT HEATING IN SOLIDS

One of the first problems with the analysis of ablative cooling is that steady state heat transfer conditions are rarely achieved, and so it is necessary to know how the engine wall warms up under a given rate of heat transfer.

For axially symmetric heat transfer, the temperature distribution in a solid is given by

$$\frac{\partial T}{\partial t} = \alpha\left\{\frac{\partial^2 T}{\partial r^2} + \frac{1}{r}\frac{\partial T}{\partial r} + \frac{\partial^2 T}{\partial z^2}\right\}, \qquad (13.1)$$

where α is the thermal diffusivity of the material ($k/\rho c$). With suitable boundary conditions it is possible to solve this by finite difference methods. However, some degree of approximation may be obtained by assuming one-dimensional heat flow, in which case the equation reduces to

$$\frac{\partial T}{\partial t} = \alpha \frac{\partial^2 T}{\partial x^2} \quad . \tag{13.2}$$

This equation is satisfied by

$$T = t^{-1/2} e^{-x^2/4\alpha t} \quad ,$$

which has the properties

$$T \to 0 \text{ as } t \to 0 , \quad x \neq 0$$
$$T \to \infty \text{ as } t \to 0 , \quad x = 0 .$$

Physically this may be regarded as the solution corresponding to the release of a quantity of heat $2\rho c(\pi\alpha)^{1/2}$ per unit area over the plane $x = 0$ at time $t = 0$.

Now it happens that if T is a solution to Equation (13.2), $\partial T/\partial x$ is also a solution. For this reason

$$T = \int_0^x t^{-1/2} e^{-x^2/4\alpha t} \, dx = 2\alpha^{1/2} \int_0^{x/2(\alpha t)^{1/2}} e^{-\xi^2} \, d\xi \tag{13.3}$$

is also a solution to Equation (13.2). The integral on the right hand side of this equation is the so-called "error function"

$$\text{erf}(x) = \frac{2}{\sqrt{\pi}} \int_0^x e^{-\xi^2} \, d\xi ,$$

so that

$$T = A \, \text{erf}\left(\frac{x}{2(\alpha t)^{1/2}}\right)$$

and

$$T = A \, \text{erfc}\left(\frac{x}{2(\alpha t)^{1/2}}\right) = A \left[1 - \text{erf} \frac{x}{2(\alpha t)^{1/2}}\right] \tag{13.4}$$

are also solutions. The problem remaining is to find a solution having the correct boundary conditions for a given situation.

Carslaw and Jaeger[1] present a solution for an infinite slab heated at one edge with a constant heat input q_w by observing that the heat transfer in the solid obeys the same differential equation as that for temperature

$$\frac{\partial^2 \ddot{q}}{\partial x^2} = \frac{\partial \ddot{q}}{\partial t} , \qquad x > 0, \; t > 0 . \tag{13.5}$$

The solution of (13.5) with

$$\ddot{q} = \ddot{q}_w , \qquad x = 0, \; t > 0$$

is

$$\ddot{q} = \ddot{q}_w \, \text{erfc}\left(\frac{x}{2(\alpha t)^{1/2}}\right) \quad . \tag{13.6}$$

Integrating, the temperature at any point (assumed initially zero) is

$$\boxed{T = \frac{2\ddot{q}_w}{k}\left[\left(\frac{\alpha t}{\pi}\right)^{1/2} e^{-x^2/4\alpha t} - \frac{x}{2} \, \text{erfc} \frac{x}{2(\alpha t)^{1/2}}\right]} \tag{13.7}$$

and the surface temperature is

$$T_w = \frac{2\ddot{q}_w}{k}\left(\frac{\alpha t}{\pi}\right)^{1/2} . \tag{13.8}$$

For constant heat transfer coefficient, Carslaw and Jaeger[1] give the solution

$$\frac{T}{T_w} = \operatorname{erfc}\left(\frac{Nu_x}{2(\tau^*)^{1/2}}\right) - e^{(Nu_x+\tau^*)} \operatorname{erfc}\left\{\frac{Nu_x}{2(\tau^*)^{1/2}} + (\tau^*)^{1/2}\right\} , \tag{13.9}$$

where

$$Nu_x = \frac{hx}{k} \quad \text{and} \quad \tau^* = \frac{h^2 t}{k\rho c} .$$

Although Equations (13.7) and (13.9) are not obviously similar, for similar heat inputs the solutions are very close. Figure 13.2 illustrates the two solution procedures used to predict the temperature within a block of copper initially at 273°K under conditions of constant heat input and constant heat transfer coefficient. We see therefore that Equation (13.7) is not sensitive to slowly changing rates of heat input.

This simplified solution to the transient heat transfer will tend to give errors as the curvature of the heated surface increases, and – for blocks of finite thickness – as the rear surface temperature increases. Under these circumstances, finite difference integration methods will be required for accurate answers.

13.3 SURFACE CONTROLLED ABLATION

Two simple cases of ablation occur, viz. when the surface evaporates on reaching a given temperature, and when there is a steadily increasing rate of chemical erosion as the surface temperature increases. In both these cases we require to know how much material has been ablated away in a given time, and what the temperature at a given depth within the material will have risen to.

The first of these cases can be treated very simply. There will be an initial period during which the wall temperature rises without any material emission from the wall. Once the sublimation or decomposition temperature of the wall has been reached, the mass-flow from the wall per unit area ($\ddot{m}$) will be given by

$$\ddot{m} = \frac{\ddot{q}_w}{\Delta H_p} , \tag{13.10}$$

where ΔH_p is the energy absorbed in gasifying unit mass of the wall. Because, from Equation (12.1), we have approximately that

$$\frac{\ddot{q}_w}{\ddot{q}_0} = 1 - 0.375\,\frac{F}{St_0}$$

and

$$\ddot{q}_0 = \rho_m u_m St_0 \Delta H_w ,$$

where ΔH_w is the enthalpy drop between the free stream and the wall surface temperature (assumed to be the decomposition temperature of the wall material T_w), it follows that

$$\frac{\ddot{q}_w}{\ddot{q}_0} = \left[1 + 0.375\,\frac{\Delta H_w}{\Delta H_p}\right]^{-1} . \tag{13.11}$$

The mass-flow per unit area of wall is thus

$$\ddot{m} = \frac{\ddot{q}_0}{\Delta H_p}\left[1 + 0.375\,\frac{\Delta H_w}{\Delta H_p}\right]^{-1} . \tag{13.12}$$

A figure of merit which is commonly used to define the performance of ablative materials is the "effective heat of ablation", which is defined as

$$Q^{\star} = \frac{\ddot{q}_0}{\ddot{m}} . \tag{13.13}$$

For the simple case considered here, the effective heat of ablation is constant for a given material and is defined by

$$\boxed{Q^{\star} = \Delta H_p \left[1 + 0.375 \frac{\Delta H_w}{\Delta H_p} \right]} . \tag{13.14}$$

Finally, one needs to know the temperature distribution in the material. In the case of evaporation on the surface the inner wall temperature is constant, and an equation similar to Equation (13.6) can be derived,

$$T = T_w \operatorname{erfc}\left(\frac{x}{2(\alpha t)^{1/2}} \right) . \tag{13.15}$$

Once again, the temperatures are above an initial temperature of "zero".

Such simple ablation only takes place with certain polymeric materials such as teflon and nylon, and with these the effective heat of ablation tends to be rather low. For other materials, e.g. silicon carbide, which absorb heat through melting rather than vaporizing the mechanism of ablation is similar, but in this case without the beneficial blocking effect of the gaseous products emitted from the surface. In this case, $Q^{\star} = \Delta H_p$, so that while the energy involved in melting or decomposing the material may be high, the advantage of transpiration cooling is absent.

A closely related group of materials are the graphites, which do not decompose or melt at a set temperature but instead undergo progressively faster reactions with the combustion gases as the wall temperature rises. In this case, while the maximum wall temperature is theoretically high, oxidizing reactions cause a progressive loss of wall material.

In most cases of chemical erosion, the mass flow of released gases from the surface will be small,and will not contribute much towards a "blocking effect" to the heat transfer from the combustion gases. The reaction rate at the surface will be a function both of temperature and mass fraction of oxidizing gases in the main combustion gas stream (mainly oxygen and water vapour). Part of the heat will be absorbed by endothermic surface reactions, and the remainder transmitted into the material. These processes have a set of three simultaneous equations which in very approximate form will be

$$\left.\begin{aligned} \ddot{q}_w &= \ddot{q}_0 - \ddot{m}\ \Delta H_p \\ \ddot{m} &= f(T_w, x_i) \\ T_w &= \frac{2\ddot{q}_w}{k} \left(\frac{\alpha t}{\pi} \right)^{1/2} \end{aligned}\right\} \tag{13.16}$$

Using a model such as this, Heath and Thackray[2] have successfully predicted erosion rates and surface temperatures in graphite nozzles. The chief problems concern the chemical reactivities of the graphites used at high pressures and temperatures. Recent work by Lewis et al.[3] has yielded chemical kinetic data on specific graphites relevant to conditions in rocket engines.

One form of carbon of particular interest in rocket engine design is pyrolytic graphite. This material is produced by the pyrolysis of hydrocarbon gases under controlled conditions, and forms a material in which the crystal planes of the graphite are highly ordered. Under these conditions a material is formed having a markedly different thermal conductivity parallel to and perpendicular to the crystal planes, as well as different chemical reaction rates. It is therefore possible to construct nozzles in which the crystal plane is perpendicular to the nozzle axis, and the surface temperature is reduced by the high thermal conductivity. Alternatively, the crystal planes can be oriented parallel to the nozzle wall, and the chemical reactivity becomes much reduced. These two nozzle designs are known as the "disk" and "shell" forms respectively. Because chemical erosion is a function both of wall temperature and mass concentration of oxidizing gases, the configuration chosen will depend on the particular application.

Equations (13.16) have the form of a feedback loop, and can obviously be inserted without difficulty into any program designed to obtain the transient temperature profile within the solid nozzle. In general, the principal

problems will involve finding adequate thermal diffusivity and oxidation kinetics data on the nozzle material.

13.4 TRANSIENT CHARRING ABLATION (SIMPLIFIED THEORY)

While many pure polymer materials simply depolymerise and gasify when exposed to the high heat transfer rates in rocket engines, there exists an important category of materials where the solid residue from the pyrolysis of the material is a porous carbonaceous "char". For the most part these are composite materials – phenolic resins containing nylon, graphite fibres, or silica fibres, and being composite materials they are to some extent susceptible to "tailoring" to meet given conditions.

The presence of the char layer in such materials imposes an additional thermal barrier on the gas-side heat transfer without losing the good thermal absorption characteristics of simple sublimating or decomposing materials, and for this reason such materials have been looked upon with somewhat more favour than materials having a simpler ablation behaviour.

Charring ablators will pass through three distinct phases in their behaviour as time progresses. Initially there will be a short period during which the surface temperature rises enough to start pyrolysis in the virgin material. Following this, a steadily thickening char layer will form, as the decomposition zone moves further back into the material. At this point the char layer will be cooled by the outflow of gaseous reaction products and to some extent heat transfer from the combustion gases will be "blocked" by the emitted gas from the surface.

As the char layer thickens the surface temperature will continue to rise, and eventually surface oxidation (or other processes) will begin to erode the char material. This is the third phase in the behaviour of a charring ablator. A dynamic equilibrium will eventually be attained when the rate of erosion at the char surface equals the rate of regression of virgin material within the material.

The first phase will be short, and is simply a case of transient heat transfer within the virgin ablative material. In this section only the transient, second phase, and in Section 7 the ultimate phase of steady, charring ablation will be dealt with.

Using the linear approximation of Equation (13.7), one can define the temperature at any point within the char layer. In particular, as the interest is in the decomposition temperature T_p,

$$\frac{\ddot{q}_w x}{k T_p} = \left[\frac{e^{-X^2}}{X\sqrt{\pi}} - \operatorname{erfc}(X) \right]^{-1} , \tag{13.17}$$

where

$$X = \frac{x}{2(\alpha t)^{1/2}} .$$

Equation (13.17) defines the depth of a given isothermal (x) in terms of the non-dimensional parameter X, and these two quantities in their turn define the time t. Thus, the x-t co-ordinates of the interface between the char and the virgin material are established*.

The heat flux to the surface of the virgin material will be (Equation (13.6))

$$\ddot{q}_x = \ddot{q}_w \operatorname{erfc}(X) .$$

If the simple form of Equation (12.1) for the surface heat transfer is employed, one obtains

$$\begin{aligned} \frac{\ddot{q}_w}{\ddot{q}_0} &= 1 - 0.375 \frac{F}{St_0} \\ &= 1 - 0.375 \frac{\Delta H_w}{\Delta H_p} \frac{q_x}{q_0} \\ &= 1 - 0.375 \frac{\Delta H_w}{\Delta H_p} \frac{q_w}{q_0} \operatorname{erfc}(X) , \end{aligned}$$

so that

$$\frac{\ddot{q}_w}{\ddot{q}_0} = \left[1 + 0.375 \frac{\Delta H_w}{\Delta H_p} \operatorname{erfc}(X) \right]^{-1} \tag{13.18}$$

* It is interesting to note that the left hand side of Equation (13.17) has the form of a Nusselt number.

From this approximate values can be found for (a) the rate of mass-loss

$$F = \frac{\Delta H_w}{\Delta H_p} St_0 \left[\frac{\text{erfc (X)}}{1 + 0.375 \frac{\Delta H_w}{\Delta H_p} \text{erfc (X)}} \right], \tag{13.19}$$

(b) for the effective heat of ablation

$$Q^* = \Delta H_p \left[\frac{1 + 0.375 \frac{\Delta H_w}{\Delta H_p} \text{erfc (X)}}{\text{erfc (X)}} \right], \tag{13.20}$$

and (c) for the position of the char-virgin material interface

$$\frac{\ddot{q}_0 x}{k T_p} = \left[\frac{1 + 0.375 \frac{\Delta H_w}{\Delta H_p} \text{erfc (X)}}{\frac{e^{-X^2}}{X\sqrt{\pi}} - \text{erfc (X)}} \right]. \tag{13.21}$$

It will be noticed that in each of these cases, only X remains as a variable on the right hand side. Equation (13.21) will determine the relation between the depth of the char and X , and thus also the time t . If we now apply this to Equations (13.19) and (13.20) we find that as the transient ablation period continues, the rate of decomposition (given by F) will decrease, and the effective heat of ablation consequently will increase. As might be expected, the equations also indicate the need for materials having a high energy absorption in the decomposition process (ΔH_p).

Such an analysis represents a simplified picture, ignoring among other things the fact that in usual charring processes chemical reactions will be taking place over the entire depth of the char (see Section 7). One class of nozzles in which there will be a well-defined heat absorbing region, however, are the so-called "self-cooled" nozzles.

13.5 SELF-COOLED NOZZLES

In solid propellant rocket motors especially there is a requirement for nozzles which do not erode, but which at the same time have the heat absorbing capacity of ablative nozzles. The so-called "self-cooled" nozzles, in which e.g. a porous tungsten body is infiltrated with a second material which can be endothermically decomposed, or vaporized, provide a means of achieving this objective.

This cooling technique appears to have been first suggested by Ziebland[15,16] who demonstrated in a series of experiments with small-scale oxygen-kerosine and RFNA-kerosine rocket engines the feasibility of this novel technique. The advantage of the system over the conventional ablation cooling is that, during the period of operation the porous metal body retains its internal configuration, a factor which is of particular importance for the efficient performance of the expansion nozzle.

The composite nozzle will act as a simple heat sink until the surface temperature reaches the boiling point or decomposition point of the coolant. After this time, a receding interface will be formed, leaving behind a porous tungsten zone cooled by the vaporized material (Fig.13.3).

In most respects such a nozzle will behave according to the simple model outlined in Section 13.4. There will be some balance between the heat absorbing capacities of the vaporizing material and the "blocking" effect of the transpired vapour on the gas-side heat transfer, so that thermal differences between various coolant materials will not be marked. Materials having a high latent heat of vaporization will have more influence on the surface temperature during the early part of a firing, while the interface is still close to the surface. Materials which are more easily vaporized will continue to give protection to the surface by transpiration cooling, but at the same time will demand greater thicknesses of nozzle material. Coolants investigated (e.g. by Gessner, Ingram and Seader at Rocketdyne[4]) include silver, zinc and lithium hydride, although the latter provides a number of practical problems in manufacture.

In making a complete analysis of self-cooled nozzles, the transient heat transfer equation in the porous tungsten zone is modified by the existence of the cooling effect of vaporized material

$$(1-P)\,\rho_w c_w \frac{\partial T}{\partial t} = k_w(1-P)\frac{\partial^2 T}{\partial x^2} + C_p \dot{m} \frac{\partial T}{\partial x}\,, \tag{13.22}$$

where P is the porosity of the tungsten. The new term will generally be small. In addition, the heat loss from the back of the evaporating interface zone must also be taken into account. Silver-infiltrated tungsten of 20% porosity, for example, has a thermal conductivity 1.8 times that of the porous tungsten.

Equation (13.19) then becomes, assuming that the nozzle may be regarded a semi-infinite slab

$$\frac{F}{St_0} = \frac{\Delta H_w}{\Delta H_p}\left[\frac{\text{erfc}\,(X)}{1 + 0.375\,\dfrac{\Delta H_w}{\Delta H_p}\,\text{erfc}\,(X)}\right] - \frac{kT_p}{\sqrt{\pi\alpha t}}\,\frac{1}{\rho_m u_m St_0}\left[\frac{1 - 0.625\,\text{erfc}\,(X)\,\dfrac{\Delta H_w}{\Delta H_p}}{1 + 0.375\,\dfrac{\Delta H_w}{\Delta H_p}\,\text{erfc}\,(X)}\right] \tag{13.23}$$

showing that the effect of heat conduction away from the vaporizing interface is to reduce the loss of coolant.

The latent heat of vaporization will vary with the gas pressure at the interface, and it will be necessary to take into account the pressure drop of the vapour in the porous material. Green[5] gives, as a basic equation of flow in porous materials,

$$\frac{dp}{dx} = a_1 \mu u + a_2 \rho u^2\,, \tag{13.24}$$

where u is the mean velocity of flow ($= \dot{m}/\rho$), μ the viscosity of the fluid and a_1 and a_2 are empirical coefficients. For a wide variety of porous materials, including wire screens and packed beds of particles, Green[5] found that these coefficients were linked by an approximate relation

$$a_1 = 2.605 \times 10^4\, a_2\,,$$

where a_1 and a_2 have units of m^{-2} and m^{-1}, respectively.

The pressure drop in the porous metal matrix will tend to limit self-cooling when the internal vapour pressure in the material becomes sufficiently large to cause material failure. This possibility may become more important at high rates of coolant flow. Assuming that the vapour behaves as an ideal gas, Equation (13.24) becomes

$$p\frac{dp}{dx} = (a_1\mu + a_2\dot{m})\,\dot{m}\,\frac{RT}{M}\,. \tag{13.25}$$

Seader, Rivers and Ingram[6] have also investigated the effect of varying the porosity of a tungsten matrix with distance from the inner surface. Their results indicate that increasing the porosity some small distance below the surface. say, from 20% to 80%, improves coolant utilization considerably, but at the same time leads to higher surface temperatures than for nozzles with a uniform porosity.

The major problems remaining with self-cooled nozzles are in the manufacture of the composite materials, particularly those with low density coolants, such as lithium hydride. The choice of a suitable coolant and matrix porosity will depend on the particular application.

13.6 FINITE DIFFERENCE SOLUTIONS FOR CHARRING ABLATION

If a more exact model than the foregoing is required for the transient processes occurring in charring types of ablation, then finite difference methods will be required for the analysis of heat conduction within the char layer. The heat conduction equation can then be used in conjunction with a more exact relation for the transpiration cooled boundary layer (Chapter 12), and for the decomposition processes within the ablating material.

A detailed one-dimensional ablation model has been developed by Rivers et al.[7] which includes most of the processes which are required in a full simulation of the transient ablation processes with internal reactions. This

model includes "in depth" pyrolysis of the virgin ablative material, instead of making the assumption of a simple decomposition temperature, and also subsequent "cracking" of the pyrolysis products as they move towards the char surface. The transient heat conduction equation within the material is now

$$\rho c \frac{\partial T}{\partial t} = \frac{\partial}{\partial y}\left(k \frac{\partial T}{\partial y}\right) - C_p \dot{m} \frac{\partial T}{\partial y} - \sum_j r_j \Delta H_j \,. \tag{13.26}$$

The above equation now includes terms for the heat convected towards the surface by the released gases, and heat absorbed by "cracking" of the higher molecular weight components of the released gases and, in the reaction zone, the pyrolysis of the polymer itself.

The pyrolysis of the decomposing ablative material is described by a relationship found by Friedman[8]

$$\frac{1}{w_0}\frac{dw}{dt} = -A_p \left[\frac{w - w_f}{w_0}\right]^n \exp\left(-\frac{\Delta E_p}{RT}\right) , \tag{13.27}$$

where w is the weight of a sample of the ablative material, w_0 is the initial weight before heating is begun, w_f its final weight after the pyrolysis has been completed and the material is completely charred, A_p the reaction rate constant and ΔE_p the activation energy.

Typical values for the constants in Equation (13.27) are given in Table 13.III for a fibreglass-reinforced phenolic resin (35% by weight resin) given by Friedman[8], and for polytetrafluoroethylene by Anderson[9].

The pyrolysis of an ablative material using a phenolic resin base will release a complex mixture of gases, some relatively low molecular weight species such as H_2, CO, and CH_4, and some high molecular weight gases such as benzene, toluene, xylene, phenol and cresol which will undergo separate decomposition reactions (or "cracking") as they enter the higher temperature region closer to the surface of the char. These reactions are generally highly endothermic and thus represent a considerable "sink" for heat absorption. For the purposes of analyzing charring ablation, Rivers et al.[7] adopted a simple first-order chemical reaction

$$r_j = A_j \rho_g \exp\left(\frac{-\Delta E_j}{RT}\right) , \tag{13.28}$$

where ρ_g is the actual spatial density of the reacting gas.

Since the required data on the chemical species available in the pyrolised material, and the necessary chemical reaction rate constants will often be unknown, Beecher and Rosensweig[10] assumed that the "unstable" fraction of the pyrolysis gas is composed entirely of o-cresol. For this, the reaction rate constants are

$$A_j = 2.1 \times 10^{14} \text{ sec}^{-1}$$

$$\Delta E_j = 2.88 \times 10^8 \text{ joule/kg mole} .$$

With these values, the cracking reaction does not occur appreciably below temperatures of about 1100°K.

Additional reactions will also take place between the char material and the reinforcement in the original material. One of the more common materials used as reinforcement is silica, which becomes fluid at temperatures of about 1700°K. At these temperatures, silica has a tendency to enter into reactions with carbon.

$$SiO_2 + 3\,C \rightarrow SiC_{(s)} + 2\,CO$$

$$SiO_2 + 2\,C \rightarrow Si_{(l)} + 2\,CO$$

$$SiO_2 + C \rightarrow SiO_{(g)} + CO \,.$$

Of these reactions, the first occurs more readily at lower temperatures, and is therefore the most likely to occur first. This reaction is known to be highly endothermic, and will therefore add to the heat absorbing capacity of the ablative material.

With all these reactions included in the overall transient heat transfer equation (13.26), and adapting the surface boundary condition to a suitable heat transfer coefficient for transpiration cooling, it is possible to perform an iterative integration of the ablative process. The resultant computer program will naturally be complex, and major difficulties arise because of lack of information about all the processes involved. However, as time progresses, the ablation process will tend towards a steady state condition, and at this point reaction rate data are no longer required.

13.7 STEADY CHARRING ABLATION

As the surface temperature of the char layer rises, erosion of the char surface will begin to take place. In due course we may expect the rate of regression of the char surface to approach that of the char-virgin material interface. This is the steady state condition for the ablating material. Kohn et al.[11] have provided a calculation procedure for this steady state which appears to predict actual behaviour quite well, and it is this method which will be presented here.

The two basic equations of the steady state are the thermal balance, and the balance between material released in the decomposition process and that diffusing through the boundary layer. These are

$$\ddot{m}\ \Delta H_p = \rho_m u_m\ St_w\ \Delta H_w \tag{13.29}$$

and

$$\ddot{m}\ (\Gamma_w - \Gamma_p) = \rho_m u_m D\ (\Gamma_m - \Gamma_w) \tag{13.30}$$

where Γ_m, Γ_w, and Γ_p represent the concentration of a given chemical species in the main flow, at the surface, and in the non-pyrolised resin respectively. D is a mass transport number, which like the Stanton number will be affected by the mass-flux $\ddot{m}$ emitted from the surface. Indeed, for a Lewis number of unity

$$St \equiv D\ . \tag{13.31}$$

Kohn et al.[11] use a relation given by Spalding[12] for the Stanton number under conditions of mass release from the surface. Although it is a little more complex than Equation (13.11), a slightly better approximation is given by

$$\frac{St_w}{St_0} = \frac{\log_e\left(1 + \dfrac{\Delta H_w}{\Delta H_p}\right)}{\dfrac{\Delta H_w}{\Delta H_p}}\ . \tag{13.32}$$

Because the Lewis number has been assumed to be unity, Equations (13.26) and (13.27) have become directly equivalent, and the concentrations can be substituted for the enthalpies in Equation (13.29). The rate of mass-loss thus becomes

$$\boxed{\ddot{m} = \rho_m u_m\ St_0\ \log_e\left(1 + \frac{\Gamma_m - \Gamma_w}{\Gamma_w - \Gamma_p}\right)\ .} \tag{13.33}$$

At first sight, this equation would seem to bring us little closer to a solution, for while the chemical composition in the free stream and of the original ablative material are both known, the compositions of the surface gases are not known because the chemical transformations take place both within the char and in the boundary layer. However, it has been shown that it is possible in some circumstances to substitute for these concentrations the concentrations of a single element, or a linear combination of several elements present.

In the case of pure polymeric resins containing only hydrogen, carbon and oxygen, Spalding[13] showed that if materials of very low concentration are neglected, the combination of the elements oxygen and carbon is also equal to the combination of the concentrations of the compounds, oxygen, carbon dioxide and water, contained in the gaseous flow.

$$\left[\frac{12}{16}\Gamma^O - \Gamma^C\right] = \frac{12}{16}\Gamma_{O_2} + \frac{12}{44}\Gamma_{CO_2} + \frac{12}{18}\Gamma_{H_2O}\ .$$

At the surface, O_2, CO_2 and H_2O are reduced by the residual carbon of the charred resin, so that

$$\left[\frac{12}{16}\Gamma^O - \Gamma^C\right]_w = 0\ .$$

With this, Equation (13.33) can be solved. Kohn et al.[11] have found satisfactory agreement between this theory and experiment for pure phenolic resin material. With phenolic resin reinforced by carbon fibres, the results of theory tended to be somewhat higher than experiment, but this was put down to errors in the determination of the experimental ablation velocity.

The temperature distribution in the material is given by[14]

$$T = T_w \exp(-\dot{m}C\, x/k)$$

so that, if the temperature of incipient carbonization of the resin is T_p, the thickness of the char layer is given by

$$x_p = \frac{k}{\dot{m}C} \log_e \left(\frac{T_w}{T_p} \right) \tag{13.34}$$

In the foregoing analysis it has been assumed that the progressive removal of the char layer takes place solely by chemical reaction. If mechanical erosion also occurs, then the rate of ablation will naturally be increased.

Where the resin is reinforced by silica, this simple theory can no longer be applied. Instead, one must consider how silicon compounds are removed from the ablating material. Kohn et al.[11] assume that SiO is the only compound controlling the ablation phenomena in such composites, and that the three reactions capable of producing SiO from SiO_2 are

$$SiO_2 \rightleftharpoons SiO_{(g)} + \tfrac{1}{2} O_2$$

$$SiO_2 + C \rightleftharpoons SiO_{(g)} + CO_{(g)}$$

$$SiO_2 + H_2 \rightleftharpoons SiO_{(g)} + H_2O_{(g)}$$

At the ablation temperatures measured (1950 – 2000°C), the dominant reaction is the reduction of SiO_2 by C.

The surface temperature will depend on the enthalpy available in the main stream combustion gases. But since the reaction rate is an exponential function of the temperature, a relatively small increase in the surface temperature will lead to a large increase in the reaction velocity and thus of the absorbed heat, so that a more or less constant surface temperature can be assumed.

If the carbon in the char material is insufficient to completely reduce the silica in the pyrolized resin, the remaining silica will form a surface layer of viscous liquid, protecting the carbon in the char from the additional oxidizing effect of the combustion gases. Under these circumstances, the limitation on the SiO_2-C reduction reaction will come from the available carbon and not the available silica.

With this information, and knowing that the surface temperature will be approximately 2250°K, it is possible to calculate both the available enthalpy difference between the main gas stream and the gas at the wall (ΔH_w), and the energy absorbing capacity of the ablative material (ΔH_p). The rate of ablation can then be calculated from the thermal balance alone (Equation (13.20)), in conjunction with Equation (13.32), and the surface concentrations of the various species are no longer needed.

13.8 CONCLUSIONS

From an analytical point of view, ablative cooling provides the greatest numbers of difficulties of all the various cooling systems used in rocket engines, both because of the complexity caused by the interaction of the various mechanisms involved, and because of lack of information as to the rate constants involved in these mechanisms. Computer programs containing reasonably accurate descriptions of all the relevant processes tend to be large, and because of existing uncertainties, doubts will tend to persist with new, untried materials. At the same time there is now a growing volume of experience in the use of various ablative materials in liquid propellant rocket engines. In solid propellant engines, various forms of ablative nozzles have been used for a long time.

Considering only heat transfer processes, silica reinforced phenolic resin composites would appear to offer better thermal protection than most other currently available ablative materials. However, the desire for a constant throat area will tend to limit the universal application of this material, and most combustion chambers can be expected to have a composite structure of ablative materials and throat inserts of some less rapidly eroding material, e.g. a tungsten-silver composite.

REFERENCES

1. Carslaw, H.S. Jaeger, J.C. — *Conduction of Heat in Solids.* 2nd ed., Clarendon Press, Oxford, 1959, Chapter 2.

2. Heath, G.A. Thackray, R.W. — *Chemical Erosion of Graphite Rocket Nozzles.* J. Brit. Interplanet. Soc., Vol.22, 1969, p.402.

3. Lewis, J.C. et al. — *A Comparative Study of the Gaseous Oxidation of Vitreous Carbon and Various Graphites at 1500–3000°K.* 8th Carbon Conference, 1967.

4. Gessner, F.B. et al. — *Self-cooled Nozzles.* Summary Report, Vol.2. Rocketdyne Rept. T-5323. Wright-Patterson AFB Technical Documentary Report RTD-TDR-63-4046, 1964.

5. Green, L., Jr — *Heat, Mass and Momentum Transfer in Flow Through Porous Media.* ASME-AIChE Heat Transfer Conference, August 11-15, 1957.

6. Seader, J.D. et al. — *Effect of Porosity Zoning and Matrix Material on the Performance of Self-Cooled Nozzle Throat Inserts.* J. Spacecraft Rockets, Vol.3, 1966, p.1138.

7. Rivers, W.J. et al. — *Effect of Rocket Engine Combustion on Chamber Materials. Part I: One-Dimensional Computer Program.* Air Force Rocket Propulsion Laboratory Rept. AFRPL-TR-63-13, January 1965.

8. Friedman, H.L. — *Kinetics of Thermal Degradation of Char-Forming Plastics from Thermogravimetry. Application of a Phenolic Plastic.* J. Polymer Science, Part C, Vol.6, 1963, p.183.

9. Anderson, H.C. — *Thermogravimetry of Polymer Pyrolysis Kinetics.* J. Polymer Science, Part C, Vol.6, 1963, p.175.

10. Beecher, N. Rosenweig, R.E. — *Ablation Mechanisms in Plastics with Inorganic Reinforcement.* ARS J., Vol.31, 1961, p.530.

11. Kohn, S. et al. — *Contribution to the Study of the Ablation of Some Materials Based on Phenolic Resins.* Pyrodynamics, Vol.6, 1968, p.315.

12. Spalding, D.B. — *Some Fundamentals of Combustion.* Butterworths, London, 1955.

13. Spalding, D.B. — *Heat and Mass Transfer in Aeronautical Engineering.* Aero. Quart., Vol.XI, 1960, p.105.

14. Bethe, H.A. Adams, M.C. — *A Theory for the Ablation of Glassy Materials.* J. Aero/Space Sci., Vol.26, 1959, p.321.

15. Ziebland, H. — *"Liquid Storage" Cooling. A New Technique for Protecting the Walls of Rocket Motors Burning High Energy Liquid Propellants.* E.R.D.E. 5/M/1955.

16. Ziebland, H. — *An Improved Method of Protecting Solid Surfaces from Hot Gases.* Brit. Pat. Appl. No.22, 512, 1956.

TABLE 13.I

Comparison of Ablative Cooling with Regenerative Cooling

Advantages of Ablative Cooling	*Disadvantages of Ablative Cooling*
1. Costs, particularly development costs.	1. Material loss from structure means that firing times cannot be indefinitely extended.
2. Good transient response, and insensitivity to throttled operation.	2. Higher mass than regenerative engines.
3. Slightly lower propellant delivery pressures required.	3. Engine dimensions (throat in particular) not constant.
4. No propellant compatability problems with tube materials.	4. Somewhat more uncertainty in design procedures.

TABLE 13.II

Material	*Approximate Decomposition Temperature* T_p °K	*Enthalpy Change in Depolymerization* H_p kj/kg	*Density* kg/m³	*Specific Heat* kj^c/kg°K
Phenolic	800		1700	1.6
refrasil			1550 (char)	
P.T.F.E.	1000	2560	2200	1.1
Nylon	550		1150	1.7
Silicon carbide	3000 (melts)	53	2800	0.8

TABLE 13.III

	Fiberglass-phenolic	*P.T.F.E.*	
A_p	2.8×10^{14}	6.7×10^{18}	sec^{-1}
ΔE_p	2.3×10^5	3.2×10^5	kj/kg mole
n	5	1	

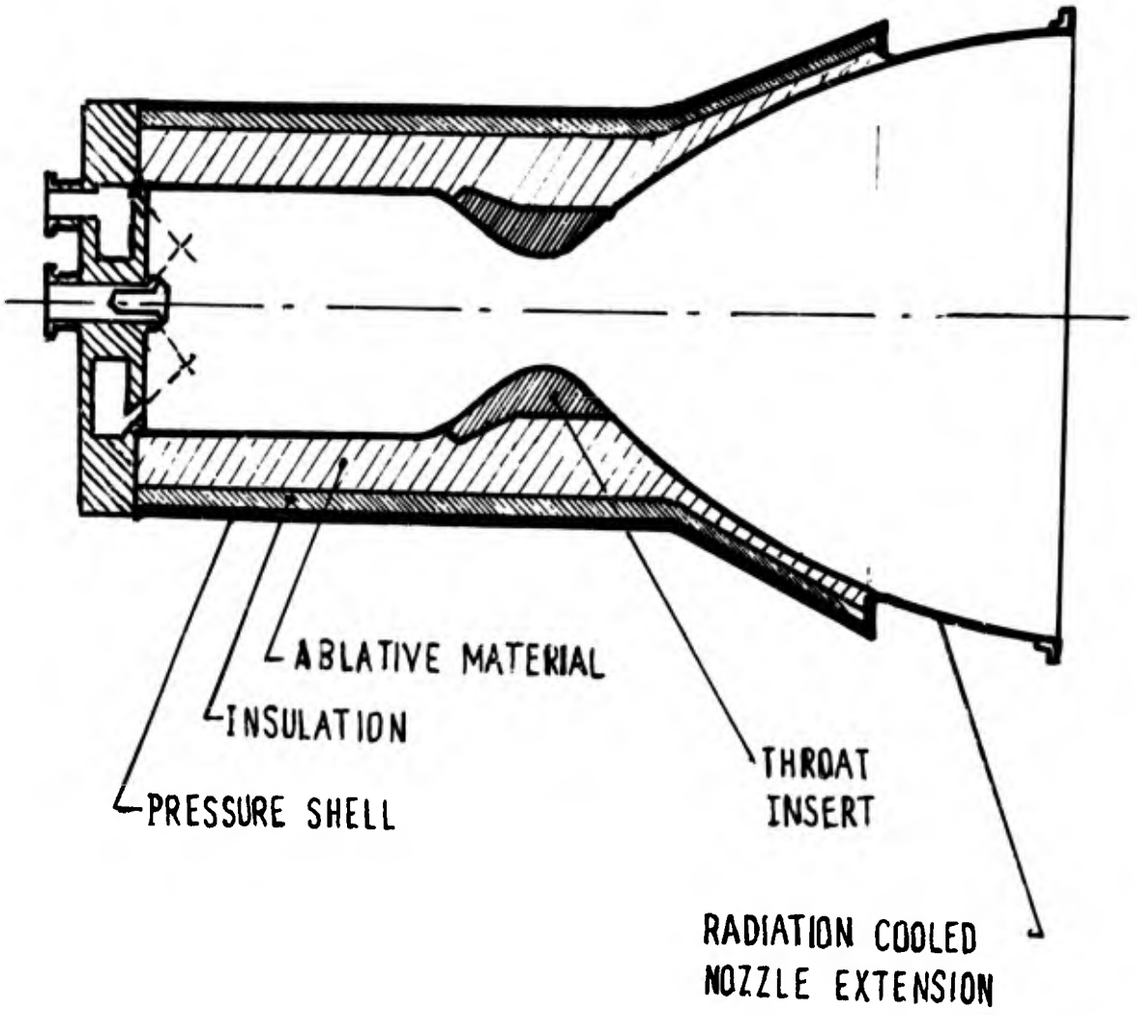

Fig.13.1 Typical ablation-cooled nozzle

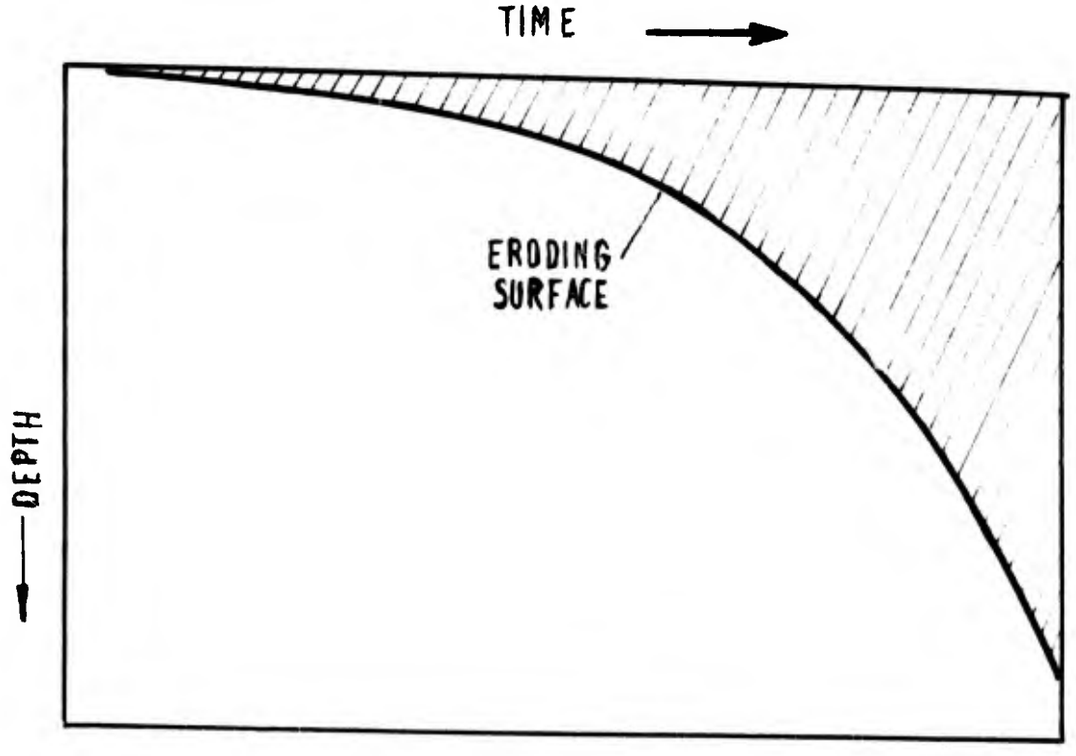

Fig.13.2 Progress of surface-controlled ablation

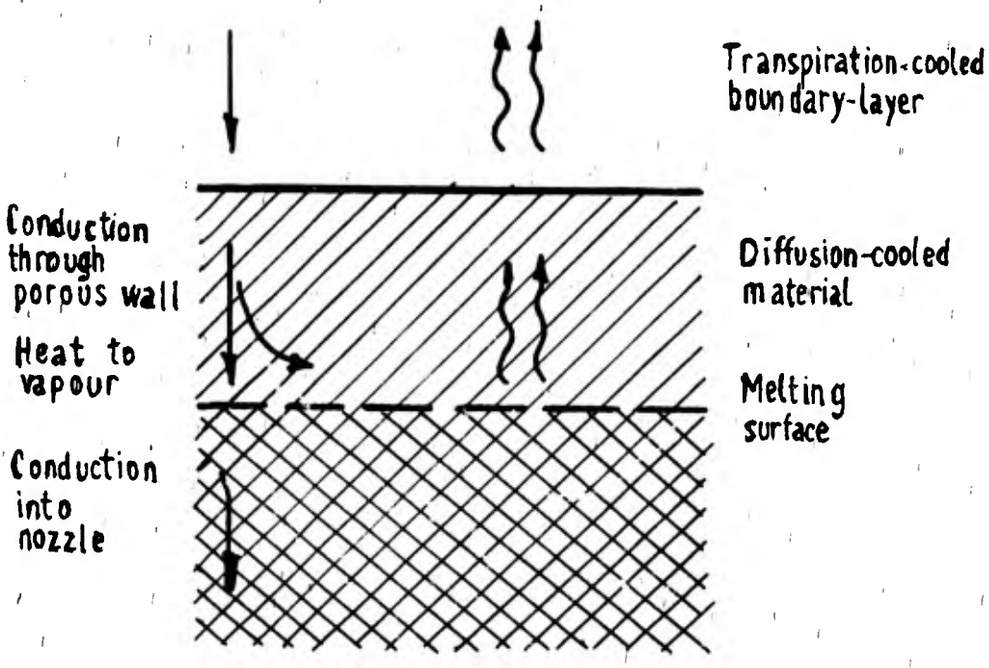

Fig.13.3 A schematic picture of energy and mass transport in a "self-cooled" wall

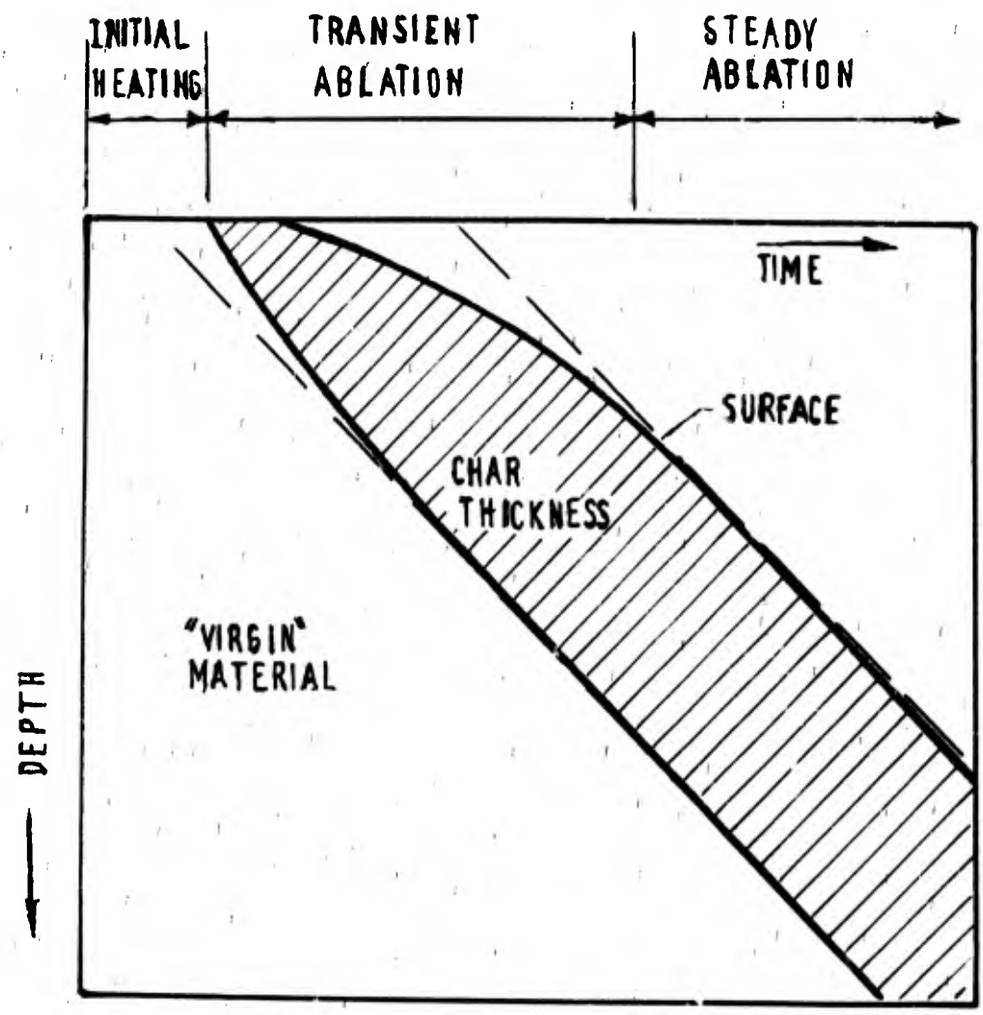

Fig.13.4 The three phases characterizing the transient and steady states of a charring ablator

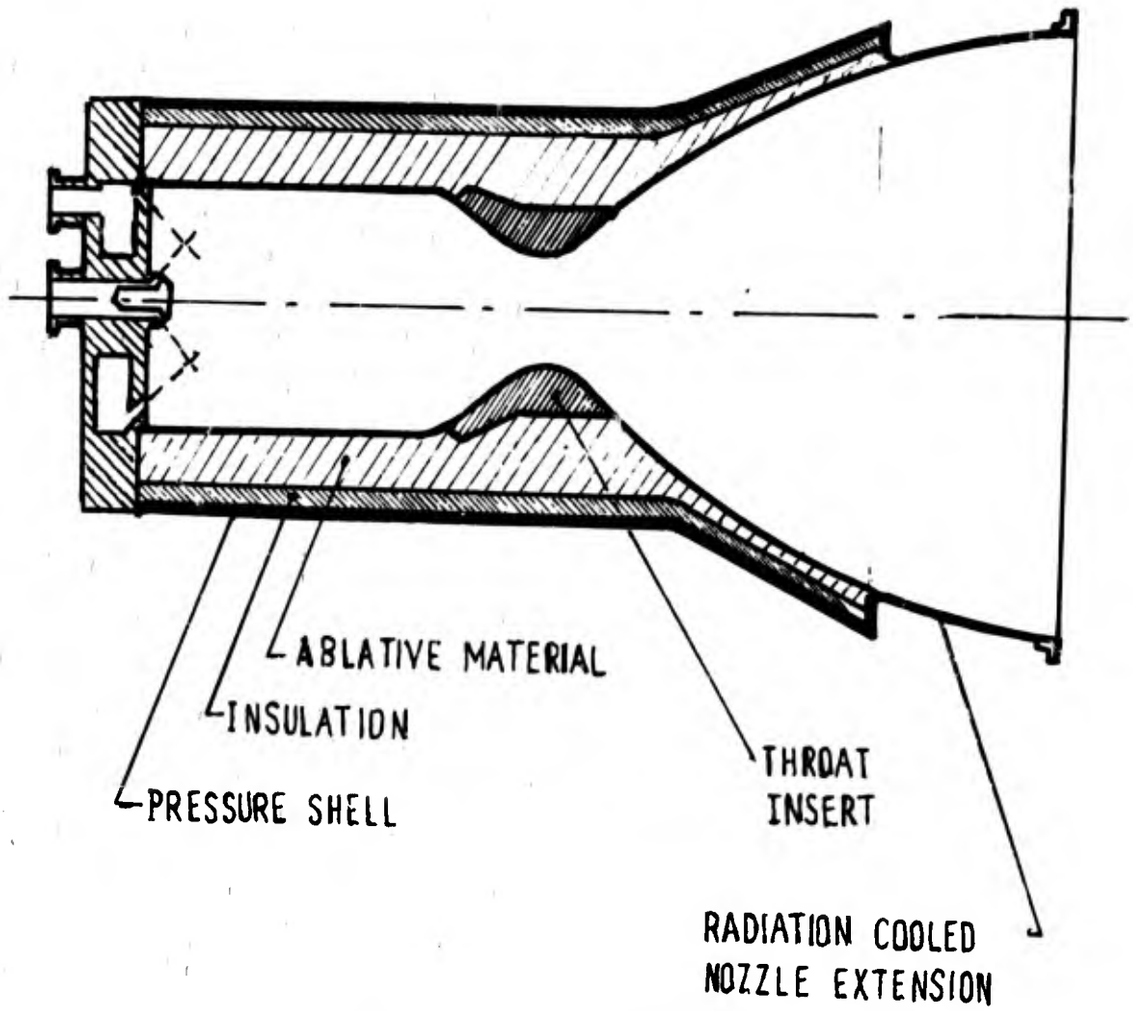

Fig.13.1 Typical ablation-cooled nozzle

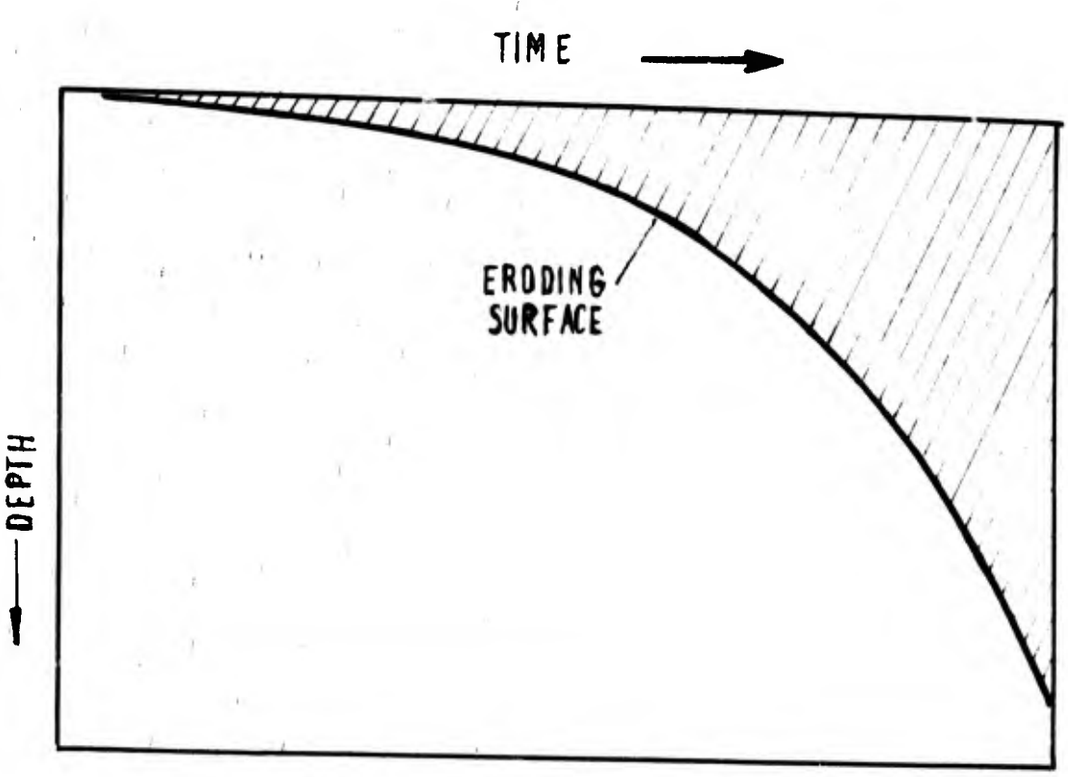

Fig.13.2 Progress of surface-controlled ablation

CHAPTER 14

RADIATION COOLING

14.1 GENERAL

In nearly all cases it will not be possible to build a rocket engine from materials capable of withstanding the full combustion temperature of the reacting gases. Such a design would, however, have the attractions of simplicity and lightness. Radiation cooling allows one approach towards this ideal.

With radiation cooling, the hot walls of the engine are allowed to radiate their heat away to their surroundings – ideally into empty space. The heat radiated away varies with the fourth power of the surface temperature, but wall temperatures of about 1600°K are required before the heat radiated away begins to be comparable with hot gas convection rates.

Radiation cooling has found major use with the very high area-ratio nozzle extensions of upper stage engines, where heat transfer rates are relatively low, and mass is at a premium. Other uses have been with small, liquid propellant thrusters for space use, and certain solid rocket motors, where the possibilities for fluid cooling are limited.

14.2 NOZZLE SKIRT EXTENSIONS

The basic theory of radiation cooling is simple. The heat radiated away from the hot wall surface at temperature T will follow the Stefan-Boltzmann law

$$\dot{q} = 5.67 \times 10^{-14} \epsilon T^4 \qquad MW/m^2 , \tag{14.1}$$

where ϵ is the emissivity of the surface. With suitable surface finishes an emissivity of 0.8 is not difficult to obtain, and errors in this value will result in only small changes of the surface temperature.

Basically the heat transferred by convection to the inner surface of the nozzle has to be equated to the heat radiated away from both the external surface and those areas of the inner nozzle surface (expansion cone) which are in radiative exchange with the outer space through the nozzle exit area. An equilibrium wall temperature may thus be calculated which will depend on the nozzle configuration and the engine operating conditions. Figure 14.1 shows the variation of the equilibrium wall temperature of the nozzle of a hydrogen-oxygen engine with area ratio for two operating pressures, viz. 2.1 and 0.7 MN/m², respectively. It will be noticed that the equilibrium temperature falls steeply with increasing area ratio.

The point at which a purely radiation cooled nozzle extension may be employed will depend on the material used. Obviously it is desirable to use a material with adequate mechanical properties at high operating temperatures, but set against this is the fact that refractory metals are also very heavy. While the nozzle skirt will only be lightly stressed, it must be constructed to withstand the additional rigours of flight. To illustrate this point the upper operating temperatures of two high-temperature metals have been shown in Figure 14.1.

In many radiation-cooled nozzles flame-sprayed refractory coatings are used. The reason for this is not to reduce the heat transfer – to do so appreciably the inner wall temperature would have to rise towards the full combustion temperature of the exhaust gases, and thermal stress problems would arise. Instead, thin coatings of alumina or zircona are to protect the refractory metal walls against oxidation, which is a serious problem at these high temperatures.

At the same time, while it may not be possible to diminish the convective heat transfer appreciably by the use of refractory coatings, the heat transfer rates in high area-ratio nozzles are sufficiently low that the equilibrium wall temperature may only be reached after some considerable interval of firing. Figure 14.2 illustrates a typical example. Heat transfer rates were assumed to be less than 0.2 MW/m².

14.3 INTERNAL RADIATION

Heat will be radiated away by the nozzle both within and from the outside of the nozzle. However, the inner surface of the nozzle will also receive heat radiated by other parts of the nozzle, and so the effective emissivity will be limited by how much of the "outside" a point on the nozzle wall sees through the nozzle exit.

In the first instance, let us suppose that the inner surface of the nozzle is at a uniform temperature, so that from everywhere except through the nozzle exit a typical point on the nozzle surface receives as much radiation from other hot surfaces as is emitted in that direction. The heat loss from the surface is then determined by that fraction (f) of a hemisphere occupied by the nozzle exit.

$$f = \frac{1}{2\pi} \iint d\theta d\phi \quad . \tag{14.2}$$

(Nomenclature is shown in Figure 14.3.)

In the same co-ordinates, the edge of the nozzle exit has the equation

$$\tan\theta = \left[\frac{r_e}{x} \pm \sqrt{\left\{ \left(\frac{r_e}{x} \right)^2 - \tan^2\phi \right\}} \right] \cos\alpha \quad . \tag{14.3}$$

Using Equation (14.3) to define the θ-limits of Equation (14.2), the fractional angular area occupied by the nozzle exit is

$$\boxed{f = \frac{1}{2\pi} \int_{-\tan^{-1}(r_e/x)}^{\tan^{-1}(r_e/x)} \tan^{-1} \left[\frac{2 \cos\alpha \sqrt{\{(r_e/x)^2 - \tan^2\phi\}}}{1 + \cos^2\alpha \tan^2\phi} \right] d\phi \quad .} \tag{14.4}$$

This function is shown in Figure 14.4. Even at the nozzle exit the surface can only radiate about half of its radiation into "space", and within half a nozzle diameter of the exit the available area has dropped to a quarter. Except very close to the nozzle exit, therefore, most of the radiation lost from the nozzle will be radiated from the outer surface of the nozzle, and that emitted from within may be left to add a factor of safety to calculations.

If the inner surface of the nozzle is not all at uniform temperature, then it is possible that cooler areas of the nozzle will absorb radiation from hotter areas, and the analysis becomes somewhat more complicated. This will rarely be a problem with chemical engines, but is a problem in solid-core nuclear engines in which radiation from the uncooled reactor face can contribute significantly to the heat transfer within the early part of the nozzle. Robbins[1] provides details of the complex analysis that is necessary in a case such as this.

14.4 MIXED SYSTEMS

One method of extending the possible application of radiation cooling to nozzle skirts is to use a mixed system with film cooling to reduce the convective heat transfer to the wall. This will involve some slight performance loss, but the two cooling processes work well together. As the film cooling effectiveness falls, so also does the possible heat transfer from the main stream, and a more or less uniform wall temperature can be maintained. If the mass flow in the film has been properly calculated, the film may acquire sufficient energy from the main stream before reaching the exit to reduce the loss in performance essentially to zero.

A further possibility is that used in the Rocketdyne J-2 and F-1 engines[2], where exhaust gas from the engine turbine is used as a film coolant. The only disadvantage in this attractive system is a slight reduction in turbine pressure ratio.

14.5 TOTALLY RADIATION COOLED NOZZLES

If one considers nozzles cooled throughout by radiation alone, then in almost all applications the maximum wall temperature must be brought up into the region above 2000°K, approaching that of the combustion temperature of the propellants. The choice of materials is now severely limited -- tungsten, tantalum, graphite and one or two others. The refractory metals are heavy, and find their main use in small control engines for space work. The main use of carbon and graphite has been in small solid rocket motors.

Pyrolitic graphite is finding increasing use in the nozzles of small solid motors and elsewhere. This material has a good thermal conductivity along one axis, and a poor conductivity in the perpendicular direction, so that by careful design heat can be "channelled" into a preferred direction. A typical design of nozzle uses the preferentially conducting direction as radially outward.

With such a design, using radiation from the outer surface as the only process of energy dissipation, it is no longer an advantage to make the nozzle walls as thin as possible. Larger, or extended surfaces on the outer wall will assist in the rejection of heat. Figure 14.5 illustrates this effect, showing to what extent the temperatures at the throat can be reduced by increasing the nozzle wall thickness. Chemical reactions between the hot gases and the wall material follow some exponential variation with temperature and a reduction of this latter quantity can be of importance in critical cases.

The outer diameter of the nozzle cannot be extended indefinitely, however, for eventually the thermal resistance due to heat conduction will outweigh the effect of increasing surface area.

The throat temperature reached in such a nozzle, other things being equal, will be dependent on the performance of the propellants used. Figure 14.6 illustrates the inner and outer wall temperatures for a nozzle of given size at a constant chamber pressure for a number of different propellant combinations. As might be expected, as the performance of the propellants increases, so cooling problems become more difficult.

14.6 CONCLUSION

Radiation cooling has an important place in the technology of rocket engines. It is significant that nearly all large liquid propellant engines use a combination of regenerative cooling for the combustion chamber and nozzle throat, and radiation cooled nozzle extensions – an optimum "mix" giving minimum performance losses and a light structure.

In addition, radiation cooling has found a use with the smallest rocket engines, where simplicity and reliability are the important factors. Here mass is of less importance, and the entire nozzle can be made in refractory metals such as tantalum or tungsten.

REFERENCES

1. Robbins, W.H. — *An Analysis of Thermal Radiation Heat Transfer in a Nuclear-Rocket Nozzle.* NASA TN D-586, 1961.

2. Sutton, G.P. et al. — *Advanced Cooling Techniques for Rocket Engines.* Astronautics and Aeronautics, Vol.3, 1966, pp.60-71.

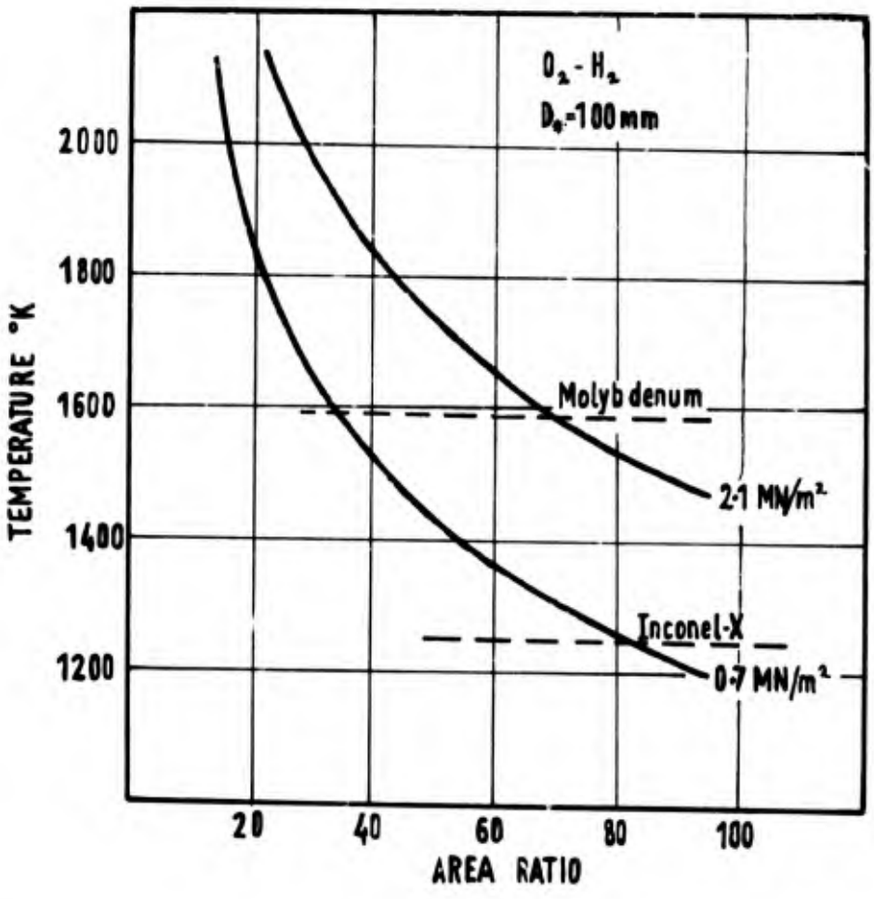

Fig.14.1 Variation of equilibrium temperatures with nozzle area ratio in a typical hydrogen-oxygen engine of 100 mm throat diameter

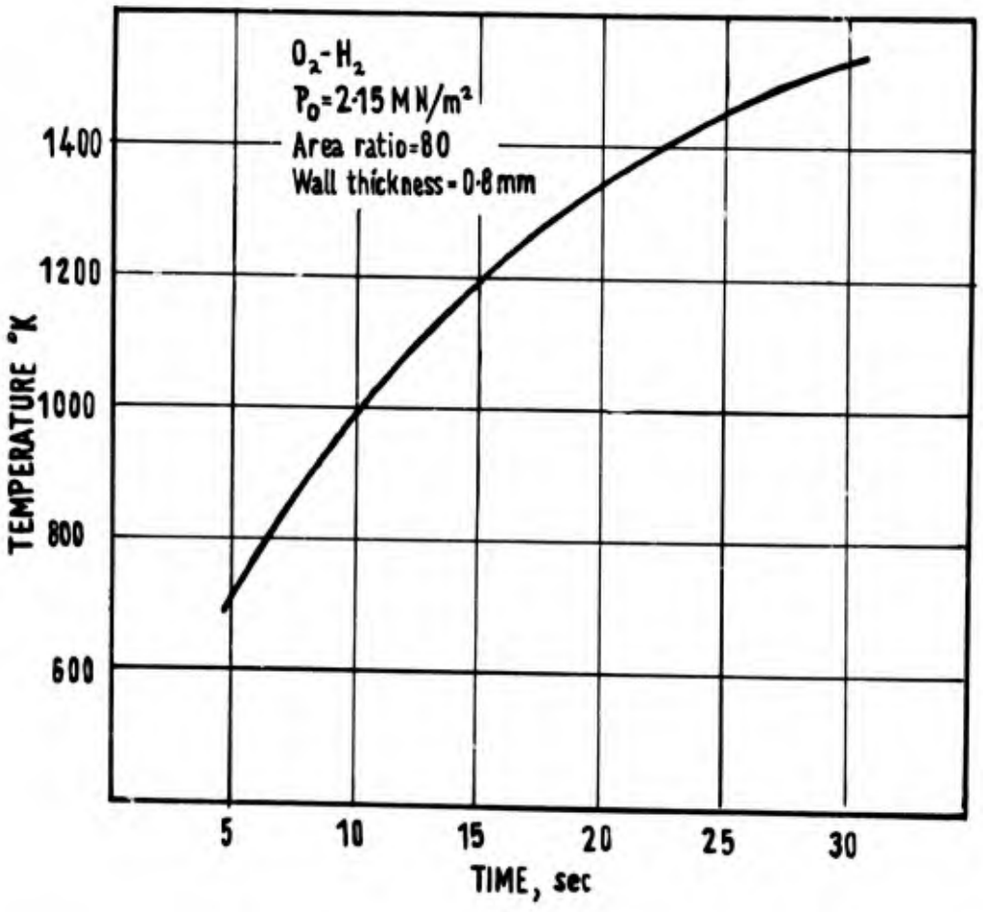

Fig.14.2 Transient temperature rise of a radiation-cooled nozzle having an area ratio of 80 at an average heat flux of less than 0.2 MW/m²

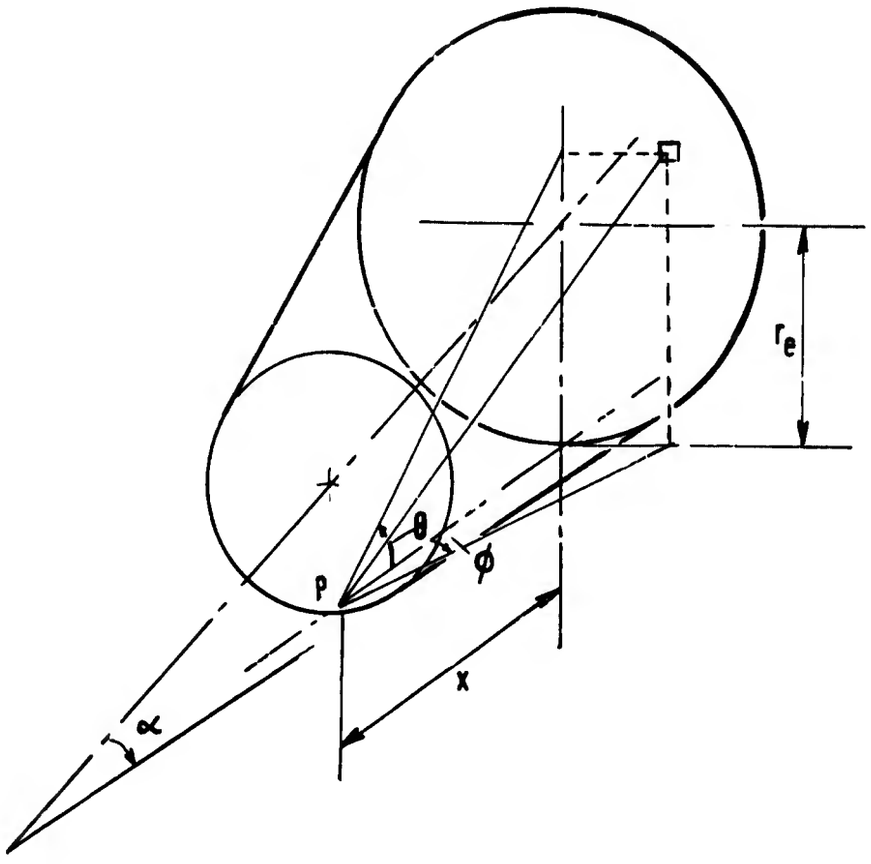

Fig. 14.3 Co-ordinate system for internal radiation in a radiation-cooled nozzle

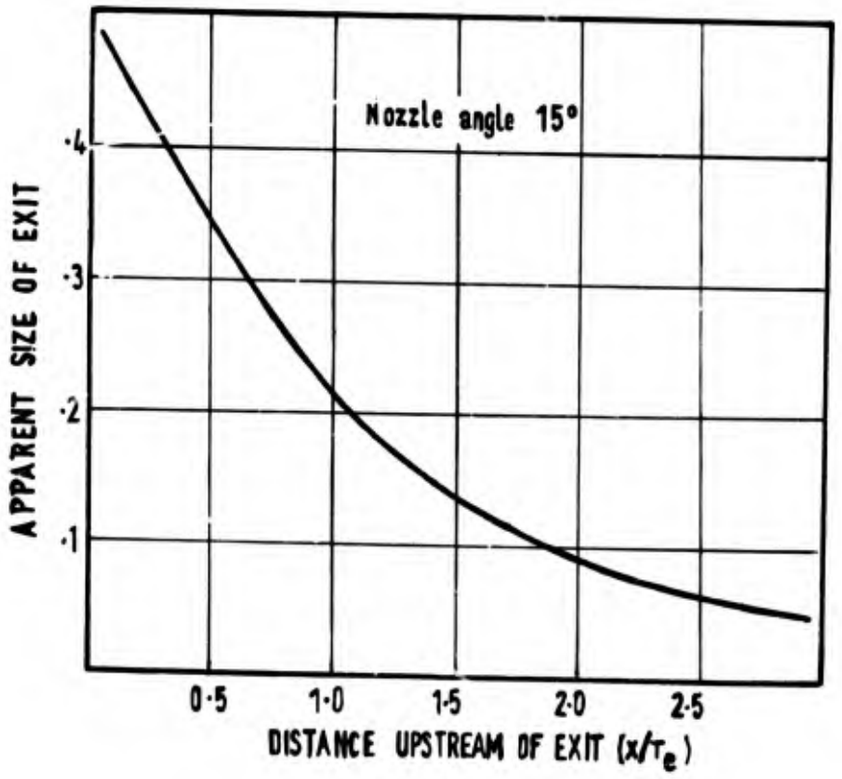

Fig. 14.4 View factors for the nozzle exit within a conical expansion nozzle

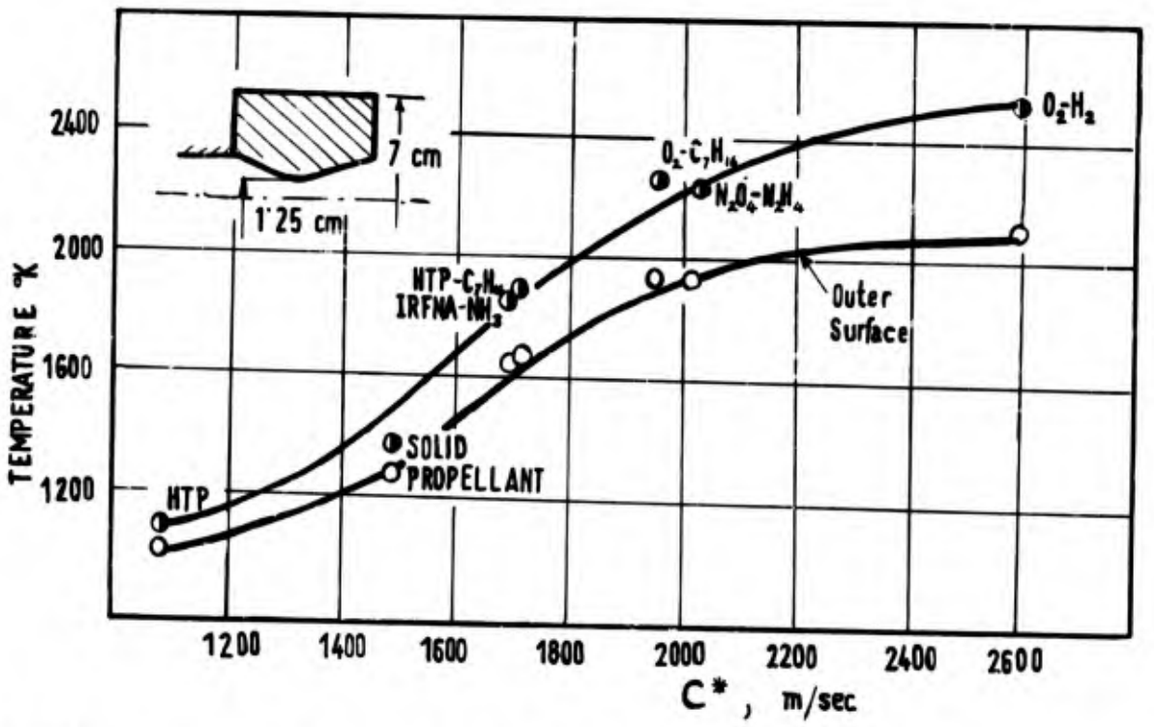

Fig.14.5 Temperatures in a pyrolytic graphite nozzle for a fixed internal configuration and variable external diameter

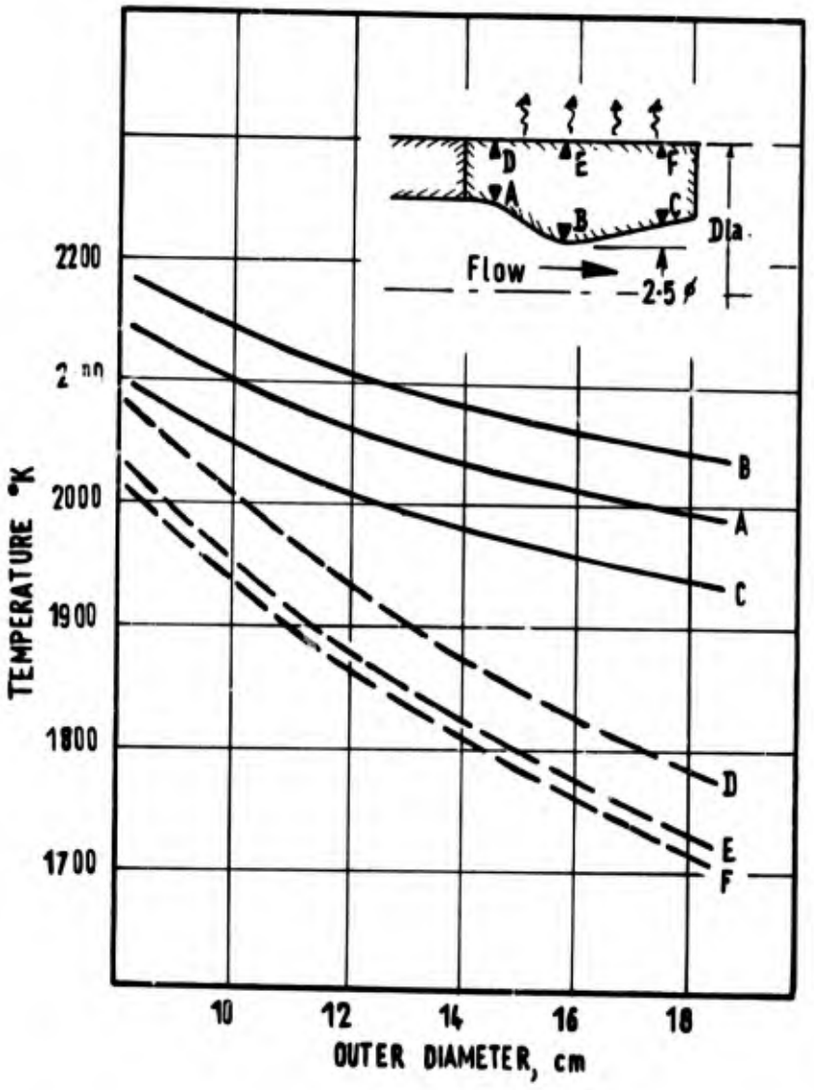

Fig.14.6 Nozzle throat temperatures in a totally radiation-cooled pyrolytic graphite nozzle with propellants of different performance

CHAPTER 15

GAS TRANSPORT PROPERTIES

15.1 INTRODUCTION

A knowledge of the transport properties of the combustion gas mixture is essential to the understanding and calculation of heat transfer processes in rocket engines. Of interest in this context are the viscosity, the thermal conductivity, the Prandtl number and the isentropic exponent of the gas.

In this chapter the available data and theoretical formulae for the transport properties of gas mixtures at high temperatures will be reviewed, and an estimate made of the uncertainty introduced into the heat transfer calculations by the use of this information.

Little experimental data is available of these properties at the temperatures relevant to rocket engines. Instead, extrapolations must be made from measurements at lower temperatures. Such extrapolation introduces uncertainties because the exact state of the gas, the accuracy which may be attached to the various constants, and the validity of the formulae used are not known.

Before all else it is necessary to know the composition and stagnation gas temperature of the mixture of combustion gases. This problem is beyond the scope of the present work, but equilibrium gas composition programs are in widespread use. Values for the various thermochemical constants are well established[1], and a good account of the methods used is given by Siegel and Schieler[2]. However, to use an equilibrium gas composition program to establish in detail the gas composition and temperature throughout the flow in a rocket engine before embarking on calculations of the heat transfer is likely to be impracticable; so that assumptions will have to be made about the nature of the flow and about changes in gas composition across the boundary layer.

The extreme assumptions about the gas composition in the boundary layer are either that the gas reaches the chemical equilibrium appropriate to the local gas temperature, or that the composition remains "frozen" at the free-stream condition. The degree of equilibrium actually achieved in the boundary layer was dealt with in Chapter 5. Here it shall merely be observed that the extremes exist.

15.2 ISENTROPIC EXPONENT

The usual assumption made about the main-stream nozzle flow is that the gas behaves according to the isentropic flow equation for an ideal gas:

$$p\rho^{-\gamma} = \text{constant} \ . \tag{15.1}$$

The true, local, isentropic exponent is thus defined as

$$\gamma = \frac{\partial \log_e p}{\partial \log_e \rho} \ . \tag{15.2}$$

For gases at moderate temperature this is approximately equal to the ratio of the specific heats of the gas at constant pressure and volume. Making the assumption that the gas is constant ("frozen") in composition throughout the flow, it is possible to assume that energy exchange occurs only between the thermal and the translational states, and thus

$$\gamma_f = \frac{C_p}{C_v} = \frac{C_p}{C_p - R} \ . \tag{15.3}$$

In rocket engines, however, it is more usual for the flow to remain close to chemical equilibrium. If the gases are otherwise ideal, it is fairly easy to show that

$$\gamma_e = \frac{C_p}{C_p(1+\alpha_2) - R(1-\alpha_1)^2} \ , \tag{15.4}$$

where

$$\alpha_1 = \left(\frac{\partial \log_e M}{\partial \log_e T}\right)_p$$

and

$$\alpha_2 = \left(\frac{\partial \log_e M}{\partial \log_e p}\right)_T ,$$

M being the mean molecular weight of the gas mixture. In general the reaction (represented by changing M) will be a much stronger function of temperature than of pressure, and so γ_f will be larger than γ_e .

Figure 15.1 shows the variations of γ_f and γ_e with pressure ratio for a typical rocket engine exhaust gas combination. It can be seen that the use of a constant isentropic exponent value for the gas flow, derived from Equation (15.2), will provide only a first approximation to the flow. A better approximation would be to use an "equivalent" exponent (γ_e'), giving the correct conditions at *two* points in the flow (most probably the chamber and the throat), and providing an approximation for conditions in the intervening range, i.e.

$$\gamma_e' = \frac{\log_e(p_0/p_\star)}{\log_e(\rho_0/\rho_\star)} , \tag{15.5}$$

where the subscripts 0 and $\star$ refer to the conditions in the combustion chamber and the throat of the expansion nozzle, respectively.

However, in heat transfer calculations one is not very interested in the relationship between the local pressure and the local density. Instead, the local free-stream temperature T_s in terms of the area ratio $A/A_\star$ is required and a value of γ is sought which best satisfies the equation

$$\frac{A}{A_\star} = \frac{\left[\frac{2}{\gamma+1}\frac{T_0}{T_s}\right]^{(\gamma+1)/(\gamma-1)}}{\left[\frac{2}{\gamma-1}\left(\frac{T_0}{T_s}-1\right)\right]^{1/2}} . \tag{15.6}$$

While it may be unnecessarily complicated to calculate the gas composition and conditions from basic thermochemical considerations throughout the nozzle, it is still fairly simple to calculate the sonic or "throat" conditions of the flow at the same time as the stagnation conditions. At the throat, where $A/A_\star = 1$, Equation (15.6) provides a very simple "equivalent" isentropic exponent,

$$\boxed{\gamma_e' = 2\frac{T_0}{T_\star} - 1 .} \tag{15.7}$$

The dependence of T_s on γ in Equation (15.6) is relatively weak. If a particular value of the area ratio $A/A_\star$ is chosen, say $A/A_\star = 2.281$, corresponding to an actual value of $p_0/p = 10$, then the variation of T_s with chosen γ may be obtained, as in Figure 15.2. As an example, the values of γ for this particular condition obtained from the ratio of the specific heats of the gas, and from the actual $p-\rho$ variation (Eqn (15.2)) are indicated, along with the temperature obtained from an equilibrium gas composition calculation (the "actual" value). There is a difference of only 170°K between the extremes of temperature calculated from the ratio of the specific heats, and the "actual" value.

Equation (15.7) probably represents the most convenient approximation of the "isentropic exponent" for heat transfer calculations, except for such applications as radiation-cooled nozzles where the area of interest lies well downstream of the throat of the nozzle.

15.3 VISCOSITY

Having found the local free-stream gas temperature, values of the corresponding transport properties and their variation across the boundary layer are needed.

Svehla[3] has provided calculations for the viscosities and thermal conductivities of a wide range of pure gas species which would seem adequate for nearly all rocket engine calculations. For these calculations, a Lennard-Jones intermolecular potential function was assumed.

$$\phi(r) = 4\epsilon\left[\left(\frac{\sigma}{r}\right)^{12} - \left(\frac{\sigma}{r}\right)^{6}\right], \tag{15.8}$$

where ϵ is the maximum energy of attraction between colliding molecules, and σ the low-velocity collision diameter. Using this model, Hirschfelder et al.[4] gives a first approximation to the viscosity of a pure gas as

$$\mu = \frac{2.6693\sqrt{(MT)}}{\sigma^2\Omega^{(2,2)\star}} \times 10^{-7}, \tag{15.9}$$

where T is the gas temperature (°K), and M the molecular weight. $\Omega^{(2,2)\star}$ is the reduced collision integral, which is a function of the reduced temperature kT/ϵ. Figure 15.3 shows the variation of this integral, values of which are tabulated by Hirschfelder et al.[4] for a wide range of reduced temperatures.

Values for the force constants, taken from Svehla[3] are given in Table 15.1 for a range of gas molecules typically found in rocket engine exhaust gases. Figure 15.4 shows a selection of viscosity-temperature variations from this source.

Bromley and Wilke[5] have provided an approximate formula for the viscosity of a gas mixture in terms of the viscosity of its component species, namely:

$$\boxed{\mu_{mix} = \sum_i \frac{\mu_i}{\left[\sum_j G_{ij}\frac{x_j}{x_i}\right]}}, \tag{15.10}$$

where

$$G_{ij} = \frac{\left[1 + \left(\frac{\mu_i}{\mu_j}\right)^{1/2}\left(\frac{M_i}{M_j}\right)^{1/4}\right]^2}{2\sqrt{2}\left[1 + \frac{M_i}{M_j}\right]^{1/2}}$$

and x_i and M_i are the mole-fraction and the molecular weight of the i^{th} species of the gas, respectively.

Amdur and Mason[6] have made comparisons of statistical gas kinetic solutions with the approximate formula of Equation (15.10). The helium-argon system provides their most severe test, and at 4000°K the deviation of the approximation from the exact equation is 1.9%. Such close agreement would seem to be a good justification for using this simple, approximate method in heat transfer calculations.

Further, Saxena and Gambhir[7] have made studies of the accuracy with which the approximation of Equation (15.10) predicts experimental results at ordinary temperatures for binary gas mixtures, finding a maximum error of approximately 3.4% at 300°K.

At high temperatures, determinations of viscosity are rare. Vasilesco[8] has measured the viscosity of air, argon, nitrogen and carbon dioxide at temperatures up to 2000°K. Results for air are illustrated in Figure 15.5, where they are compared with the theoretical prediction as outlined above. For pure gases, the correlation with theory is about 1% over the entire range. For air, there is a discrepancy of about 4% at 2000°K.

Except at very high pressures, the viscosity may be assumed to be independent of pressure.

Combining all these results, the uncertainty involved in using Svehla's data and a formula for the viscosity of a gas mixture as given in Equation (15.10) is probably about 6%.

It has also been assumed (Eqn (2.22)) that the viscosity within the boundary layer varies according to some exponential function of the temperature. Figure 15.4 shows that such a relation holds quite well for temperatures of above about 600°K. Since the temperature in the boundary layer will vary from a wall temperature of about this value to the stagnation combustion temperature, such an assumption would seem quite reasonable.

15.4 THERMAL CONDUCTIVITY

As with viscosity, Svehla[3] has provided calculations for the thermal conductivity of a wide range of pure gas species. The equation used to calculate the thermal conductivity is

$$k = \frac{R}{M}\left[\frac{15}{4} + 1.32\left(\frac{C_p}{R} - \frac{5}{2}\right)\right]\mu = k' + k'' , \tag{15.11}$$

where

$$k' = \frac{15R}{4M}\mu$$

and

$$k'' = 1.32\,\frac{R}{M}\left(\frac{C_p}{R} - \frac{5}{2}\right)\mu .$$

In this equation k' represents the translational thermal conductivity and k'' the contribution of the internal degrees of freedom to the conductivity. This is an approximate variation only, tending to overestimate k' and underestimate k''. At high temperatures Equation (15.11) may be expected to be moderately accurate. At lower temperatures, experimental thermal conductivities should be used in preference to the calculated values. However, Equation (15.11) should be suitable for all rocket engine applications.

For gas mixtures, the approximate mixture formula given by Mason and Saxena[9] is similar to that for the viscosity of a gas mixture

$$k_{mix} = \sum_i \frac{k_i}{\left[\sum_j G'_{ij}\,\frac{x_j}{x_i}\right]} , \tag{15.12}$$

where

$$G'_{ij} = \frac{1.065\left[1 + \left(\frac{k'_i}{k'_j}\right)^{1/2}\left(\frac{M_i}{M_j}\right)^{1/4}\right]^2}{2\sqrt{2}\left[1 + \frac{M_i}{M_j}\right]^{1/2}} .$$

It should be noted that k' appearing in the function G_{ij} is the translational component of the thermal conductivity only. From Equation (15.11),

$$\frac{k'_i}{k'_j} = \frac{\mu_i M_j}{\mu_j M_i} .$$

As in the case of viscosity, Amdur and Mason[6] have made comparison between the exact gas kinetic solutions and this approximation, and – with the helium-argon mixture again representing the worst case – found a deviation of 5.1% at 4000°K.

Experimental determinations of the thermal conductivity at high temperatures are limited, both in temperature range and species. Westenberg and de Haas[10,11] have made measurements on N_2-CO_2 and O_2-H_2O mixtures up to temperatures of 1100°K. There is general agreement with Svehla's calculations to about 7%, with a maximum of about 12.5% in the case of a carbon dioxide-nitrogen mixture. This probably represents the approximate limits of the accuracy of the experiments.

At higher temperatures additional effects complicate the measurement of the thermal conductivity. With polyatomic gases, heat transfer by the diffusion of dissociated species across a temperature gradient, and their subsequent recombination, can increase the effective thermal conductivity. However, such ideal "equilibrium" conditions may not be met with in the boundary layer of a rocket engine. This subject has been dealt with in Chapter 5.

15.5 PRANDTL NUMBER

The Prandtl number of the gas is derived from the viscosity, the thermal conductivity, and the specific heat at constant pressure

$$Pr = \frac{\mu C_p}{k} .$$

The Prandtl number is thus the ratio of the momentum and thermal diffusivities of the gas, and is a separate property of the gas. However, it is nearly impossible to measure the Prandtl number directly, and it must therefore be calculated from the other properties of the gas.

The viscosity and the thermal conductivity have already been discussed. Knowledge of the specific heat of the gas at constant pressure is somewhat more difficult to come by. Very few direct measurements of the specific heat of a gas have been made. On the other hand, the specific heat is the rate of change of gas enthalpy with temperature, and the enthalpy of a gas of given composition may be fairly readily calculated. Furthermore, such calculations – based on the law of conservation of energy – involve relatively few assumptions about the behaviour of the gas, and thus enthalpies may be considered moderately reliable. Thermochemical data for most gas species are collected in NBS Circular 500 (Ref.12) and are well established.

The specific heat of a mixture is simply the sum of the products of the individual specific heats with the mass-fraction of the species involved, since for near-ideal gases the "heat of mixing" will be negligible, so that

$$C_{p_{mix}} = \sum_i \frac{x_i C_{p_i}}{M_i} \,. \tag{15.13}$$

Once again, if the gas composition changes with temperature, the heat of the reaction will contribute to the final result, and must be taken into account.

A simple equation relating thermal conductivity to viscosity for a gas is

$$k = f\mu C_v \,, \tag{15.14}$$

where C_v is the specific heat of the gas at constant volume, and f is a pure number. Eucken has proposed a formula connecting f with γ, the ratio of the specific heats of the gas,

$$f = \tfrac{1}{4}(9\gamma - 5) \,,$$

from which it would follow that

$$Pr = \frac{4\gamma}{9\gamma - 5} \,. \tag{15.15}$$

At 273°K the Eucken formula holds to within a few percent for simple molecules. However, a comparison of the value of Equation (15.15) with the Prandtl number calculated from k, C_p and μ suggests that the formula does not hold at high temperatures. The reason for this is that the simple relationship between conductivity and viscosity only applies to the translational thermal conductivity (k'), and at high temperatures internal modes of heat transfer become important.

It is therefore desirable to calculate the Prandtl number from the gas properties themselves to prevent serious error. For this reason also we cannot expect the uncertainties in viscosity and thermal conductivity to cancel one another completely. Summing the component uncertainties leads to an estimated overall uncertainty in Prandtl number of about 19%. The error in practice will almost certainly be less than this.

15.6 CONCLUSION

Using the methods detailed above, the probable uncertainties are 6% in the viscosity, 12% in the thermal conductivity, and 19% in Prandtl number. The use of a simple isentropic exponent to calculate the free stream temperature of the gas can lead to a maximum error of about 7½% in temperature, but this will give much smaller errors in heat transfer calculations.

Applying these results to the heat transfer equation would lead to an uncertainty of about 17% in heat transfer rate due to unreliability in knowledge of the gas transport properties. These uncertainties will, however, tend to produce systematic errors in the heat transfer, and since experimental measurements will in general be rather more accurate than this, it becomes possible to modify the gas transport properties in the light of the heat transfer measurements. It is found that if the data given here are used, any such systematic errors are lost in the general experimental inaccuracies. We may therefore expect that the actual error lies in the region of 5-10%.

REFERENCES

1. JANAF *Interim Thermochemical Tables.* Dow Chemical Co., Midland, Michigan, Dec.1960.

2. Siegel, B. Schieler, L. *Energetics of Propellant Chemistry.* Wiley, New York, 1964.

3. Svehla, R.A. *Estimated Viscosities and Thermal Conductivities of Gases at High Temperatures.* NASA R-132, 1962.

4. Hirschfelder, J.O. et al. *Molecular Theory of Gases and Liquids.* Wiley, New York, 1954.

5. Bromley, L.A. *Viscosity Behaviour of Gases.* Ind. Eng. Chem., Vol.43, 1951, p.1641.

6. Amdur, I. Mason, E.A. *Properties of Gases at Very High Temperatures.* Phys. Fluids, Vol.1, 1958, p.370.

7. Saxena, S.C. Gambhir, R.S. *The Viscosity and Translational Thermal Conductivity of Gas Mixtures.* Brit. J. Appl. Phys., Vol.14, 1963, p.436.

8. Vasilesco, V. *Recherches Expérimentales sur la Viscosité des Gaz aux Températures Elevées.* Ann. Phys., Vol.20, 1945, pp.137 & 292.

9. Mason, E.A. Saxena, S.C. *Approximate Formulae for the Thermal Conductivity of Gas Mixtures.* Phys. Fluids, Vol.1, 1958, p.361.

10. Westenberg, A.A. de Haas, N. *Gas Thermal Conductivity Studies at High Temperatures. I: Line-Source Technique and Results in N_2, CO_2 and N_2-CO_2 Mixtures.* Phys. Fluids., Vol.5, 1962, p.266.

11. Westenberg, A.A. *Gas Thermal Conductivity Studies at High Temperatures. II: Results for O_2 and O_2-H_2O Mixtures.* Phys. Fluids, Vol.6, 1963, p.617.

12. Rossini, F.D. et al. *Selected Values of Chemical Thermodynamic Properties.* Nat. Bureau of Standards, Circular 500, 1952.

TABLE 15.I

Molecule	σ(A.U.)	ϵ/k	M
CO	3.690	91.7	28.01
CO_2	3.941	195.2	44.01
Cl	3.613	130.8	35.457
Cl_2	4.217	316.0	70.91
F	2.968	112.6	19.00
F_2	3.357	112.6	38.00
H	2.708	37.0	1.008
HCl	3.339	344.7	36.47
HF	3.148	330	20.01
H_2	2.827	59.7	2.016
H_2O	2.641	809.1	18.02
NH	3.312	65.3	15.02
NH_3	2.900	558.3	17.03
NO	3.492	116.7	30.01
N_2	3.798	71.4	28.02
O	3.050	106.7	16.00
OH	3.147	79.8	17.01
O_2	3.467	106.7	32.00

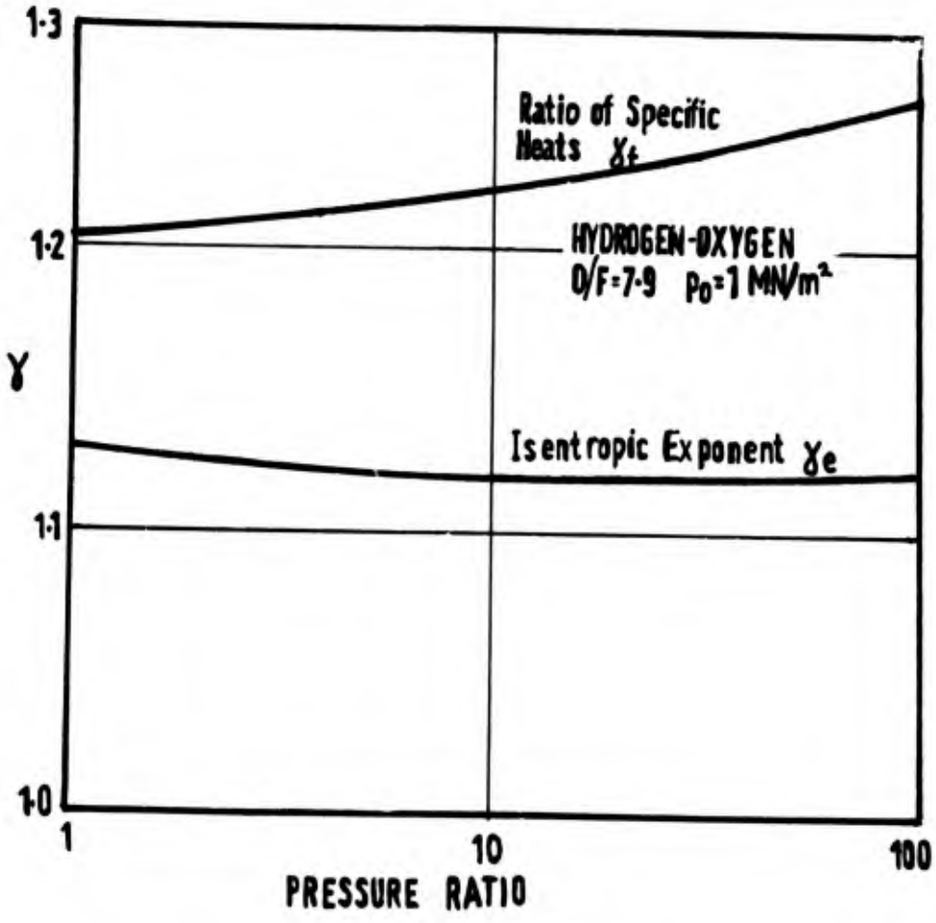

Fig.15.1 Variation of local frozen and equilibrium isentropic exponent with pressure ratio in a typical rocket engine

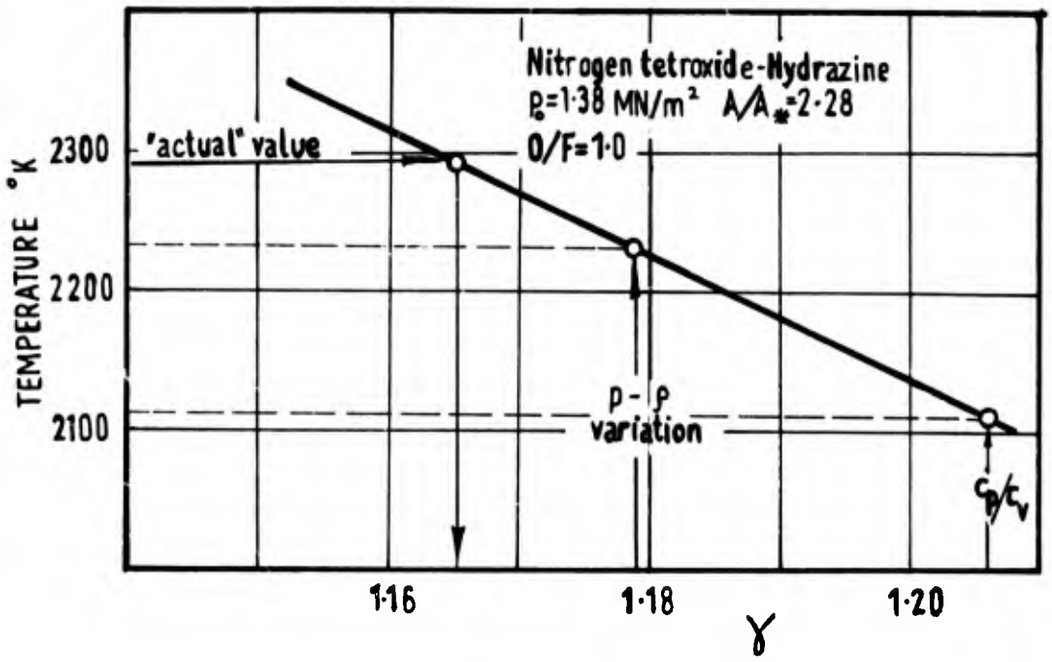

Fig.15.2 Variation of free stream temperature with isentropic exponent for a given area ratio

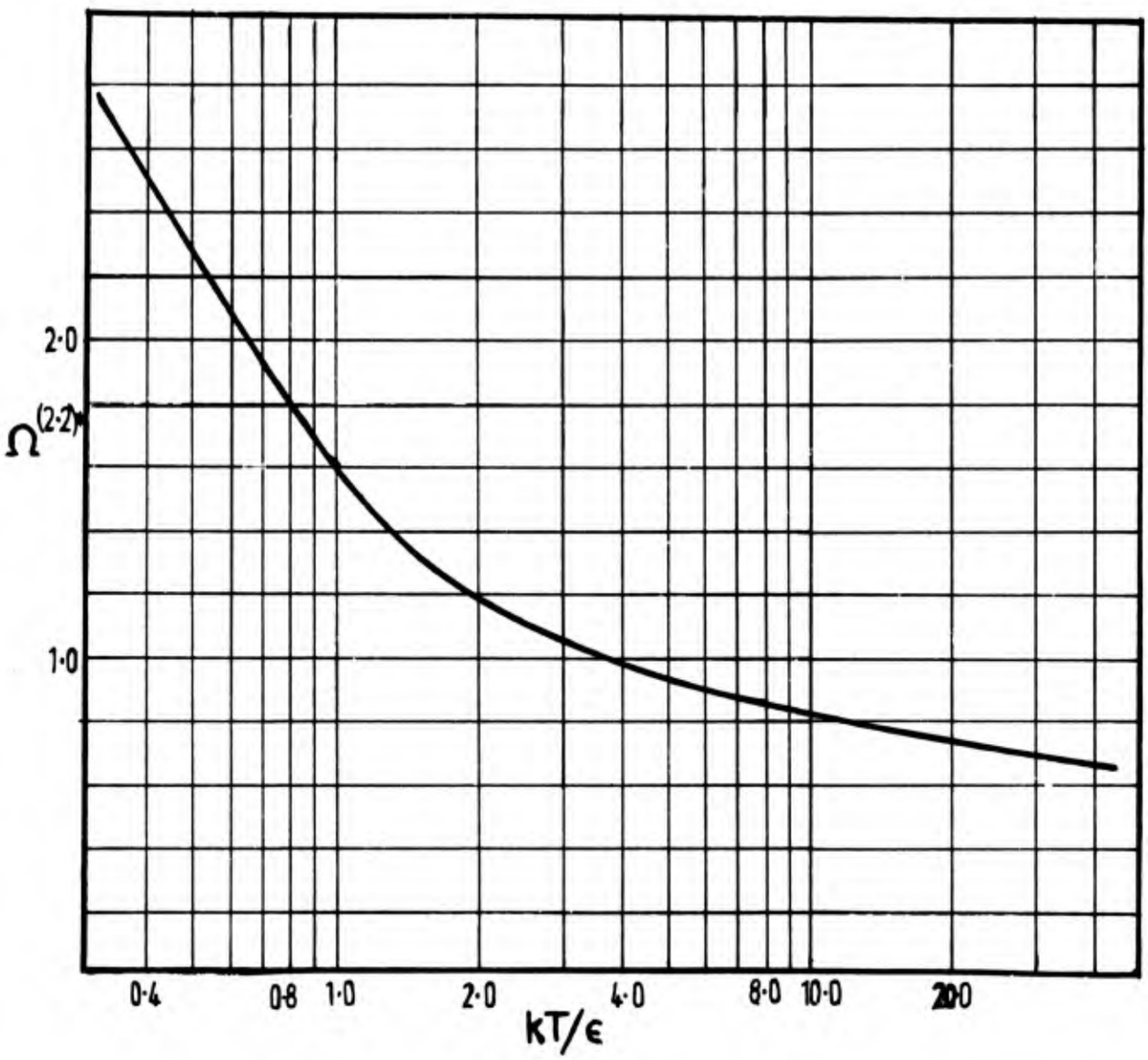

Fig.15.3 Reduced collision integral for calculating transport coefficients for the Lennard-Jones intermolecular potential function

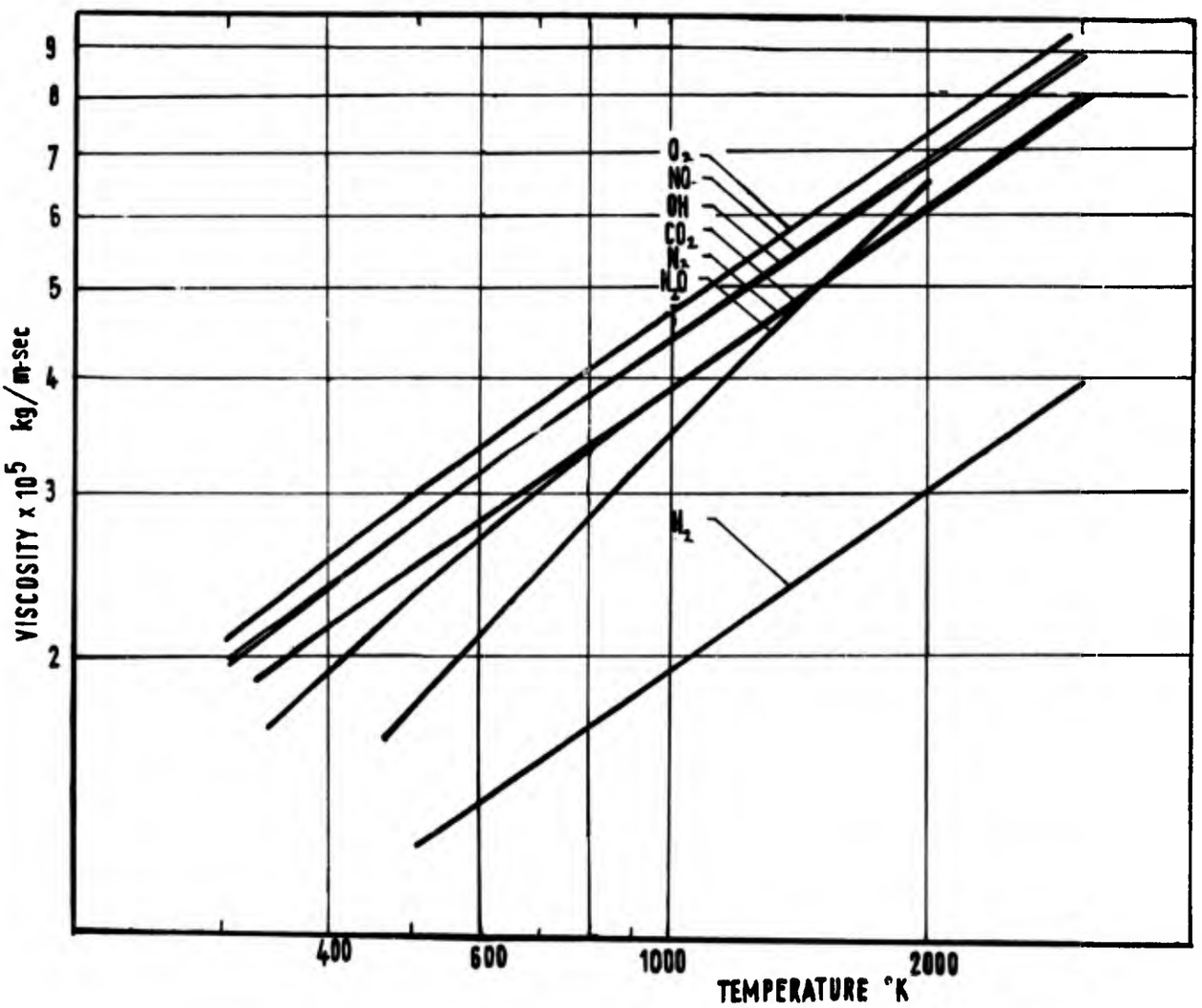

Fig. 15.4 Typical variation of viscosity with temperature for rocket engine exhaust products

CHAPTER 16

MATERIALS FOR REGENERATIVELY COOLED ENGINES

16.1 INTRODUCTION

Compared with the considerable effort expended over the last 30 years on many aspects of liquid propulsion systems, only scant attention seems to have been given to the optimisation of thrust chamber materials. This apparent neglect has its cause in the fact that past requirements were adequately, but not necessarily best, met by an intuitive choice from a range of well tried engineering materials. However, as has already been shown in Chapter 10, better materials are available, and as higher performance is demanded of engines, more attention will have to be given to the choice of materials from which the thrust chamber is manufactured.

The loads imposed on the thrust chamber structure will come from a combination of thermal and pressure stresses (see Figure 16.1). The pressure stress will reach its maximum in the nozzle exit plane, the thermal stress in the region of maximum heat transfer. In most engines it will be this latter area, i.e. the vicinity of the throat of the expansion nozzle, which provides the critically stressed region.

But critical stress conditions will depend not only on the operating conditions within the chamber, but also on the design adopted. A configuration favoured in the early days of rocket engineering consisted of two co-axial shells with an annular passage of suitable width for the controlled flow of coolant (e.g. the German V-2 thrust chamber). In this arrangement the outer shell is subjected to the full pressure of the coolant (always in excess of the combustion pressure), but thermal stresses are practically absent. The inner shell, on the other hand, has to withstand the locally variable coolant excess pressure and, as a result of the heat flux through the wall, also a considerable thermal stress. The limitations on such a design are for smaller thrust chambers, the narrow cooling passage required, and for high-thrust chambers, the fact that pressure stresses demand an increase in wall thickness with consequent weight penalties and thermal stress problems.

For small thrust chambers, the twin shell design is modified to provide a helical passage for the coolant flow, thereby providing a higher coolant passage for the same flow area. But for high thrusts, multi-tube chambers are now universal. In this chapter each of these designs will be dealt with in turn, examining the way in which pressure and thermal stresses limit the choice of design and material.

16.2 MATERIAL OPTIMISATION FOR PRESSURE STRESSES

For engines in which pressure stresses are dominant, one is concerned in general with materials which can conduct maximum heat flux per unit mass of unit area of wall.

If we have a wall of unit surface area and thickness Δx, thermal conductivity k, and with a temperature difference ΔT across it, the heat flux normal to the plate will be

$$\ddot{q} = \frac{k\,\Delta T}{\Delta x} \quad . \tag{16.1}$$

The mass of the heat exchange surface of unit surface area is given by

$$W = \Delta x \rho \, , \tag{16.2}$$

where ρ is the density of the material. The thickness of the wall (Δx) depends on the stress that it is subjected to, and on the mechanical properties of the material. In the case of pure tension or compression, for example

$$\Delta x \propto \frac{1}{\sigma_{max}} \, , \tag{16.3}$$

where σ_{max} is the maximum permissible stress for the material at the mean operating temperature. For bending, the more likely situation with multi-tube chambers, the relationship is

$$\Delta x \propto 1/\sqrt{\sigma_{max}} \ . \tag{16.4}$$

Therefore, eliminating the wall thickness from Equations (16.1) and (16.2) we have

$$\text{for tension} \quad \ddot{q}/W \propto k\Delta T\sigma^2{}_{max}/\rho \tag{16.5}$$

$$\text{and for bending} \quad \ddot{q}/W \propto k\Delta T\sigma_{max}/\rho \ . \tag{16.6}$$

It will be noticed that both expressions contain the term σ_{max}/ρ , the so-called specific stress, a quantity which is used for the assessment of materials in aerospace structures.

To evaluate Equations (16.5) and (16.6) assumptions concerning the reference temperature for the relevant material properties and the operating temperature difference $\Delta T = T_{w,g} - T_{w,c}$ have to be made. The highest gas-side wall temperature $T_{w,g}$ a material can sustain is clearly limited by its melting point T_{MP} . However, a marked loss of mechanical strength is generally observed on approaching the melting point and considering this point and other possible effects, such as chemical interaction of the wall material with the hot combustion gases, a maximum temperature of 60 per cent of the respective melting points was taken as the limiting gas-side wall temperature for each material investigated. This assumption was thought to allow a fair comparison between materials of widely different melting points.

The coolant-side wall temperature is a variable quantity and depends on the local heat transfer conditions and the conductance of the thrust chamber wall. Changes in the coolant-side wall temperature will obviously affect the temperature dependent physical and mechanical material properties. For this reason the thermal conductivity and the maximum permissible stress were evaluated at the respective mean wall temperature, given by $(0.6\ T_{MP} + T_{w,c})/2$. Bearing in mind the short operating periods of rocket engines and the consequent relative unimportance of creep, it seemed justifiable for the purpose of a material intercomparison to use short-time, high temperature ultimate tensile strength data for σ_{max} in Equations (16.5) and (16.6). With these limiting assumptions the results presented in Figures 16.2 and 16.3 were calculated.

For relatively low coolant-side wall temperatures the heat resistant Y-alloy is superior in tension and bending to the other materials and even surpasses the intuitively favoured copper. Where the coolant is a cryogenic fluid this, or similar types of alloys appear to be an attractive choice. A somewhat surprising result is the relative position of stainless steel. With the exception of the temperature range below 100°C it is superior to all other materials in tension and second best choice to copper for bending loads at coolant-side wall temperatures in excess of 250°C.

It must be remembered, however, that this analysis applies only to cases where simple, pressure induced stresses predominate. At high heat fluxes large temperature differences between the gas-side and the coolant-side wall surfaces will be set up and considerable thermal stresses will be superimposed over the coolant pressure stresses. This situation may alter the relative order of merit of the materials as shown in Figures 16.2 and 16.3.

16.3 MATERIAL OPTIMISATION FOR THERMAL STRESSES

By applying classical similarity laws, Hagen[1] has provided criteria for material optimisation where thermal stresses are important. His method of deriving material characteristics led to the discovery of a previously unknown similarity law describing the thermo-elastic behaviour of solid materials.

Consider an element ΔV in a flat plate of homogenous material subject to heating. Of the energy input into ΔV one part (Q_c) will serve to increase the temperature of the volume element, and a second part (Q_k) will be conducted to adjacent material. As a result of the temperature rise of the volume element elastic forces are set up in the material.

Inside ΔV the following energies have to be considered:–

Heat capacity

$$Q_c = c\rho\Delta T\Delta V \ , \tag{16.7}$$

Heat conduction

$$Q_k = k\left(\frac{dT}{dx}\right)\frac{\Delta V}{\Delta x}\ \Delta t \ , \tag{16.8}$$

where $\Delta V/\Delta x$ represents the cross-sectional area of the volume element, and Δt the period of time during which heating takes place.

The specific thermally induced stresses are proportional to the temperature excess and the thermal expansion coefficient

$$\epsilon \propto \alpha \Delta T \tag{16.9}$$

which, on introducing Hooke's law

$$\sigma = \epsilon E , \tag{16.10}$$

leads to a stress τ_p in the direction of the temperature gradient

$$\tau_p \propto E\alpha\Delta T \tag{16.11}$$

and laterally

$$\tau_l \propto \nu E\alpha\Delta T . \tag{16.12}$$

Combining these quantities with the external conditions (i.e. the temperature gradient ΔT and the time increment Δt), a general expression for the stress in any part of the plate will be of the form

$$F(\sigma , Q_c , Q_k , \tau_p , \tau_l , \Delta x , \Delta T , \Delta t) = 0 . \tag{16.13}$$

Introducing Equations (16.11) and (16.12) into this expression, one may obtain characteristic terms in non-dimensional quantities, viz.

$$\Phi(\sigma/E\alpha\Delta T, c\rho/E\alpha, k\Delta t/E\alpha\Delta x^2, \nu) = 0 . \tag{16.14}$$

The non-dimensional quantity $(\Delta t/\Delta x^2)(k/E\alpha)$ is characteristic of the transient conditions during heating, and important in engines where steady-state conditions are not achieved. For steady-state conditions we may ignore it.

The remaining terms in Equation (16.14) then state that stresses in geometrically similar structures exposed to similar external temperature distributions will be physically similar provided that the dimensionless parameter $c\rho/E\alpha$ and the Poisson ratio ν have identical numerical values. The property $c\rho/E\alpha$ represents a new similarity criterion, and is a measure of the conversion of thermal energy into elastic energy. Analogous to the Prandtl number for fluids, it contains only material properties and thus represents a characteristic dimensionless property of solid materials.

Comparing the data for different materials (Table 16.I) the interesting and unexpected result emerges that $c\rho/\alpha E$ has nearly the same value for all metallic materials listed, whereas for non-metallic (ceramic) materials it may assume widely different values. This fact reveals a fundamental difference in the thermo-elastic behaviour of some metals and non-metals.

In view of the near-constancy of the independent variable $c\rho/E\alpha$, Equation (16.14) can be simplified to

$$\frac{\sigma_{max}}{E\alpha\Delta T} = \text{constant}$$

or

$$\Delta T \propto \frac{\sigma_{max}}{E\alpha} . \tag{16.15}$$

If ΔT is converted to the equivalent heat-flux the same equation as has been previously quoted as Equation (10.10) is obtained,

$$\ddot{q}_{max} \propto \frac{\sigma_{max} k}{E\alpha\Delta x} . \tag{16.16}$$

The two important quantities in this expression will tend to be thermal conductivity and Young's modulus (k and E). As already previously noted, the consequence of this is that typical high temperature materials (ceramics) are likely to fail earlier than materials chosen for their high thermal conductivity and low Young's modulus (e.g. copper).

However, apart from the mechanical and physical properties which can be conveniently combined into characteristic quantities, there are others not so easy to express in numerical form.

Wall materials, especially those used for the construction of multi-tube chambers, must be capable of being fabricated by most conventional methods, such as hot and cold forming, welding, brazing and machining by cutting tools. Further, some of the coolants may possess properties incompatible with certain metals. However, these factors are not likely to much alter the choice of materials. Copper and copper alloys remain good choices for

high performance chambers. Steels and nickel alloys, merely by their familiarity, will probably retain their traditional place for a little while longer.

If fabrication problems were ever to be considered important, then a significant contender might be aluminium and its alloys. The chief disadvantage of aluminium alloys is their very low softening points, but from a fabrication point of view entire chambers might be constructed from hydraulically formed double-taper tubes, salt-bath brazed for very low cost, and the heat transfer problems overcome by judicious use of film cooling.

16.4 DOUBLE-SHELL CHAMBERS

It has already been shown in Chapter 10 that the height of the cooling channel in a simple regeneratively cooled engine is roughly proportional to the chamber diameter for a wide range of conditions. At low thrusts, therefore, the double-shell chamber is limited merely by the problem of maintaining this annulus between two concentric shells.

At high thrusts the double-shell chamber is limited by the conflicting requirements of thermal and pressure stresses. The inner shell must withstand the external load imposed on it by the difference between the coolant pressure and the combustion gas pressure. As the pressure and/or diameter increase, this will lead to increasing wall thickness, which in turn will lead to increased thermal stresses (Equation (16.16)).

Cylindrical shells and other rotationally symmetric shells, when subjected to external pressure, may fail in two ways:

(i) In the elastic regime, where the wall will collapse by buckling at a critical pressure giving stresses considerably below the elastic limit of the material. The critical pressure for cylindrical shells is given approximately by

$$p_B \simeq 2E\left(\frac{\Delta x}{D}\right)^3 . \qquad (16.17)$$

In this region the elastic modulus E controls the behaviour, and there is little point in selecting materials merely for high strength.

(ii) In the plastic range, where the material is stressed up to and beyond its yield point failure occurs through continuing plastic flow. Here

$$p_{max} \simeq 2\sigma_{max}\left(\frac{\Delta x}{D}\right) . \qquad (16.18)$$

For this condition, the yield strength $\sigma_{0.2}$ of the material is the limiting quantity.

The two regions are consecutive for increasing values of wall thickness to diameter ($\Delta x/D$). At low values of this ratio, Equation (16.17) holds, up to the point at which the linear relation of Equation (16.18) intersects the previous cubic relation. An illustration for aluminium, copper and iron is given in Figure 16.4.

Now, if we allow an excess pressure of perhaps 10 atm in the annular space of the thrust chamber (to allow for flow pressure drops and the injector pressure drop), then even for stiff materials such as iron, a minimum value for ($\Delta x/D$) is going to be about 0.0135 (see Figure 16.4). Thus, a thrust chamber with an internal diameter of 80 cm (perhaps about 300 kN thrust) would have wall thicknesses of about 1.1 cm. Even if thermal stresses were not limiting, the weight of such a construction would be quite unacceptable.

Conversely, by choosing an acceptable wall thickness, we find an upper limit to the thrust with such chamber construction – somewhere about 50 kN.

It can therefore be concluded that the double-shell construction has a useful operating region only in the thrust range from about 10 – 50 kN, and really represents the division between chambers with helical cooling passages, and tubular construction chambers.

16.5 HELICALLY COOLED CHAMBERS

For small thrust chambers, and consequent low coolant flow rates, helical coolant passages are arranged between the inner and outer shells, so that the cross-section of the flow duct can be adjusted to suit the operating conditions. These passages can be either machined directly on the inner wall, or formed by winding a wire about the inner shell

and brazing. Because of the larger total length of the helical flow ducts, the pressure drop in such chambers will be increased.

The helical fins on the inner shell have a useful stiffening effect on the inner shell. However, a problem that may occur, and therefore limit the lower size at which this sort of design can be used, is the reduction in cooling effectiveness that takes place under the fin. A simplified analysis of this problem has been carried out by Bartas[2].

A diagram of the rib is shown in Figure 16.5. The thickness of the rib is $2a$, on a wall thickness X, and an additional, "equivalent" wall thickness of $\bar{k}/h$ has been introduced to account for the hot gas heat transfer coefficient h ($\bar{k}$ is the average thermal conductivity of the wall). The apparent wall thickness is thus

$$X_{tot} = X + \frac{\bar{k}}{h} . \tag{16.19}$$

In Figure 16.6, the reduced temperature

$$T_r = \frac{(T_g - T_{wg})}{(T_g - T_{wc})} \tag{16.20}$$

is plotted against the reduced thickness $(\bar{k}/h)X_{tot}$ for different values of the reduced thickness of the rib (a/X_{tot}). T_{wg} is the temperature on the hot-gas side of the wall, and T_{wc} the coolant-side wall temperature.

As an example, if one takes a gas temperature of 2800°K, a coolant-side wall temperature of 530°K, a wall thickness of 0.4 cm and an equivalent thickness for the boundary layer of 0.9 cm, one finds from Figure 16.6 that the undisturbed wall temperature i.e. the temperature in the absence of a rib ($a = 0$) amounts to 1235°K. If the gas-side wall temperature in the centre-line of the rib is not to exceed, say, 1400°K, the reduced temperature is now

$$(2800 - 1400)/(2800 - 530) = 0.615 ,$$

and with the help of Figure 16.6 one obtains $a/X_{tot} = 0.4$ and thus $2a \leq 1.04$ cm. This example shows that while the presence of ribs on cooled walls does not pose an insuperable problem, it must be taken into account if the wall temperature must not exceed a certain critical value.

16.6 MULTI-TUBE CHAMBERS

At higher thrust levels, tubular construction chambers are all but universally used for regeneratively cooled chambers. In this design, suitable formed and tapered tubes are assembled together and brazed to form a pressure tight wall, and then the assembly is supported by external pressure bands or a wire wrapped outer casing. It is now possible to use glass-fibre windings to contain this pressure stress, and the tubes then have only to support their own internal pressure and thermal stresses. The propellant used as coolant may either be introduced at the nozzle exit and made to flow up towards the injector, or if heating problems are too severe, a double-pass arrangement can be used introducing the coolant closer to the injector, flowing it to the nozzle exit through one set of tubes, and then returning to the injector through adjacent tubes.

The major limitation on the wall thickness for a tubular construction chamber will be the manufacturing techniques used. For the most part wall thicknesses of between 0.2 and 0.3 mm can be expected. At this point one would like to know how wide such a tube could be made without exceeding the maximum permissible stress of the material.

The tube wall will act as a uniformly loaded beam fixed at both ends (Figure 16.7). If we consider unit axial length, the required minimum section modulus Z at the point of maximum stress is

$$Z = \frac{\Delta x^2}{6} = \frac{\Delta p\, w^2}{12\sigma_{max}}$$

so that

$$w = \Delta x \left(\frac{2\sigma_{max}}{\Delta p} \right)^{1/2} , \tag{16.21}$$

where

Δx is the thickness of duct wall,

w the width of the duct,

Δp the local pressure difference between the coolant and the combustion gases,

σ_{max} the maximum permissible stress at the given operating temperature.

Conditions will be severest at the start of the firing, when the coolant pressure is applied to all ducts before the combustion pressure rises to its steady operating condition, or at any time at the end of the exhaust nozzle where the coolant pressure will be highest, and the gas pressure lowest.

For stainless steel, using $\sigma_{max} \equiv \sigma_{0.2} = 4200$ bar, one finds from (16.21) that for an engine operating at $p = 30$ bar the width w of the tube is about 17 times the wall thickness Δx, so that for a wall thickness of 0.2 mm, a maximum tube width of only 8.5 mm is permissible. This limitation, in the case of high expansion ratio engines, may lead to the necessity of bifurcating the tubes in the expansion cone.

It is important to realise that this maximum width depends on the local coolant excess pressure and the wall thickness only. Since the heat transfer through the wall (and thus the limiting performance condition for the design) depends only on the wall conductance ($k/\Delta x$), multi-tube chambers will not be limited by chamber diameter. For this reason, multi-tube construction permits the building of very large thrust chambers using high energy propellants.

16.7 CONCLUSION

This chapter has considered the design problems related to material selection in particular types of regeneratively cooled engines. Of the three major variants in design – double-shell, helically cooled and multi-tube chambers – only the last two are really of importance, the former at low thrusts, the latter at high thrusts. Material problems are the ability to withstand the pressure and thermal stress loads imposed on the structure by the design.

The choice of "best" materials will vary with the particular design conditions. At the moment very many regeneratively cooled engines are constructed from high temperature steels and nickel alloys. As time passes, however, it is expected that there will be a shift to materials with higher thermal conductivities, at least for high performance, high pressure engines, and copper alloys would appear to be a likely new contender.

REFERENCES

1. Hagen, H. *Die Beurteilung der Werkstoffeignung für statische, dynamische und thermische Beanspruchung auf Grund des Ähnlichkeitsprinzips.* Die Technik, Vol. 3, 1948, pp.6-14.

2. Bartas, G.J. *Wall Temperatures in Ribbed Combustion Chambers.* Jet Propulsion, Vol. 24, 1957, pp.228-234.

TABLE 16.I

Values of some Physical Properties for Selected Metallic and Ceramic Materials (Reference 1 and others)

Material		*Density* ρ g/cm³	*Specific Heat* c cal/g °C	$\alpha \times 10^6$, *Linear Thermal Expansion Coefficient* (Range in °C) –	$E \times 10^{-6}$ *Modulus of Elasticity* bar	$\frac{c\rho}{E\alpha}$ –
Aluminium	(Al)	2.70	0.212 (0 ÷ 100)	23.8 (0 ÷ 100)	0.700	1.46
Iron	(Fe)	7.876	0.111 (0 ÷ 100)	12.3 (0 ÷ 100)	2.107	1.44
Nickel	(Ni)	8.9	0.1086 (18 ÷ 100)	13.0 (0 ÷ 100)	2.050	1.55
Copper	(Cu)	8.93	0.0928 (18 ÷ 100)	16.98 (0 ÷ 100)	1.300	1.60
Titanium	(Ti)	4.53	0.1125 (0 ÷ 100)	8.8 (0 ÷ 200)	1.12	2.21
Tantalum	(Ta)	16.6	0.033 (14 ÷ 100)	6.5 (0 ÷ 100)	1.900	1.89
Tungsten	(W)	19.3	0.0338 (20 ÷ 100)	4.5 (17 ÷ 100)	3.700	1.67
Quartz	(SiO_2)	2.65	0.263 (20 ÷ 1000)	4.6 (300 ÷ 1300)	0.74	8.75
Silicon Carbide	(SiC)	3.2	0.19 (20 ÷ 1000)	5.2 (20 ÷ 1000)	4.7	1.06
Alumina	(Al_2O_3)	3.98	0.304 (20 ÷ 1000)	8.5 (0 ÷ 100)	3.94	1.54

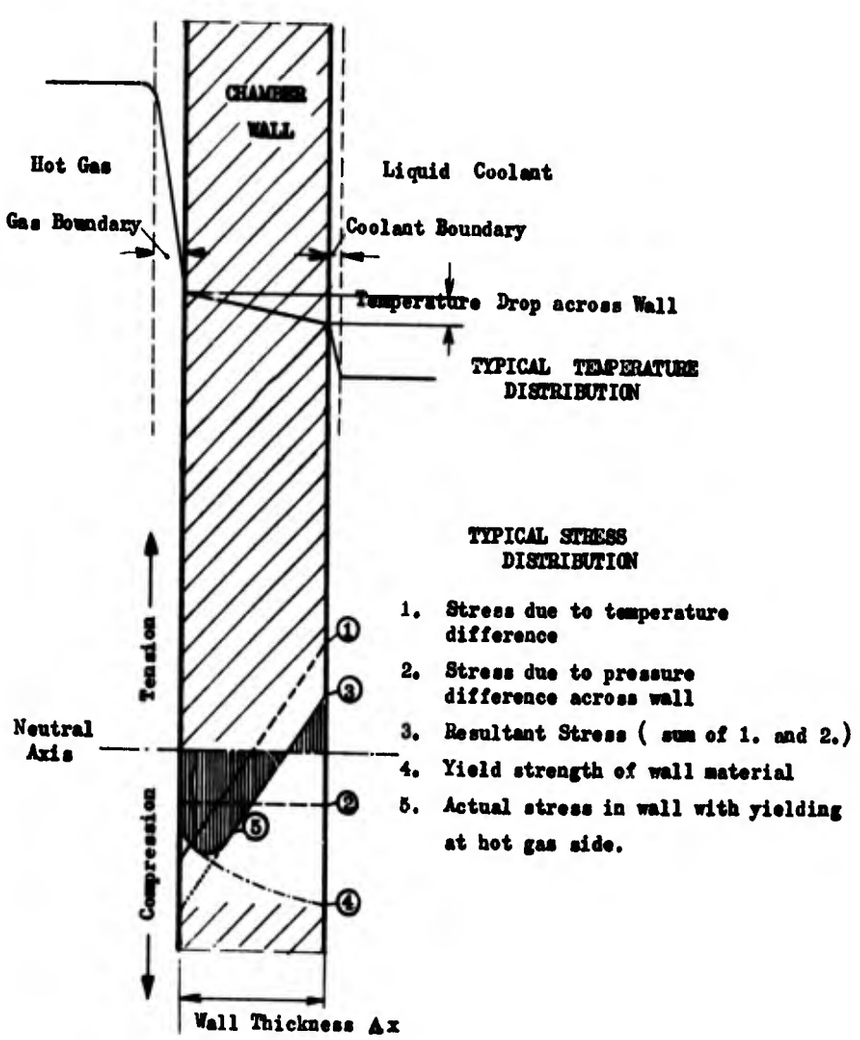

Fig.16.1 Typical stress and temperature distribution in a cooled thrust chamber wall

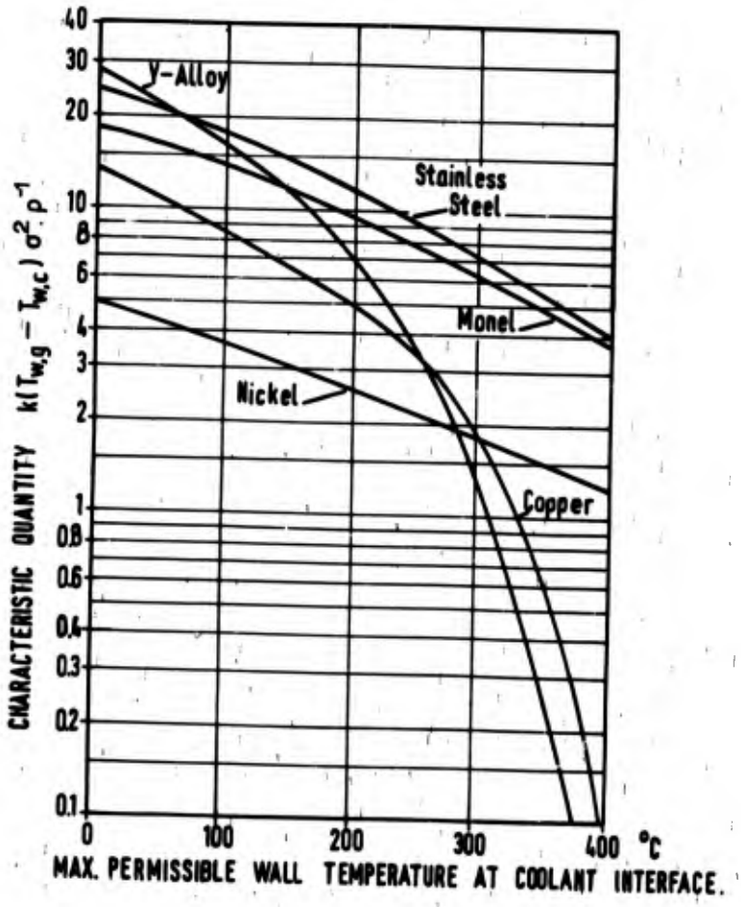

Fig.16.2 Variation in the order of merit of several wall materials exposed to tensile loads as a function of the permissible coolant-wall temperature

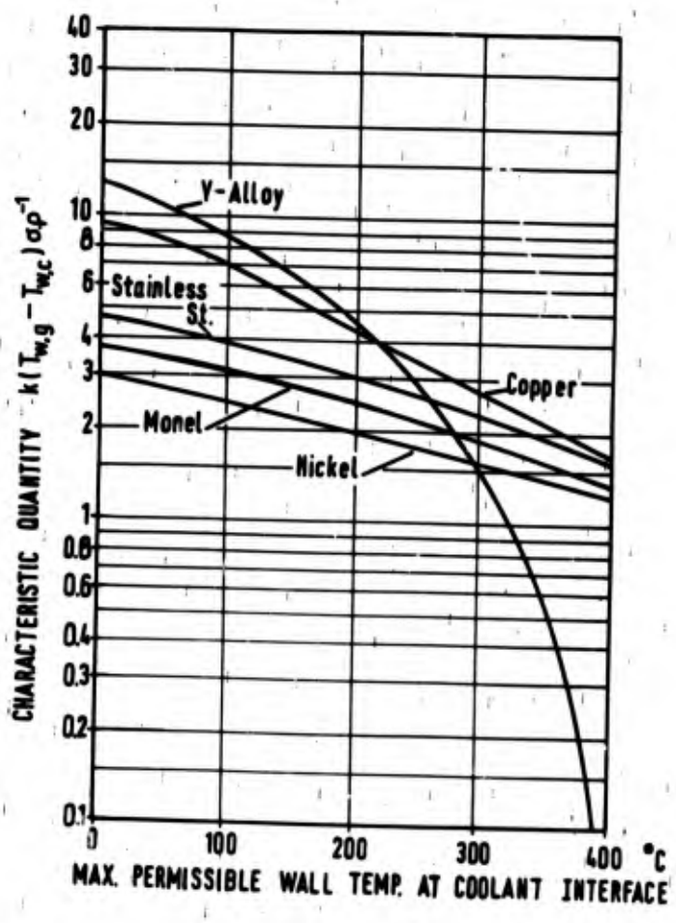

Fig.16.3 Variation in the order of merit of several wall materials exposed to bending loads as a function of the permissible coolant-wall temperature

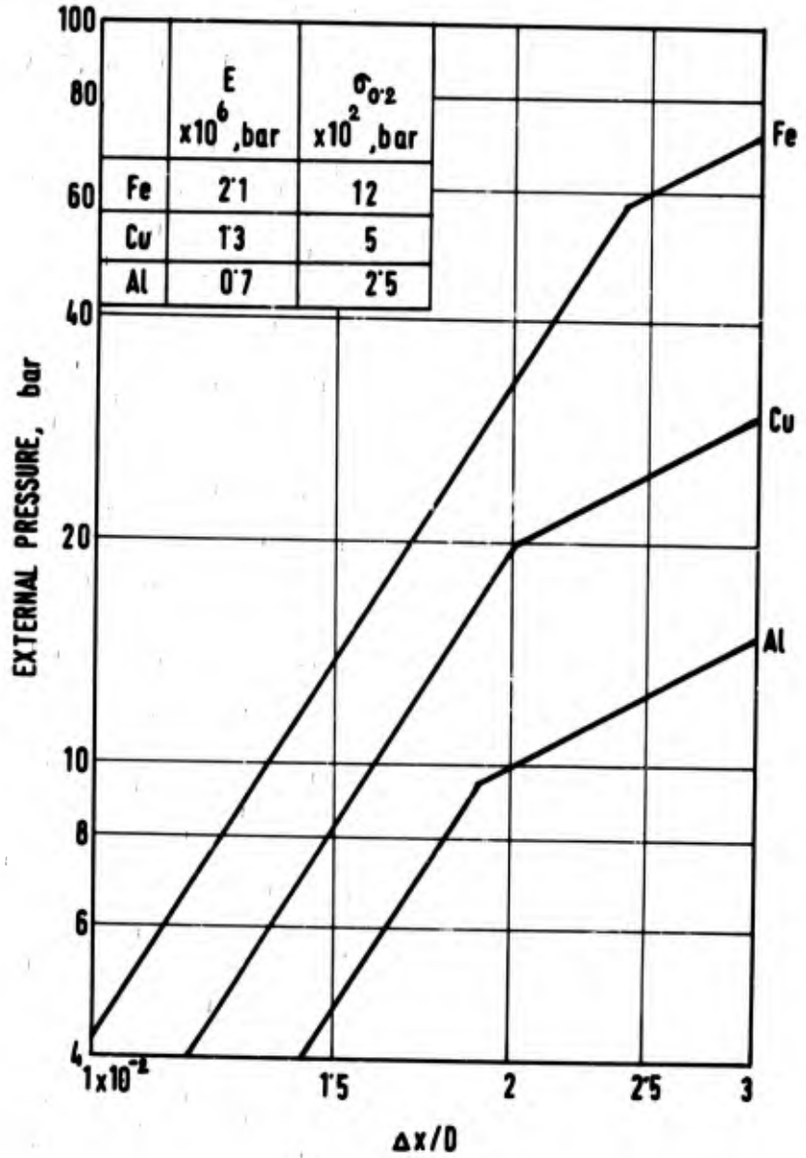

Fig.16.4 Limiting coolant pressures for cylindrical, double-shell thrust chambers

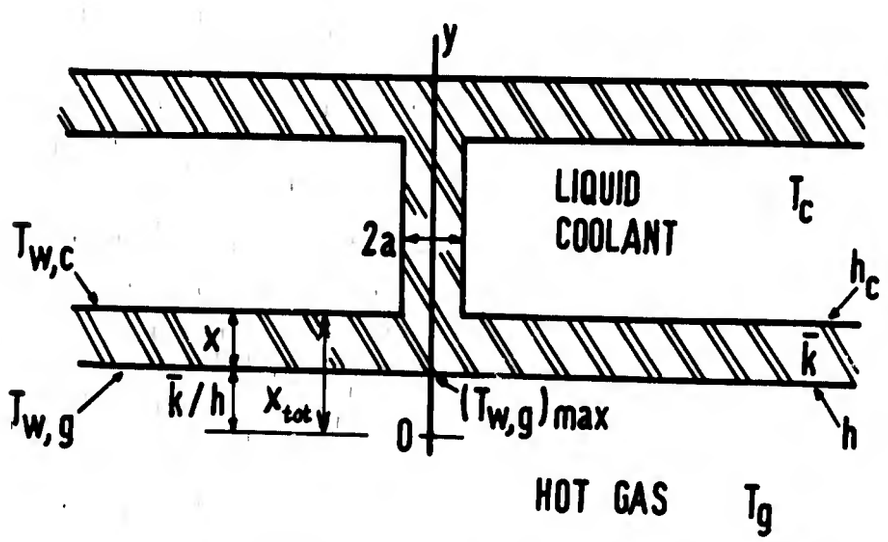

Fig.16.5 Rib configuration in helically cooled chambers (after Bartas[2])

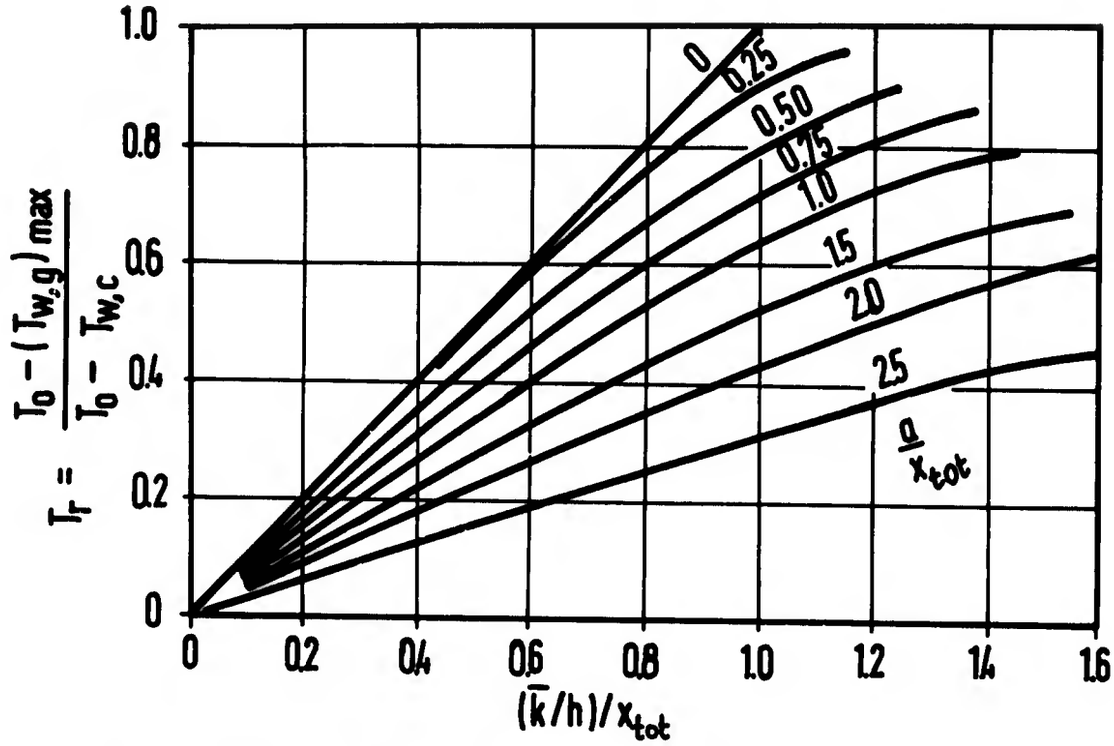

Fig.16.6 Chart for the evaluation of gas-side wall temperatures in ribbed combustion chambers (after Bartas[2])

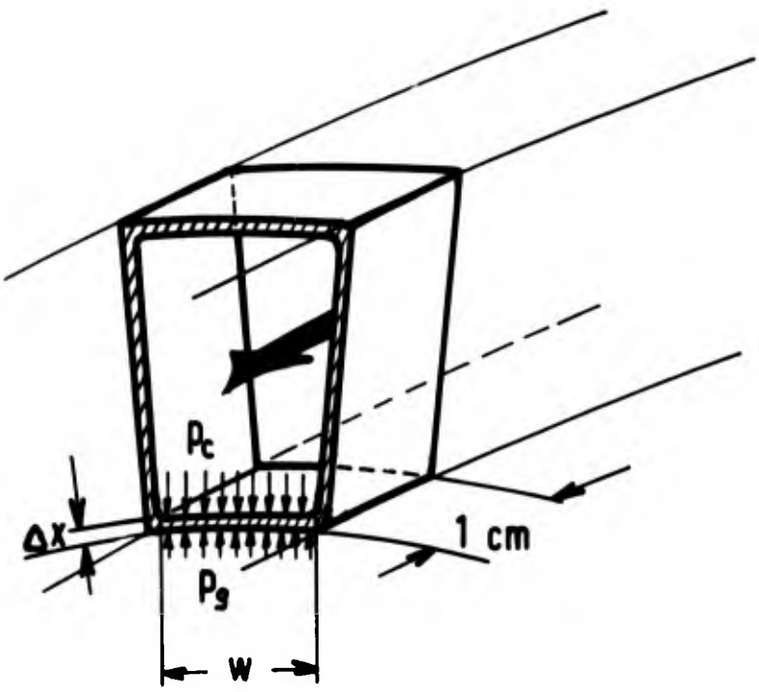

TYPE OF BEAM MODEL

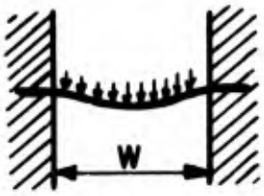

Maximum Stress at both Ends

$$(p_c - p_g)w^2/\Delta x^2 . 2 = \sigma_{max}$$

Fig.16.7 Simplified model of the loading of the cooled tube wall in a multi-tube chamber